Solvent- and Time-dependent Fluorescence of Photoacids based on Pyranine

Dissertation

zur Erlangung des Grades

des Doktors der Naturwissenschaften

der Naturwissenschaftlich-Technischen Fakultät III

Chemie, Pharmazie, Bio- und Werkstoffwissenschaften

der Universität des Saarlandes

von

Dipl. Chem. Christian Spies

Saarbrücken

2014

Tag des Kolloquiums: 10.07.2014

Dekan: Prof. Dr. Volkhard Helms

Berichterstatter: Prof. Dr. Gregor Jung

                         Prof. Dr. Michael Springborg

                         Prof. Dr. Patrick Nürnberger

Vorsitz: Prof. Dr. Gerhard Wenz

Akad. Mitarbeiter: Dr. Bernd Morgenstern

„An experiment, like every other event which takes place, is a natural phenomenon; but in a scientific experiment the circumstances are so arranged that the relations between a particular set of phenomena may be studied to the best advantage. "

James Clerk Maxwell, 1876

Danksagung

Bedanken möchte ich mich zunächst und zutiefst bei Prof. Gregor Jung für die Gelegenheit diese Arbeit in den letzten dreieinhalb Jahren in seiner Arbeitsgruppe anzufertigen. Sein unerschütterlicher Optimismus sowie sein ständige Hilfsbereitschaft haben enorm zur gelungenen Bearbeitung dieses interessanten Themengebiets beigetragen.

Danken möchte ich ebenso Prof. Michael Springborg für die Übernahme der Zweitkorrektur und dafür, dass er mir jederzeit mit Rat und Tat zur Seite stand.

Dank ist ebenso dem Team der Feinmechanik-Werkstatt um Herrn Skohoutil für die Herstellung benötigter Kleinteile geschuldet.

Ohne die großartige Arbeitsatmosphäre im AK Jung wäre es mir definitiv schwerer gefallen, jeden Morgen ins Büro zu kommen. Daher möchte ich allen Leuten von Herzen danken, die in den letzten fünf Jahren dazu beigetragen haben. Ich hatte eine echt tolle Zeit mit euch.

Ein ebenso großes Dankeschön gebührt meiner gesamten Familie, insbesondere meinen Eltern Gudrun und Stefan Spies, welche mich jederzeit unterstützt und ermutigt haben, diesen Weg zu beschreiten. Danke!

Ein riesiges Dankeschön geht auch an meine Freundin Gudrun Nürenberg, die mir schon während des Studiums und insbesondere in den letzten langen Jahren eine enorme Stütze und Rückhalt war. Ohne dich wäre ich nicht der Mensch, der ich heute bin. Danke dafür!

Finally, I want to thank Prof. Ehud Pines and Dan Huppert, for giving me the opportunity to do part of my research in their labs. They put an enormous effort in realizing and organizing my visit in Israel. Due to them and all the people at their labs, I had a great time in those four months, both from a scientific as well as personal perspective.

Table of Contents

1 Abstract

The process of excited-state proton transfer (ESPT) is frequently found in aromatic alcohols. Upon electronic excitation, the acidity of these molecules increases by 5-10 orders of magnitude. While being in the excited state, the proton can be transferred to a suitable acceptor unit due to the high photoacidity. In this thesis, the ESPT behavior of five new photoacids in different solvents as proton acceptor is investigated. The new molecules are based on the well-known pyranine photoacid, with electronic transitions in the visible part of the electromagnetic spectrum. Steady-state and time-resolved spectroscopy is used to characterize the new molecules and prove them as "super"-photoacids, which are capable of ESPT in organic solvents. The combination of steady-state measurements with a solvatochromic analysis showed that it is an intramolecular charge transfer on the photoacid side, which correlates best with the photoacidity of the molecule. The proton transfer rate constants could be measured by using time-resolved methods with picosecond time resolution. The experimental rate constants of the molecules in the solvents water, methanol and ethanol could be correlated by empirical Marcus-like free energy correlations. The decreased proton transfer efficiency in alcohols compared to water is mainly due to equilibrium solvation energies.

Protonentransfer aus dem angeregten elektronischen Zustand ist ein Phänomen, das bei den meisten aromatischen Alkoholen zu beobachten ist. Die Azidität dieser Moleküle nimmt durch Absorption eines UV-Vis-Photons um 5-10 Größenordnungen zu. Aufgrund dieser hohen Photoazidität wird das azide Proton während der Lebensdauer des angeregten Zustandes auf einen geeigneten Protonenakzeptor übertragen. In dieser Arbeit werden fünf neue Photosäuren hinsichtlich ihrer ESPT-Fähigkeit in verschiedenen Lösemitteln getestet. Diese Moleküle, die ausgehend von dem gut untersuchten HPTS Molekül hergestellt wurden, absorbieren und emittieren im sichtbaren Wellenlängenbereich. Ihre Charakterisierung mittels stationärer und zeitaufgelöster Spektroskopie zeigte, dass sie den sogenannten „Super"-Photosäuren zuzuordnen sind, die auch organische Lösemittel protonieren. Durch die

1. Abstract

Kombination von stationärer Spektroskopie mit einer solvatochromen Analyse konnte gezeigt werden, dass die Stärke eines internen Ladungstransfers vor dem Protonentransferschritt proportional zur Photoazidität ist. Die Ratenkonstanten des Protonentransfers wurden mittels zeitaufgelöster Methoden mit Pikosekundenauflösung bestimmt. Diese in Wasser, Methanol und Ethanol gefundenen Ratenkonstanten können durch Freie-Energie Beziehungen basierend auf der Marcus Theorie beschrieben werden. Die geringere Transfereffizienz in Alkoholen konnte auf kleinere Gleichgewichts-Lösemittelenthalpie zurückgeführt werden.
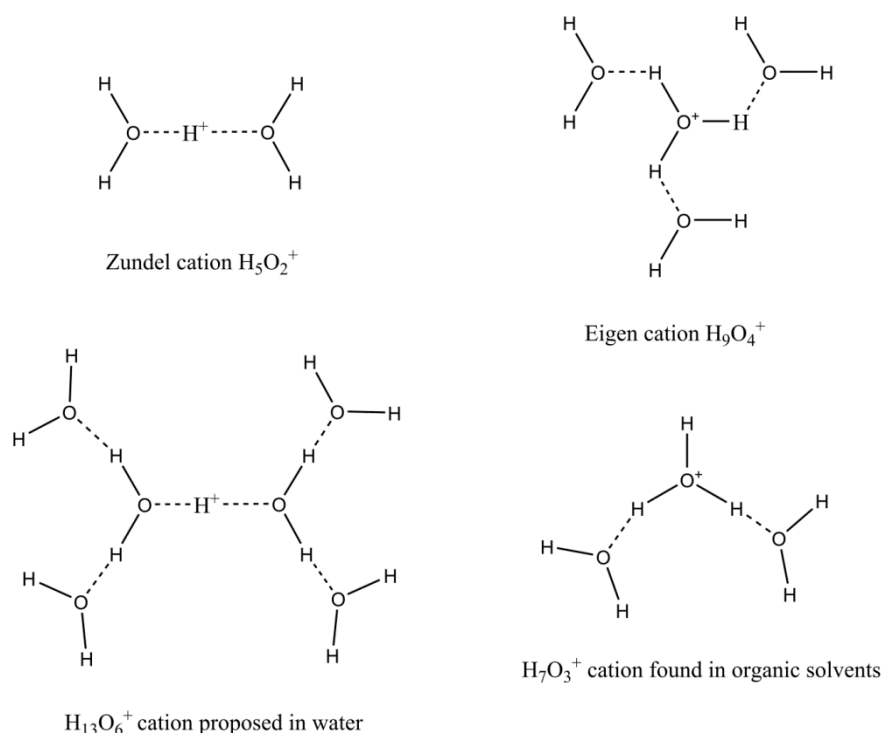
2 General Part

2.1 Introduction

The proton is one of the most important particles in chemistry. It is related to almost every field of chemistry: Its properties and dynamics can easily be calculated in theoretical models; it serves as stabilizing part by forming hydrogen-bonds and therefore influences the stability of DNA, proteins and polymers; the hydrogen-bonding network in water is responsible for its high boiling point and thus enables life on earth; the proton concentration in water defines the pH-value and through this controls chemical and biochemical processes – in a flask or in a living cell.

Most of the abovementioned examples rely on the proton coupled to water to form the hydronium ion, H_3O^+. This simplified picture has been questioned several times and it is known today that the proton forms a stronger clustered structure in condensed media. Many theoretical and experimental studies have been conducted to find the structure and dynamics of the hydronium ion,[1-7] a problem still under investigation in current days[8, 9]. Most prominent are the structures named after Eigen,[10] $H_9O_4^+$, and Zundel,[11, 12] $H_5O_2^+$. Nevertheless, it has been proposed in recent years, that the prominent cluster around the proton in water is $H_{13}O_6^+$,[13] whereas in wet organic solvents the proton is preferentially surrounded by three water molecules to form $H_7O_3^+$ (see Scheme 1).[9, 14] If another solvent is added to water, e.g. alcohol, the situation becomes even more complicated.[14, 15] The structure and energetics in pure polar protic solvents, e.g. alcohols and amines, or polar aprotic solvents like DMSO is also largely unknown. The small amount of water usually present in organic solvents enables the proton to form small water clusters around the proton, its structure determined by the solvent and the water content.[9]

Zundel cation $H_5O_2^+$

Eigen cation $H_9O_4^+$

$H_{13}O_6^+$ cation proposed in water

$H_7O_3^+$ cation found in organic solvents

Scheme 1. Different structures of the proton described in the literature.[8-11, 13, 14]

Besides the structure of the proton, the dynamics of hydrogen bonds formed in a solvent or between a solvent and a probe are also of great interest in chemical research.[16] They were traditionally probed using infra-red (IR) spectroscopy. The appearance of short-pulsed laser systems nowadays allows studying dynamics down to the femtosecond (fs) scale. Techniques like (UV-) pump – (UV/IR) probe spectroscopy, fluorescence up-conversion and time-correlated single photon counting (TCSPC) provided many insights into those dynamics. Many of these methods are based on the absorption of a UV-Vis photon to generate an excited state that can be probed by the respective spectroscopy. To establish these methods for probing hydrogen bonds, a suitable reporter molecule has to be used. Such probes need to change their electronic distribution in the excited state to induce a change in the hydrogen bonds under investigation. Strong perturbations are caused by those molecules, which release an acidic proton in the excited state. Suchlike molecules with a higher acidity upon electronic excitation are called photoacids and are in the focus of the present work.

The first description of an excited state proton transfer (ESPT) is dated back to Theodor Förster,[17, 18] who explained correctly the observations of Weber[19]. In 1931, Weber had observed a change of the fluorescence spectrum of 1,4-naphthylaminosulfonate upon changing the pH of the solution – maintaining an unchanged absorption spectrum. Förster found the same observation true for other aromatic amines and alcohols and stated that this is due to different protolytic equilibrium in the excited state compared to the ground state. The

processes occurring in an ESPT reaction can be depicted in the Förster cycle (Figure 1), a thermodynamic cycle that is named after Theodor Förster, who was the first to use this method for the calculation of pK_a^* values.[18]
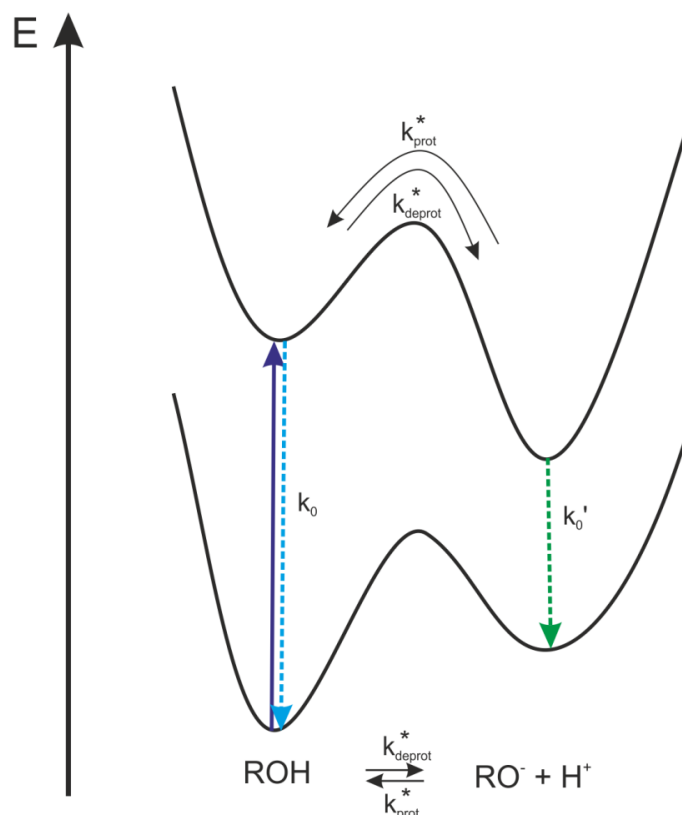
Figure 1. The Förster cycle displays the basic processes that occur in a photoacid system.

Upon electronic excitation hv_a, an usually weak acid ROH increases its acidity in the ES by some orders of magnitude, $pK_a^* < pK_a$, with pK_a defined by equation (1) and the asterisk denoting the ES.

$$pK_a = -\log\left(k_{deprot}\Big/k_{prot}\right) = -\log(K_a) \tag{1}$$

In the ES both ROH* as well as RO^{-*} can return to the ground state by emitting a fluorescence photon. The emission of the deprotonated form is shifted to longer wavelengths compared to the acid form. Therefore, both species are observable by fluorescence methods. The transition wavelengths of the photoacid and the base can be used to calculate the pK_a^* value by use of the Förster cycle (Figure 1), given that the pK_a in the ground state is known. If that is not the case, only the increase of acidity upon excitation, ΔpK_a, can be determined (equation (2)).

$$\Delta pK_a = pK_a - pK_a^* = \frac{E_{ROH} - E_{RO^-}}{kT ln(10)} \tag{2}$$

In equation (2), k is the Boltzmann constant, T the temperature and E_{ROH} and E_{RO^-} the energy of the electronic transition in photoacid and anion, respectively.[20, 21]

In the years after Försters seminal work, it was mainly Weller[22-25] who contributed significantly to developments in this new field of photochemistry. New molecules capable of ESPT were discovered, including alcohols and amines based on naphthalene, pyrene, cyanine or fluorescein. It was also Weller who accounted an intramolecular excited-state proton transfer for the large observed Stokes shift observed in salicylic acid.[26] The term excited-state proton transfer itself was first used by Trieff and Sundheim in 1965,[27] but it was only in the 1980s that ESPT reactions gained more interest in scientific research. Even today this interest is still increasing, reaching a maximum number of articles concerning ESPT reactions in the years 2012 and 2013. The use of modern spectroscopy methods with a better temporal resolution has opened the doorway to directly measure much shorter time constants. Thus, very strong photoacids having proton transfer rate constants even in the femtosecond regime can be investigated today.[28]

In this work, the ESPT behavior of a new series of strong photoacids based on pyrene is described. Starting from the commonly used pyranine molecule (8-hydroxy-1,3,6-pyrenetrisulfonate, HPTS), five new photoacids that only differ in their substituents on the aromatic pyrene core have been synthesized in our research group (Scheme 2).

HPTS: R = -O⁻
HPTA: R = -N(CH₃)₂
   1a: R = -OCH₂CF₃
   1b: R = -OCH(CF₃)₂
   1c: R = -N(CH₃)(OCH₃)
   1d: R = -N((CH₂)₂OCH₃)₂
   1e: R = -N(CH₃)((CH₂)₂OH)

MPTS: R = -O⁻
MPTA: R = -N(CH₃)₂
   2a: R = -OCH₂CF₃
   2b: R = -OCH(CF₃)₂
   2c: R = -N(CH₃)(OCH₃)
   2d: R = -N((CH₂)₂OCH₃)₂
   2e: R = -N(CH₃)((CH₂)₂OH)
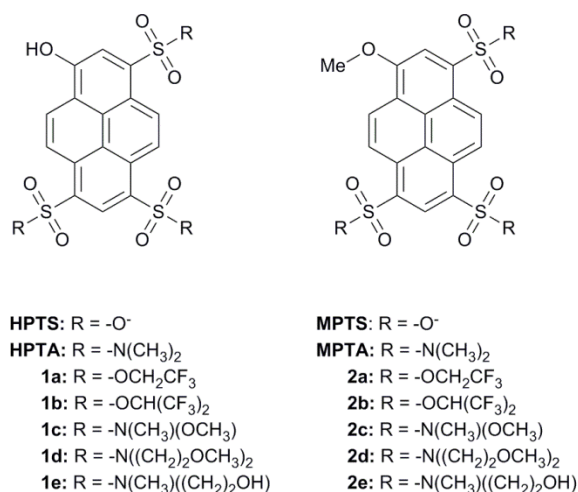
Scheme 2. The photoacids used in this study and their corresponding methylated counterparts.

The use of stationary and time-resolved spectroscopy sheds light onto the underlying mechanism of ESPT in these molecules. The chemical similarity, but yet different photoacidity of the new photoacids is very useful in finding common phenomena proceeding or accompanying the proton transfer step. To ensure the assignment of certain processes to the

proton transfer event, the hydroxyl group of each photoacids has also been modified to yield the methoxy derivatives of the photoacids. The replacement of the proton by a methyl group disables the photoacidity of the molecule, leaving all other properties beside the missing hydrogen bond unchanged. In the following chapters, a short overview over the principles and mechanisms of ESPT reactions is given and the experimental methods used in this study are explained. The results are presented as articles that appeared in peer-reviewed scientific journals.

2.2 Basic principles of excited-state proton transfer

2.2.1 Observation and verification of ESPT

Excited-state proton transfer is a phenomenon that is nowadays widely known to occur in many hydroxyaryl compounds. The combination of the aromatic ring system and the attached hydroxyl group sets gives all the preconditions for an increased excited-state acidity compared to the ground state. The pK_a values of most simple aromatic alcohols are in the range of p$K_a \approx$ 7-10.[29-31] Upon electronic excitation, their pK_a values drop by 5-10 units, turning them into medium or very strong acids in the excited-state (ES). The extent of this acidity increase, i.e. the strength of a photoacid, can easily be modified by varying the substituents on the aromatic core (see chapter 2.2.3). The reason for the ongoing and still increasing interest in the photoacidity phenomenon has its origin in the possibility to create "protons on demand" at a specific point in time and position. By using short laser pulses, the photoacid reaches the ES in a few femtoseconds and transfers the acidic proton to a suitable acceptor in its environment with a specific rate constant k_{prot}. This rate constant depends on the photoacidity of the molecule as well as the acceptor and the solvent used. The investigation of suchlike systems offers the possibility to analyze the hydrogen-bonding behavior under specifically set preconditions.

The basic concepts and steps of ESPT reactions have often been reviewed in the last 20 years.[21, 32-35] Nevertheless, there is still some debate going on how to correctly describe different scenarios (see also Chapter 2.3). A general indication of the occurrence of an ESPT reaction can be seen in the steady-state absorption and fluorescence spectra of photoacids (Figure 2). Whereas only a single band can be seen in the absorption spectra of the neutral species ROH, the resulting emission spectrum consists of two different bands, indicating the existence of two different species in the excited state (Figure 2(a)).
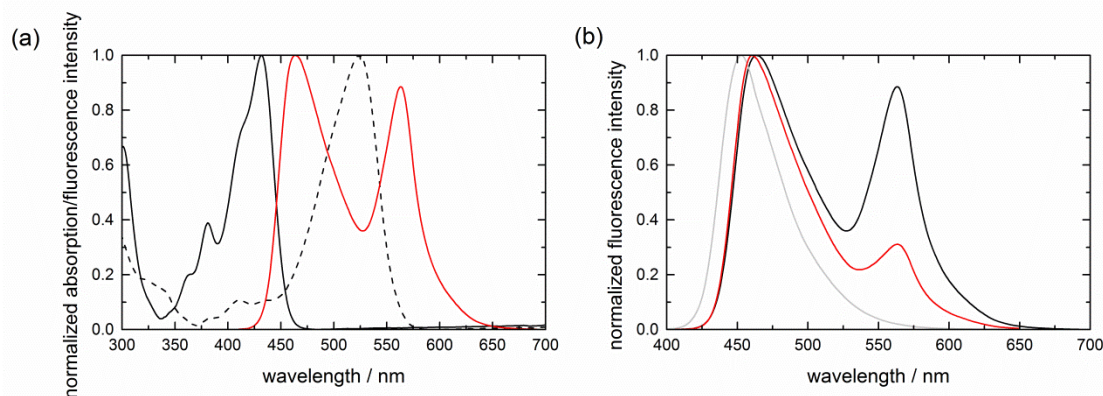
Figure 2. (a) Absorption spectrum of **1c** in ethanol without (black dashed line) and with addition of trifluoroacetic acid (black solid line). The red line shows the emission spectrum in the acidified solution. (b) Comparison of the emission of **1c** in acidified ethanol (black) and in deuterated ethanol (red) with its methylated counterpart **2c** (gray).

The explanation of this was first given by Förster[17] and is visualized using Figure 2 and equation (3).

$$ROH \rightarrow ROH^* \rightleftharpoons RO^{-*} + H^+ \qquad\qquad (3)$$
$$\downarrow k_0 \qquad \downarrow k_0'$$

In the ground state, only the protonated ROH form of the photoacid is present, depending on the solvent conditions. As can be deciphered in Figure 2, in some cases the solution needs to be slightly acidified to ensure a complete shift to the ROH species. In the ES, due to the increased acidity, the photoacid dissociates into the anionic, excited RO^{-*} molecule and a proton. Both ROH^* and RO^{-*} are fluorescent, but at different transition wavelengths, which simplifies the analysis of the reaction. The anion is shifted bathochromically compared to the free photoacid, owing to better resonance stabilization of the product of the photoreaction,[22] which lowers the energy of the $n \rightarrow \pi^*$ transition, as defined by Kasha.[36] Nowadays, it is known that in most photoacids, e.g. those based on pyrenol or naphthol, the lowest electronic transition is of a $\pi \rightarrow \pi^*$ type, with a significant contribution of the $n \rightarrow \pi^*$ transition that transfers charge from the oxygen of the hydroxyl group.[35] However, usually the classification of transitions according to Platt's notation[37] is more suitable and therefore used in the discussion of aromatic molecules (see also chapter 2.3.2).[38-40]

Further proof of ESPT being responsible for the observations seen in Figure 2(a) is achieved by using the methoxy derivative of the molecule under discussion.[41, 42] The much higher activation energy to split the oxygen-carbon bond compared to the oxygen-hydrogen bond[43, 44] suppresses the protolytic equilibrium in equation (3). Consequently, the observation of a single emission band in the methoxy derivative compared to the free photoacid as shown in

Figure 2(b) is a direct proof of the protolytic equilibrium in the ES.[42, 45] In Figure 2(b) is also shown the emission spectra of a photoacid in deuterated ethanol, which serves as another indicator of the ESPT reaction of equation (3). The change from hydrogen to deuterium in the solvent alcohol function induces a corresponding H-D exchange on the OH group of the photoacid, increasing the activation energy of dissociation. This larger activation energy for k_{deprot} – while the back-reaction rate constant k_{prot} is less influenced – shifts the protolytic equilibrium to the ROH form. Thus, both the fluorescence intensity ratio $\frac{I_{RO^-}}{I_{ROH}}$ and the proton transfer rate constant k_{deprot} are lowered, which is known as kinetic isotope effect (KIE).[46-48] The strength of the KIE in different photoacids was in the focus of many studies concerning the mechanisms of ESPT reactions,[49, 50] and the debate still continues.[51-54]

A final tool to validate an ES-reaction is the measurement of the time-dependent fluorescence intensity. The decay of a photoacid which undergoes an ES deprotonation is expected to undergo a complex decay, induced by the different processes that can occur after photoexcitation (see also chapter 2.3). On the other hand, observation of the RO^{-*} fluorescence should be characterized by a rise time. This is due to the measurement of fluorescence photons of a species that first has to be formed in the ES with the rate constant k_{deprot}. This is indeed observed with all photoacids in ESPT-capable solvents and an example is shown in Figure 3. Contrary to the decay of the photoacid, the methylated photoacids show a monoexponential decay at all emission wavelengths.
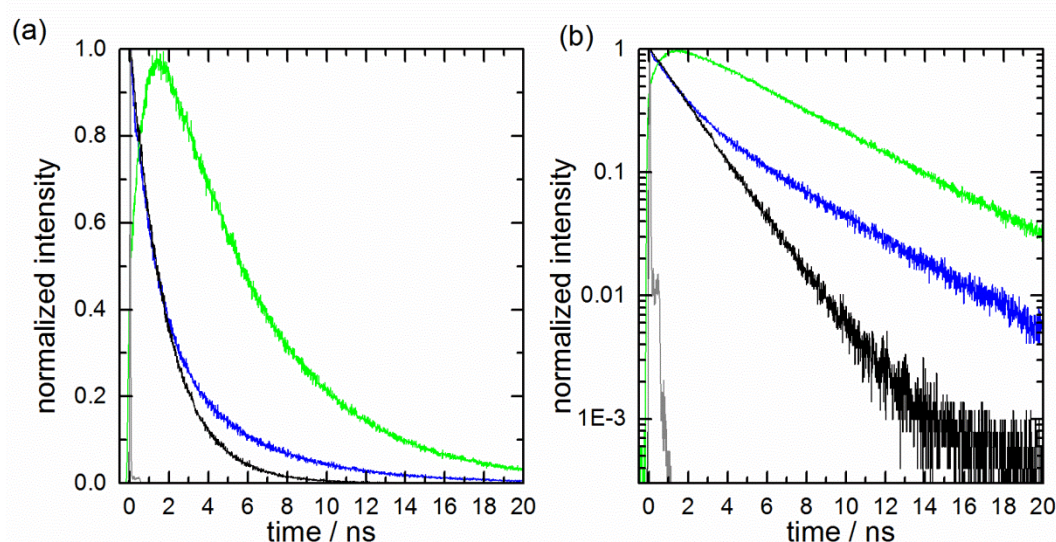
Figure 3. Fluorescence decay of HPTA, measured at $\lambda_{det} = 450$ nm (blue) and 570 nm (green), on a linear (a) and semilogarithmic (b) scale. The decay of MPTA is shown in black as a comparison; the IRF is displayed in gray.

The observation of ESPT is always linked to having a suitable proton acceptor in proximity of the photoacid. The acceptor is most often a polar solvent, e.g. water, methanol or DMSO,[28, 55-66] but proton transfer to Brönstedt bases[67] like acetate or carboxylates is also investigated intensively.[68-78] Due to its unique ability to stabilize a proton, water is the most prominent and important medium concerning ESPT reactions to solvents. Moreover, it is the only solvent that enables ESPT of weak photoacids to a solvent. Only photoacids having a negative pK_a^* value are able to transfer the proton to other polar solvents, which are named "super"-photoacids. These molecules offer the possibility to extend the research of proton transfer beyond water as a medium and to study the influence of the solvent. Many studies have been dedicated to the proton transfer behavior in water-methanol mixtures, to understand the differences in their proton accepting capability.[62, 79-82] Furthermore, mixtures of water with aprotic solvents like dioxane or acetonitrile have been investigated.[65, 83-85] Those studies indicate that both the dielectric constant of the solvent, that stabilizes the presence of the negatively charged anion, and the high delocalization of the proton in water are both important for the ease of ESPT in water. The importance of solvent effects, which also play an important role in direct proton transfer reactions to a base, are further discussed in chapter 2.4.

A special case of proton transfer is found, when the proton acceptor is located within the same molecule as the acidic group. Such an excited-state intramolecular proton transfer (ESIPT)[86] has been in the focus of many studies as it serves as a special case of the general form of ESPT.[87-90] Due to the fixed location of the groups towards each other, proton transfer is usually easier and therefore very fast. Furthermore, tunneling is known to occur in many ESIPT reactions.[86] Although ESIPT reactions served well in the investigation of ESPT mechanism,[89, 91-93] in the following parts, this work will focus on ESPT-to-solvent reactions.

2.2.2 Photoacidity

All of the methods above validate the existence of an ESPT reaction. One of the most important characteristics of a photoacid after the validation is the identification of its photoacidity strength, i.e. the determination of its pK_a^* value. The simplest way to estimate this value is the use of the Förster cycle (Figure 1 and equation (2)). Application of the Förster cycle is only strictly valid when the system reaches equilibrium during the lifetime of the ES.[40] This is not the case if quenching reactions compete with the radiative decay of the excited state. Furthermore, the use of the Förster cycle requires the entropy of protonation to be the same in the ground and excited state, as well as the exact energy of the 0-0 electronic transition.[34] In solution, the accurate determination of the 0-0 transition energy of the photoacid is not straightforward and several approaches have been analyzed.[94] The method recommended and usually applied is using the average of the transition energies as measured in absorption and emission. Both base and photoacid have to be fluorescent to apply this method, but this precondition is usually fulfilled by all photoacids under discussion in this work.

A more experimental approach to determine the pK_a^* value is the method of fluorescence titration.[95-97] Here, the fluorescence intensities of photoacid and corresponding base are monitored over a range of pH values (Figure 4(a)). From the infliction point of such curves, the pK_a^* value can be extracted. The method is expected to be more accurate in the determination of ES acidities, given a constant quantum yield and good solubility over the pH range of interest. The robustness of the titration method can further be improved by using a ratiometric approach of fluorescence intensities.[98, 99] By dividing both intensity values and plotting their ratios, the sensitivity towards a constant quantum yield and the concentration is reduced (Figure 4(b)).
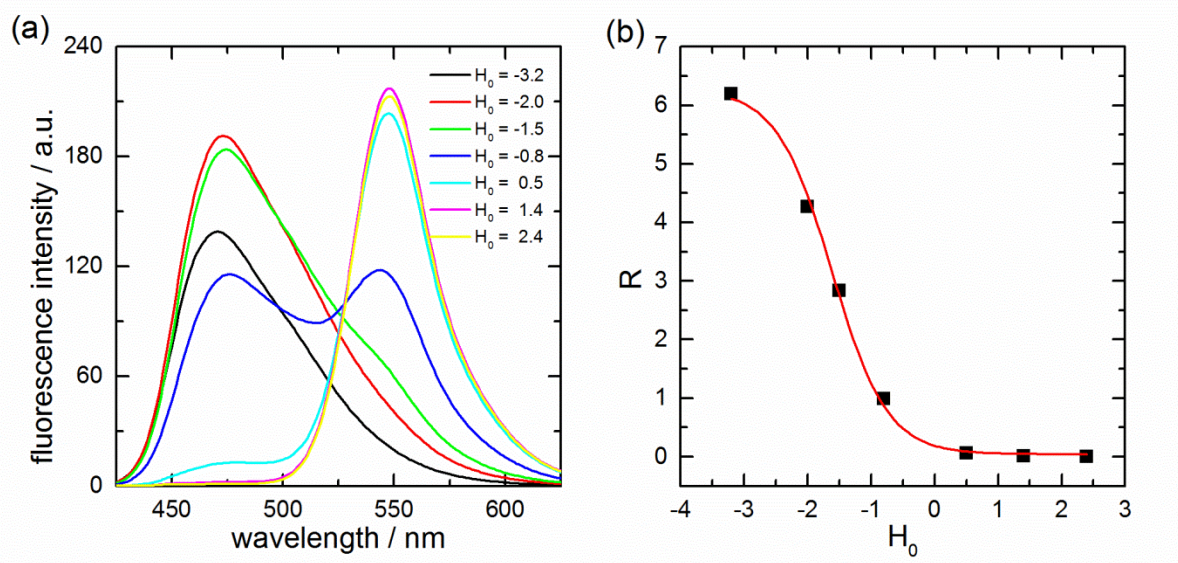
Figure 4. (a) Fluorescence spectra of 1e at different H_0 values. (b) Plot of the corresponding ratio R of fluorescence intensities at the emission wavelengths of ROH and RO⁻.
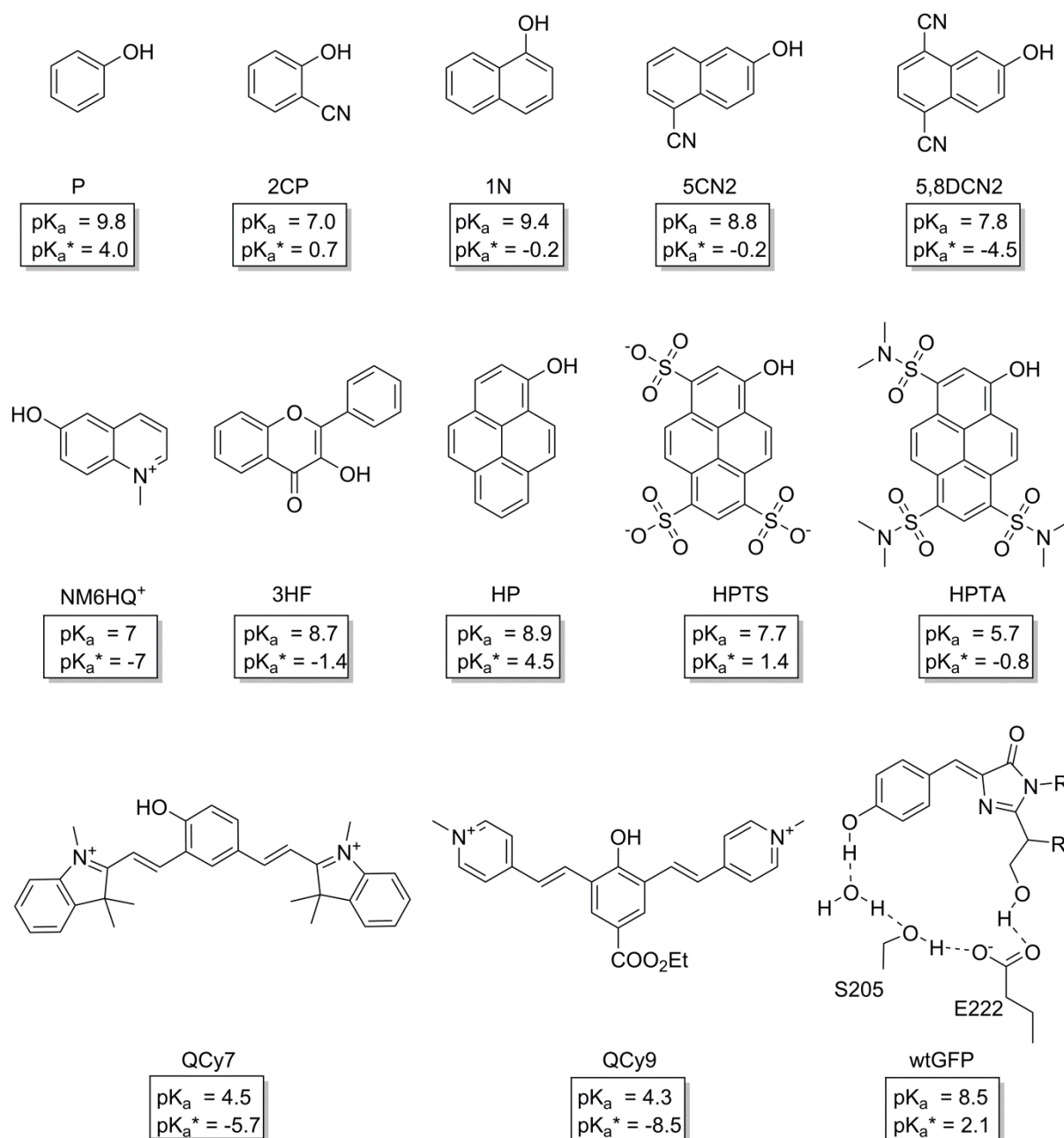
The fluorescence titration method is preferentially applicable with photoacids having a pK_a^* value in the pH range 3-11. For stronger photoacids with pK_a^* value that are negative, so-called "Super"-photoacids,[21, 58, 100] the Hammett acidity scale has to be used (Figure 4(a)).[101, 102] The Hammett acidity function H_0 is a measure of the acidity of very strong acids and an extension of the pH-scale beyond the leveling effect of water. The high acidity and, thus, harsh conditions in such solutions can complicate the analysis of these mixtures, inducing quenching reactions in some photoacids. Quenching of photoacid fluorescence is an additional pathway that can occur in a reaction scheme such as in (3) and has been observed especially in 1-naphthol.[103-106] Given the fact that quenching reactions might occur, the best possibility to determine pK_a^* values is a correct kinetic analysis, calculating by using the rate constants k_{deprot} and k_{prot} (Equation (4)).[32, 40, 107]

$$pK_a^* = -\log\left(\frac{k_{deprot}^*}{k_{prot}^*}\right) \tag{4}$$

The usefulness of the kinetic approach is limited to cases in which the correct modelling of the reaction is used. The different models that are used in description of ESPT reactions are discussed in Chapter 2.3. Using an inaccurate model or not well-behaving photoacids with complicated time-dependent decays usually results in a large discrepancy between pK_a^* values estimated with the Förster cycle and the experimental ones.[40] It should also be mentioned here that computational methods nowadays are getting more and more accurate and pK_a^* values can be computed theoretically with a rather good precision.[78, 108-110]

2.2.3 Photoacids

As mentioned before, the chemical structure of most photoacids consists of an aromatic system with an attached protolytic functional group. Most often, an alcoholic function is used and investigated, but also photoacids bearing a protonated amine group (NX_3H^+) are well-known. Some examples of commonly used (hydroxylic) photoacids are shown in Scheme 3.

P	2CP	1N	5CN2	5,8DCN2
pK_a = 9.8 pK_a^* = 4.0	pK_a = 7.0 pK_a^* = 0.7	pK_a = 9.4 pK_a^* = -0.2	pK_a = 8.8 pK_a^* = -0.2	pK_a = 7.8 pK_a^* = -4.5

NM6HQ$^+$	3HF	HP	HPTS	HPTA
pK_a = 7 pK_a^* = -7	pK_a = 8.7 pK_a^* = -1.4	pK_a = 8.9 pK_a^* = 4.5	pK_a = 7.7 pK_a^* = 1.4	pK_a = 5.7 pK_a^* = -0.8

QCy7	QCy9	wtGFP
pK_a = 4.5 pK_a^* = -5.7	pK_a = 4.3 pK_a^* = -8.5	pK_a = 8.5 pK_a^* = 2.1

Scheme 3. Aromatic alcohols that are known and well investigated as photoacids and their acidity constants: phenol (P),[111, 112] 2-cyano-phenol (2CP),[113] 1-naphthol (1N),[103, 114] 5-cyano-2-naphthol (5CN2),[95] 5,8-dicyano-2-naphthol (5,8CN2),[113] N-methyl-6-hydroxyquinolinium (NM6HQ$^+$),[100, 115] 3-hydroxyflavone (3HF),[116, 117] 1-hydroxypyrene (HP),[118] 8-hydroxypyrene-1,3,6-trisulfonate (HPTS),[119] 8-hydroxy-N,N,N,N,N,N-hexamethylpyrene-1,3,6-trisulfonamide (HPTA),[30] quinone-cyanine-7 (QCy7),[120] phenol-carboxyether dipicolinium cyanine (QCy9),[61] and wild-type green fluorescent protein chromophore (wtGFP)[121].

Most of them are small organic molecules; however, a chromophore capable of ESPT can also be found in larger molecules. As an example, the chromophore of the Green Fluorescent Protein (GFP) transfers a proton to nearby amino acids in the ES,[122-125] and also other proteins and biomolecules are known for ESPT reactions.[126, 127] A more special case is the artificial combination of a small ESPT capable chromophore with a larger (bio-)chemical structure. These systems offer the possibility to investigate the influence of the direct environment of a photoacid. Studies have shown that HPTS can transfer a proton to the Human Serum albumin (HSA) protein[128] or cyclodextrin[128, 129]. Another example that is also relevant to study proton transfer events in cells is the inclusion of a photoacid in micelles or membranes.[85, 130-132]

Generally, photoacids can be classified by multiple criteria. They can differ in molecular size, photoacidity strength, absorption and emission wavelength, charge, polarity and/or chemical functionality. Thus, a wide variety of molecules is at hand and a suitable photoacids for any scientific question related to proton transfer may be found. The smallest molecule with ESPT capability is phenol, which is also one of the weakest photoacids. Due to its small molecular size, its absorption and emission wavelengths are also small and located in the UV wavelength region. An extension of the aromatic system to naphthols or pyrene is accompanied with a bathochromic shift. All of these molecules may be grouped as uncharged photoacids. Charged photoacids usually contain an aromatic nitrogen cation unit, e.g. pyridinium (QCy9, NM6HQ$^+$). In general, they have lower pK_a^* values, but a kinetic analysis is more complicated because of the anisotropic charge distribution in the deprotonated form and additional coulombic interactions of the counteranion with the proton.[133] Another member of the group of charged photoacids is HPTS, which is unique among the other molecules of this group because of its effective negative sum charge of -4 in the anion form. Therefore, this highly charged molecule served as a paradigm for the observation of the phenomenon of *geminate recombination* (Chapter 2.3).[119] It should be mentioned here, that all photoacids based on an amino group as proton donor also belong to the group of cationic photoacids. After protonation of the amine function, they usually become a strong photoacid, at least compared to their hydroxylic analogue.[134] In their neutral form on the other hand, they represent weak photoacids and barely transfer a proton at all.

Beside the structure of the molecules, also their ground- and excited-state acidity constants are given in Scheme 3. It is evident that, based on the chemical structure, these pK_a and pK_a^* values are quite different. The stabilization of the negative charge on the photoproduct, the

corresponding base, is one of the main factors that governs the acidity in the ES.[35] The better the resonance stabilization, the higher is the acidity. A general observation is that in most photoacids, e.g. 2-naphthol and HPTS, the negative charge of the oxygen is partly transferred to the ring system, a process named as *intramolecular charge transfer* (ICT).[22, 29, 35] This ICT on the photoacid side has been used as the explanation for ES acidity. However, it has been found out both theoretically[29, 135] and experimentally[74], that the ICT effect is much stronger on the anion side. Until today, no satisfying reasoning that is applicable to all photoacids has been given to explain the exact processes that lead to ESPT.[35, 40, 136] Some of the mechanisms given in the literature are summarized in chapter 2.3.

For the same reasons as outlined above, electron withdrawing substituents on the aromatic system further stabilize the ICT state and, hence increase the ES acidity.[95, 107, 137] As can be deciphered in Scheme 3, introducing a cyano group in ortho position of the weak photoacid phenol lowers both pK_a and pK_a^* values by about 3 units.[113] Despite this finding, the substituent effect is usually not the same in GS and ES. The important factor is the (re)localization of the negative charge, i.e. on which atoms of the molecule it increases upon excitation. Thus, as an example, the effect of cyano-substituents on position 5 and 8 of 2-naphthol (Scheme 3) is stronger in the ES. The reason for this is that these are the positions to which the negative charge from the oxygen atom is transferred to upon excitation.[135] A similar observation can be found upon sulfonation of HP, leading to the HPTS molecule. Whereas the pK_a value only decreases by one, the pK_a^* value drops by approximately 3 units. The electron distribution on several photoacids and the influence of substituent position has been investigated both theoretically and experimentally in the past decade.[29, 38, 113, 135, 138]

The stronger acidity of HPTA compared to HPTS is due to the much better electron-withdrawing strength of sulfonamides. A quantification of these inductive (and mesomeric) effects is given by the Hammett coefficient.[102] The strongest photoacids are created by the introduction of very strong electron-withdrawing substituents on suitable positions. For many years, 5,8DCN2 has been known as the strongest photoacid.[135, 139] Recently, stronger photoacids have been realized, yet they all contain charged nitrogen substituents.[28, 100] The strongest photoacid known today is QCy9, with an approximated pK_a^* value of -8.5. However, no stronger neutral photoacid than 5,8DCN2 has been synthesized yet. Furthermore, the strong photoacids based on cyanine (QCy7, QCy9) have only a small fluorescence quantum yield due to the lack of a rigid aromatic system.[54]

For the naphthol photoacids, many molecules with different substituents and thus, different photoacidity are available, creating a family of photoacids with chemical similiarity.[51] Such a family is not available for photoacids based on pyrene, where only HP, HPTS and HPTA are known in the literature. Pyrene photoacids that absorb in the visible part of the electromagnetic spectrum have come to our attention as a probe for possible substrates for visualizing the proton transfer on the single-molecule level. To avoid a large background in single-molecule spectroscopy, no UV-light should be used for excitation of the probe. Therefore, photoacids of the naphthol family are not useful for this purpose. However, it was found out that the widely used HPTS molecule does not have a sufficient photostability for single-molecule investigations.[140] On the other hand, the photoacidity of HP is not high enough to effectively observe ESPT in different media. The only molecule at hand for our purpose is HPTA, but this photoacid is strongly apolar and not good soluble in water. This situation promoted us to synthesize new photoacids in order to vary both photoacidity and photostability, as well as solubility. The synthesis of the new photoacids (Scheme 2) and their properties are presented in Chapter 3.1.
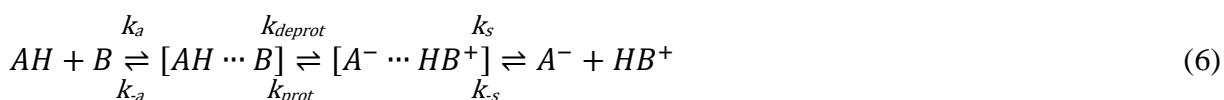
2.3 Mechanisms of proton transfer reactions

2.3.1 Kinetic description

The kinetic description of proton transfer reactions has been under discussion for a very long time. Various models have been used for different variations of this type of reactions, owing to the large variety of proton transfer conditions. It is widely accepted today that photoacidity depends on both electronic structure of the molecule and the solvent. For example, Strandjord et al. demonstrated that the ESIPT rate of different 3-hydroxyflavones measured in aprotic solvents decreases when changing to a hydrogen-bonding solvent.[91] The HB to a solvent molecule competes with the intramolecular HB, slowing down the rate of the intramolecular proton transfer.

The relation of the proton transfer rate to the strength of acidity by linear free-energy relationships is usually applied (chapter 2.3.3). The first of this kind of correlations was noted by Brönsted and Petersen, who stated that the rate of deprotonation k_{deprot} and protonation k_{prot} are correlated to the equilibrium constant of an acid catalyst.[141]

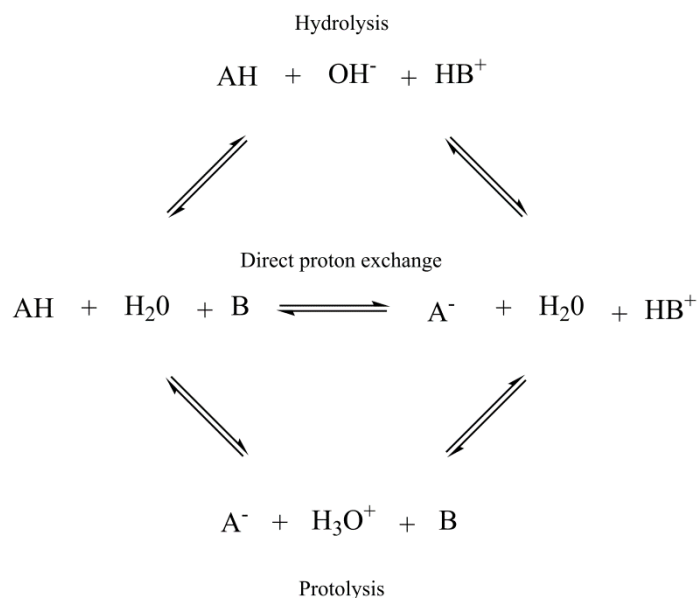$$k_{deprot} = G_{deprot}K_a{}^{\alpha} \quad and \quad k_{prot} = G_{prot}K_a{}^{1-\alpha} \tag{5}$$

The parameter α in equation (5) has the same value for acids of the same type, whereas the values of G are dependent on the substrate and further variables like temperature and solvent. The Brönsted relation was successfully used in a few cases, but is only applicable if the proton transfer step is rate-limiting. Thus, it can only be used over a very small range of acidity values and fails in the case of strong acids, where diffusion of reactants limits the rate constant. This limitation was pointed out by Weller[24, 25] and Eigen[10], who introduced a reaction scheme that allows for diffusion of reactants and products in bimolecular acid-base reactions, equation (6).

$$AH + B \underset{k_{-a}}{\overset{k_a}{\rightleftharpoons}} [AH \cdots B] \underset{k_{prot}}{\overset{k_{deprot}}{\rightleftharpoons}} [A^- \cdots HB^+] \underset{k_{-s}}{\overset{k_s}{\rightleftharpoons}} A^- + HB^+ \tag{6}$$

In the Eigen-Weller scheme, the proton transfer step is preceded by the association of the acid AH and the base B, to form an encounter complex. After the proton is transferred to the base in the encounter complex, the molecules separate by diffusive motion and may eventually recombine again. In 2003, the groups of Pines and Nibbering could show by using fs-IR spectroscopy that this model has to be refined.[70] The formation of the "loose" encounter complex is followed by a "tight" complex, in which the proton is transferred along the hydrogen bond. The proton transfer step in the tight complex of the investigated HPTS-

acetate system occurs then within hundreds of femtoseconds.[70] Using smaller base concentrations, the effective proton transfer rate is lowered to about 6 ps due to solvent reorganization and is even slower when diffusion limited.[142] These authors could also show that the three different proton transfer mechanisms – direct, hydrolysis and protolysis – as discussed by Eigen[10] (Scheme 4) needs to be refined.[69]

Hydrolysis

$$AH \quad + \quad OH^- \quad + \quad HB^+$$

Direct proton exchange

$$AH \quad + \quad H_2O \quad + \quad B \quad \rightleftharpoons \quad A^- \quad + \quad H_2O \quad + \quad HB^+$$

$$A^- \quad + \quad H_3O^+ \quad + \quad B$$

Protolysis

Scheme 4. Reaction scheme for aqueous acid-base reactions as proposed by Eigen.[10]

Hydrolysis, which is the deprotonation of water by the base with subsequent neutralization by the acid, is too slow to occur on the ps time scale. As could be shown,[69] there are many rearrangement steps occurring between the other limits of direct (tight complex) proton transfer and protolysis. Each of these configurations that differ in the amount of solvent separation results in an own proton transfer rate. Recently, the group of Fang could verify this multidimensional reaction coordinate by femtosecond stimulated Raman spectroscopy using HPTS and acetate.[74, 77] In these studies, the vibrational marker bands of the deprotonated HPTS appear faster than the acetic acid peak. The different time constants between 0.3 and 6 ps are indicative of different amounts of intervening water molecules between the photoacid and acetate.

Similarly to the Eigen-Weller reaction scheme for a bimolecular proton transfer reaction in equation (6), the unimolecular acid dissociation in a solvent, e.g. water, can be divided in a 2-step mechanism that involves the formation of an encounter complex, which separates by diffusion (equation (7)).

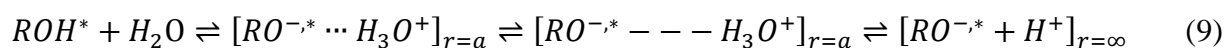$$AH \rightleftharpoons [A^- \cdots H^+] \rightleftharpoons A^- + H^+ \tag{7}$$

The idea of an encounter pair in equation (7) has also found its way into the description of ESPT reactions. In 1988, Agmon, Pines and Huppert introduced a reaction model that was found suitable to describe the nonexponential kinetics found two years before in the time-resolved emission of HPTS.[143, 144] In the reaction scheme of equation (8), the excited photoacid first dissociates into a solvent-stabilized ion pair which separates by diffusion. The dissociation and recombination on contact distance a are described by a backreaction boundary condition.[145, 146] The diffusional motion is modeled using the Debye-Smoluchowski equation (DSE).[119, 147, 148]

$$ROH^* \rightleftharpoons [RO^{-,*} \cdots H^+]_{r=a} \rightleftharpoons [RO^{-,*} + H^+]_{r=\infty} \qquad (8)$$
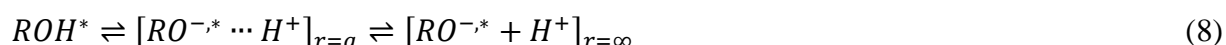
An important outcome of this model is the influence of geminate recombination (GR), the adiabatic recombination process of the proton released by the photoacid with the excited anion. This leads to a power law behavior instead of exponential decay kinetics of the excited photoacid, thus at times longer than the twice the inverse of the PT rate, the decay can be fitted by a $t^{-3/2}$ power law.[149] The GR is of particular importance when a highly negatively charged molecule as HPTS is used, due to the high Coulomb interaction with the proton, that leads to high recombination rates.[81] Many studies using the DSE as a model have been published and the model was refined to also account for nonadiabatic recombination (quenching) and different lifetimes of acid and base forms.[76, 103-106, 150-154] It has been found that geminate quenching leads to a $t^{-1/2}$ power law as observed in 1-naphthol.[103] This power-law shows a reduced dimensionality in comparison to the GR power-law, due to the one-dimensionality of diffusion space for the geminate quenching reaction. Very useful in many of these studies was the SSDP program, developed by Krissinel and Agmon, that solves the DSE with boundary conditions numerically.[155]

Huppert and coworkers, inspired by an internal dynamic study of HPTS by Tran-Thi et al. and theoretical calculations by Ando[156, 157], proposed a different explanation for the intermediate time component found in the HPTS dissociation (chapter 2.3.2). Ando and Hynes showed by *ab initio* calculations that the dissociation of a mineral acid, i.e. HCl and HF, in water involves two steps.[156, 157] First, the acid dissociates to form a contact ion-pair, that becomes solvent separated in a consequent step. Therefore, the new model to explain the ESPT of HPTS in water by Huppert et al. involves three steps as shown in equation (9).[158, 159]

$$ROH^* + H_2O \rightleftharpoons [RO^{-,*} \cdots H_3O^+]_{r=a} \rightleftharpoons [RO^{-,*} --- H_3O^+]_{r=a} \rightleftharpoons [RO^{-,*} + H^+]_{r=\infty} \qquad (9)$$

As in the old two-step model (equation (8)), the last diffusional step is described by the DSE and hence, a nonexponential decay of the photoacid is expected. The three-step model, that accounts the intermediate component to be a part of the deprotonation process, has been supported by the group of Fayer. [39] They identified the lowest excited state of HPTS to be of ^1L_a type, which is in disagreement to the state-inversion model proposed by the Hynes group (see chapter 2.3.2). Moreover, visible pump-probe spectroscopy gave further agreement with the results of Huppert.[42] The photophysics of photoacids complicate the analysis of the kinetic of ESPT reactions. Therefore, the strongly investigated internal dynamcis of HPTS and the different ways to interpret these are discussed in the next chapter.

2.3.2 Internal dynamics of photoacids

Although the use of the DSE has proven to be valuable in the analysis of TCSPC traces of HPTS and also some further strong photoacids, it is rather difficult to observe the GR in decays of neutral photoacids. Due to the small Coulomb attraction in these acids, a high signal-to-noise ratio needs to be achieved to verify the non-exponentiality. A further limitation of the reaction scheme in equation (8) was discovered when HPTS was studied with fs-resolved spectroscopy.[160] In the study by Tran-Thi et al. two ultrafast steps with time constants of 150 fs and 2.5 ps were observed before the 87 ps proton transfer step. The shortest time component can be assigned to solvation dynamics after electronic excitation of the acid. The intermediate time component has aroused some controversies as how to interpret this finding. The authors of the study[160] claimed therein and in a following study[38] that it is due to the relaxation into an intermediate state, which has charge transfer character. A tentative model as shown in Figure 5 was proposed that involves the locally excited state (LE) to be of nonpolar character.
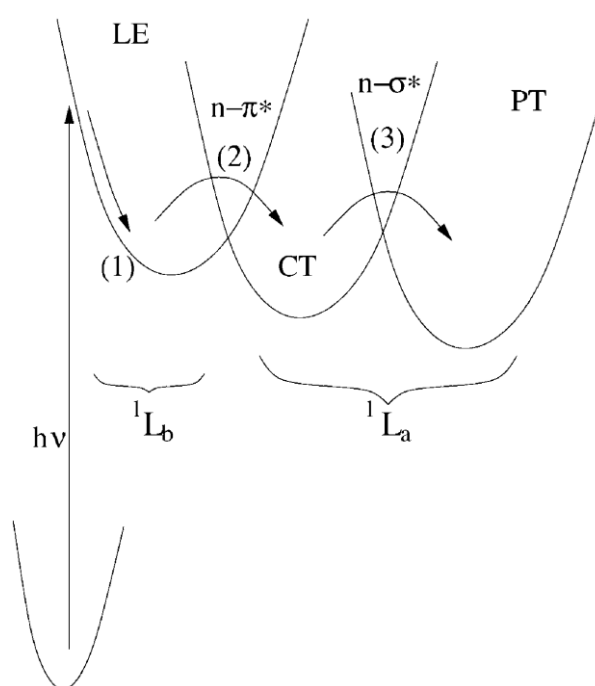
Figure 5. Scheme for the excited-state dynamics of HPTS in water, as proposed by Hynes and coworkers.[136]

The intermediate state has a significant amount of CT character, due to the $n \rightarrow \pi^*$ transition (Chapter 2.2.1) and is the state in which the ESPT occurs. The role of the nonpolar ^1L_b and more polar ^1L_a state has often been discussed in the photochemistry of 1N and 2N.[40, 161, 162] This notation for the description of electronic states of aromatic molecules is based on the work of Platt.[37] Shortly, Platt stated that for cata-condensed aromatic systems, the electronic

states are classified based on the angular moment of the transition and the orientation of the transition dipole moment. The lowest electronic states of these hydrocarbons are named ^1L_a, ^1L_b, ^1B_a and ^1B_b. In this notation, the number 1 symbolizes a singulet state, B and L correspond to an angular momentum of Q=1 and Q=2n+1, respectively, with n as the number of condensed rings. The subscripts a and b refer to the direction of the transition dipole moment along the long axis (through the atoms) or the short axis (through the bonds) of the molecule, respectively.

The photoacids based on pyrene investigated in this work (Scheme 2) also have two close lying excited states. As can be seen in Figure 2 (a) they are visible in the absorption spectra at 430 nm and 380 nm. For HPTS, the excited states are heavily mixed, but the lowest transition is primarily of L_a type, whereas the S_2 can be mainly assigned as L_b.[39] The same is true for the HPTA molecule,[163] and therefore most probably also for all photoacids of this family.

The state inversion model of Hynes (Figure 5) was supported by visible pump-IR-probe spectroscopy by Mohammed et al.[164] However, further studies by the Fayer group have given hints that a slow charge transfer occurs in the stronger, but closely related HPTA photoacid, which may be a general process in all neutral photoacids.[134, 163, 165] It should be mentioned that the model of Figure 5 offers a different explanation of the underlying reason for photoacidity (see also Chapter 2.2.1). The ICT effect as described in this model was thought in earlier studies to occur simultaneously with the excitation,[34] whereas in the $^1L_a/^1L_b$ state inversion picture[166], the inversion happens during the proton transfer step.[136]

The discussion of the different models above and in chapter 2.3.1 shows the complexity of the processes that happen upon electronic excitation of a photoacid. Several years of intense research have not resulted in a congruent and unified view on the ESPT, and may be even impossible due to the different electronic properties of different molecules. Thus, the importance to study a class of chemically related molecules with varying photoacidity becomes clear. The new photoacids shown in Scheme 2 are thus very useful to investigate the mechanisms of ESPT in a closely related family of photoacids. The solvatochromism analysis in Chapter 3.2 indeed proves a charge transfer happening on the photoacid side before any proton transfer occurs.
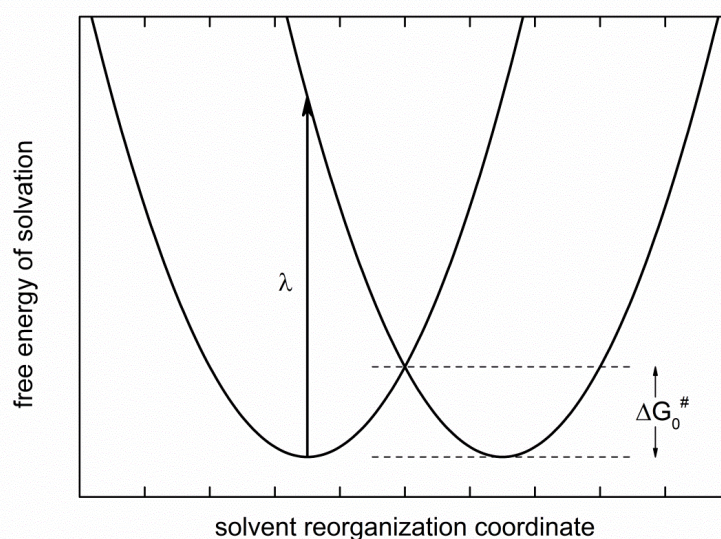
2.3.3 Linear free energy relationships

Most of the approaches outlined in chapter 2.3.1 aim to model all steps occurring during an ESPT reaction. Returning now to the Brönstedt equation (5), a different way to rationalize the ESPT is based on the proton transfer step itself and correlating the intrinsic k_{deprot} used in the models above with the free energy of the reaction, ΔG_0. Due to the well-known correlation of ΔG_0 with the equilibrium constant of a reaction K_{eq} (equation (10)), k_{deprot} is therefore also directly linked to the photoacidity.

$$\Delta G_0 = -RTln(K_{eq}) = RTln(10) \cdot pK_a \tag{10}$$

Eigen used the basic equations of Brönsted and correlated the overall rate constants of proton transfer derived from equation (6) with the acidity difference.[10] Although some acids apply to these equations, many other examples do not show an idealized behavior due to the neglect of any solvent barriers. A large success in the field of linear free energy relationships applied to proton transfer reactions was the introduction of Marcus theory for these reactions.[167-169] Marcus originally developed a theory for nonadiabatic (and therefore, with weak interaction) outer-sphere electron transfer reactions in solution. Marcus stated that these reactions proceed along a solvent coordinate that exhibits an activation energy $\Delta G^{\#}$ (equation (11)), composed of a term he called "solvent reorganization energy λ", equation (12). This reorganization energy is the energy needed for a vertical transition from reactant to product, when the solvent motion would be frozen. It is also equal to four times the intrinsic activation energy of a symmetric transfer, $\Delta G_0^{\#}$, where the total free energy change ΔG_0 following the electron transfer is zero (Figure 6).

$$k_{deprot} = A \cdot exp(-\frac{\Delta G^{\#}}{RT}) \tag{11}$$

$$\Delta G^{\#} = (1 + \frac{\Delta G_0}{\lambda})^2 \cdot \frac{1}{4\lambda} = (1 + \frac{\Delta G_0}{4\Delta G_0^{\#}})^2 \Delta G_0^{\#} \tag{12}$$

Figure 6. Diabatic potential energy curves visualizing the definition of the reorganization energy factor λ.

Marcus theory was successfully applied to proton transfer reactions, even though the precondition of weak overlap does not hold for atom transfer reactions and thus, can only be classified as a semiempirical method.[50, 51, 68, 72, 168, 170-172] Due to the intrinsic restrictions of his theory in PT reactions, Marcus applied also a bond-energy-bond-order (BEBO) model – originally developed by Johnston and Parr[173] – semiempirically to PT along a hydrogen bond, equation (13).[167] In the BEBO model, the reaction coordinate is along the hydrogen bonds and the sum of bond orders of reactant and product is constant and equal to unity.

$$\Delta G^{\#} = \frac{\Delta G_0}{2} + \Delta G_0^{\#} + \frac{\Delta G_0^{\#}}{ln(2)} ln\left(cosh\left(\frac{\Delta G_0 ln(2)}{2\Delta G_0^{\#}}\right)\right) \tag{13}$$

The application of the Marcus theory, equation (12), and the BEBO model of equation (13) yield very similar results in the endothermic branch of reaction free energies. However, whereas Marcus theory predicts a reappearance of activation energy with high reaction exothermy and thus, a decrease in reaction rate, the BEBO model reaches a constant reaction rate for very strong photoacids (Chapter 3.3).[51] The inverted regime has not been verified for ESPT reactions yet. The few examples reported in the literature[174, 175] do not involve proton transfer reactions from the singlet excited state and are only observed in organic media.[35] For example, the "well-behaved" QCy9 molecule with pK_a^* ≈ -8.5 in water does not show an inverted behavior.[28, 61, 120]

Similar to the BEBO model are the structure-reactivity correlations given by Agmon and Levine, equation (14).[176, 177] They use a mixing entropy argument, in which the activation energy is governed by the location of the transition state, expressed as a fractional bond order parameter $n^{\#}$ of the product. A small value for the bond order corresponds to an early transition state along the reaction coordinate, whereas a large value of $n^{\#}$ is observed with endothermic reactions and their late transition state. The Agmon-Levine model was also successfully applied to ESPT reactions.[58, 72, 178]

$$\varDelta G^{\#} = \Delta G_0 - \Delta G_0^{\#} \frac{\ln(n^{\#})}{\ln(2)} \tag{14}$$

A further model based on the same principles as the BEBO method is the intersecting-state model (ISM) introduced by Formoshino and Barandas.[179, 180] It is based on two diabatic "dressed" Morse potentials that represent the reactant and product states and accounts for the effect of both species on each other. Instead of the assumption of constant bond order as in the BEBO model, the ISM method introduces the difference of the minima of both states (see Figure 6) as the most important parameter in proton transfer reactions. The ISM has been applied successfully to ESPT reactions of naphthols.[181]

All of the models mentioned above – although they served well in correlating PT reaction rates with the reaction free energy – basically arise from relatively crude assumptions (e.g. weak electronic coupling, which is usually not fulfilled if covalent bonds are involved), as pointed out by Kiefer and Hynes.[182, 183] These authors introduced a nonlinear free energy correlation for adiabatic proton transfer reaction, which is based on a rigorous quantum mechanical treatment of the proton vibration. In this treatment the quantum proton is viewed to undergo a proton transfer reaction in a solvent reaction coordinate, in which solvent reorganization is reasoned for the activation barrier. It turned out that the strictly analytical treatment yields a result that is only slightly different to the empirical Marcus equation. Thus, although Marcus theory is based on crude assumptions and $\Delta G_0^{\#}$ is basically a numerical fit parameter, the results obtained out of it are very reasonable.[182, 183] The theory was further developed to rationalize kinetic isotope effects and it was shown that inclusion of higher vibronic levels in the theory delays the appearance of the inverted region.[49, 184]

An important difference of the Kiefer and Hynes treatment to the Marcus theory is that the PT in this view is not a classical "over-the-barrier" mechanism as in the other models. The quantum description of the proton in the adiabatic limit reasons the PT resulting from the

vibrational zero point energy at the transition state (in the solvent coordinate) lying over the energy barrier (Figure 7).
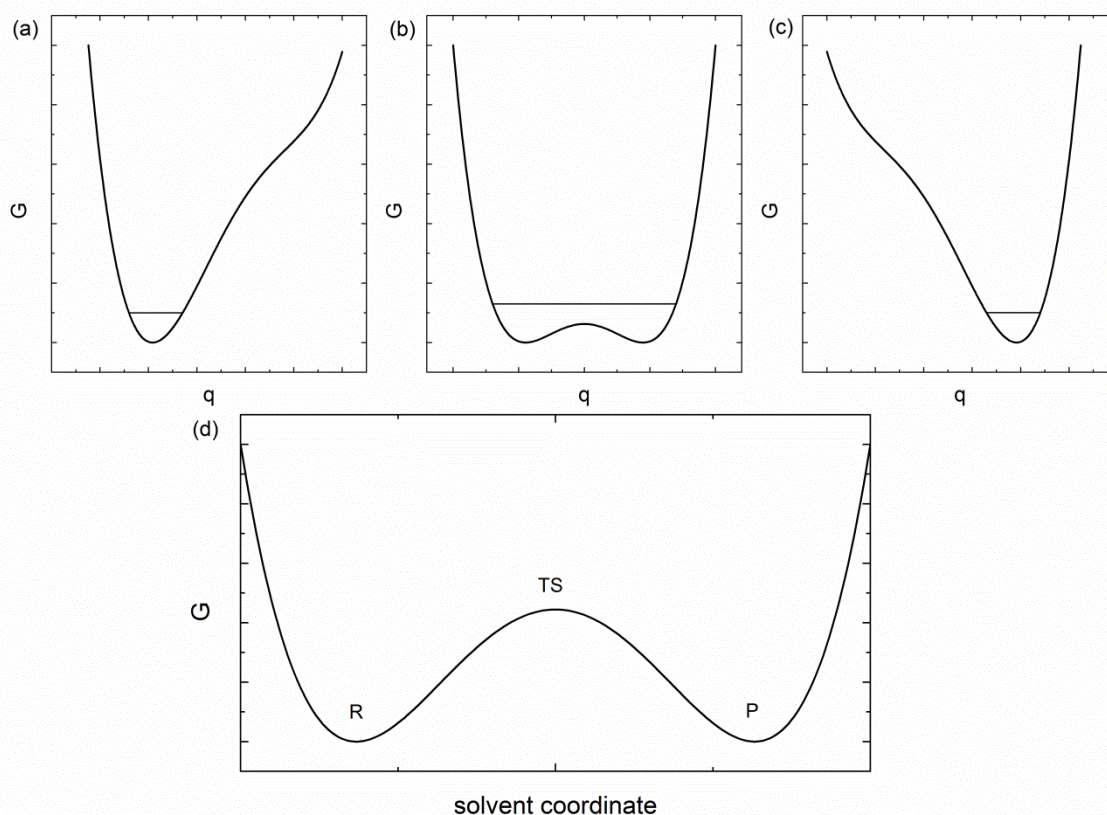
Figure 7. Free energy curves versus proton position q for fixed proton donor-acceptor separation Q and at (a) the reactant, (b) transition state and (c) product state solvent configurations. In each case, the ground-state proton vibrational energy level is indicated. (d) Free energy of the PT system, with the proton quantized in its vibrational ground state, versus solvent reaction coordinate. The solvent coordinate critical points corresponding to the proton potentials in panels (a)-(c) are indicated.[adapted from[182]]

This limitation cannot hold true if the heavy atom distance in the PT pair is increased, and thus lowering the interaction and, correspondingly, increasing the barrier in the proton coordinate q. In this case, which they named nonadiabatic proton transfer regime, the PT can only happen by tunneling.[71, 185-188] The proton transfer at the nonadiabatic reaction limit was investigated experimentally,[162, 174, 175, 189] and intermediate cases were found, showing a transition between nonadiabatic and adiabatic PT at different temperatures.[190, 191] The PT rate can be expressed in the nonadiabatic limit by equation (15), in which C_{AB} is the proton coupling in the diabatic states (Figure 8).[188]

$$k_{PT} = \frac{2\pi}{\hbar} |C_{AB}|^2 \frac{1}{\sqrt{4\pi\lambda RT}} exp(-\frac{\Delta G^{\#}}{RT}) \tag{15}$$
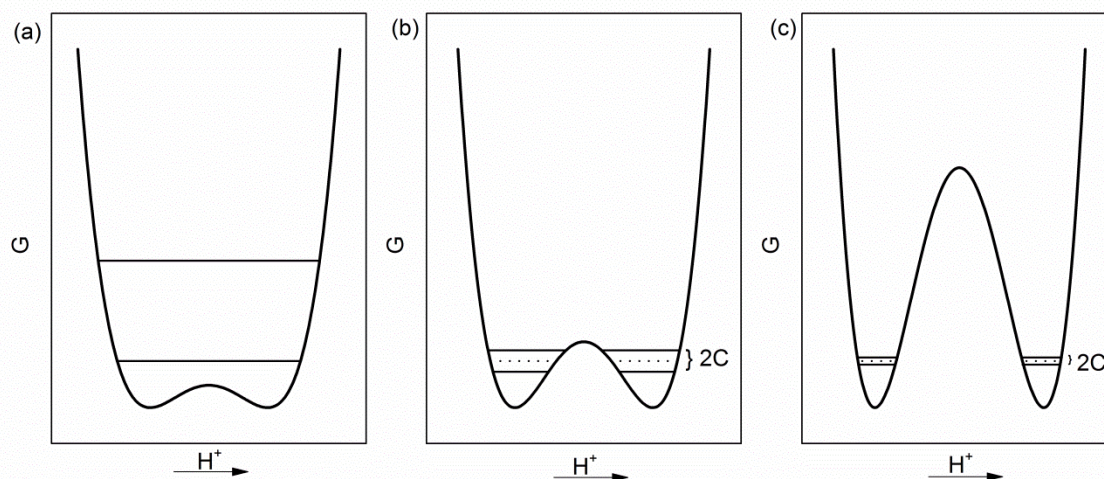
Figure 8. Variation of proton potentials, at the reaction transition state, with increasing H-bond coordinate, going from (a) to (c). Solid line: both the ground and first excited proton vibrational levels. Dotted lines in (b) and (c): the diabatic proton vibrational levels for each well.[adapted from[188]]

Equation (15) has the form of a transition-state-theory reaction rate, due to the fact that the reaction coordinate is the solvent. However, the PT in this limit is governed by tunneling and the activation energy is isotope dependent, due to the zero point energy and quantum nature of the proton.

It is clear from the above considerations, that the solvent plays a crucial role in ESPT reactions. Changing the solvent can even transform a reaction from the adiabatic to the nonadiabatic limit. Therefore careful attention has to be given to solvent effects, which will be in the focus of the next chapter.

2.4 Solvatochromic scales

2.4.1 Solvent scales based on physical models

The importance of solvent effects on the properties of molecules in the condensed phase is known in chemistry for a long time.[192] The solvent molecules form a continuum medium around the solute, which influences its electronic distribution. Furthermore, specific interactions play a significant role if the solvent or solute is protic and its structure contains heteroatoms with lone electron pairs, which are able to accept a hydrogen bond, or vice versa. Many studies aimed at the understanding of these solvent-solute interactions and their influence on reaction rates, chemical equilibrium or spectral shifts. Some of the earliest ways to describe solvent effects were focused on the polarity of the solvent. Solvent polarity itself is a very complex property and very difficult to account for on a quantitative basis.[192] Physical constants as the dielectric constant ε_r, the refractive index n or the dipole moment of a solute molecule were used more or less successfully, as specific interactions are neglected in this kind of treatment. Up to date there is no general theory based on physical properties and rigorous mathematical treatment that allows predicting reaction rates or equilibrium constants of reactions in different solvents.

In this section, only one example that has proven to be useful in the context of this work is to be mentioned. Based on the work of Liptay to yield a correlation between absorption maxima in different solvents,[193] an equation that correlates the Stokes shift Δv of a fluorophore with the change of its permanent dipole moment upon electronic excitation $\Delta\mu$ was developed.[194] Its name, Lippert-Mataga equation (16), accounts also for the contributions of Lippert[195] and Mataga[196].

$$hc\Delta v = \frac{2|\mu_e - \mu_g|^2}{4\pi\varepsilon_0 a^3}\left[\frac{\varepsilon_r - 1}{2\varepsilon_r + 1} - \frac{n^2 - 1}{2n^2 + 1}\right] = \frac{2|\mu_e - \mu_g|^2}{4\pi\varepsilon_0 a^3}\Delta f \qquad (16)$$

The solvent dependence in equation (16) is based on dielectric constant and refractive index of the solvent. The main source of error is the accurate determination of the solute molecular volume. The derivation of the Lippert-Mataga equation neglects all terms describing the polarizability of the solvent, which was taken account of in the rigorous treatment of Liptay.[192, 193] The Lippert-Mataga equation has been used to determine the change of the dipole moment of a fluorophore upon excitation.[84, 197]

2.4.2 Empirical one-parameter solvent scales

The relative failure of the description of solvent effects with physical constants led to the use of empirical solvent polarity functions. Many empirical solvatochromic scales have been developed to describe the effects upon solvation.[192] These solvent scales are used as linear-free-energy relationships, to correlate kinetics, thermodynamics and spectroscopy of a reaction series with solvent properties. This systematic is similar to the description of substituent effects by Hammett coefficients[101] or reagent effects as done by Brönsted for acid catalysis[141] (Chapter 2.3). The reasoning behind this can be grasped if the solvent is regarded as a "loose" substituent that influences the electronic properties of the probe in a similar matter as a covalently linked substituent.[192]

Solvatochromic scales can be roughly divided in two groups: the first group uses only one generalized solvent parameter to classify the solvent and correlate physical parameters with it. The other set of solvatochromic scales are based on a multiparameter approach to distinguish between specific and non-specific solvent-solute interactions. This section will focus on the solvent scales obtained from spectroscopic data as compared to scales obtained from kinetic and thermodynamic data. Examples for solvent scales based on equilibrium measurements are Gutmann's donor number (DN),[198] describing Lewis basicity of the solvent, or the Hansch-Leo partition coefficient $P_{o/w}$ as a hydrophobicity measure[199]. Winstein's Y-scale[200] as an example of a solvent polarity parameter based on a kinetic property may be mentioned here as well. Spectroscopic properties are usually obtained with greater precision and variety than kinetic or thermodynamic data, and are thus, better suited for linear free-energy correlations. Kosower and coworkers were the first to report a spectroscopic "Hammett scale", based on the absorption spectrum of a chromophore with different substituents.[201] They observed a bathochromic shift of the CT band of a pyridinium compound with electron-withdrawing substituents. In a similar way, a hypsochromic band shift of a similar compound ((I), Scheme 5) with increasing solvent polarity was used to introduce a solvent polarity scale, known as Kosower Z scale.[202]

$$Z \equiv h \cdot c \cdot N_A \cdot \tilde{v} \tag{17}$$

Solvents with increasing polarity stabilize the zwitterionic ground state much more than the excited state, that is more of neutral character, and thus, increase the energy difference between GS and ES. Hence, the more polar a solvent, the larger is its Z value according to equation (17).
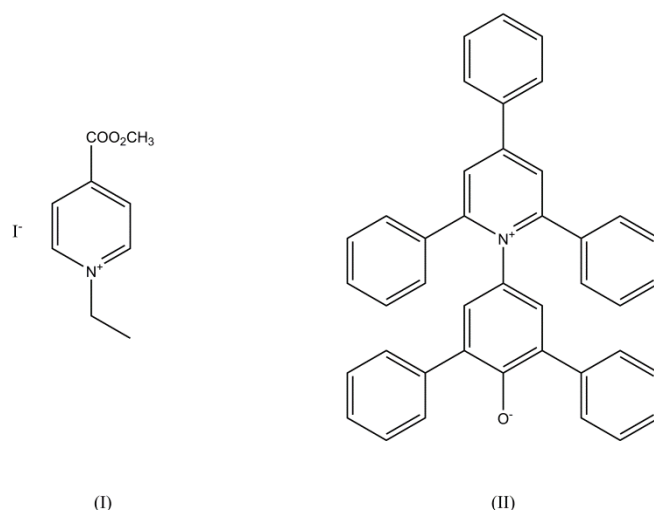
Scheme 5. Solvatochromic dyes to establish the Kosower Z scale (I) and the $E_T(30)$ scale (II).

An alternative empirical solvent polarity scale was introduced by Dimroth and Reichardt, the $E_T(30)$ scale.[203, 204] Similar to the Kosower scale, $E_T(30)$ values are based on the absorption maximum of a solvatochromic dye, equation (17). For this scale, the longest $\pi \rightarrow \pi^*$ absorption band of the most solvatochromic dye known, pyridinium-N-phenoxide betaine (II), is used. The advantage of the $E_T(30)$ scale compared to the Z-scale is the absorption wavelength in the visible part and the stronger solvatochromism of this dye, which makes it a more sensitive reference compound. It has been found more suitable to use a normalized solvent scale, due to the dimensions of kcal/mol for both scales. $E_T(30)$ values were chosen to normalize using tetramethylsilane (TMS) and water, equation (18).[205]

$$E_T^N = \frac{E_T(solvent) - E_T(TMS)}{E_T(TMS) - E_T(solvent)}$$
(18)

The $E_T(30)$ scale was found to describe solvent polarity effects, as well as being sensitive to solvents donating a hydrogen bond. The sensitivity to hydrogen-bond donating solvents and Lewis acids is due to the localized charge on the phenolic oxygen, whereas the positive charge on the pyridinium unit is delocalized, rendering the molecule insensitive to Lewis bases (Scheme 5). An important aspect, if solvatochromism is investigated in solvent mixtures, can be deciphered in analysis of solvent mixtures of dye (II). Already the addition of a small amount of polar solvent to an apolar solvent leads to a large band shift, which is due to preferential solvation of the dye.[206]

2.4.3 Empirical multi-parameter solvent scales

One parameter solvent scales as, e.g. the Kosower and the ET_{30} scale were found suitable to describe polarity effects, but fail if the molecule under investigation is able to form hydrogen-bonds with the solvent. In that case, multiparameter approaches have proven to give more insights into the solvatochromic behavior. Important multiparameter scales are those introduced by Kamlet and Taft[207-210] (equation (19)) and, more recently, by Catalán[211-214], equation (20).

$$v_i = v_{0,i} + a_i \cdot \alpha + b_i \cdot \beta + p_i \cdot \pi^* \qquad (19)$$

$$v_i = v_{0,i} + A_i \cdot SA + B_i \cdot SB + P_i \cdot SdP + Q_i \cdot SP \qquad (20)$$

The solvent parameters for the specific interactions are their acidity (i.e. hydrogen-bond donating ability), expressed by α and SA, respectively, as well as their basicity (or hydrogen-bond accepting ability), expressed by β and SB. The dipolarity and polarizability of the medium, just the single parameter π^* in the Kamlet-Taft relation, is considered in Catalán's equation as the factors SdP and SP, respectively. The specific interactions that are possible in these scales are exemplified in Scheme 6 for the HPTA molecule.
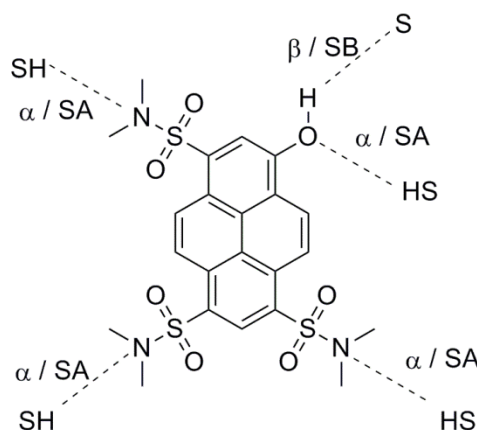

Scheme 6. Possible hydrogen-bond interactions with the HPTA molecule.

All of the solvent parameters in both scales are normalized by arbitrary chosen reference points. As an example, π^* values are defined by the reference values of 0 in cyclohexane and 1 in DMSO. However, due to refined measurements, also values larger than 1 are known. A revised π^* scale has been presented by Laurence.[215] By using special conditions the three- and four-parameter correlations can be simplified. If only nonprotic solvents are used, the α (or SA) dependence in equation (19) (or (20), respectively) vanishes. On the other hand, if the solute does not donate a hydrogen-bond, β (or SB) can be eliminated of the correlation. A

special way of simplifying these equations offers the differential solvatochromism.[41] A solute bearing a hydroxyl group as only HB donor may be replaced by a methoxy group and hence, the β-dependence can be eliminated. Similarly, a specific solvent dependence can be assigned to a specific proton, if the solute exhibits further protic sides.

The Kamlet-Taft scale has been employed many times in a solvatochromic analysis of different molecules.[197, 216-222] Furthermore, many studies concerning the ESPT mechanism made use of this correlation.[38, 41, 58, 223-225] A correlation of the ESPT capability with the parameter β has been found. This finding seems reasonable, as the photoacidity may increase with increasing strength of the hydrogen bond formed by the hydroxyl group. However, the results presented in Chapter 3.2 point to a correlation with the parameter π^* only, at least for the pyranine group of photoacids. The solvatochromism of HPTS was found to deviate from this correlation.[41, 226] A possible reasoning thereof implies that the charge separation in the CT step of this molecule is hidden in a solvatochromic analysis due to the three permanent negative charges (Scheme 7).

HPTA
neutral substituents

HPTS
anionic substituents
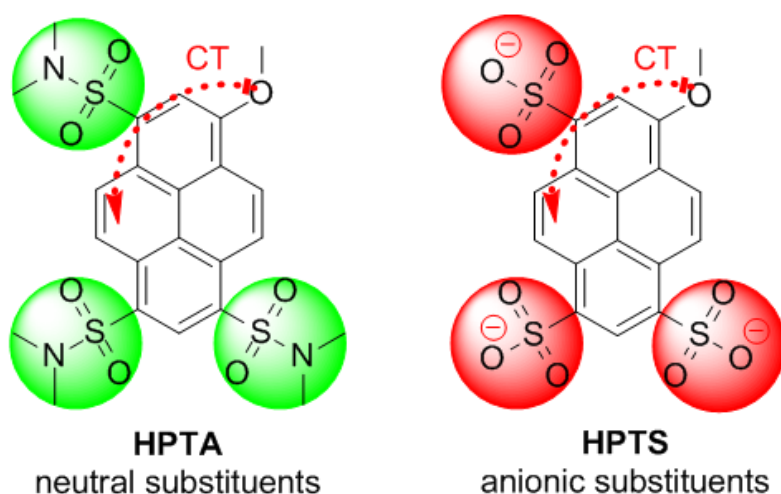
Scheme 7. The charge transfer step in HPTS cannot be seen in a π^* dependence due to the shielding of the sulfonate groups.

3 Publications of the results

1) *Highly Photostable "Super"-Photoacids for Ultrasensitive Fluorescence Spectroscopy*; B. Finkler, C. Spies, M. Vester, F. Walte, K. Omlor, I. Riemann, M. Zimmer, F. Stracke, M. Gerhards, G. Jung, *Photochem. Photobiol. Sci.*, 2014, **13 (3)**, 548-562.

2) *Solvatochromism of of pyranine-derived photoacids*; C. Spies, B. Finkler, N. Acar, G. Jung, *Phys. Chem. Chem. Phys.*, 2013, **15**, 19893-19905.

3) *Solvent Dependence of Excited-State Proton Transfer from Pyranine-derived Photoacids*; C. Spies, S. Shomer, B. Finkler, D. Pines, E. Pines, D. Huppert, G. Jung, *Phys. Chem. Chem. Phys.*, 2014, DOI: 10.1039/C3CP55292F.

Highly Photostable "Super"-Photoacids for Ultrasensitive Fluorescence Spectroscopy

Björn Finkler[a], Christian Spies[a], Michael Vester[a], Frederick Walte[a], Kathrin Omlor[a], Iris Riemann[b], Manuel Zimmer[c], Frank Stracke[b], Markus Gerhards[c], Gregor Jung[a*]

The photoacid 8-hydroxypyren-1,3,6-trisulfonic acid (HPTS, pyranine) is a widely used model compound for the examination of excited state proton transfer (ESPT). We synthesized five "super"-photoacids with varying hydrophilicity and acidity on the basis of HPTS. By chemical modification of the three sulfonic acid substituents, the photoacidity is enhanced by up to more than five logarithmic units from pK_a* ≈ 1.4 to ~ -3.9 for the most acidic compound. As a result, nearly quantitative ESPT in DMSO can be observed. The novel photoacids were characterized by steady-state and time-resolved fluorescence techniques showing distinctively red shifted spectra compared to HPTS while maintaining a high quantum yield near 90%. Photostability of the compounds was checked by fluorescence correlation spectroscopy (FCS) and found to be adequately high for ultrasensitive fluorescence spectroscopy. The described photoacids present a valuable palette for a wide range of applications, especially when the properties of HPTS, i.e. highly charged, low photostability and only moderate excited state acidity, are limiting.

Introduction

Many aromatic alcohols like phenol-[1–5] and naphthol-derivatives[5–23] undergo an increase of acidity upon electronic excitation, facilitating an excited state proton transfer (ESPT) to the solvent or an appropriate base molecule. Among these, the pyrenol derivative HPTS (8-Hydroxypyren-1,3,6-trisulfonic acid, pyranine) is one of the most investigated photoacids.[5,24–46] Theodor Förster was the first to describe ESPT of HPTS to water more than 60 years ago,[24,25] but this molecule is still under investigation.[40,41] One important reason for the ongoing interest in this dye is that the use of short excitation pulses to trigger proton transfer reactions allows for monitoring the molecular events which follow the dissociation of the acid (ROH) by time-resolved fluorescence spectroscopy.[28,30,31,33,35,39,42–45] Besides the examination of proton transfer, HPTS has been used for various biological applications due to its high water solubility[47] and low toxicity. Hence, a fluorogenic substrate for different enzymes was developed by modification of the hydroxyl group of the molecule.[48] Having a pK_a within the physiological range, the chromophore has been suggested for measuring of cytoplasmic and acidic organelle pH in different cell types.[49] However, the lack of cell permeability due to of the negatively charged sulfonic acid substituents yet limits the use of HPTS as intracellular indicator.[50]

The pK_a of HPTS drops from 7.3[49] to 1.4 upon excitation (pK_a*).[27] The latter value indicates a rather moderate photoacidity in the excited state. 8-Hydroxypyren-*N,N,N',N',N'',N''*-hexamethyl-1,3,6-trisulfonamide (HPTA, **3f**) is a more recently introduced derivative of HPTS which also exhibits photoacidic properties.[5,44,45,51,52] The substitution of the three sulfonic acid groups of HPTS with more electron-withdrawing dimethyl sulfonamide groups results in an increased aqueous acidity in the ground state (pK_a = 5.6) and even more in the excited state (pK_a* ~ -0.8). Suchlike molecules with pK_a* < 0 are referred to as "super"-photoacids.[15,53] The high acidity in the excited state induces ESPT to non-aqueous solvents like methanol, dimethylformamide or dimethyl sulfoxide,[8] which in turn enables the investigation of solvent effects on the process.[18] Furthermore, proton transfer in organic solvents is characterized by simpler kinetics than in water.[9] In fact, HPTA is hardly soluble in water.[52]

In the past years, significant efforts were undertaken to develop even stronger photoacids. Tolbert and co-workers modified and intensively studied 1- and 2-naphthol derivatives with several electron-withdrawing functional groups to enhance the photoacidity of the dye.[8,9,14] The most acidic compound among these is 5,8-dicyano-2-naphthol (DCN2) with a pK_a* = -4.5 calculated by use of the Förster cycle.[9] DCN2 has become an elaborately studied and valuable compound for examination of ESPT.[19–22,53] However, the examination of proton transfer to water is challenging, because DCN2 is nearly insoluble in this solvent as well.[54]

This limitation was overcome with N-methyl-6-hydroxyquinolinium (NM6HQ$^+$) iodide.[53,55–57] Analysis of the time-resolved data of its ESPT in water revealed a pK_a* of -7. This high photoacidity was attributed to an intramolecular charge transfer from the hydroxylate group to the positively charged pyridinium ring.[53] In another recent publication, quinone cyanine photoacids were reported.[54,58,59] The aqueous pKa* of these dyes

was estimated to be ~ -6 and below. Compared to the ground state pKa of ~ 4.5, electronic excitation results in an increase by at least 10 orders of magnitude. For both classes of molecules, deprotonation rate constants above 1012 s-1 were reported, which are the highest values recorded up to date. Nevertheless, the positive charge present in both classes of photoacids aggravates the analysis of ESPT kinetics, since the typical description, by the spherically symmetric Debye-Smoluchowski equation for reversibility cannot be applied.53,54 In addition, quantum yield of the RO*- form of the cyanine based dyes hardly reaches 10%.54 Finally, virtually all systems on the basis of naphthol and hydroxyquinoline are excited by UV- or near UV-light. As a consequence Raman scattering, photodestruction and background fluorescence are intensified, which complicates the investigation of ESPT by ultrasensitive spectroscopic methods and their application for live-cell imaging.

The above mentioned shortcomings of existing photoacids kindled our interest in the searchfor the search of new "super"-photoacids for various purposes. In the present manuscript, we describe several highly photostable, bright "super"-photoacids on the basis of pyranine. Sulfonic acid groups of HPTS were converted by use of amines and alcohols to more electron-withdrawing sulfonamide and sulfonic ester groups. All described molecules exhibit a higher photoacidity than HPTS and partially even higher than HPTA. Two of these derivatives are well soluble in water. The lack of the negatively charged substituents in contrast to HPTS enables the use of the more lipophilic compounds as a fluorescent probe for intracellular use *in vivo*. Photostability, as verified by fluorescence correlation spectroscopy (FCS), is comparable to rhodamine 6G.

Results

Scheme 1 displays the overall synthesis of the photoacids starting from HPTS. Compounds **3d** and **3e** were conceived as highly hydrophilic probes. To achieve this aim, we used substituents with structural elements which are known for good water solubility

while maintaining the similar electron withdrawing capability as the dimethyl sulfonamides of HPTA.

The rationale of dyes **3a-c** was to increase photoacidity. Fluorinated alcohols were chosen for the synthesis of **3a** and **3b** due to higher chemical stability of the corresponding sulfonic esters compared to the hydrocarbon analogs.60 The synthesis of **3a-f**, as illustrated in Scheme 1, followed a modified procedure of Singaram *et al.*61 HPTS was converted into 8-acetoxypyrene-1,3,6-trisulfonic acid (**1**) for protection of the hydroxyl group in the following reaction. Subsequently, the sulfonic acid groups of **1** were activated as sulfonyl chloride substituents (**2**) by use of thionyl chloride. Photoacids **3a-f** were obtained from a reaction of **2** with the corresponding alcohols and amines in moderate to good overall yields (62-91%). The complete substitution of the three sulfonic acid groups could be proven by NMR-spectroscopy for all compounds, while the pyrene core itself remained unaltered.

Spectroscopic characterization with absorption and steady-state fluorescence spectroscopy

For spectroscopic characterization, DMSO was chosen as aprotic solvent due to its excellent dissolving properties and because putative ESPT of "super"-photoacids might occur in this medium. Other solvents are discussed in a parallel publication62 and time-resolved data with higher time-resolution will be presented elsewhere.63

In pure DMSO, all compounds dissociate to a large extent without addition of a base, as can be anticipated from the absorption spectra (Figure 1a). A tentative explanation of this high degree of dissociation is that it could originate from the acidity constant in DMSO which is similar to that in water, in combination with the low dye concentration. This effect would not be surprising due to the highly delocalized charge in the anion.64 Also, spurious amounts of water might support the dissiciation.65 The absorption maxima $\lambda_{abs,\ max}$ of anionic compounds 3a-f are found between $\lambda = 554$ and 576 nm (Table 1).
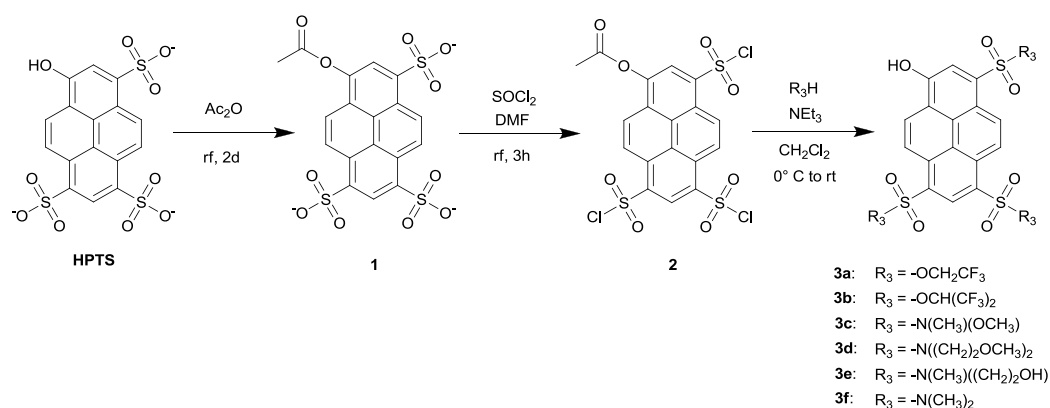
Scheme 1: Synthesis of HPTS-derivatives **3a-f**.
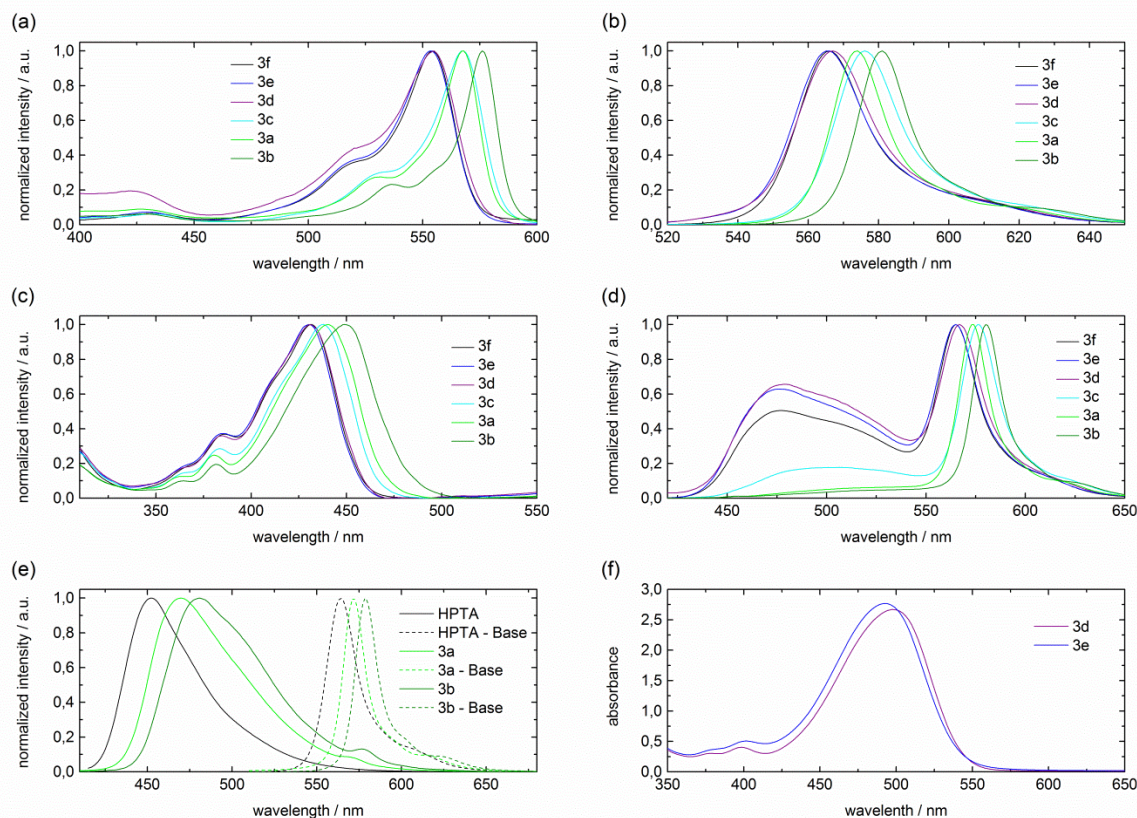
Figure 1: (a) Absorption and (b) emission spectra (λ_{exc} = 500 nm or 520 nm) of the base form of the photoacids. (c) Absorption and (d) emission spectra (λ_{exc} = 400 nm) of the neutral photoacids in DMSO. (e) Emission spectra of the photoacids (solid line, acetone+TFA) and their base forms (dashed, acetone+NaOH). (f) Absorption spectra of two photoacids in water before normalization, showing the excellent water solubility of **3d** (10 mm path length) and **3e** (1 mm path length).

Emission spectra in pure DMSO (Figure 1b) exclusively exhibit fluorescence of the anionic dyes ($\lambda_{em, max}$ = 565-581 nm). Stokes shifts of the anionic species decrease from $\Delta\tilde{v}$ = 380 cm^{-1} (12 nm) for **3e** to $\Delta\tilde{v}$ = 150 cm^{-1} (5 nm) for the sulfonic ester derivative **3b**. Molar absorption coefficients (Table 1) are highest for the sulfonic esters (**3a**, **3b**) and slightly smaller for the sulfonamide derivatives.Molar absorption coefficients (Table 1) are highest for the sulfonic esters (**3a**, **3b**) and slightly smaller for the sulfonamide derivatives. Addition of 3 μL trifluoroacetic acid to DMSO (1 mL) assures a complete protonation of the dyes in the electronic ground state (Figure 1c, 1d). The normalized absorption spectra (Figure 1c) display a shape similar to that previously described for neutral **3f**[5] ($\lambda_{abs, max}$ = 430-449 nm), whereas no absorption of the anionic species is discernible. Absorption spectra of neutral and anionic **3d** and **3e** almost coincide with those of **3f**,[5] whereas absorption bands of **3a-c** are distinctly red shifted. A similar red shift is also present in the fluorescence emission of the excited RO$^-$ form, only the order of the close lying maxima of **3a** and **3c** is reversed.

All corresponding fluorescence emission spectra (Figure 1d) show maxima at λ = 565-581 nm, which coincide with those of the excited base. This finding hints to the occurrence of ESPT to DMSO. A second maximum at higher energies in the spectra of **3c-f** arises from the excited photoacid.[5] While the peak height at $\lambda_{em, max}$ (ROH) is about 50-70% of the anionic emission for **3d-f**, it is just around 20% for compound **3c**. In the spectra of **3a** and **3b** nearly no emission of an excited neutral photoacid is visible, indicating a high efficiency of the ESPT process for these compounds in DMSO. Stokes shifts as the phenomenological difference between absorption of ROH and emission maxima of the conjugated base RO$^-$ lie in the range between $\Delta\tilde{v}$ = 5000 and 5600 cm^{-1} (132-138 nm).

The pure emission of the neutral species can be observed in less polar solvents. Fluorescence emission spectra of **3a**, **3b** and **3f** in acetone are shown in Figure 1e. Interestingly, whereas **3f** shows exclusive emission of the excited neutral species, a second distinct band at higher wavelength is discernible in the spectrum of **3a** and even more **3b**.

Table 1: Spectroscopic properties of **3a-f** in DMSO.

	3a	**3b**	**3c**	**3d**	**3e**	**3f**
$\lambda_{abs, max}$, nm(ROH)	440	449	438	431	430	431
$\lambda_{em, max}$, nm (ROH)	-[a]	-[a]	506	479	477	477
$\lambda_{abs, max}$, nm (RO⁻)	568	576	568	555	554	554
$\lambda_{em, max}$, nm(RO⁻)	574	581	576	567	566	565
Φ_{fl}	0.87[b]	0.91[b]	0.98[b]	0.87[c]	0.95[c]	0.84[c]
$\varepsilon_{abs, max}$ (RO⁻), L mol⁻¹ cm⁻¹	60000	60000	53000	-[d]	35000	37000

[a] could not be determined due to nearly quantitative ESPT in DMSO.

[b] comparative quantum yield; sulforhodamine 101 (Φ_{fl} = 0.95 (EtOH)[70]) and rhodamine 101(Φ_{fl} = 1.00 (EtOH)[71]) used as reference.

[c] comparative quantum yield; rhodamine 6G (Φ_{fl} = 0.94 (EtOH)[72]) and fluorescein (Φ_{fl} = 0.95 (0.1M NaOH)[73]) used as reference.

[d] could not be determined due to hygroscopy of the compound.

The maximum of this peak ($\lambda \approx 570$ nm) coincides with that of the excited RO⁻species in this solvent. Consequently, we attribute this observation to some ESPT of **3a** and **3b** to the solvent acetone.Finally, absorption spectra before normalization demonstrate the solubility of compounds **3d** and **3e** in water (Figure 1f). Both compounds are readily soluble in concentrations > 10^{-4} mol/L, yielding an optical density above 2. From the necessary dilution, we could estimate a saturation concentration of **3e** above 10 mM. This should be adequately high for biological use and for transient absorption measurements in water.[66–69]

Acidity constants

Photoacids are characterized by their acidity constants in ground and excited state. pK_a values of **3c-f** were analyzed in aqueous solution via absorption titration. Absorption spectra of **3e** in buffer solution with various pH values are shown in Figure 2a. An isosbestic point indicates a proper conversion from ROH to RO⁻ with increasing pH. Fluorescence correlation spectroscopy, which provides an alternative access to pK_a at very low concentrations, was used for pK_a determination of the hardly water-soluble sulfonic ester derivatives **3a** and **3b** (see *supporting information* for details).[74] pK_a values are roughly the same within the experimental error for all sulfonamide based photoacids (p$K_a \approx 5.6$), but formal substitution of the sulfonamide by sulfonic ester groups decreases the pK_a by roughly one logarithmic unit (p$K_a \approx 4.4$-4.7).

Fluorescence titration and Förster calculations were used to evaluate the pK_a* of the photoacids **3a-f**. Figure 2b shows absorption and emission spectra of compound **3a** in perchloric acid of different concentration, characterized by their Hammett acidity values H_0.[75,76] At all H_0 values, only the neutral species is present in the ground state. Its absorption is deformed at H_0 = -0.2 presumably due to the formation of non-fluorescent aggregates as a result of reduced solubility at low perchloric acid concentrations, i.e. high water content. For the same reason, fluorescence emission intensity is diminished at low acid concentrations. Nevertheless, with decreasing H_0 values the emission of anionic molecule decreases, since the high proton concentration shifts the dissociation equilibrium towards the fluorescence emission of the excited ROH form. Figure 2c illustrates the fluorescence intensity ratios of acid to base emission for all photoacids. pK_a* values (Table 2) were evaluated according to equation 1.[77]

$$R = R_1 + (R_2 - R_1)\frac{1}{1+10^{pH-pK_a}} \quad (1)$$

In equation 1, R is the fluorescence or absorbance ratio of λ_{max} (ROH) and λ_{max} (RO⁻), whereas R_1 resp. R_2 represent the minimal and maximal ratio values observed at very high and low proton concentrations. Among the sulfonamide based dyes, **3f** seems to be the less acidic compound, whereas **3c** and **3e** are the strongest, which is slightly different to the ordering of the RO⁻/ROH ratios in the steady-state fluorescence spectra in DMSO (Table 2). However, the differences are cancelled in the excited state acidities calculated by use of the Förster cycle. The change of the pK_a value ΔpK_a can be calculated from the fluorescence excitation and emission maxima in aqueous solution according to equation 2. The so determined pK_a* values will be refered to as Förster-pK_a* (see Table 2). With exception of **3a** and **3d**, the Förster-pK_a* values are found to be lower than those calculated from ratiometric titration.
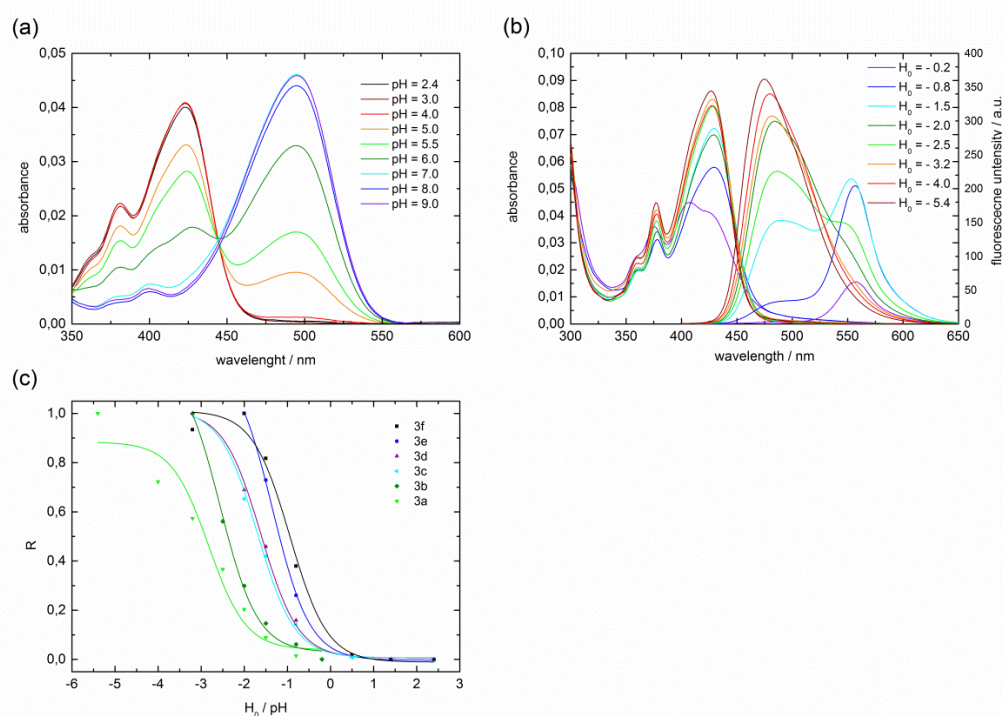
Figure 2: (a) Absorption titration of **3e** in buffer with the acid form absorbing at λ = 423 nm and the base form at λ = 495 nm. (b) Absorption and emission spectra of **3a** in perchloric acid of different concentration. The solubility decreases with higher water content. (c) Fluorescence intensity ratios of acid to base peak signals (λ_{max} see Table 1).

Table 2: pK_a-values; $\lambda_{abs,\ max}$ (H$_2$O) and $\lambda_{em,\ max}$ (H$_2$O) given in nm. Perchloric acid was used for acidification.

	3a		3b		3c		3d		3e		3f	
	RO$^-$	ROH	RO$^-$	ROH	RO$^-$	ROH	RO$^-$	ROH	RO$^-$	ROH	RO$^-$	ROH
$\lambda_{abs,\ max}$	516	426	526	414	509	429	499	427	495	423	494	422
$\lambda_{em,\ max}$	558	480	564	490	555	481	551	478	548	476	547	473
pK_a	4.7[a]		4.4[a]		5.6[b]		5.7[b]		5.6[b]		5.6[b]	
pK_a*[c]	-2.7		-3.9		-1.2		-0.8		-0.9		-1.0	
pK_a*[d]	-2.9		-2.5		-1.0		-1.0		-0.6		-0.3	

[a] determined by FCS.

[b] determined via absorption titration.

[c] determined via Förster cycle.

[d] evaluated by fluorescence titration.

In any case, the sulfonic ester derivatives turned out to be about two logarithmic units more acidic than the sulfonamide based molecules independent of the method.

$$\Delta pK_a = \frac{(h\nu_{ROH} - h\nu_{RO^-})}{kT\ln(10)} \qquad (2)$$

Time-resolved spectroscopy

ESPT of the photoacids to DMSO was studied in more detail by time-correlated single-photon counting (TCSPC). The TCSPC histograms of the excited bases in neat DMSO (Figure 3a) follow a mono-exponential decay. Fluorescence lifetimes for all bases lie between 5.5 and 5.7 ns (see Table 3) indicating that the variation

of the substituents does not greatly affect the fluorescence lifetime of the excited RO$^-$ form in this solvent. A similar value was previously reported for **3f**.[45] In agreement to this long fluorescence lifetime, the fluorescence quantum yield in DMSO is found to be close to 90% or even higher for all excited RO$^-$ species (Table 1).

Both the mono-exponential decay and the high quantum yield indicate that competitive processes to fluorescence are negligible. Furthermore, no distinct triplet population can be found in FCS experiments (see below).

In TFA acidified DMSO (Figure 3b) the fluorescence decay of neutral **3a-f** (λ_{det} = 420-460 nm) follows

complex kinetics, which could not be entirely resolved by our experimental setup (IRF ~ 300 ps). Average decay time constants ($\tau_{\text{fl,avg}}$) are in the range of 2.2-0.4 ns (see Table 3). The fluorescence signals of neutral **3d-f** appear to decay similar, but slower than those of the

further photoacids. Especially **3a** and **3b** exhibit rapid fluorescence decays.
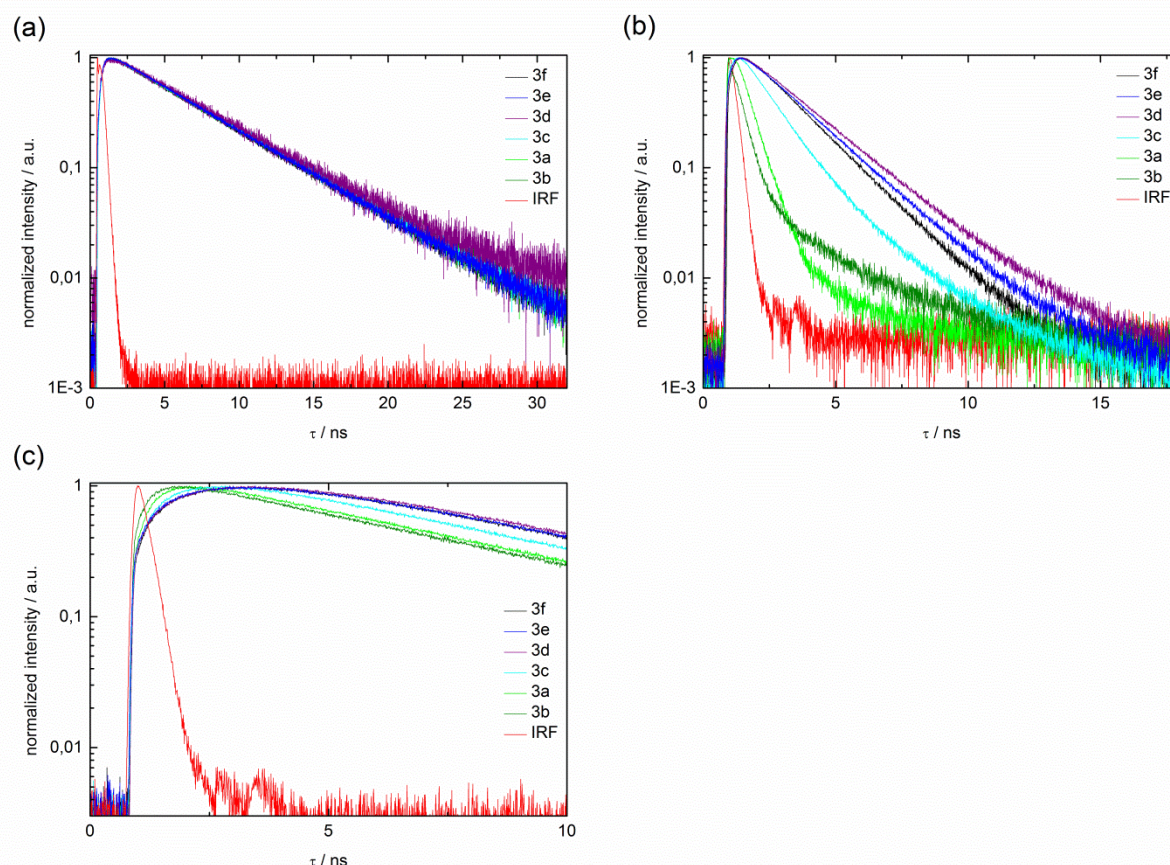
Figure 3: TCSPC-Histograms of the various photoacids: (a) λ_{ex} = 470 nm, λ_{det}= 550-600 nm, DMSO. (b) λ_{ex} = 405 nm λ_{det} = 420-460 nm, DMSO+TFA. (c) λ_{ex} = 405 nm, λ_{det}= 560-610 nm, DMSO+TFA.

Fluorescence decay of the excited acid ROH ($\tau_{\text{fl,ROH}}$) is expected to be determined by the sum of the natural radiative rate constant of the photoacid k_{rad} and the rate constant of the proton transfer in the excited state k_{ESPT} (equation 3).[46] A mono-exponential decay is thus anticipated.

$$\tau_{\text{fl,ROH}} = \frac{1}{k_{\text{rad}} + k_{\text{ESPT}}} \qquad (3)$$

However, the observed fluorescence decay is non-exponential and deviates especially at longer times from purely exponential progression. This indicates that more processes influence the fluorescence lifetime of the ROH form. Aberration from an exponential decay of the ROH* fluorescence has been observed for different photoacids in water and was attributed to arise from a geminate proton recombination process.[19,26,27,46] Currently, experiments are undertaken to explore

whether diffusional processes or recombination in the excited state could be the reason for the unexpected behavior here as well.

At λ_{det} = 560-610 nm, TCSPC histograms of **3a-f** (Figure 3c) are described by two exponentials. The longer time component,
i.e. the decay, agrees with the lifetime of the anionic species determined by the histograms in Figure 3a. The short, rise time component with negative amplitude is attributed to the formation of the excited RO⁻ form caused by ESPT. Short time-components obtained by reconvolution analysis span the range between 1.8 and 0.2 ns and show similar values as the component determined at λ_{det} = 420-460 nm but are slightly smaller. Yet, the average decay time of **3b** at λ_{det} = 420-460 nm obtained by reconvolution fit (τ ~ 0.8 ns) seems to differ from this trend. This constant is about four times longer than the rise time component at λ_{det} = 560-610 nm (τ ~

0.2 ns), which in turn is in good agreement with the excited state acidity of this compound (see discussion). This deviation is attributed to an enhanced detection of background fluorescence due to the low intensity of the ROH emission in the case of this strong photoacid. However, it is assumed that the rise time component of the RO$^-$ form mirrors the same process as the main decay component of the ROH fluorescence. Consequently, these values reflect time component of the proton transfer in the excited state (τ_{ESPT}) (see Table 3).

Table 3: Fluorescence lifetimes of **3a-f**.

|	**3a**	**3b**	**3c**	**3d**	**3e**	**3f**
$\tau_{\text{fl,avg}}$, ns (DMSO, ROH)	0.4	0.8	1.4	2.2	2.0	1.8
τ_{ESPT}, ns (DMSO, RO$^-$)	0.4	0.2	0.9	1.8	1.7	1.6
$\tau_{\text{fl,RO}^-}$, ns (DMSO, RO$^-$)	5.6	5.6	5.7	5.5	5.5	5.5

Photostability

A fundamental factor for usability of a chromophore in ultrasensitive spectroscopy is the resistance to photobleaching. The use of HPTS in such assays is hampered by its low photostability which is assumed to arise from the permanent negative charges.[78,79] Especially for microscopic applications, a good photostability is a key feature. Since all dyes are sufficiently soluble in water for FCS measurements, we determined their relative photostability in aqueous buffer solution (pH = 7.5) by use of this technique.[80] At the employed pH, almost two units above the highest pK_a values, all dyes exist solely in the anionic RO$^-$ form. Furthermore, RO$^-$ is the exclusively emissive form in water and its direct excitation with green light results in a lower background and simplifies the analysis since protonation can be ignored as a competitive source of fluctuations.

Shortly, fluorescence fluctuations arising from molecules into and out of the detection volume are autocorrelated. The longest time component of the autocorrelation decay, hence, results from diffusion through the detection volume. However, any light-driven, irreversible process competing with diffusion, leads to a smaller apparent diffusion time τ_{diff}. The extent, by which τ_{diff} is reduced upon increased excitation intensities, is a measure of the photostability. Equation 4 represents the kinetic description of photobleaching as competitive process to diffusion in analogy to the Stern-Volmer analysis.[80] k_{bl} is the photobleaching rate constant and can be determined by plotting $\tau_{\text{diff}}(0)/\tau_{\text{diff}}(I)$ against the excitation intensity I.

$$\frac{\tau_{\text{diff}}(0)}{\tau_{\text{diff}}(I)} = 1 + k_{\text{bl}} \cdot \tau_{\text{diff}}(0) \cdot I \qquad (4)$$
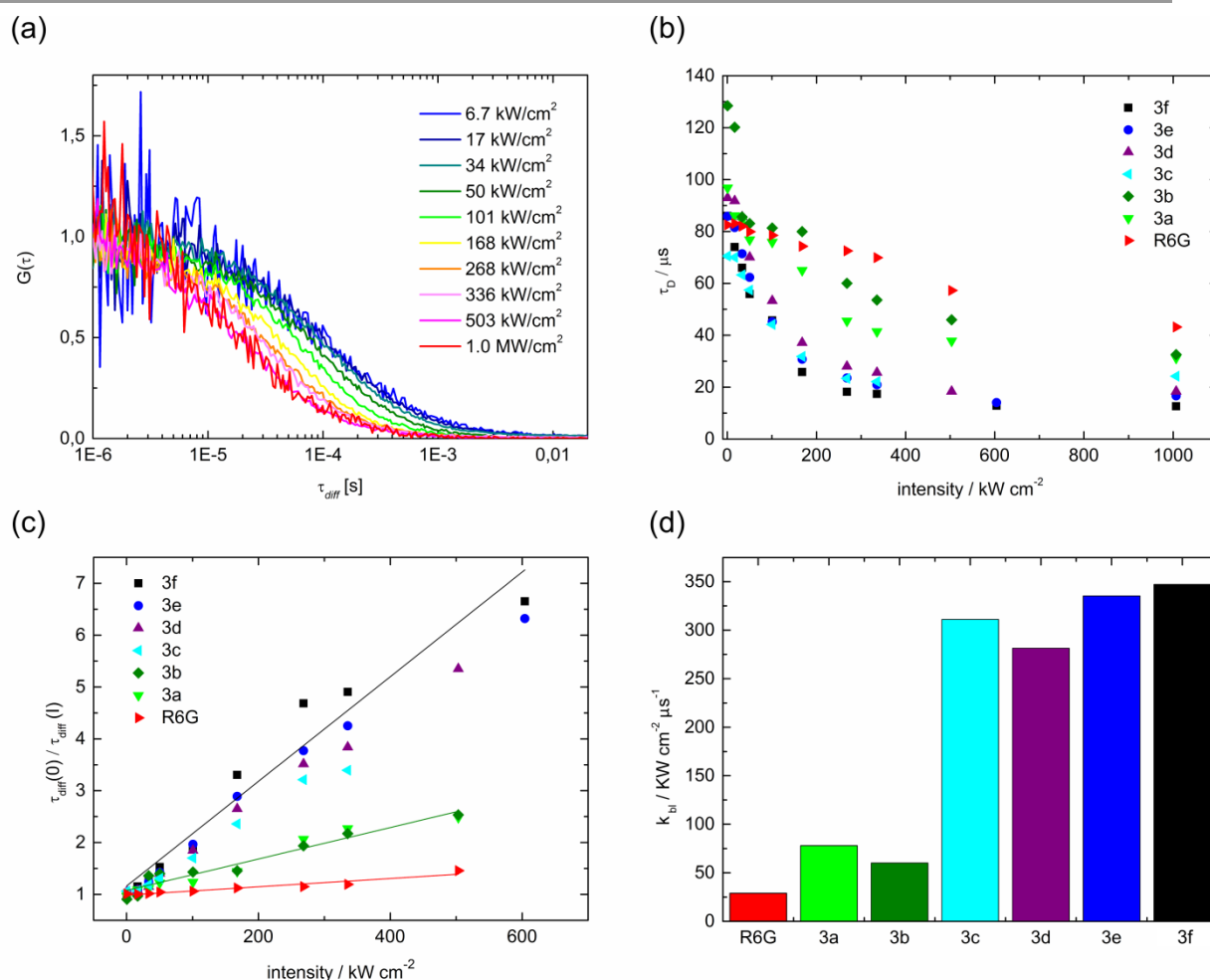
Figure 4: Investigation of the photostabilities of the photoacids in an aqueous medium. (a) Normalized FCS-curves of **3d** at various laser-intensities (λ_{exc} = 488 nm). (b) Measured diffusion times for all photoacids. (c) Stern-Volmer type analysis. (d) Rate constants of photobleaching after correction with the relative excitation cross sections.

All dyes were excited with intensities spanning more than two orders of magnitude. As reference, we selected rhodamine 6G (R6G) which is used for single-molecule experiments and known for its excellent photostability.[81,82] Its excitation and emission maxima beneficially are similar to those of deprotonated **3a-f**. Figure 4a shows the normalized auto-correlation functions of compound **3d** at intensities ranging from 6.7 to 1000 kW cm^{-2}. It turns out that the higher the laser intensity, the shorter τ_{diff}. This behavior is also observed for all other measured dyes (Figure 4b) and obeys the linear form of equation 4. Electronic saturation of all analyzed dyes was calculated to occur above 300 kW cm^{-2}. Accordingly, deviations of the linear relation at high intensities (> 500 kW cm^{-2}) likely result from saturation[80] and were therefore excluded from the analysis. The k_{bl} values shown in Figure 4d were obtained from dividing the slope of Figure 4c by $\tau_{diff}(0)$ and further correction by the varying extinction coefficient at λ = 488 nm. Thus, the photostability of the examined molecules can be unequivocally compared due to the same experimental conditions.

It turns out, that the photostabilities of the fluorinated sulfonic esters are very close to the reference dye R6G. **3a** exhibits a bleaching rate constant k_{bl} less than the triple of R6G, while this value is even more lowered for **3b** being only about twice as high. All sulfonamide derivatives are commonly less photostable. Nevertheless, even the sulfonamide derivatives show sufficient photostability for *in vivo* fluorescence measurements.

Perspectives for biological application

Finally, we also investigated the capability of the photoacids for a potential *live cell* use. As mentioned before, highly negatively charged HPTS cannot penetrate intact cell membranes leading to a negative fluorescence staining (Figure 5a).

Although **3d** and especially **3e** can be dissolved in millimolar concentrations (Figure 1f), incubation for all cultures can be performed at lower concentrations.

Unfortunately, compound **3e** does not cross the membrane of an intact cell, presumably due to the high hydrophilicity. Subsequently, we chose dyes with higher lipophilicity **3a** and **3c** and incubated Hep-G2 cells. Figure 5b-d show multiphoton fluorescence micrographs after treatment of Hep-G2 cells with **3a** and **3c**. The used dyes apparently cross the cell membrane within 20 minutes (**3c**) to 1 hour (**3a**) and accumulate in the cytosol. The accumulation may be due to adsorption of the lipophilic molecules to cellular compounds which are absent in the nucleus. Especially compound **3c** appears appropriate as fluorescence in the cytoplasma can be found within 1 minute after incubation (Figure 5c). A further staining of the nucleus is not observed.
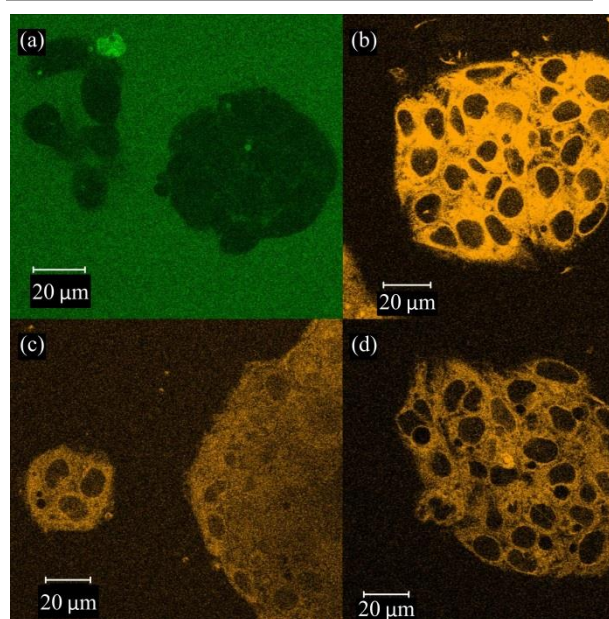
Figure 5: Clusters of Hep-G2 cells (λ_{ex}= 800 nm) incubated with (a) HPTS, λ_{det} = 495-591 nm, after 60 minutes; (b) **3a**, λ_{det} = 495-623 nm, after 60 minutes; (c) **3c**, λ_{det} = 495-591 nm, after 1 minutes and (d) 20 minute.

Discussion

A series of new photoacids, all derived from pyranine as starting material, is presented. They can be divided into two groups, i.e. the sulfonamides and sulfonic esters. The variation of the acidity of the sulfonamide derivatives can be understood by comparing the properties of the substituents. The acidity of the protonated 2-methoxy-N-(2-methoxyethyl)ethanamine and 2-(methylamino)ethanol lies in a similar range as that of dimethylamine (pK_a ~ 9-10).[83–85] Consequently, the electron-withdrawing strength of the corresponding sulfonamides is expected to be similar to that of **3f**. In contrast, the protonated form of N,O-dimethylhydroxylamine shows a pK_a of 4.75,[83] indicating an increased electron withdrawing strength

of the corresponding sulfonamide in relation to the above mentioned amines. An even higher electron-withdrawing strength is anticipated for the sulfonic esters, due to the higher electronegativity of the oxygen atoms of **3a** and **3b** compared to the nitrogen atoms of the sulfonamides **3c-f**. A pK_a of 9.3[86] for 1,1,1,3,3,3-hexafluoro-2-propanol in contrast to pK_a = 12.4 for 2,2,2-trifluoroethanol[86] reveals the reduced charge density of the oxygen atom and hence points to a higher electron-withdrawing strength of the corresponding sulfonic ester. Accordingly, compound **3b** is expected to exhibit the highest acidity of all derivatives, even higher than that of **3a**. Therefore, although the Hammett-coefficients are not known for all substituents, acidity is expected to decrease in the order **3b** > **3a** > **3c** > **3d** ≈ **3e** ≈ **3f**. Actually, the substituents influence the experimental ground state acidity in the anticipated order with exception of **3c**.

The small change in pK_a by only one unit from the esters to the sulfonamides compared to the enhancement of the excited state acidity by more than two orders of magnitude, illustrates the greater impact of the substituents on the excited state properties. This behavior is also observed for substituted 1-naphtols.[17] The tendency of the excited state acidity is established in the computed Förster-pK_a* values. While **3d** and **3e** exhibit the lowest and **3c** the highest acidity of the sulfonamide photoacids, the pK_a* of **3b** was calculated to be the lowest of all compounds. As these values are calculated from spectroscopic data, i.e. Stokes shifts, it is understandable that absorption maxima of the ROH species as well as the emission maxima of RO⁻ largely follow the same ordering. However, specific interactions are analyzed elsewhere.[62]

The ESPT kinetics observed by TCSPC correlate well with the Förster-pK_a values, yielding a good agreement between thermodynamical and kinetic analysis. The acceleration of the fluorescence decay is attributed to the rising efficiency of the ESPT from **3e** to **3b**. The ESPT time constants τ_{ESPT} of **3a** and **3b** are more than twice as small as for the strongest sulfonamide based acid **3c** (0.9 ns), which is half of the ESPT time constant of the other sulfonamide derivatives. Accordingly, the ratio of the emission intensity of the neutral species to that of the corresponding base by excitation of the ROH species is a measure of the ESPT efficiency. While compounds with the most electron-withdrawing substituents **3a** and **3b** show nearly quantitative ESPT in DMSO, **3d** and **3e** which contain less electron withdrawing groups only partly dissociate after excitation.

Besides some minor variations like the different rate constants for the similar sulfonamides **3d-f**, noteworthy deviations from the general tendency derived above can be found. pK_a* values determined by fluorescence titration do not exactly match the ordering of the ROH/RO⁻ ratios observed in the steady-state spectra in

DMSO. Especially the weakly water soluble derivative **3b** points to lower excited state acidities by more than one order of magnitude compared to pK_a^* determined via Förster calculations. In addition, the pK_a^* of **3f** ($pK_a^* \approx -0.3$) is slightly different to previous results[5] and does not fit to the above mentioned ordering. Also, the apparent higher pK_a^* of **3a** in comparison to that of **3b** also contradicts the findings of the steady-state and time-resolved fluorescence spectroscopy in acidic DMSO. The divergence is ascribed to the fact that especially neutral **3b**, and to a lesser extent **3a** as well, is hardly soluble in water, which results in a low absorption and fluorescence intensity. The weak solubility of these two compounds is likely due to the increasing quantity of fluorine atoms in the molecule. Hence, titration experiments are affected by the low solubility of some neutral species as the ratio of the ROH and RO$^-$ form at low pH-values is vague. This hypothesis is supported by the observation that the values of the strongly water-soluble photoacids are distinctly less diverse. Nevertheless, the experimentally determined pK_a^* values serve as a good approximation as a change of the ratio is clearly visible, but the ordering of the excited state acidities determined by Förster calculation is in better agreement with all other spectroscopic observations. Yet, it should be noted that also the Förster-pK_a^* values present an approximation, since changes in the molecular geometry and solvation relaxation are not taken into account.[9,11]

Some more correlations of the Förster-pK_a^* values with other spectroscopic data can be found. The Stokes shift of the bases and also the width of the anionic fluorescence emission band from $\lambda_{FWHM} = 25$ nm for **3d** and **3e** to $\lambda_{FWHM} = 18$ nm for **3b**, are diminished in the same order. Both observations could be qualitatively understood if one takes into account that the excited bases are the conjugated bases to the photoacids. Therefore, their spectroscopic behavior reflects the tendency of the acid in reversed order, i.e. the corresponding base of the strongest photoacid is the less interacting with the surrounding.

It is also worth to note that the photostability follows the trend **3b** > **3a** > sulfonamides. A unified picture, which comprises all mechanisms of photobleaching, is still lacking. Triplet states, higher excited states and/in combination with molecular oxygen are commonly regarded as reason for this degradation process.[80,87,88] It was reported for numerous chromophores that fluorination or trifluoromethylation of the aromatic core leads to an enhanced photostability.[89–93] Yet, the stabilizing effect of core-fluorination and -trifluoromethylation is ascribed mainly to the strong electron withdrawing properties of fluorine substituents.[91] Moreover, there are several examples of chromophores substituted with electron withdrawing cyano groups, that are also characterized by higher photostability compared to the unsubstituted molecule.[94–96] So, the electron withdrawing strength of the substituents could be the explanation for the enhanced photostability of the sulfonate based compounds **3a** and **3b**, and could explain why photoacidity and photostability are related. The fact that a clear and reproducible FCS-trace is observed for each dye can be interpreted as hint for sufficiently high photostability for further single-molecule experiments, especially as no triplet population could be detected by FCS.

Conclusions

We have synthesized a series of five new derivatives of HPTS. The physical- and photophysical properties of the HPTS backbone can be greatly modified to give a palette of photoacids with varying properties. Substitution of the sulfonic acid substituents can increase the excited state acidity up by to ~ 5 logarithmic units. Especially the chemical and photostable sulfonic ester derivatives exhibit almost quantitative ESPT in DMSO. In contrast to HPTS, all compounds lack negative charges and are sufficiently photostable for ultrasensitive fluorescence spectroscopy. All derivatives exhibit high quantum yields. While showing similar photochemical properties as **3f**, compounds **3d** and **3e** exhibit a significant solubility in aqueous media, whereas **3c** is strongly membrane permeable. Various applications in life sciences can be foreseen. Recently, we have addressed the origin of the enhanced photoacidity compared to HPTS in detail by solvatochromic studies.[62] Furthermore, the kinetics of the ESPT are investigated by femtosecond time-resolved spectroscopy and allow for examining its solvent-dependence.[63] Altogether, worthwhile and improved alternatives to HPTS are reported.

Experimental Section

General

8-Hydroxypyrene-1,3,6-trisulfonic acid (purity > 98%) was purchased from Acros Organics. All other reagents and solvents were obtained from Sigma-Aldrich, Merck or Acros Organics and used without further purification. For the chromatographic purification of **3e**, silica gel was washed prior to use with an 8:2 mixture of methylene chloride and methanol and dried in vacuo.

UV/Vis and Fluorescence Spectroscopy

Absorption spectra were recorded with Jasco Spectrophotometer V-650, fluorescence emission and excitation spectra with Jasco Spectrofluorometer FP-6500. Concentrations of the measured solutions were in micromolar range if not otherwise stated.

Time-Correlated Single-Photon Counting

TCSPC measurements were performed with a home-built setup. Excitation was done with pulsed laser diodes (PicoQuant, LDH-P-C-405, λ = 405 nm resp. PicoQuant, LDH-P-C-470, λ = 470 nm; pulse width = 60-120 ps) which were controlled by a diode laser driver unit (PDL 808 MC SEPIA, PicoQuant). A single-photon avalanche detector (PDM 100ct SPAD, Micro Photon Devices) in combination with a photon counting device (PicoHarp 300, PicoQuant) was used for detection. The overall instrumental response function was ~ 300 ps (FWHM). Obtained data were analysed by the SymPhoTime (PicoQuant) and FluoroFit (PicoQuant) software.

Fluorescence Correlation Spectroscopy

FCS measurements were performed using a custom built setup. Continuous-wave lasers (Picarro, Soliton, λ = 488 nm resp. Guided Laser Technologies, Fiber Laser FL546, λ = 546 nm) with a beam diameter of 0.7 mm were used as excitation source. The laser was coupled into an inverted microscope (Axiovert 200, Zeiss) and reflected by a dichroic mirror (495 DRLP resp. 555 DRLP Omega) into a water-immersion objective lens (PlanApo 63x, NA 1.2 WI, Zeiss). The beam was focused into a diffraction limited spot above the cover slide (0.17 ± 0.01 mm, Assistent). A drop of nanomolar dye solution placed on top of the cover slip served as sample. Emitted fluorescence was collected by the same objective, passed the dichroic mirror and focused by the tube lens onto a 50 μm pinhole. After filtering through a band pass filter (HQ 585/50 or HQ 590/70, AHF Analysentechnik), the light was split into two beams by 50:50 beam splitter. Photons were detected by two avalanche photodiodes (SPCM-14-AQR, Perkin-Elmer Optoelectronics). The output of these modules was cross-correlated by a hardware correlator (FLEX 02-01D/C, Correlator.com). Laser power was varied from 20 μW to 3 mW, corresponding to an intensity of 6.7-1000 kW/cm^2. Correlation data was analysed according to the 2D model consistent with Ref [80].

Two-photon-excitation laser scanning microscopy

Laser scanning microscopy was performed with a confocal laser microscope (LSM510 META, Zeiss; Objective: Plan-Neofluar 40x/1.3, Zeiss). Excitation was performed with a Ti:Sa laser (Chameleon XR, Coherent) operating at λ = 800 nm.

Cell culture

HepG2 cells were grown in IBIDI μ-dishes (Ø 35 mm ibiTreat 33327), RPMI 1640 medium with 10% FCS (Gibco, w/o phenol red) and incubated at 37°C, 5% CO_2 for 1-2 days. Before the experiment the cells were washed with PBS and new medium was added.

FTIR-spectroscopy

FTIR measurements were performed with a Bruker Vertex 80v spectrometer using a home-built liquid cell with a path length of 1 cm. This cell contains a stainless steel housing, PTFE spacer, a viton gasket and CaF_2-windows. In case of **3e**, a home-built liquid cell with a variable pathlength has been used, in case of **3e** a space of 75 μm was chosen. The IR spectra are measured by a using a HgCdTe photoconductive detector. An average of 64 spectra (in case of **3e** 128 spectra) at a resolution of 1 or 2 cm^{-1} has been recorded. All substances (except **3e**) have been solved in CCl_4 by using concentrations in the 10^{-4} mol/L range. Species **3e** has been solved in CD_3OD with a concentration of $2*10^{-2}$ mol/L. The IR measurements are used to characterize the structure of the investigated substances in the electronic ground state.

Syntheses

Trisodium 8-acetoxypyrene-1,3,6-trisulfonic acid (1): Trisodium 8-hydroxypyrene-1,3,6-trisulfonic acid (2.28 g; 4.35 mmol) and sodium acetate (35.7 mg, 0.44 mmol) were suspended in acetic anhydride (25 mL) and refluxed for 35 hours. After the suspension was cooled down to room temperature, it was diluted with THF and filtered off. The residue was washed with acetone and dried in vacuum yielding a grey powder (2.26 g, 3.99 mmol, 92%). UV/Vis (H_2O): λ_{max} = 368 nm; fluorescence (H_2O): λ_{max} = 389 nm. ^{1}H-NMR (400 MHz, DMSO-d6, 25°C): δ = 9.24 (1 H, d, ^3J(H,H)= 9.6 Hz, Ar-*H*), 9.15 (1 H, d, ^3J(H,H) = 9.6 Hz, Ar-*H*), 9.12 (1 H, d, ^3J(H,H) = 9.6 Hz, Ar-*H*), 9.08 (1 H, s, Ar-*H*), 8.27 (1 H, s, Ar-*H*), 8.13 (1 H, d, ^3J(H,H) = 9.6 Hz, Ar-*H*), 2.57 ppm (3 H, s, COC*H*$_3$), ^{13}C-NMR (100 MHz, DMSO-d6, 25°C): δ = 169.9, 143.0, 142.6, 141.1, 140.9, 127.7, 127.3, 127.0, 125.9, 125.7, 125.1, 124.7, 124.6, 124.5, 122.9, 119.8, 119.2, 20.8 ppm. MS (ESI): *m/z* calc. for $C_{18}H_9Na_3O_{11}S_3$: 565.90 [M]$^+$, found: 566.48.

8-Acetoxypyrene-1,3,6-trisulfonyl chloride (2): Compound **1** (1.09 g, 1.93 mmol) was suspended in thionylchloride (5 mL). After addition of dimethylformamide (30 μL), the mixture was heated to reflux for 5 hours. The solution was cooled down to ambient temperature and poured on ice. After precipitation, **2** was filtered off and was obtained as orange powder after drying in vacuo. (1.04 g, 1.88 mmol, 97%). ^{1}H-NMR (400 MHz, DMSO-d6, 25°C): δ = 9.67 (1 H, d, ^3J (H,H) = 10.0 Hz, Ar-*H*), 9.62 (1 H, s, Ar-*H*), 9.50 (1 H, d, ^3J (H,H) = 10.0 Hz, Ar-*H*), 9.44 (1 H, d, ^3J (H,H) = 9.6 Hz, Ar-*H*), 8.91 (1 H, s, Ar-*H*), 8.82 (1 H, d, ^3J (H,H) = 10.0 Hz, Ar-*H*), 2.68 ppm (3 H, s, COC*H*$_3$).

General procedure for synthesis of derivatives 3a-e: Triethylamine (see individual procedure) was added to a solution of alcohols resp. amines in methylene chloride (1 mL / 0.5 mmol of reagent) and the mixture was cooled to 0 °C. Compound **2** was dissolved in methylene chloride (5 mL / 0.1 mmol of **2**) and added drop-wise to the reaction mixture. After warming up to room temperature and stirring for 48 h, hydrochloric acid (1 M, 20 mL) was added to the solution. The organic phase was separated, extracted three times with hydrochloric acid (1 M) and saturated sodium chloride-solution before being dried over sodium sulfate. After evaporation, the crude product was purified via column chromatography.

Tris(2,2,2-trifluoroethyl) **8-hydroxypyrene-1,3,6-trisulfonate (3a):** Following the general procedure, 2,2,2-trifluoroethanol (118.5 mg, 1.18 mmol) was reacted with **2** (131.2 mg, 0.24 mmol) after addition of trietylamine (132.3 mg, 1.30 mmol). Column chromatographic purification (eluent: ethyl acetate/petrolether 40-65 = 3.5 : 6.5) gave a yellow powder of **3a** (121,0 mg, 0.17 mmol, 73%). UV/Vis (DMSO+TFA): λ_{max} = 440 nm, (DMSO): λ_{max} = 568 nm, $\varepsilon_{(568)}$ (RO$^-$) = 60000 L mol^{-1} cm^{-1}, fluorescence (DMSO; DMSO+TFA): λ_{max} = 574 nm. IR (CCl$_4$): $\tilde{v}$ = 1377, 1742, 2855, 2928, 2959, 3118, 3531 cm^{-1}. ^{1}H-NMR (400 MHz, acetone-d6, 25°C): δ = 9.38 (1 H, s, Ar-*H*), 9.27 (1 H, d, ^3J (H,H) = 10.0 Hz, Ar-*H*), 9.15 (1 H, d, ^3J (H,H) = 9.2 Hz, Ar-*H*), 9.04 (1 H, d, ^3J (H,H) = 9.2 Hz, Ar-*H*), 8.99 (1 H, d, ^3J (H,H) = 10.0 Hz, Ar-*H*), 8.62 (1 H, s, Ar-*H*), 4.90 ppm (6 H, m, 3 C*H*$_2$-CF$_3$). ^{13}C-NMR (100 MHz, acetone-d6, 25°C): δ = 156.5, 135.4, 134.1, 133.6, 132.4, 130.5, 129.1, 127.1, 126.9, 126.4, 126.1 (q, ^1J (C,F) = 277.3 Hz, 3 C, 3 *C*F$_3$), 125.2, 123.3, 122.9, 122.0, 121.0, 118.4, 66.5 ppm (q, ^2J (C,F) = 37.4 Hz, 3 C, 3 *C*H$_2$-CF$_3$), ^{19}F-NMR (376 MHz, DMSO-d6, 25°C): δ = -74.96, -74.98, -74.99 ppm. MS (ESI): *m/z* calc. for C$_{22}$H$_{13}$F$_9$O$_{10}$S$_3$: 702.94 [M-H]$^-$, found: 702.84.

Tris(1,1,1,3,3,3-hexafluoropropan-2-yl) **8-hydroxypyrene-1,3,6-trisulfonate (3b):** Compound **3b** was obtained following the general procedure. After application of triethylamine (213.3 mg, 2.11 mmol), 1,1,1,3,3,3-hexafluoroisopropanol (322.1 mg, 1.92 mmol) was reacted with compound **2** (214.2 mg, 0.38 mmol). Compound **3b** was purified by column chromatography (eluent: ethyl acetate/petrolether 40-65 = 3 : 7) and was obtained as orange powder (274.0 mg, 0.30 mmol, 79%). UV/Vis (DMSO+TFA): λ_{max} = 449 nm, (DMSO): λ_{max} = 576 nm, $\varepsilon_{(576)}$ (RO$^-$) = 60000 L mol^{-1} cm^{-1}, fluorescence (DMSO; DMSO+TFA): λ_{max} = 581 nm. IR (CCl$_4$): $\tilde{v}$ = 1053, 1112, 1186, 1300, 1380, 1413, 1622, 2857, 2928, 2975, 3129, 3464 cm^{-1}. ^{1}H-NMR (400 MHz, acetone-d6, 25°C): δ = 9.41 (1 H, s, Ar-*H*), 9.36 (1 H, d, ^3J

(H,H) = 9.8 Hz, Ar-*H*), 9.25 (1 H, d, ^3J (H,H) = 9.5 Hz, Ar-*H*), 9.08 (1 H, d, ^3J (H,H) = 9.5 Hz, Ar-*H*), 9.06 (1 H, d, ^3J (H,H) = 9.8 Hz, Ar-*H*), 8.67 (1 H, s, Ar-*H*), 6.48 (1 H, hep, ^3J (H,F) = 5.8 Hz, C*H*(CF$_3$)$_2$), 6.39 (1 H, hep, ^3J (H,F) = 5.8 Hz, C*H*(CF$_3$)$_2$), 6.35 ppm (1 H, hep, ^3J (H,F) = 5.8 Hz, C*H*(CF$_3$)$_2$), ^{13}C-NMR (100 MHz, acetone-d6, 25°C): δ = 157.3, 136.0, 134.5, 134.0, 132.4, 131.2, 130.3, 126.7, 126.5, 126.4, 126.1, 125.0, 123.3, 123.2, 120.9, 119,8 (6 C, q, ^1J (C,F) = 278.8 Hz, 6 *C*F$_3$), 118.8, 73.4 ppm (3 C, hep, ^2J (C,F) = 35.2 Hz, 3 *C*H-(CF$_3$)$_2$), ^{19}F-NMR (376 MHz, DMSO-d6, 25°C): δ = -74.34; -74.37, -74.41 ppm. MS (ESI): *m/z* calc. for C$_{25}$H$_{10}$F$_{18}$O$_{10}$S$_3$: 906.91 [M-H]$^-$, found: 906.97.

8-Hydroxy-*N,N',N''*-trimethoxy-*N,N',N''*-trimethylpyrene-1,3,6-trisulfonamide (3c): Synthesis of compound **3c** follows the general procedure. N,O-Dimethylhydroxylamine hydrochloride (164.4 mg, 1.69 mmol) was deprotonated with triethylamine (312.8 ml, 3.09 mmol) and reacted with **2** (156.1 mg, 0.23 mmol). After column chromatographic purification (eluent: ethyl acetate/petrolether 40-65 = 6 : 4), **3c** was obtained as yellow powder (103.0 mg, 0.18 mmol, 62%). UV/Vis (DMSO+TFA): λ_{max} = 438 nm, (DMSO): λ_{max} = 568 nm, $\varepsilon_{(568)}$ (RO$^-$) = 53000 L mol^{-1} cm^{-1}, fluorescence (DMSO; DMSO+TFA): λ_{max} = 576 nm. IR (CCl$_4$): $\tilde{v}$ = 1157, 1346, 2856, 2929, 2980, 3137, 3452, 3589 cm^{-1}. ^{1}H-NMR (400 MHz, acetone-d6, 25°C): δ = 9.51 (1 H, d, ^3J (H,H) = 9.8 Hz, Ar-*H*), 9.48 (1 H, d, ^3J (H,H) = 9.5 Hz, Ar-*H*), 9.32 (1 H, d, ^3J (H,H) = 9.8 Hz, Ar-*H*), 9.29 (1 H, s, Ar-*H*), 9.01 (1 H, d, ^3J (H,H) = 9.5 Hz, Ar-*H*), 8.50 (1 H, s, Ar-*H*), 3.78 (3 H, s, OC*H*$_3$), 3.76 (6 H, s, 2 OC*H*$_3$), 2.96 (3 H, s, NC*H*$_3$), 2.95 (3 H, s, NC*H*$_3$), 2.92 ppm (3 H, s, NC*H*$_3$), ^{13}C-NMR (100 MHz, acetone-d6, 25°C): δ = 154.9, 136.5, 135.5, 135.3, 131.3, 131.0, 127.3, 126.8, 126.7, 126.3, 125.8, 125.7, 124.0, 123.5, 123.0, 119.1, 63.9, 63.8, 63.7, 39.2, 39.1, 39.0 ppm. MS (ESI): *m/z* calc. for C$_{22}$H$_{25}$N$_3$O$_{10}$S$_3$: 586.06 [M-H]$^-$, found: 586.07.

8-Hydroxy-*N,N,N',N',N'',N''*-hexakis(2-methoxyethyl)pyrene-1,3,6-trisulfonamide (3d): Following the general procedure, **2** (62.3 mg, 0.11 mmol) was reacted with 2-methoxy-N-(2-methoxyethyl)ethanamine (51.2 mg, 0.39 mmol) in presence of triethylamine (61.2 mg, 0.61 mmol). The crude product was purified by column chromatography (eluent: ethyl acetate/petrolether 40-65 = 9 : 1). After the solvent was removed in vacuo, **3d** was obtained as yellow, highly hygroscopic powder (Yield could not be determined). UV/Vis (DMSO+TFA): λ_{max} = 431 nm, (DMSO): λ_{max} = 555 nm, fluorescence (DMSO; DMSO+TFA): λ_{max} = 567 nm. IR (CCl$_4$): $\tilde{v}$ = 1115, 1151, 1373, 1687, 2931, 2984, 3591 cm^{-1}. ^{1}H-NMR (400 MHz, acetone-d6, 25°C): δ = 9.26 (1 H, d, ^3J (H,H) = 10.0 Hz, Ar-*H*), 9.24 (1 H, s, Ar-*H*), 9.09 (1 H,

d, ^3J (H,H) = 9.8 Hz, Ar-*H*), 9.01 (1 H, d, ^3J (H,H) = 10.0 Hz, Ar-*H*), 8.90 (1 H, d, ^3J (H,H) = 9.8 Hz, Ar-*H*), 8.44 (1 H, s, Ar-*H*), 3.65 (12 H, m, 6 NCH$_2$C*H*$_2$O), 3.48 (12 H, m, 6 NC*H*$_2$CH$_2$O), 3.13 (6 H, s, 2 OC*H*$_3$), 3.08 (6 H, s, 2 OC*H*$_3$), 3.07 ppm (6 H, s, 2 OC*H*$_3$), ^{13}C-NMR (100 MHz, DMSO-d6, 25°C): δ = 154.6, 136.9, 132.1, 131.8, 130.9, 130.8, 130.7, 128.9, 128.1, 126.1, 125.8, 125.5, 123.7, 121.6, 119.1, 115.5, 70.1 (2 C), 70.0 (2 C), 69.9 (2 C), 58.0 (2 C), 57.9 (4 C), 47.3 (2 C), 46.9 (4 C) ppm. MS (ESI): *m/z* calc. for C$_{34}$H$_{49}$N$_3$O$_{13}$S$_3$:826.23 [M+Na]$^+$, found: 826.21.

8-Hydroxy-*N,N',N''*-tris(2-hydroxyethyl)-*N,N',N''*-trimethylpyrene-1,3,6-trisulfonamide (3e):
Compound **3e** was synthesized according the general procedure. 2-(Methylamino)ethanol (55.9 mg, 0.74 mmol) was reacted with **2** (82.7 mg, 0.15 mmol) after addition of triethylamine (82.9 mg, 0.82 mmol). Crude **3e** was purified by column chromatography (eluent: methanol/methylene chloride = 1 : 9) to give a yellow powder (85.4 mg, 0.14 mmol, 91%). UV/Vis (DMSO+TFA): λ_{max} = 430 nm; (DMSO): λ_{max} = 554 nm; $\varepsilon_{(554)}$ (RO$^-$) = 35000 L mol^{-1} cm^{-1}, fluorescence (DMSO; DMSO+TFA): λ_{max} = 566 nm. IR (CD$_3$OD): $\tilde{v}$ = 1337, 1415, 2615, 3345 cm^{-1}. ^{1}H-NMR (400 MHz, DMSO-d6, 25°C): δ = 9.14 (1 H, d, ^3J (H,H) = 9.8 Hz, Ar-*H*), 8.97 (1 H, d, ^3J (H,H) = 9.6 Hz, Ar-*H*), 8.94 (1 H, s, Ar-*H*), 8.86 (1 H, d, ^3J (H,H) = 9.8 Hz, Ar-*H*), 8.80 (1 H, d, ^3J (H,H) = 9.6 Hz, Ar-*H*), 8.23 (1 H, s, Ar-*H*), 3.49 (6 H, m, 3 NCH$_2$C*H*$_2$O), 3.26 (6 H, m, 3 NC*H*$_2$CH$_2$O), 2.88 (3 H, s; NC*H*$_3$), 2.86 (3 H, s, NC*H*$_3$), 2.85 ppm (3 H, s, NC*H*$_3$), ^{13}C-NMR (100 MHz, DMSO-d6, 25°C): δ = 154.6, 135.6, 132.2, 131.0, 129.8, 129.6, 129.0, 128.3, 126.1, 126.0, 125.6, 123.7, 121.6, 120.5, 119.2, 115.5, 59.1, 59.0 (2C), 51.7, 51.5 (2 C), 35.4, 35.2 ppm (2 C). MS (ESI): *m/z* calc. for C$_{25}$H$_{31}$N$_3$O$_{10}$S$_3$: 652.11 [M+Na]$^+$, found: 652.27.

8-Hydroxypyren-*N,N,N',N',N'',N''*-hexamethyl-1,3,6-trisulfonamide (3f, HPTA):
Compound **2** (168.5 mg, 0.30 mmol) was suspended in a cooled (0° C) 5 mL dimethyl amine solution (40% in H$_2$O). After stirring for 24h and warming up to room temperature, the solution was acidified with hydrochloric acid (1M) causing a precipitation of crude **3f**. The yellow solid was filtered off, dissolved in ethyl acetate and washed twice with saturated sodium chloride-solution. After being dried over sodium sulfate and evaporation, **3f** was purified by column chromatography (eluent: ethyl acetate/petrolether 40-65 = 6 : 4) and obtained as yellow powder (102.8 mg, 0,190 mmol, 63%). UV/Vis (DMSO+TFA): λ_{max} = 431 nm, (DMSO): λ_{max} = 554 nm, $\varepsilon_{(554)}$ (RO$^-$) = 37000 L mol^{-1} cm^{-1}, fluorescence (DMSO; DMSO+TFA): λ_{max} = 565 nm. IR (CCl$_4$): $\tilde{v}$ = 1114, 1162, 2855, 2928, 2960, 3280 cm^{-1}. ^{1}H-NMR (400 MHz, DMSO-d6, 25°C): δ =

9.27 (1 H, d, ^3J (H,H) = 10.0 Hz, Ar-*H*), 9.15 (1 H, d, ^3J (H,H) = 10.0 Hz, Ar-*H*), 9.02 (1 H, d, ^3J (H,H) = 10.0 Hz, Ar-*H*), 8.98 (1 H, s, Ar-*H*), 8.87 (1 H, d, ^3J (H,H) = 10.0 Hz, Ar-*H*), 8.31 (1 H, s, Ar-*H*), 2.83 (6 H, s, 2 NC*H*$_3$), 2.81 ppm (12 H, s, 4 NC*H*$_3$), ^{13}C-NMR (100 MHz, DMSO-d6, 25°C): δ = 154.7, 133.8, 132.7, 131.6, 130.0, 128.0, 127.8 (2 C), 126.3, 125.5 (2 C), 123.8, 121.7, 120.7, 119.6, 116.3, 37.4 (2 C), 37.3 ppm (4 C). MS (ESI): *m/z* calc. for C$_{22}$H$_{25}$N$_3$O$_7$S$_3$: 539.09 [M]$^+$, found: 539.10.

Acknowledgements

Notes and references

*a*Biophysical Chemistry, Saarland University, Campus B2 2, 66123 Saarbrücken, Germany.
*b*Fraunhofer-IBMT, Ensheimer Straße 48, 66386 St. Ingbert, Germany.
*c*Technische Universität Kaiserslautern & Research Center Optimas, Fachbereich Chemie, Erwin-Schrödinger-Str., 67663 Kaiserslautern, Germany.

Electronic Supplementary Information (ESI) available: [details of any supplementary information available should be included here]. See DOI: 10.1039/b000000x/

1. J. Steadman and J. A. Syage, Picosecond mass • selective measurements of phenol • (NH3)n acid-base chemistry in clusters, *J. Chem. Phys.*, 1990, **92**, 4630–4632.
2. J. Syage and J. Steadman, Picosecond measurements of phenol excited-state proton transfer in clusters, *J. Chem. Phys.*, 1991, **95**, 2497–2510.
3. J. A. Syage, Tunneling mechanism for excited-state proton transfer in phenol-ammonia clusters, *J. Phys. Chem.*, 1993, **97**, 12523–12529.
4. S. Kaneko, S. Yotoriyama, H. Koda, and S. Tobita, Excited-state proton transfer to solvent from phenol and cyanophenols in water, *J. Phys. Chem. A*, 2009, **113**, 3021–3028.
5. E. Pines, in *The Chemistry of Phenols*, ed. Z. Rappoport, John Wiley & Sons, Ltd. **2003**, pp. 491–527.
6. I. Martynov, A. Demyashkevich, B. M. Uzhinov, M. G. Kuz'min, Proton transfer reactions in the excited electronic states of aromatic molecules, *Russ. Chem. Rev.*, 1977, **46**, 3–31.
7. A. Jankowski, P. Stefanowicz, and P. Dobryszycki, Excited state proton transfer in 2-naphthol derivatives bound to selected sites of proteins, *J. Photochem. Photobiol. A Chem.*, 1992, **69**, 57–66.

8. L. M. Tolbert and J. E. Haubrich, Enhanced photoacidities of cyanonaphthols, *J. Am. Chem. Soc.*, 1990, **112**, 8163–8165.

9. L. M. Tolbert and J. E. Haubrich, Photoexcited proton transfer from enhanced photoacids, *J. Am. Chem. Soc.*, 1994, **116**, 10593–10600.

10. S. Kim, J. Breen, D. Willberg, L. W. Peng, A. Heikal, J. A. Syage and A. H. Zewail, Solvation ultrafast dynamics of reactions. 8. Acid-base reactions in finite-sized clusters of naphthol in ammonia, water, and piperidine, *J. Phys. Chem.*, 1995, **99**, 7421–7435.

11. D. Huppert, L. M. Tolbert, and S. Linares-Samaniego, Ultrafast excited-state proton transfer from cyano-substituted 2-naphthols, *J. Phys. Chem. A*, 1997, **101**, 4602–4605.

12. K. Solntsev, D. Huppert, L. M. Tolbert and N. Agmon, Solvatochromic shifts of "super" photoacids, *J. Am. Chem. Soc.*, 1998, **120**, 7981–7982.

13. R. Knochenmuss, K. M. Solntsev, and L. M. Tolbert, Molecular beam studies of the "super"photoacid 5-cyano-2-naphthol in solvent clusters, *J. Phys. Chem. A*, 2001, **105**, 6393–6401.

14. C. Clower, K. M. Solntsev, J. Kowalik, L. M. Tolbert, and D. Huppert, Photochemistry of "super" photoacids. 3. Excited-state proton transfer from perfluoroalkylsulfonyl-substituted 2-naphthols, *J. Phys. Chem. A*, 2002, **106**, 3114–3122.

15. L. M. Tolbert and K. M. Solntsev, Excited-state proton transfer: from constrained systems to "super"photoacids to superfast proton transfer, *Acc. Chem. Res.*, 2002, **35**, 19–27.

16. F. De Vleeschouwer, W. Yang, D. N. Beratan, P. Geerlings, and F. De Proft, Inverse design of molecules with optimal reactivity properties: acidity of 2-naphthol derivatives, *Phys. Chem. Chem. Phys.*, 2012, **14**, 16002–16013.

17. M. Prémont-Schwarz, T. Barak, D. Pines, E. T. J. Nibbering, and E. Pines, Ultrafast excited state proton transfer reaction of 1-naphthol-3,6-disulfonate and several 5-substituted 1-naphthol derivatives, *J. Phys. Chem. B*, 2013, **117**, 4593–4594.

18. K. M. Solntsev, D. Huppert, and N. Agmon, Photochemistry of "super"-photoacids. Solvent effects, *J. Phys. Chem. A*, 1999, **103**, 6984–6997.

19. I. Carmeli, D. Huppert, L. M. Tolbert, and J. E. Haubrich, Ultrafast excited-state proton transfer from dicyano-naphthol, *Chem. Phys. Lett.*, 1996, **260**, 109–114.

20. B. Cohen, J. Segal, and D. Huppert, Proton transfer from photoacid to solvent, *J. Phys. Chem. A*, 2002, **106**, 7462–7467.

21. K. M. Solntsev, L. M. Tolbert, B. Cohen, D. Huppert, Y. Hayashi, and Y. Feldman, Excited-state proton transfer in chiral environments. 1. Chiral solvents, *J. Am. Chem. Soc.*, 2002, **124**, 9046–9047.

22. N. Agmon, Elementary steps in excited-state proton transfer, *J. Phys. Chem. A*, 2005, **109**, 13–35.

23. D. Pines, E. T. J. Nibbering, and E. Pines, Relaxation to equilibrium following photoacid dissociation in mineral acids and buffer solutions, *J. Phys. Condens. Matter*, 2007, **19**, 065134 1-14.

24. T. Förster, Fluoreszenzspektrum und Wasserstoffionenkonzentration, *Naturwissenschaften*, 1949, **6**, 186–187.

25. T. Förster, Dissoziation angeregter Moleküle, *Zeitschrift für Elektrochemie*, 1950, **54**, 42–46.

26. E. Pines, D. Huppert, and N. Agmon, Geminate recombination in excited-state proton-transfer reactions: Numerical solution of the Debye–Smoluchowski equation with backreaction and comparison with experimental results, *J. Chem. Phys.*, 1988, **88**, 5620–5630.

27. N. Agmon, E. Pines, and D. Huppert, Geminate recombination in proton-transfer reactions. II. Comparaison of diffusional and kinetic schemes, *J. Chem. Phys.*, 1988, **88**, 5631–5638.

28. T.-H. Tran-Thi, T. Gustavsson, C. Prayer, S. Pommeret, and J. T. Hynes, Primary ultrafast events preceding the photoinduced proton transfer from pyranine to water, *Chem. Phys. Lett.*, 2000, **329**, 421–430.

29. J. T. Hynes, T.-H. Tran-Thi, and G. Granucci, Intermolecular photochemical proton transfer in solution: new insights and perspectives, *J. Photochem. Photobiol. A Chem.*, 2002, **154**, 3–11.

30. P. Leiderman, L. Genosar, and D. Huppert, Excited-state proton transfer : Indication of three steps in the dissociation and recombination process, *J. Phys. Chem. A*, 2005, **109**, 5965–5977.

31. D. B. Spry, A. Goun, and M. D. Fayer, Deprotonation dynamics and stokes shift of pyranine (HPTS), *J. Phys. Chem. A*, 2007, **111**, 230–237.

32. G. Jung, S. Gerharz, and A. Schmitt, Solvent-dependent steady-state fluorescence spectroscopy for searching ESPT-dyes: Solvatochromism of HPTS revisited, *Phys. Chem. Chem. Phys.*, 2009, **11**, 1416–1426.

33. W. Liu, F. Han, C. Smith, and C. Fang, Ultrafast conformational dynamics of pyranine during excited state proton transfer in aqueous solution revealed by femtosecond stimulated Raman spectroscopy, *J. Phys. Chem. B*, 2012, **116**, 10535–10550.

34. E. Pines, D. Huppert, and N. Agmon, Salt effects on steady-state quantum yields of ultrafast, diffusion-influenced, reversible photoacid dissociation reactions, *J. Phys. Chem.*, 1991, **25**, 666–674.

35. M. Rini, B.-Z. Magnes, E. Pines, and E. T. J. Nibbering, Real-time observation of bimodal proton transfer in acid-base pairs in water, *Science*, 2003, **301**, 349–352.

36. E. Pines and D. Huppert, Observation of geminate recombination in excited state proton transfer, *J. Chem. Phys.*, 1986, **84**, 3576–3577.

37. D. Pines, E. Pines, in *Hydrogen-Transfer Reactions*, ed. J. T. Hynes, J. P. Klinman, H.-H. Limbach, R. L. Schowen, Wiley-VCH Verlag GmbH & Co. KGaA, Weinheim **2006**, pp. 377–415.

38. N. Barrash-Shiftan, B. B. Brauer, and E. Pines, Solvent dependence of pyranine fluorescence and UV-visible

absorption spectra, *J. Phys. Org. Chem.*, 1998, **11**, 743–750.

39. D. Pines and E. Pines, Direct observation of power-law behavior in the asymptotic relaxation to equilibrium of a reversible bimolecular reaction, *J. Chem. Phys.*, 2001, **115**, 951–953.

40. Y. Wang, W. Liu, L. Tang, B. Oscar, F. Han, and C. Fang, Early time excited-state structural evolution of pyranine in methanol revealed by femtosecond stimulated Raman spectroscopy, *J. Phys. Chem. A*, 2013, **117**, 6024–6042.

41. F. Han, W. Liu, and C. Fang, Excited-state proton transfer of photoexcited pyranine in water observed by femtosecond stimulated Raman spectroscopy, *Chem. Phys.*, 2013, **422**, 204–219.

42. T.-H. Tran-Thi, C. Prayer, P. Millié, P. Uznanski, and J. T. Hynes, Substituent and solvent effects on the nature of the transitions of pyrenol and pyranine. identification of an intermediate in the excited-state proton-transfer reaction, *J. Phys. Chem. A*, 2002, **106**, 2244–2255.

43. O. F. Mohammed, D. Pines, J. Dreyer, E. Pines, and E. T. J. Nibbering, Sequential proton transfer through water bridges in acid-base reactions, *Science*, 2005, **310**, 83–86.

44. D. B. Spry and M. D. Fayer, Charge redistribution and photoacidity: Neutral versus cationic photoacids, *J. Chem. Phys.*, 2008, **128**, 084508 1–9.

45. D. B. Spry and M. D. Fayer, Observation of slow charge redistribution preceding excited-state proton transfer, *J. Chem. Phys.*, 2007, **127**, 204501 1–10.

46. E. Pines and D. Huppert, Geminate recombination proton-transfer reactions, *Chem. Phys. Lett.*, 1986, **126**, 88–91.

47. Z. Zhujun and R. W. Seitz, A fluorescence sensor for quantifying pH in the range from 6.5 to 8.5, *Anal. Chim. Acta*, 1984, **160**, 47–55.

48. O. S. Wolfbeis and E. Koller, Fluorimetric assay of hydrolases at longwave excitation and emission wavelengths with new substrates possessing unique water solubility, *Anal. Biochem.*, 1983, **129**, 365–370.

49. O. S. Wolfbeis, E. Fürlinger, H. Kroneis, and H. Marsoner, A study on fluorescent indicators for measuring near neutral ("physiological") pH-Values, *Fresenius Zeitschrift für Anal. Chemie*, 1983, **314**, 119–124.

50. J. Han and K. Burgess, Fluorescent indicators for intracellular pH, *Chem. Rev.*, 2010, **110**, 2709–2728.

51. E. Pines, D. Pines, Y.-Z. Ma, and G. R. Fleming, Femtosecond pump-probe measurements of solvation by hydrogen-bonding interactions, *ChemPhysChem*, 2004, **5**, 1315–1327.

52. D. B. Spry and M. D. Fayer, Proton transfer and proton concentrations in protonated Nafion fuel cell membranes, *J. Phys. Chem. B*, 2009, **113**, 10210–10221.

53. E.-A. Gould, A. V Popov, L. M. Tolbert, I. Presiado, Y. Erez, D. Huppert, and K. M. Solntsev, Excited-state proton transfer in N-methyl-6-hydroxyquinolinium salts: solvent and temperature effects, *Phys. Chem. Chem. Phys.*, 2012, **14**, 8964–8973.

54. N. Karton-Lifshin, I. Presiado, Y. Erez, R. Gepshtein, D. Shabat, and D. Huppert, Ultrafast excited-state intermolecular proton transfer of cyanine fluorochrome dyes, *J. Phys. Chem. A*, 2012, **116**, 85–92.

55. T. G. Kim and M. R. Topp, Ultrafast excited-state deprotonation and electron transfer in hydroxyquinoline derivatives, *J. Phys. Chem. A*, 2004, **108**, 10060–10065.

56. J. L. Pérez Lustres, S. A. Kovalenko, M. Mosquera, T. Senyushkina, W. Flasche, and N. P. Ernsting, Ultrafast solvation of N-methyl-6-quinolone probes local IR spectrum, *Angew. Chem. Int. Ed. Engl.*, 2005, **44**, 5635–5639.

57. J. L. Pérez-Lustres, F. Rodriguez-Prieto, M. Mosquera, T. A. Senyushkina, N. P. Ernsting, and S. A. Kovalenko, Ultrafast proton transfer to solvent: Molecularity and intermediates from solvation- and diffusion-controlled regimes, *J. Am. Chem. Soc.*, 2007, **129**, 5408–5418.

58. I. Presiado, N. Karton-Lifshin, Y. Erez, R. Gepshtein, D. Shabat, and D. Huppert, Ultrafast proton transfer of three novel quinone cyanine photoacids, *J. Phys. Chem. A*, 2012, **116**, 7353–7363.

59. R. Simkovitch, N. Karton-Lifshin, S. Shomer, D. Shabat, and D. Huppert, Ultrafast excited-state proton transfer to the solvent occurs on a hundred-femtosecond time-scale, *J. Phys. Chem. A*, 2013, **117**, 3405–3413.

60. S. C. Miller, Profiling sulfonate ester stability: Identification of complementary protecting groups for sulfonates, *J. Org. Chem.*, 2010, **75**, 4632–4635.

61. F. E. Cappuccio, J. T. Suri, D. B. Cordes, R. A. Wessling, and B. Singaram, Evaluation of pyranine derivatives in boronic acid based saccharide sensing: Significance of charge interaction between dye and quencher in solution and hydrogel, *J. Fluoresc.*, 2004, **14**, 521–533.

62. C. Spies, B. Finkler, N. Acar, and G. Jung, Solvatochromism of pyranine-derived photoacids, *Phys. Chem. Chem. Physic*, 2013, **15**, 19893–19905.

63. C. Spies, S. Shomer, B. Finkler, D. Pines, E. Pines, D. Huppert, and G. Jung, Solvent dependence of excited-state proton transfer from pyranine-derived photoacids, *submitted*.

64. F. G. Bordwell, Equilibrium acidities in dimethyl sulfoxide solution, *Acc. Chem. Res.*, 1988, **21**, 456–463.

65. C. A. Reed, The nature of H+ in condensed media, *Acc. Chem. Res.*, 2013, **46**, 2567–2575.

66. G. Schweitzer, L. Xu, B. Craig, and F. DeSchryver, A double OPA femtosecond laser system for transient absorption spectroscopy, *Opt. Commun.*, 1997, **142**, 283–288.

67. C. Buehler, C. Y. Dong, P. T. So, T. French, and E. Gratton, Time-resolved polarization imaging by pump-probe (stimulated emission) fluorescence microscopy, *Biophys. J.*, 2000, **79**, 536–549.

68. M. Fukuda, O. Kajimoto, M. Terazima, and Y. Kimura, Application of the transient grating method to the investigation of the photo-thermalization process of malachite green in room temperature ionic liquids, *J. Mol. Liq.*, 2007, **134**, 49–54.

69. R. Berera, R. van Grondelle, and J. T. M. Kennis, Ultrafast transient absorption spectroscopy: principles and application to photosynthetic systems, *Photosynth. Res.*, 2009, **101**, 105–118.

70. R. a Velapoldi and H. H. Tønnesen, Corrected emission spectra and quantum yields for a series of fluorescent compounds in the visible spectral region, *J. Fluoresc.*, 2004, **14**, 465–72.

71. T. Karstens and K. Kobs, Rhodamine B and rhodamine 101 as reference substances for fluorescence quantum yield measurements, *J. Phys. Chem.*, 1980, **84**, 1871–1872.

72. M. Fischer and J. Georges, Fluorescence quantum yield of rhodamine 6G in ethanol as a function of concentration using thermal lens spectrometry, *Chem. Phys. Lett.*, 1996, **260**, 115–118.

73. J. H. Brannon and D. Magde, Absolute quantum yield determination by thermal blooming. Fluorescein, *J. Phys. Chem.*, 1978, **82**, 705–709.

74. J. Widengren, B. Terry, and R. Rigler, Protonation kinetics of GFP and FITC investigated by FCS - aspects of the use of fluorescent indicators for measuring pH, *Chem. Phys.*, 1999, **249**, 259–271.

75. L. P. Hammett and A. J. Deyrup, A series of simple basic indicators. I. The acidity functions of mixtures of sulfuric and perchloric acids with water, *J. Am. Chem. Soc.*, 1932, **54**, 2721–2739.

76. M. J. Jorgenson and D. R. Hartter, A Critical re-evaluation of the hammett acidity function at moderate and high acid concentrations of sulfuric acid. New H 0 values based solely on a set of primary aniline indicators, *J. Am. Chem. Soc.*, 1963, **85**, 878–883.

77. Y. Avnir and Y. Barenholz, pH determination by pyranine: Medium-related artifacts and their correction, *Anal. Biochem.*, 2005, **347**, 34–41.

78. A. B. Kotlyar, N. Borovok, S. Raviv, L. Zimanyi, and M. Gutman, Fast redox perturbation of aqueous solution by photoexcitation of pyranine, *Photochem. Photobiol.*, 1996, **63**, 448–454.

79. J. Yang, X.-P. Xing, X.-B. Wang, L.-S. Wang, A. P. Sergeeva, and A. I. Boldyrev, Negative electron binding energies observed in a triply charged anion: Photoelectron spectroscopy of 1-hydroxy-3,6,8-pyrene-trisulfonate, *J. Chem. Phys.*, 2008, **128**, 091102 1–4.

80. B. Hinkeldey, A. Schmitt, and G. Jung, Comparative photostability studies of BODIPY and fluorescein dyes by using fluorescence correlation spectroscopy, *Chemphyschem*, 2008, **9**, 2019–2027.

81. V. Vukojevic, M. Heidkamp, Y. Ming, B. Johansson, L. Terenius, and R. Rigler, Quantitative single-molecule imaging by confocal laser scanning microscopy, *Proc. Natl. Acad. Sci. U. S. A.*, 2008, **105**, 18176–18181.

82. J. Hu and C.-Y. Zhang, Simple and accurate quantification of quantum yield at the single-molecule/particle level, *Anal. Chem.*, 2013, **85**, 2000–2004.

83. H. K. J. Hall, Correlation of the base strengths of amines, *J. Am. Chem. Soc.*, 1957, **79**, 5441–5444.

84. J. King, M. Gill, and P. Ciubotaru, Benzenesulfonyl chloride with primary and secondary amines in aqueous media–Unexpected high conversions to sulfonamides at high pH, *Can. J. Chem.*, 2005, **1535**, 1525–1535.

85. E. Hamborg and G. Versteeg, Dissociation constants and thermodynamic properties of amines and alkanolamines from (293 to 353) K, *J. Chem. Eng. Data*, 2009, **54**, 1318–1328.

86. A. Kundu and N. Kishore, 1,1,1,3,3,3-Hexafluoroisopropanol induced thermal unfolding and molten globule state of bovine alpha-lactalbumin: Calorimetric and spectroscopic studies, *Biopolymers*, 2004, **73**, 405–420.

87. J. Widengren, U. Mets, and R. Rigler, Fluorescence correlation spectroscopy of triplet states in solution: A theoretical and experimental study, *J. Phys. Chem.*, 1995, **99**, 13368–13379.

88. T. Ha and P. Tinnefeld, Photophysics of fluorescent probes for single-molecule biophysics and super-resolution imaging, *Annu. Rev. Phys. Chem.*, 2012, **63**, 595–617.

89. W.-C. Sun, K. R. Gee, D. H. Klaubert, and R. P. Haugland, Synthesis of fluorinated fluoresceins, *J. Org. Chem.*, 1997, **62**, 6469–6475.

90. W.-C. Sun, K. R. Gee, and R. P. Haugland, Synthesis of novel fluorinated coumarins: Excellent UV-light excitable fluorescent dyes, *Bioorg. Med. Chem. Lett.*, 1998, **8**, 3107–3110.

91. G. Y. Yang, M. Hanack, Y. W. Lee, Y. Chen, M. K. Y. Lee, and D. Dini, Synthesis and nonlinear optical properties of fluorine-containing naphthalocyanines, *Chem. - An Eur. J.*, 2003, **9**, 2758–2762.

92. Z. R. Woydziak, L. Fu, and B. R. Peterson, Synthesis of fluorinated benzophenones, xanthones, acridones, and thioxanthones by iterative nucleophilic aromatic substitution, *J. Org. Chem.*, 2012, **77**, 473–481.

93. H. Sun, A. Putta, J. P. Kloster, and U. K. Tottempudi, Unexpected photostability improvement of aromatics in polyfluorinated solvents, *Chem. Commun.*, 2012, **48**, 12085–12087.

94. S. H. Kim and S. H. Hwang, Synthesis and photostability of functional squarylium dyes, *Dye. Pigment.*, 1997, **35**, 111–121.

95. A. Toutchkine, D.-V. Nguyen, and K. M. Hahn, Merocyanine dyes with improved photostability, *Org. Lett.*, 2007, **9**, 2775–2777.

96. N. I. Shank, K. J. Zanotti, F. Lanni, P. B. Berget, and B. A. Armitage, Enhanced photostability of genetically encodable fluoromodules based on fluorogenic cyanine dyes and a promiscuous protein partner, *J. Am. Chem. Soc.*, 2009, **131**, 12960–12969.

5

Supporting Information

Highly Photostable "Super"-Photoacids for Ultrasensitive Fluorescence Spectroscopy

10 Björn Finkler[a], Christian Spies[a], Michael Vester[a], Frederick Walte[a], Kathrin Omlor[a], Iris Riemann[b], Manuel Zimmer[c], Frank Stracke[b], Markus Gerhards[c], Gregor Jung[a]

[a] *Biophysical Chemistry, Saarland University, Campus B2 2, 66123 Saarbrücken, Germany.*

[b] *Fraunhofer-IBMT, Ensheimer Straße 48, 66386 St. Ingbert, Germany.*

15 [c] *Technische Universität Kaiserslautern & Research Center Optimas, Fachbereich Chemie, Erwin-Schrödinger-Str.*
67663 Kaiserslautern, Germany.

Email corresponding author: g.jung@mx.uni-saarland.de

20

25

30

Determination of pK_a values via fluorescence correlation spectroscopy (FCS)

For determination of the pK_a values of the weakly water soluble photoacids, we followed the experimental procedure of Widegren *et al*. [S1]

The actual system consists of an acid, the corresponding base and buffer HB$^+$/B for stabilizing the equilibrium. A 20 mM HPCE-buffer (citric acid / sodium citrate, Fluka) was employed for the pH values 4 and 4.5. Protonation and deprotonation is widely mediated by HB$^+$ and B with the bimolecular rate constants k_{prot}^{bi} and k_{deprot}^{bi} (Equation S1), which are experimentally determined to lie in the range of $\sim 10^8$ M^{-1}s^{-1}. At a total buffer concentration of 20 mM, where $[\text{HB}^+] \approx [\text{B}]$, direct, diffusion-controlled protonation by H$^+$ and deprotonation can be neglected at pH-values > 4.[S1]

$$\text{ROH} + \text{B} \; \underset{k_{prot}^{bi}}{\overset{k_{deprot}^{bi}}{\rightleftharpoons}} \; \text{RO}^- + \text{HB}^+ \qquad\qquad (\text{S1})$$
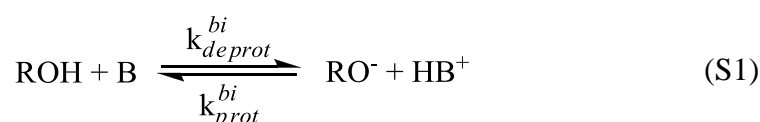
The kinetic description for the equilibrium leads to:

$$\frac{d[\text{RO}^-]}{dt} = -k_{prot}^{bi}[\text{RO}^-][\text{HB}^+] + k_{deprot}^{bi}[\text{ROH}][\text{B}] = 0 \qquad\qquad (\text{S2})$$

The effective rates are defined as $k_{prot}^{eff} = k_{prot}^{bi} \cdot [\text{HB}^+]$ and $k_{deprot}^{eff} = k_{deprot}^{bi} \cdot [\text{B}]$, so equation S2 can be converted into:

$$\frac{[\text{ROH}]}{[\text{RO}^-]} = \frac{k_{prot}^{eff}}{k_{deprot}^{eff}} \qquad\qquad (\text{S3})$$

$$K_a^{-1} = \frac{[\text{ROH}]}{[\text{H}^+][\text{RO}^-]} \qquad\qquad (\text{S4})$$

Combination of (S3) and (S4) leads to a relation for the pK_a:

$$\text{p}K_a = \text{pH} + log\,\frac{k_{prot}^{eff}}{k_{deprot}^{eff}} \qquad\qquad (\text{S5})$$

The rate constants k_{prot}^{eff} and k_{deprot}^{eff} are directly accessible in a FCS-experiment by photoexcitation of RO⁻ and detection of its fluorescence (Figure S1).

RO⁻* ———— S_1

546 nm   557 nm

k_{prot}^{eff}

ROH k_{deprot}^{eff} RO⁻ S_0
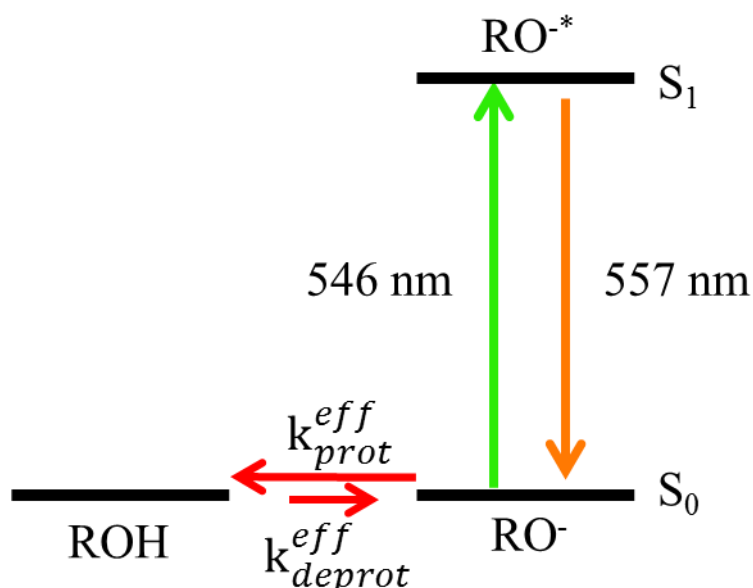
Figure S1: Schematic representation for pK_a-determination: excitation of RO⁻ (**3b**) was performed at λ_{exc} = 546 nm ($\lambda_{abs, max}$ = 515 nm at pH 4; $\lambda_{em, max}$ = 557 nm at pH 4), fluorescence was detected at λ_{det} = 555-625 nm. The dark state ROH is populated with the rate constant k_{prot}^{eff}, whereas k_{deprot}^{eff} describes the depopulation the dark state.

Fitting the obtained correlation functions G(τ) according to equation S6 (Figure S2) gives the rates k_{prot}^{eff}, k_{deprot}^{eff} and consequently the pK_a value depicted in Table 2. The outcome of this approach was verified with **3f**.

$$G(\tau) = \frac{1}{\langle N \rangle} \frac{1}{1+\frac{\tau}{\tau_D}} \left(1 + \frac{k_{prot}^{eff}}{k_{deprot}^{eff}} \exp\left(-(k_{prot}^{eff} + k_{deprot}^{eff})\tau\right) \right) \qquad (S6)$$

$$\tau_D = 107 \, (\pm 5) \, \mu s$$

$$k_{prot}^{eff} = 1.55 \, (\pm 0.13) \, MHz$$

$$k_{deprot}^{eff} = 2.21 \, (\pm 0.14) \, MHz$$
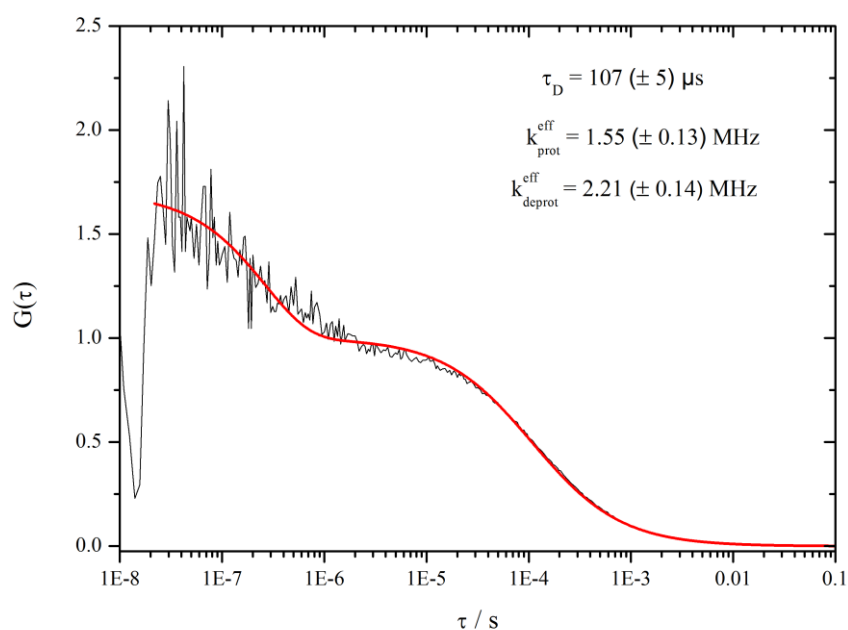
Figure S2: Normalized correlation function of **3b**. Excitation was performed at $\lambda = 546$ nm with a laser intensity of 168 kW cm^{-1} in a 20 mM citrate-buffer at pH 4.5. Fluorescence was detected at $\lambda_{det} = 555$-625 nm. A pK_a of 4.4 is calculated as a mean value of two measurements.

Characterisation of the described compounds with NMR- and mass spectroscopy:

3a: R^3 = -OCH$_2$CF$_3$
3b: R^3 = -OCH(CF$_3$)$_2$
3c: R^3 = -N(CH$_3$)(OCH$_3$)
3d: R^3 = -N((CH$_2$)$_2$OCH$_3$)$_2$
3e: R^3 = -N(CH$_3$)((CH$_2$)$_2$OH)
3f: R^3 = -N(CH$_3$)$_2$
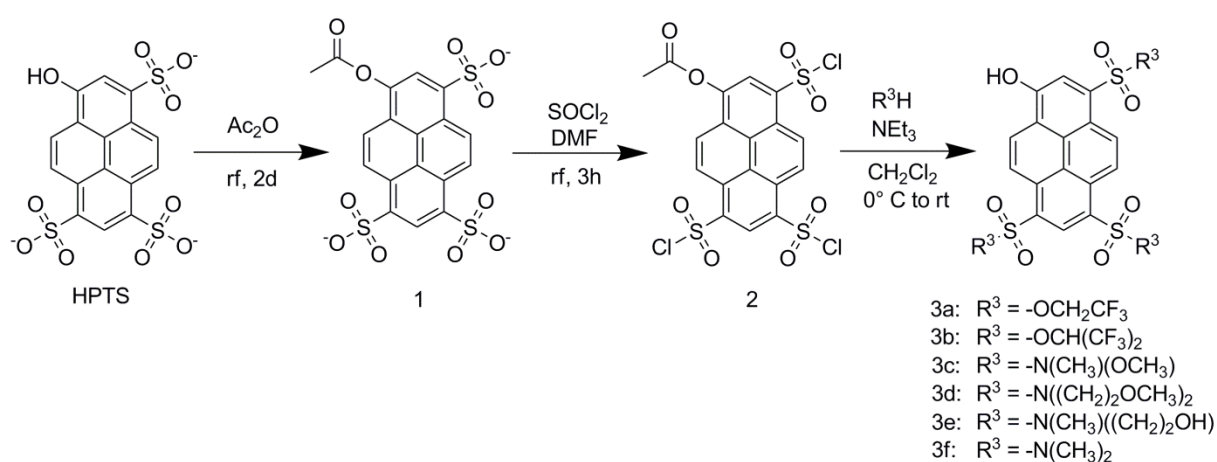
Scheme S1: Synthesis of HPTS-derivatives **3a-f**.

Compound **1**:
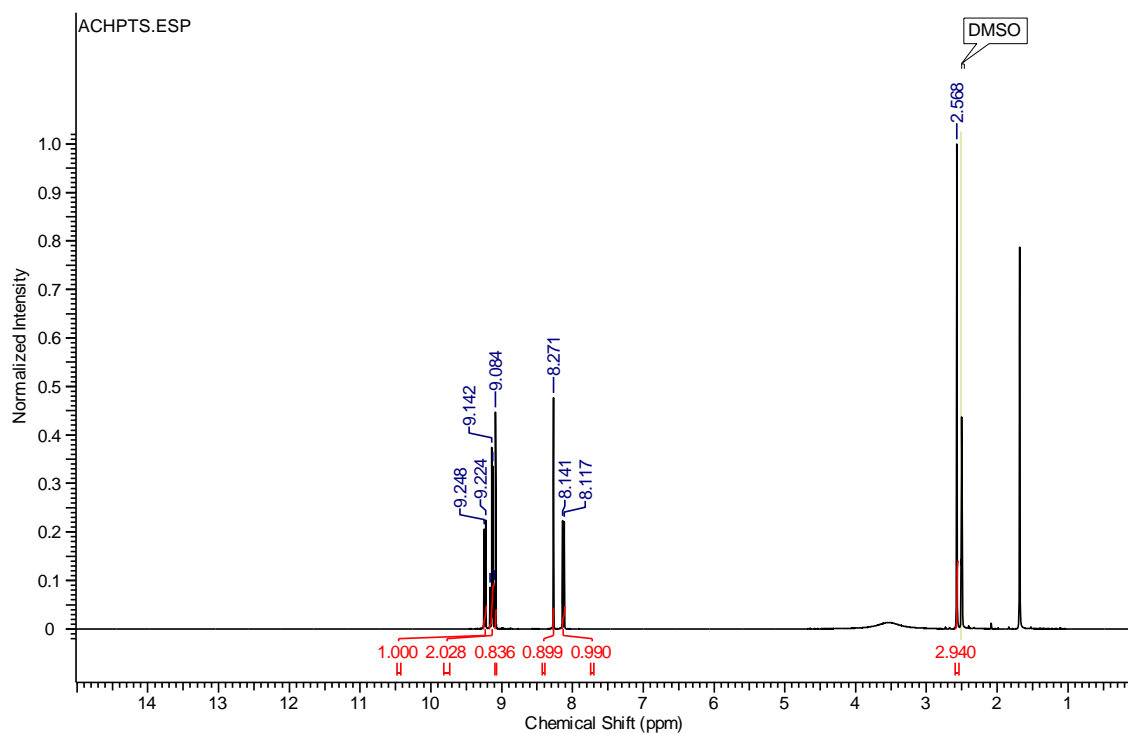
Figure S3: ^{1}H-NMR spectrum of **1**.
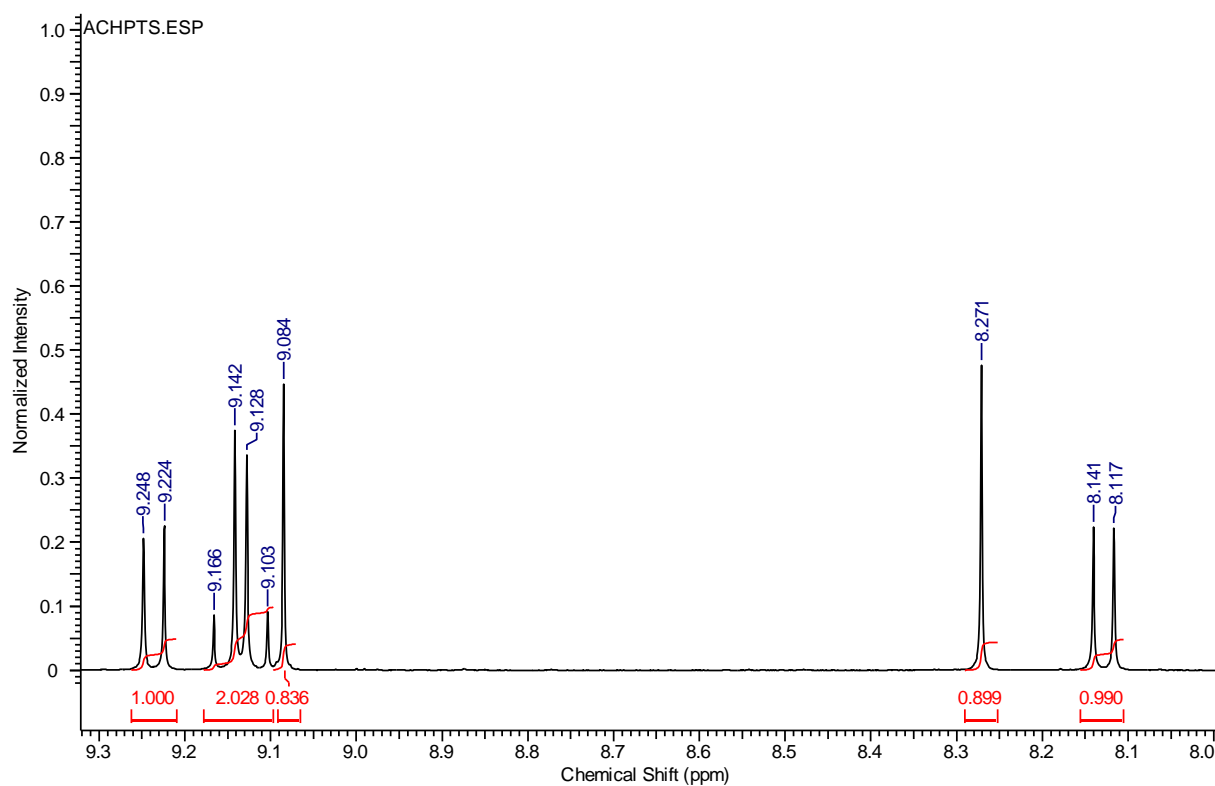
Figure S4: ^{1}H-NMR spectrum of **1** (zoomed).
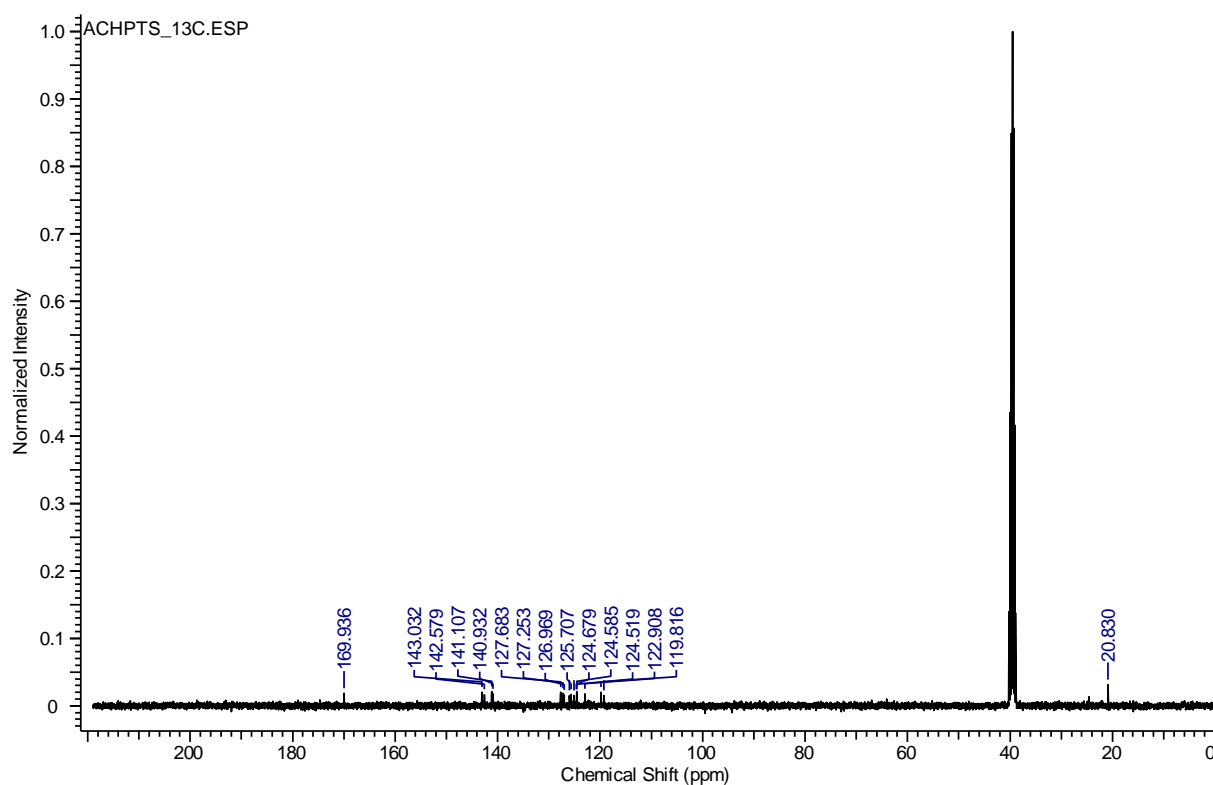
Figure S5: ^{13}C-NMR spectrum of **1**.
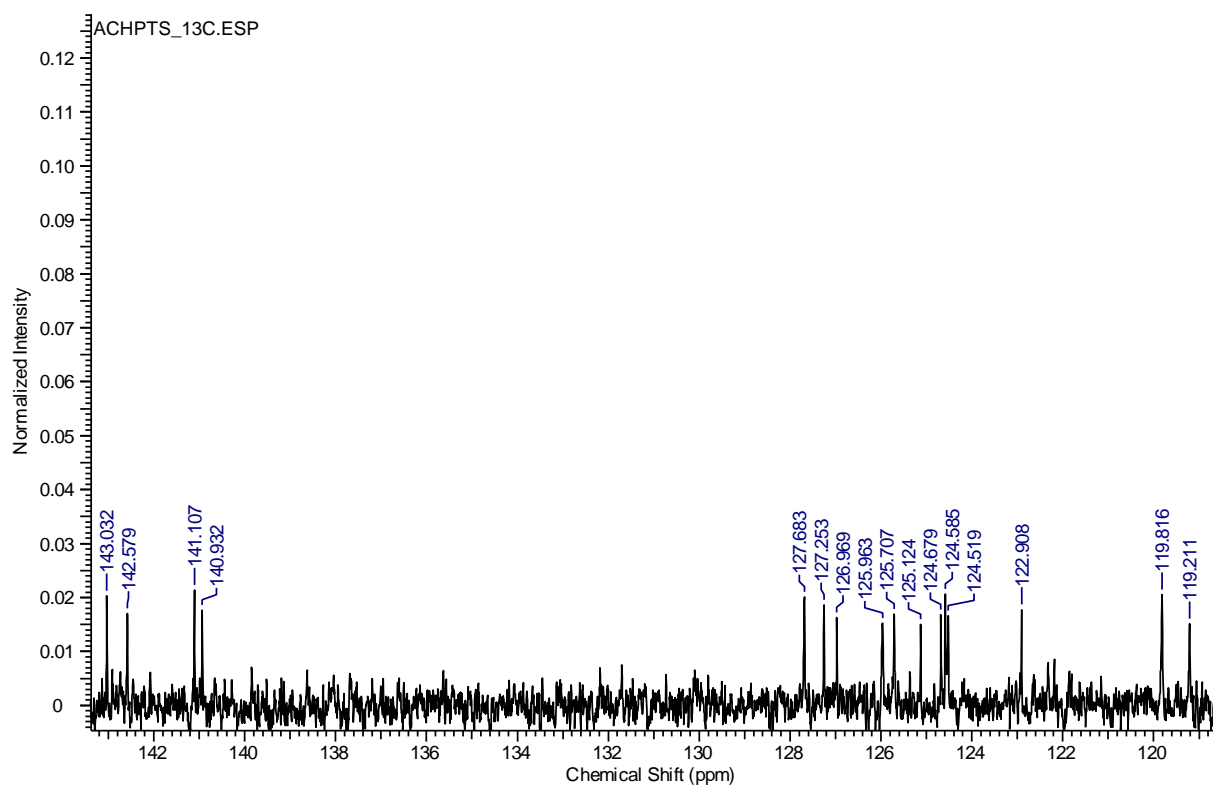
Figure S6: ^{13}C-NMR spectrum of **1** (zoomed).
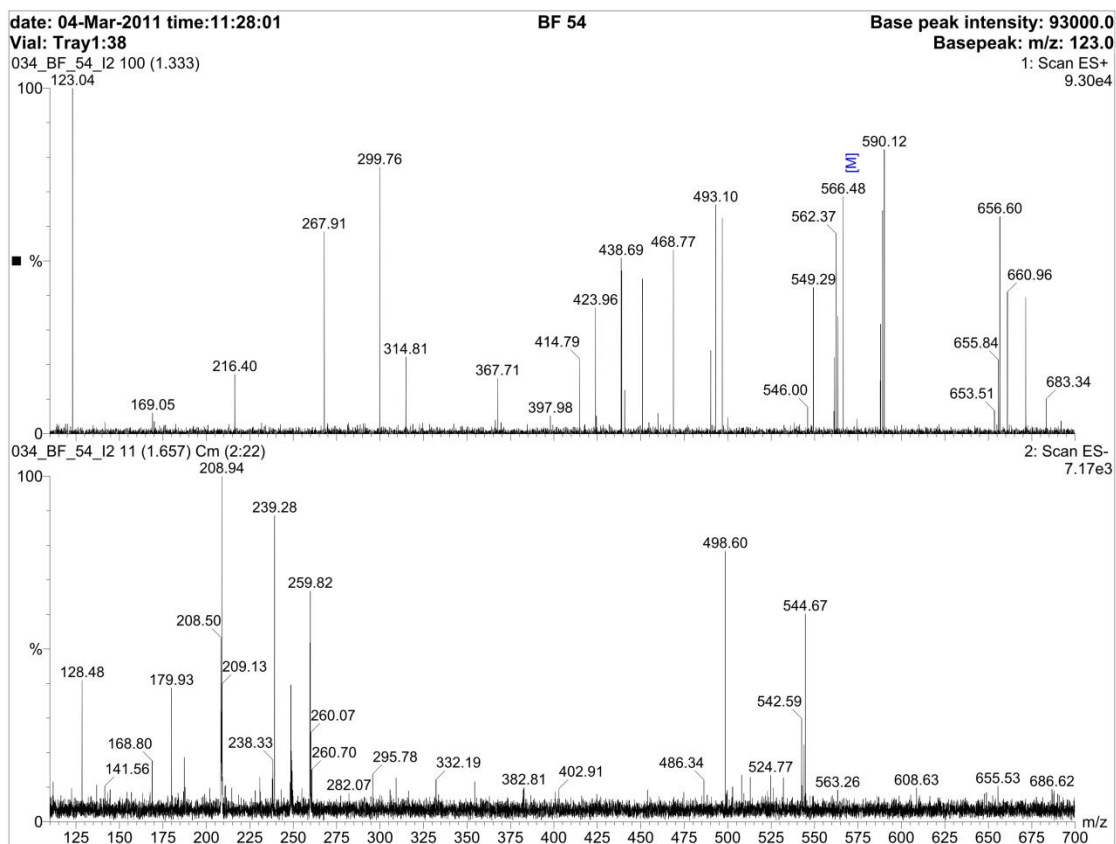
Figure S7: mass spectrum of **1**.
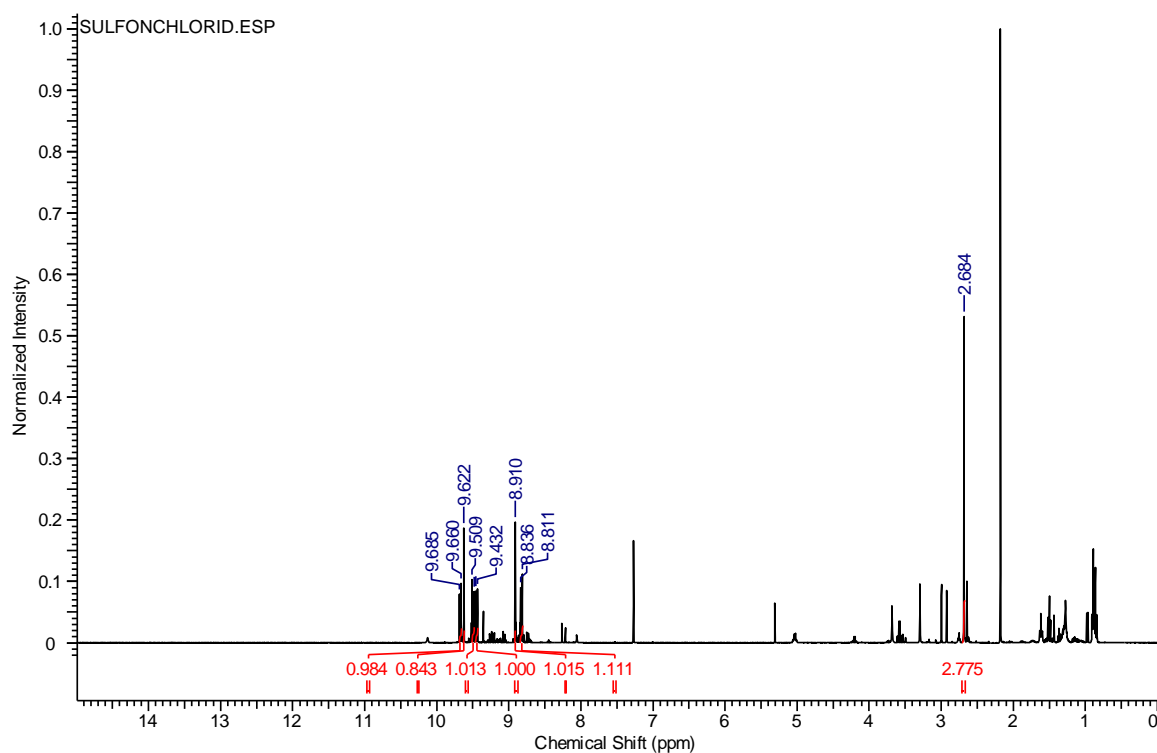
Compound **2**:

Figure S8: ^{1}H-NMR spectrum of **2**.
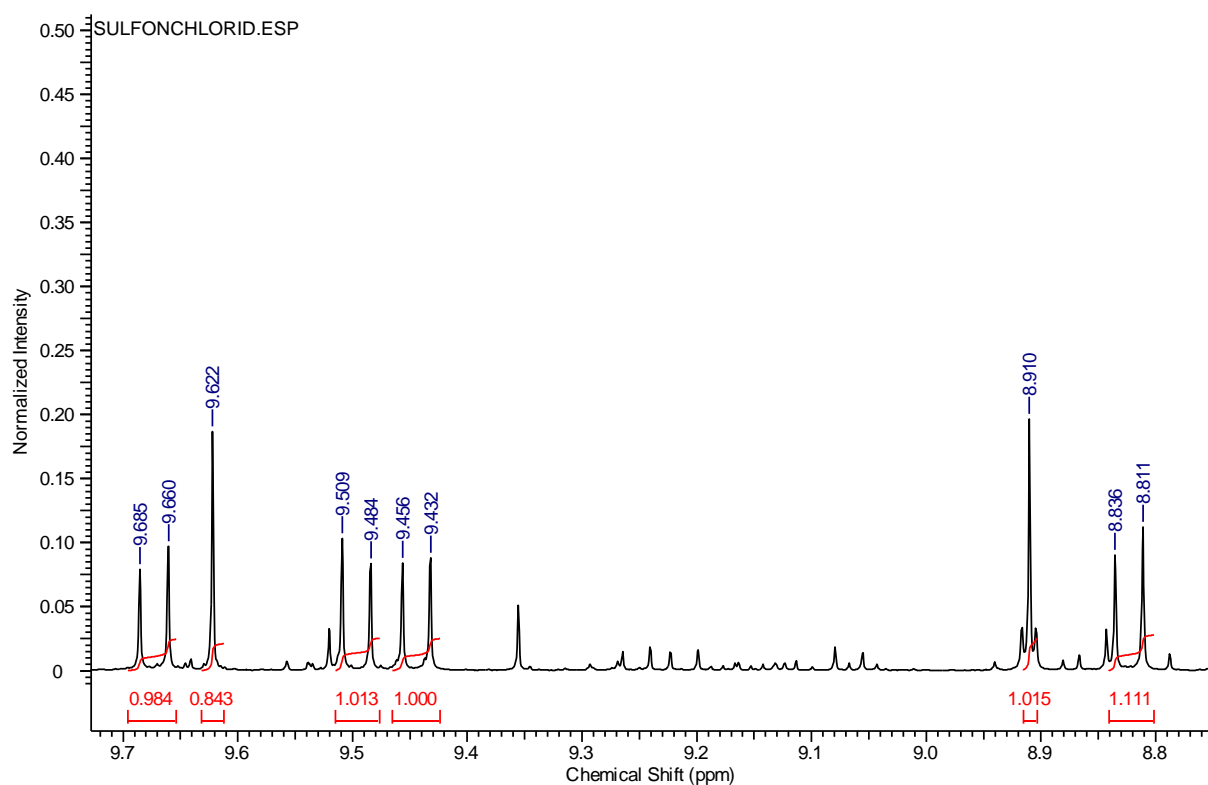
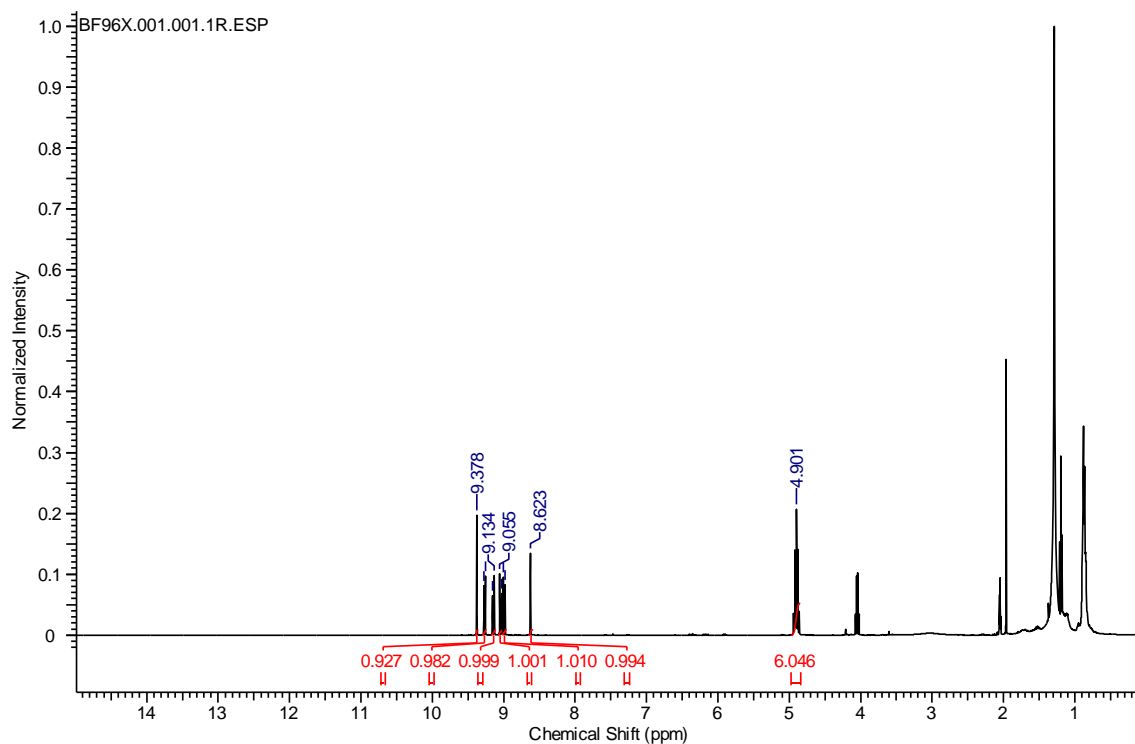Figure S9: ^{1}H-NMR spectrum of **2** (zoomed).
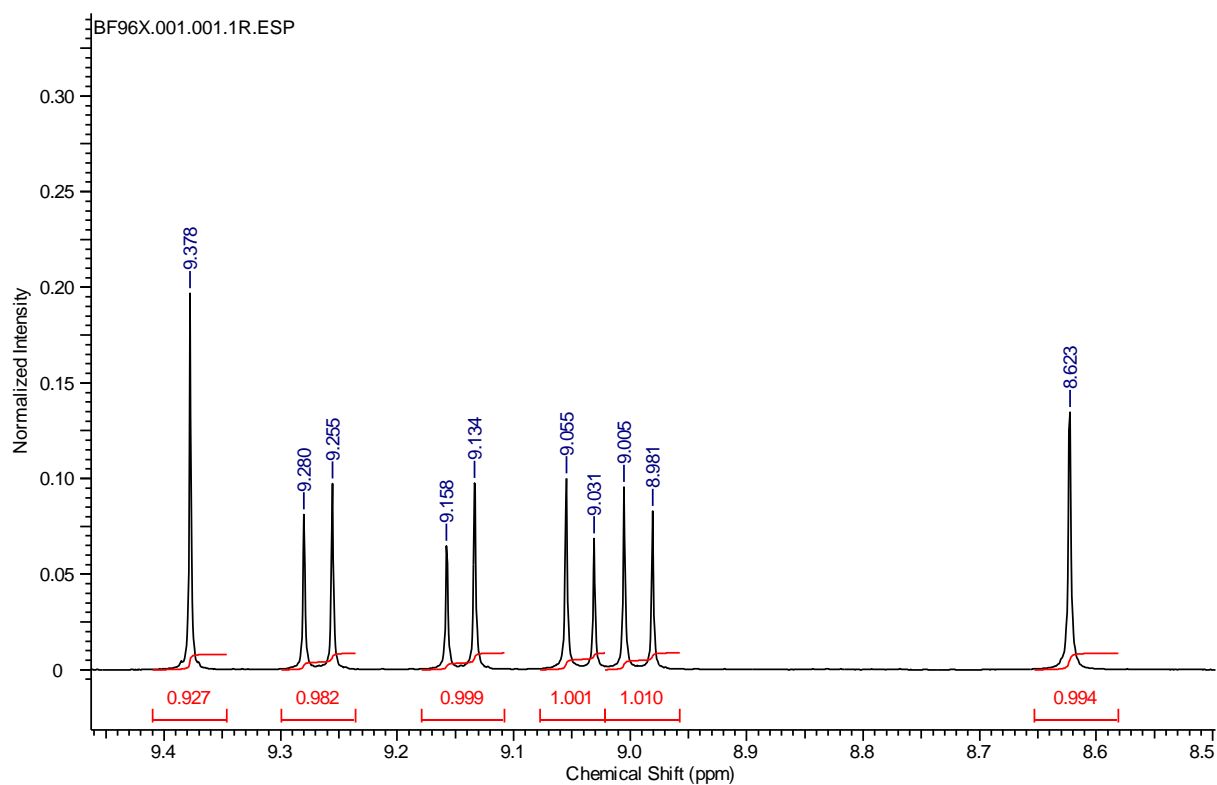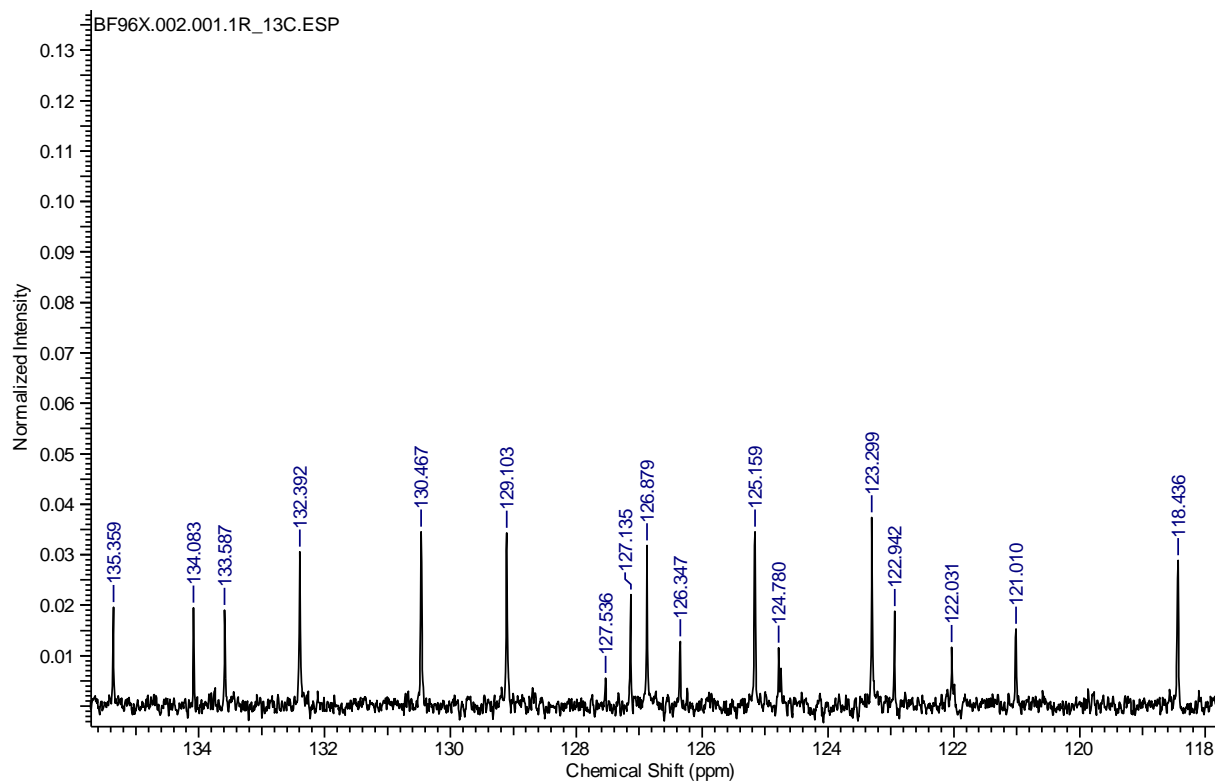
Compound **3a**:

Figure S10: ^{1}H-NMR spectrum of **3a**.

Figure S11: ^{1}H-NMR spectrum of **3a** (zoomed).
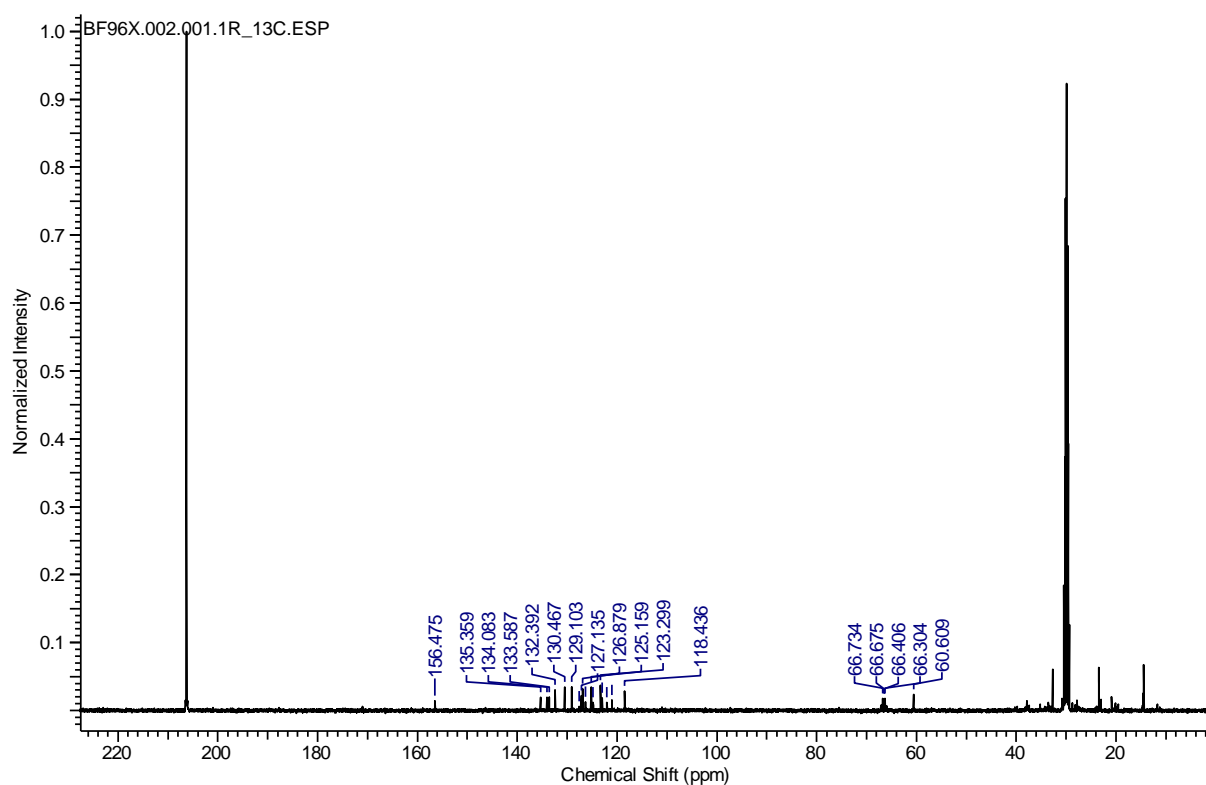
Figure S12: ^{13}C-NMR spectrum of **3a**.
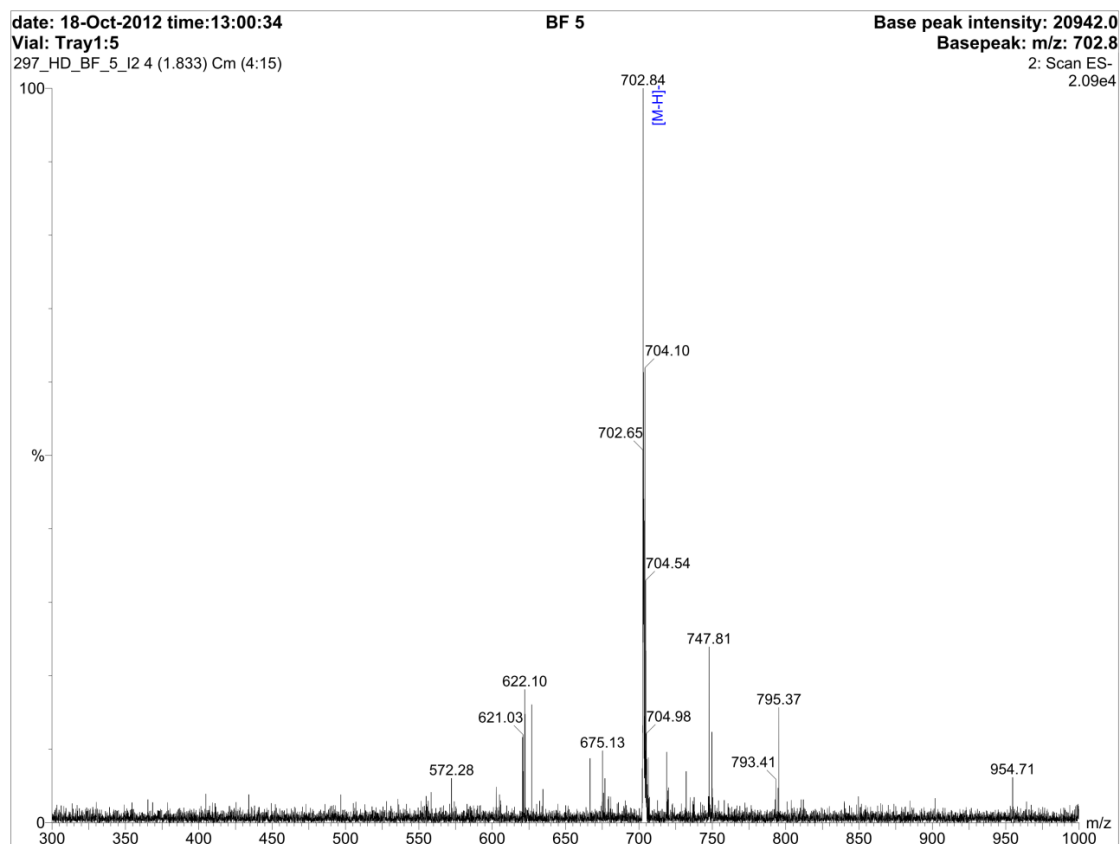
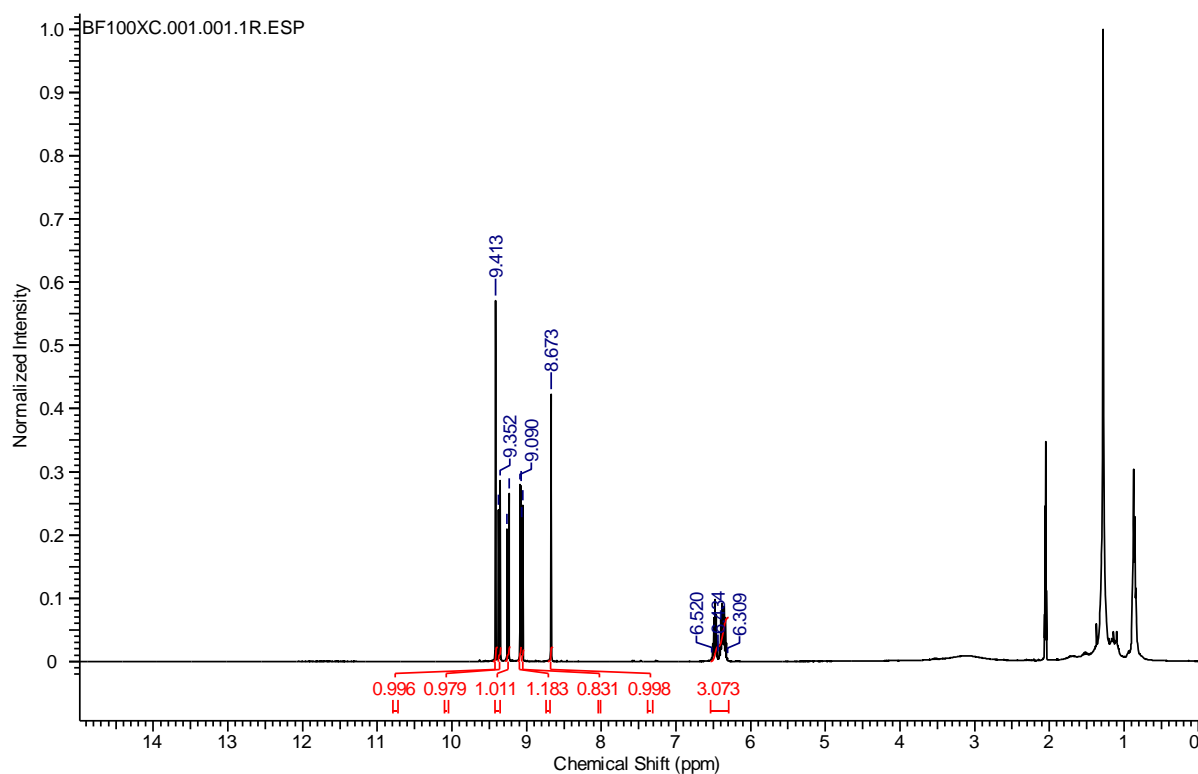

5

Figure S13: ^{13}C-NMR spectrum of **3a** (zoomed).

Figure S14: mass spectrum of **3a**.

5

10

Compound **3b**:

Figure S15: ^{1}H-NMR spectrum of **3b**.

Figure S16: ^{1}H-NMR spectrum of **3b** (zoomed).

Figure S17: ^{13}C-NMR spectrum of **3b**.

Figure S18: ^{13}C-NMR spectrum of **3b** (zoomed).
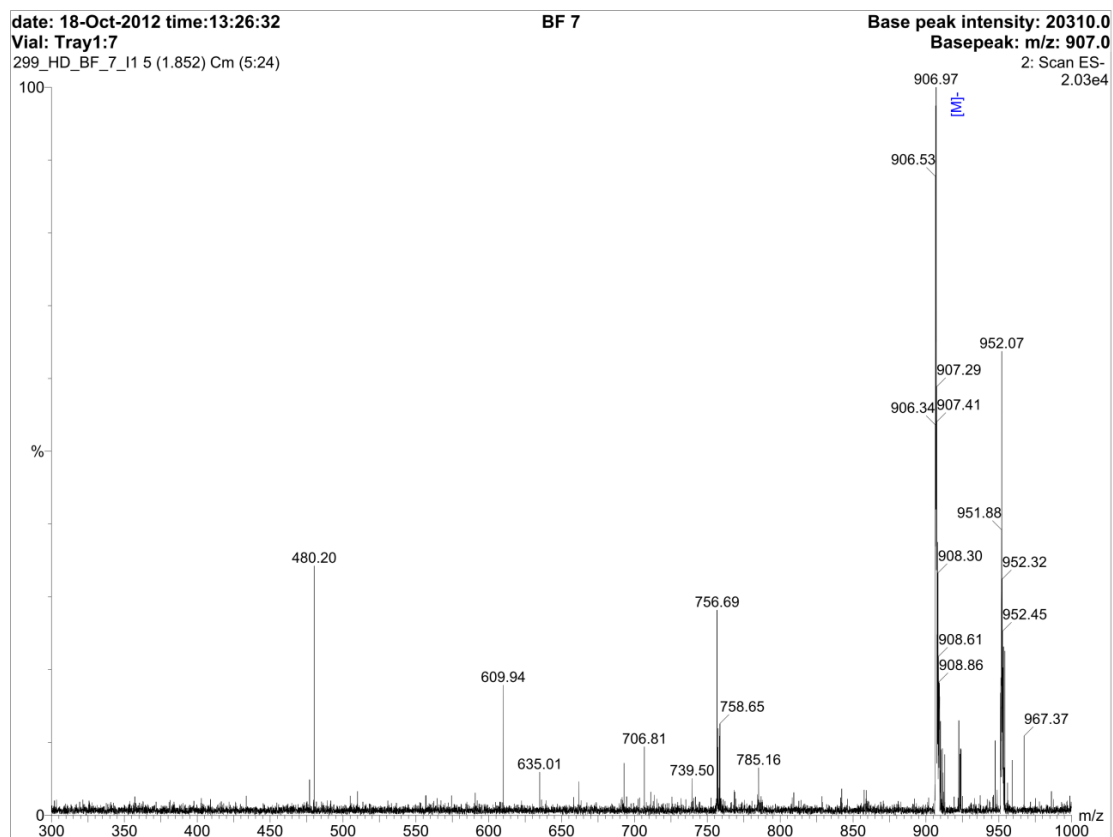
Figure S19: mass spectrum of **3b**.

5

10

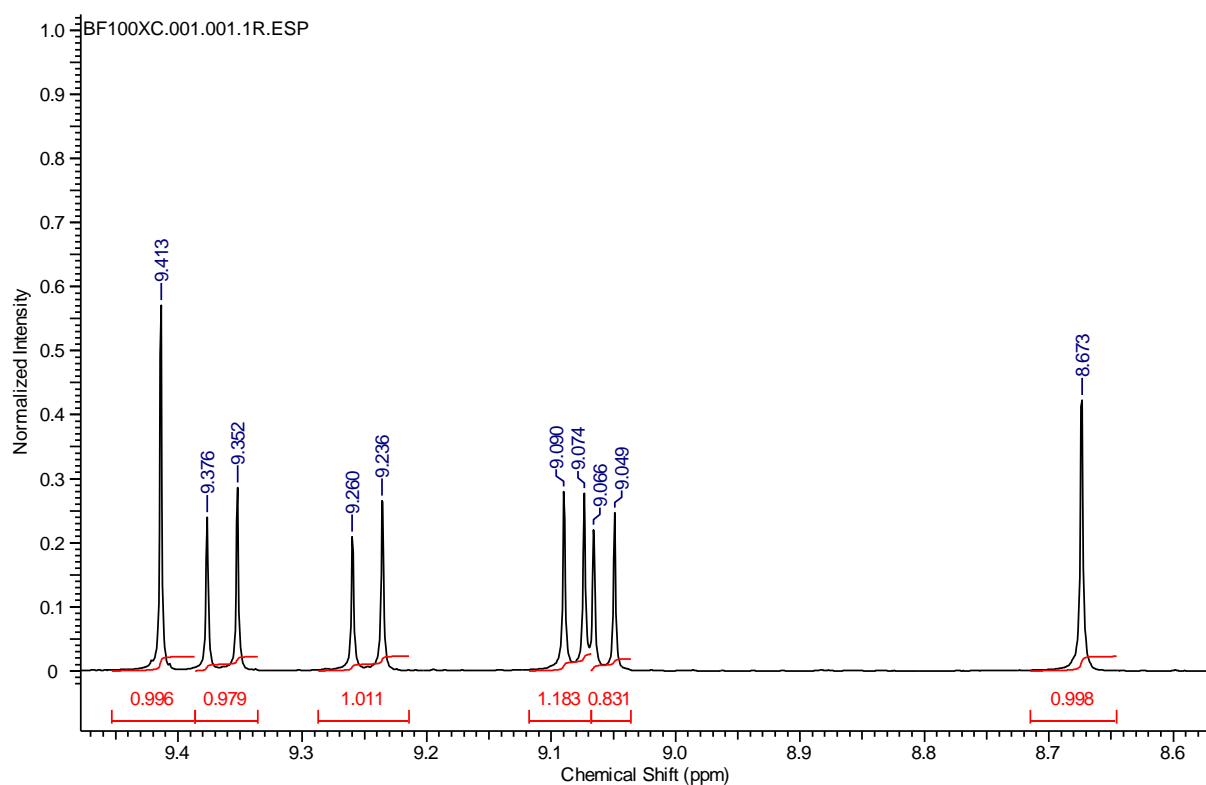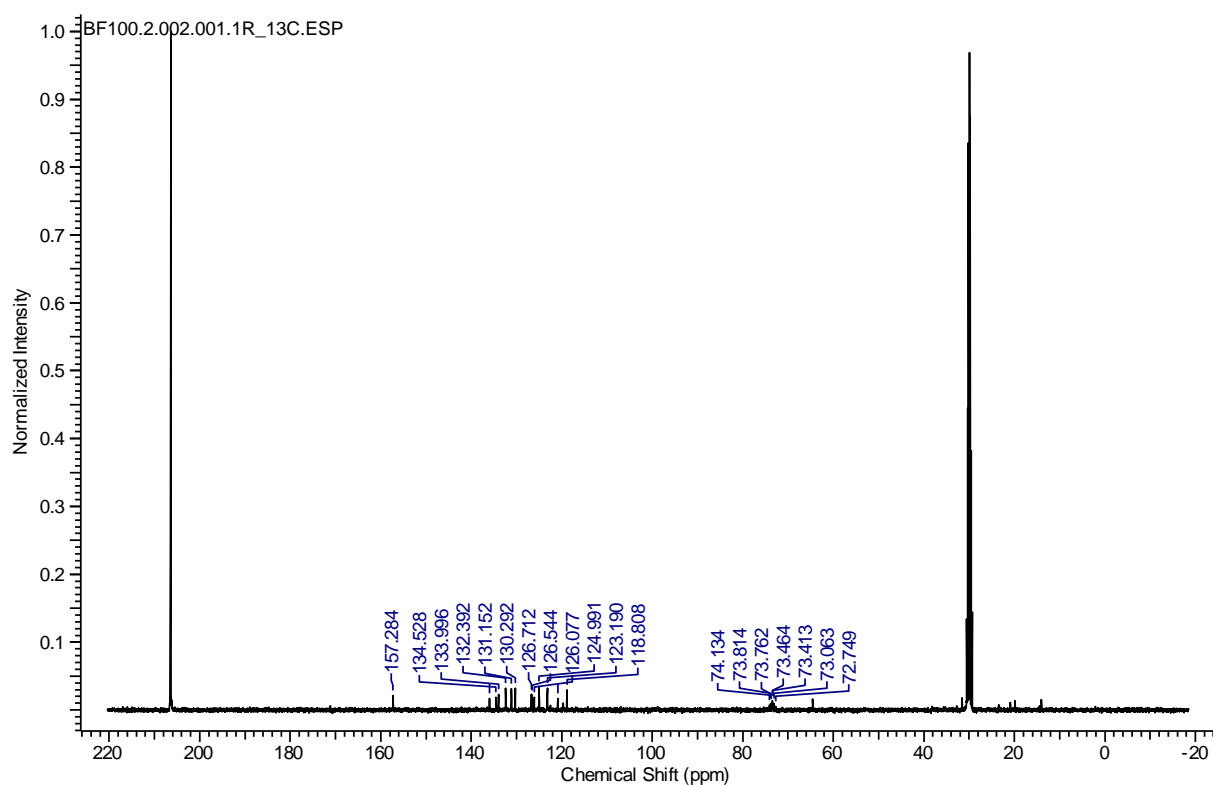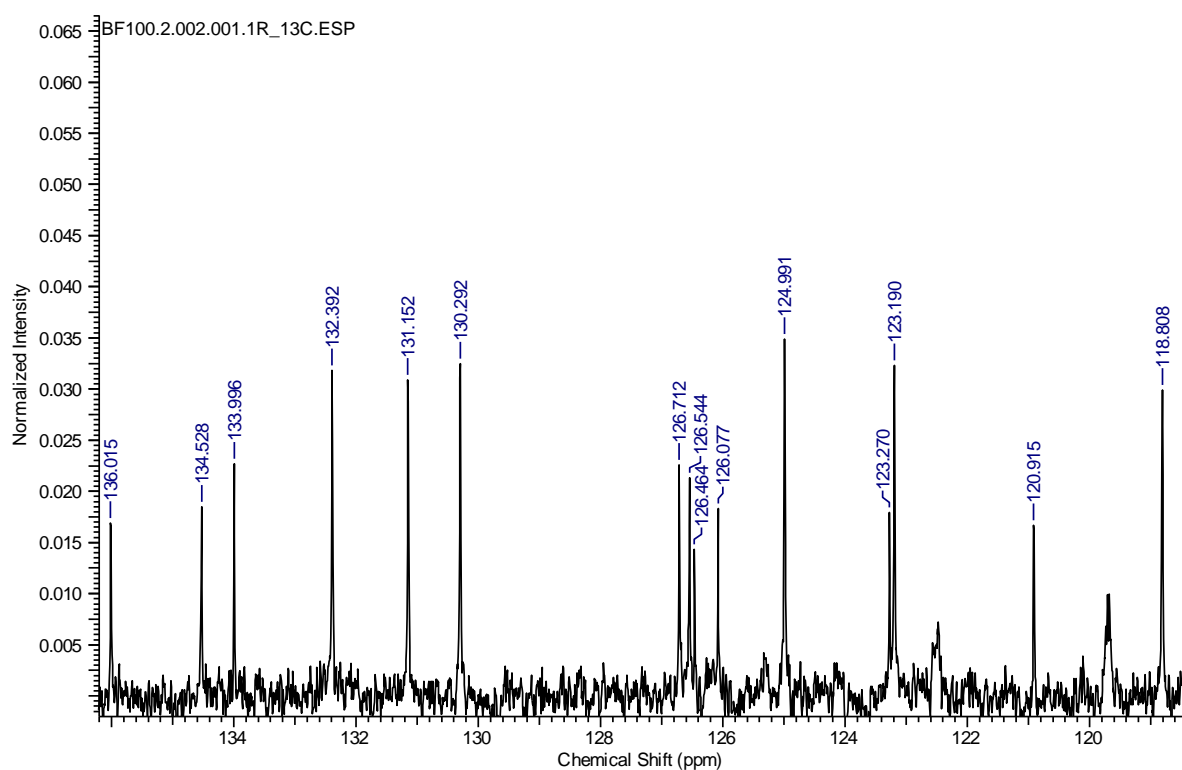Compound **3c**:

Figure S20: ^{1}H-NMR spectrum of **3c**.
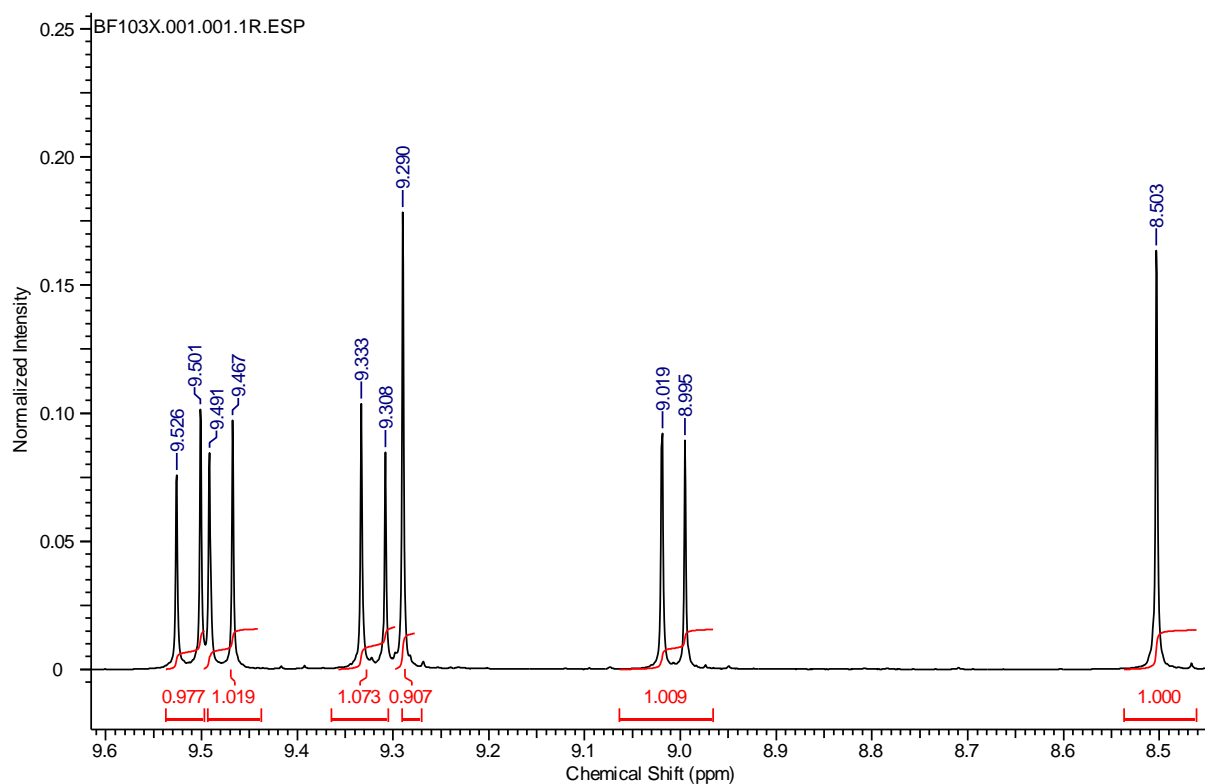
Figure S21: ^{1}H-NMR spectrum of **3c** (zoomed).
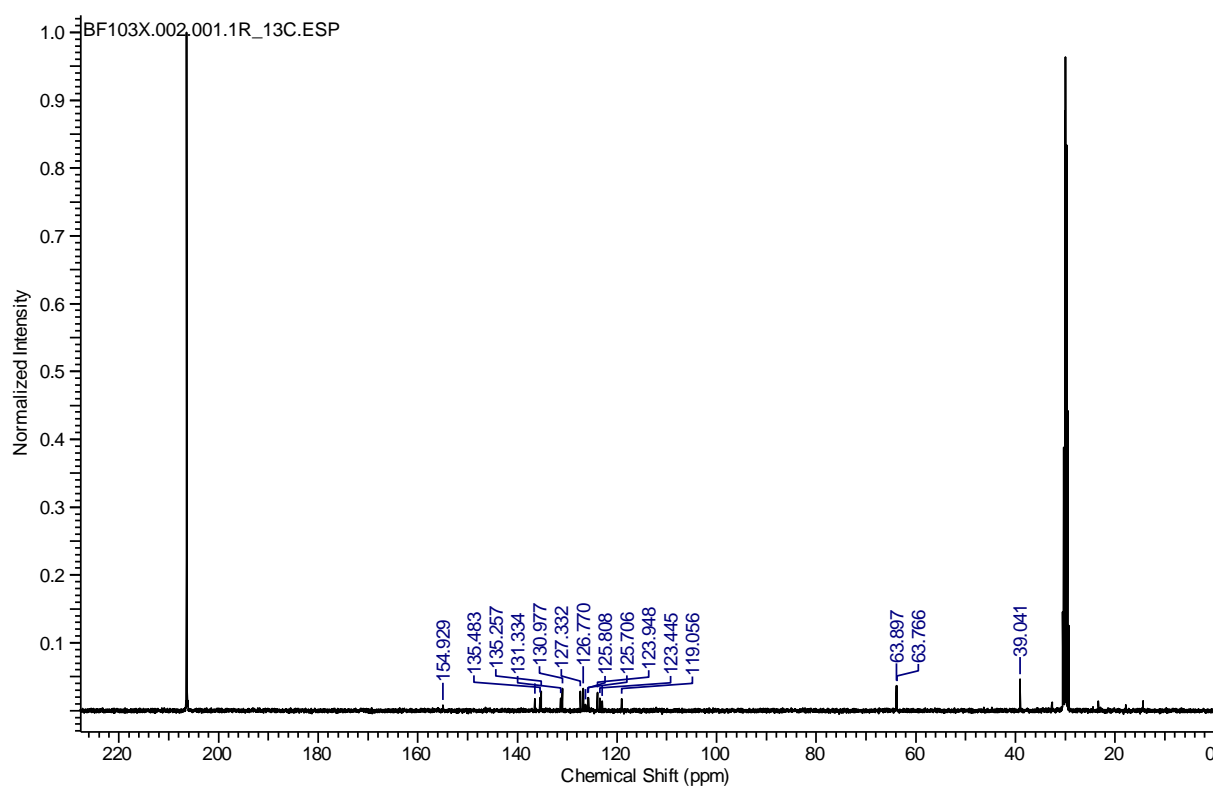
Figure S22: ^{13}C-NMR spectrum of **3c**.
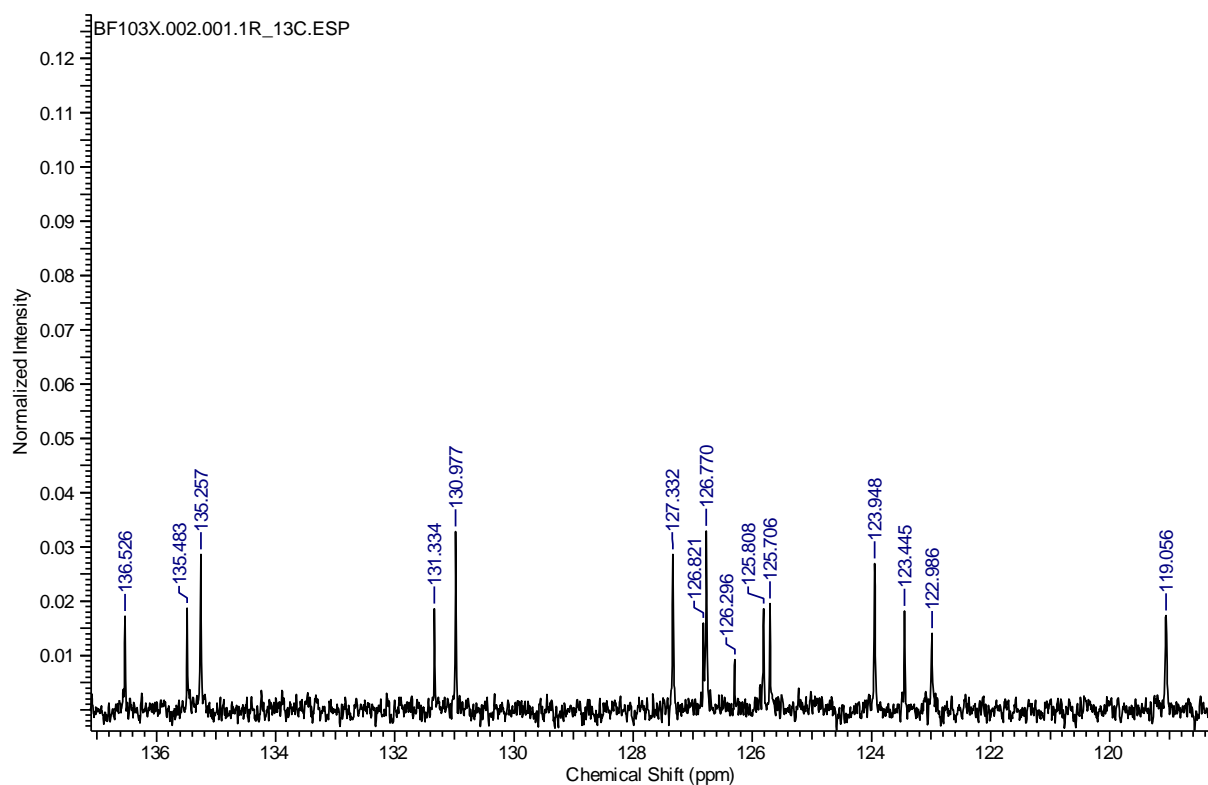
Figure 23: ^{13}C-NMR spectrum of **3c** (zoomed).
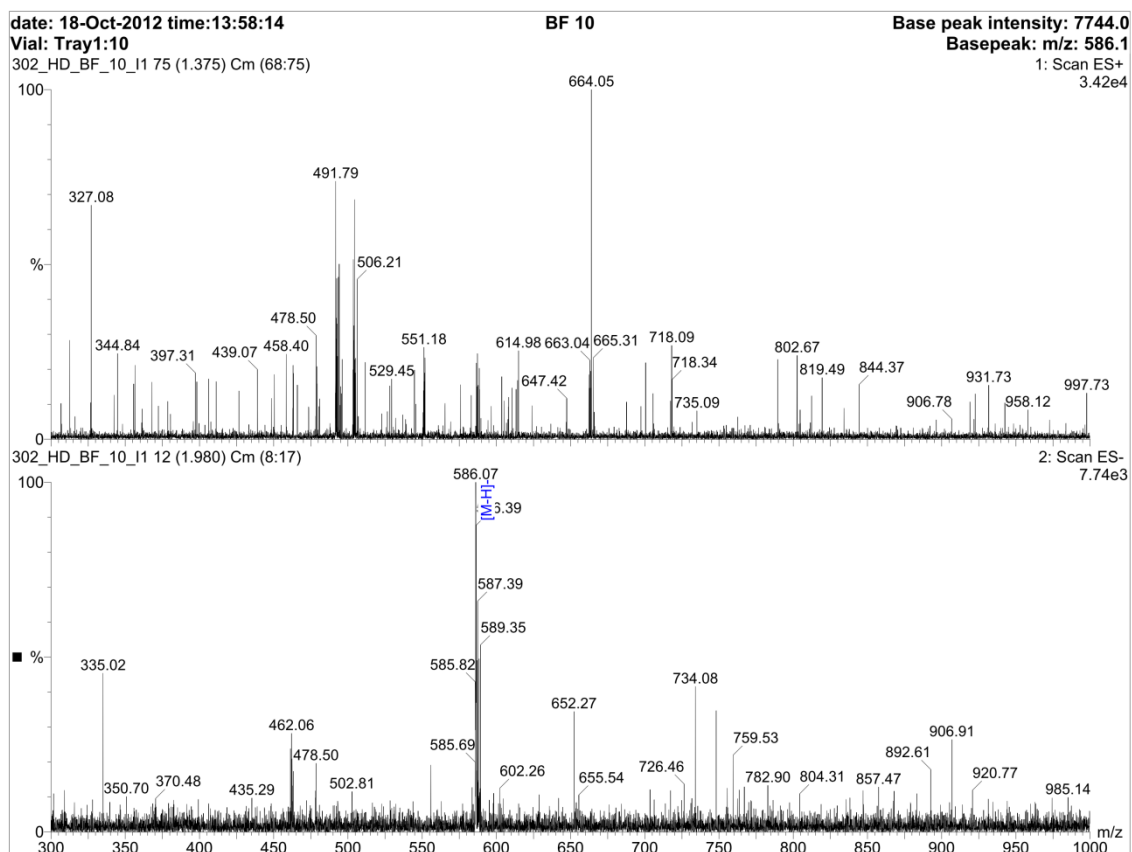
Figure S24: mass spectrum of **3d**.
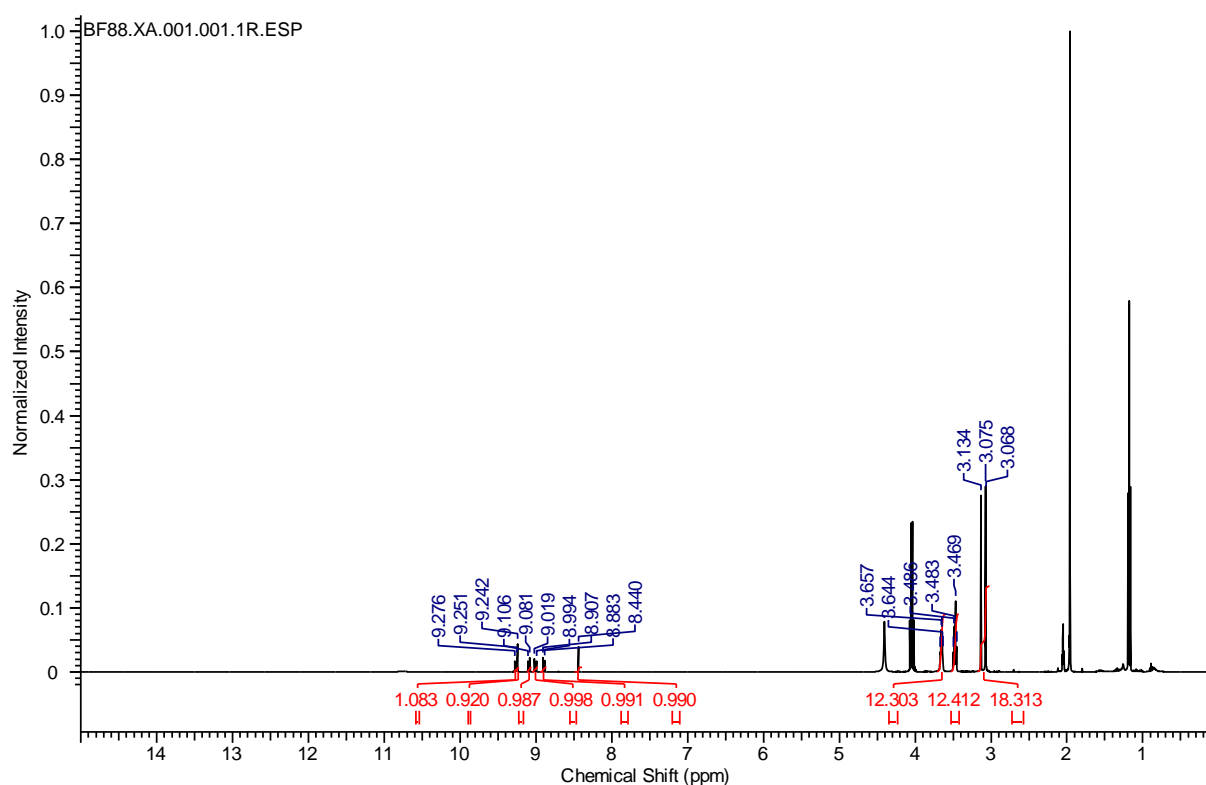
Compound **3d**:

Figure S25: ^{1}H-NMR spectrum of **3d**.
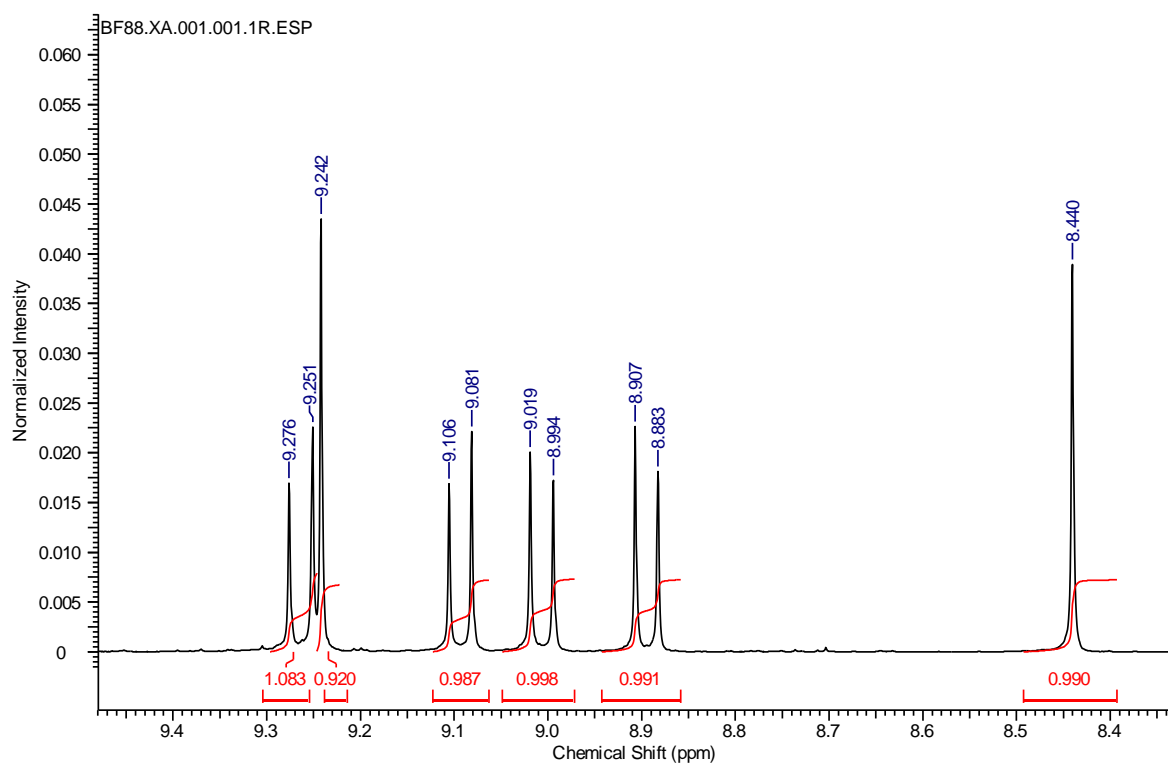
Figure S26: ^{1}H-NMR spectrum of **3d** (zoomed).
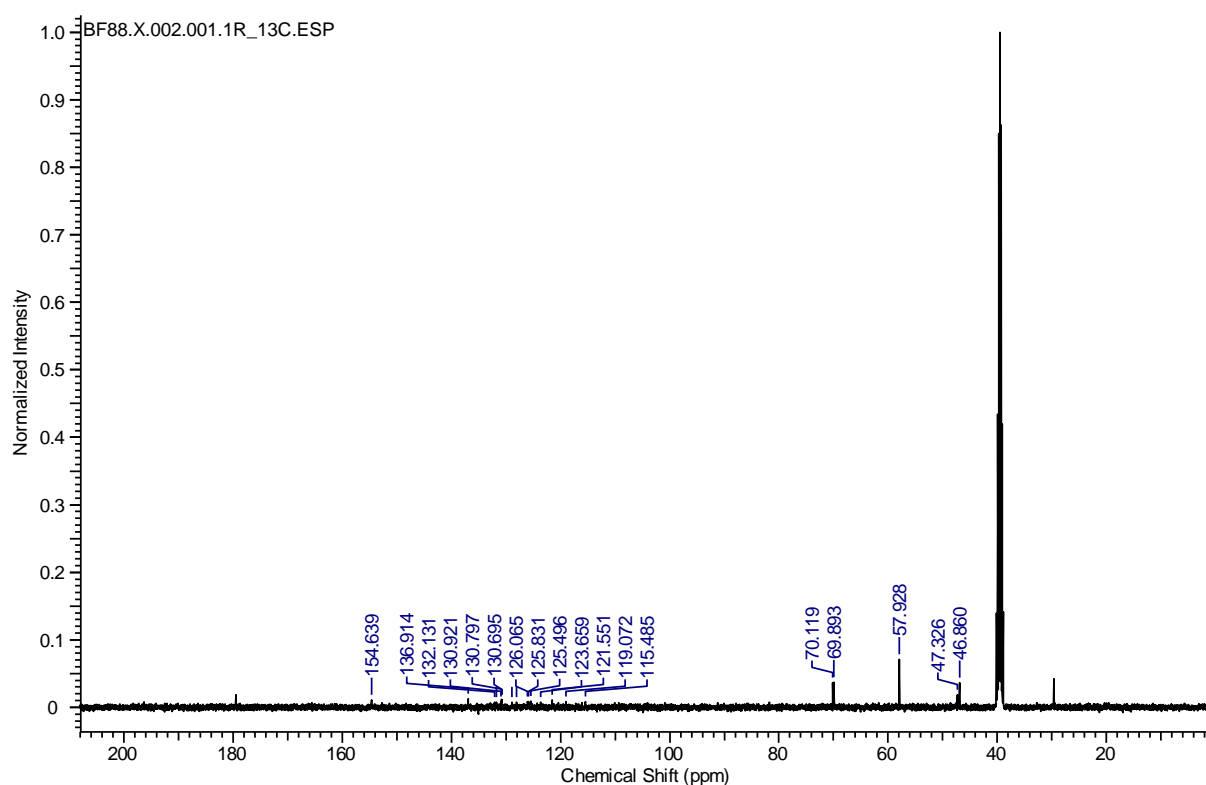
Figure S27: ^{13}C-NMR spectrum of **3d**.

Figure S28: ^{13}C-NMR spectrum of **3d** (zoomed).
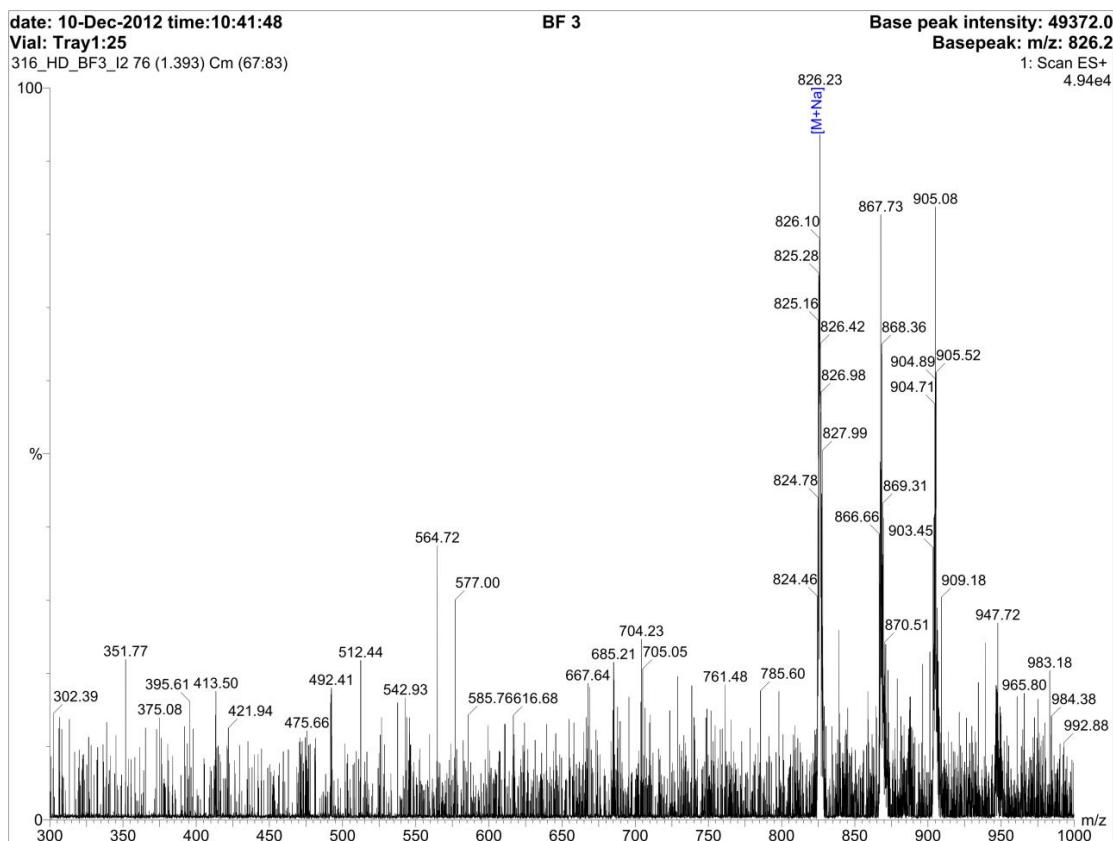
Figure S29: mass spectrum of **3d**.
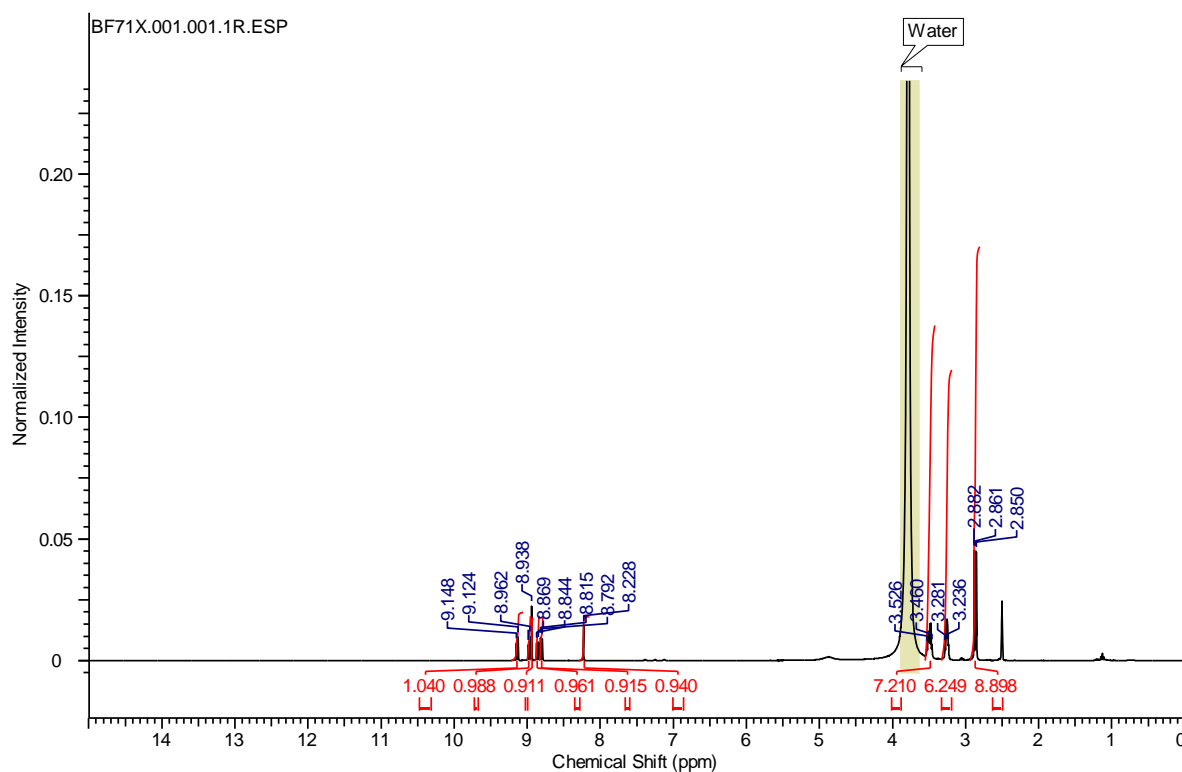
Compound **3e**:

Figure S30: ^{1}H-NMR spectrum of **3e**.

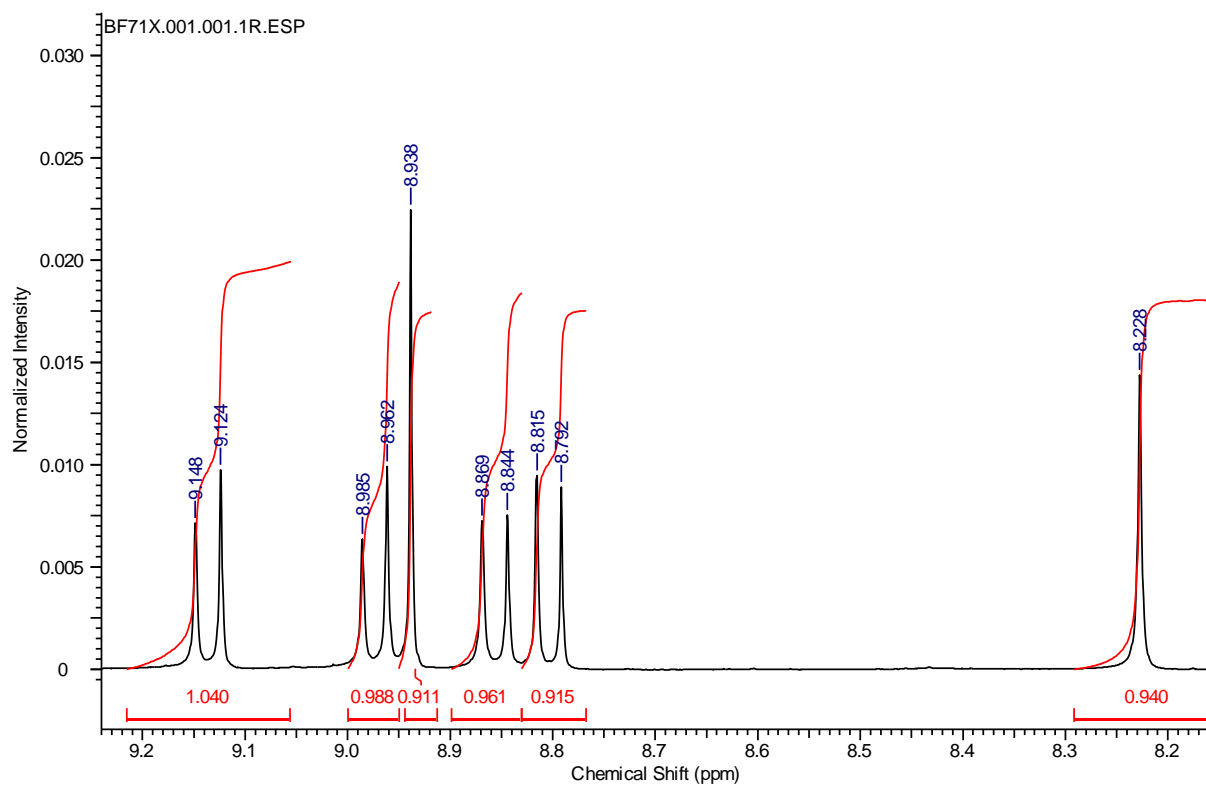
Figure S31: ^{1}H-NMR spectrum of **3e** (zoomed).
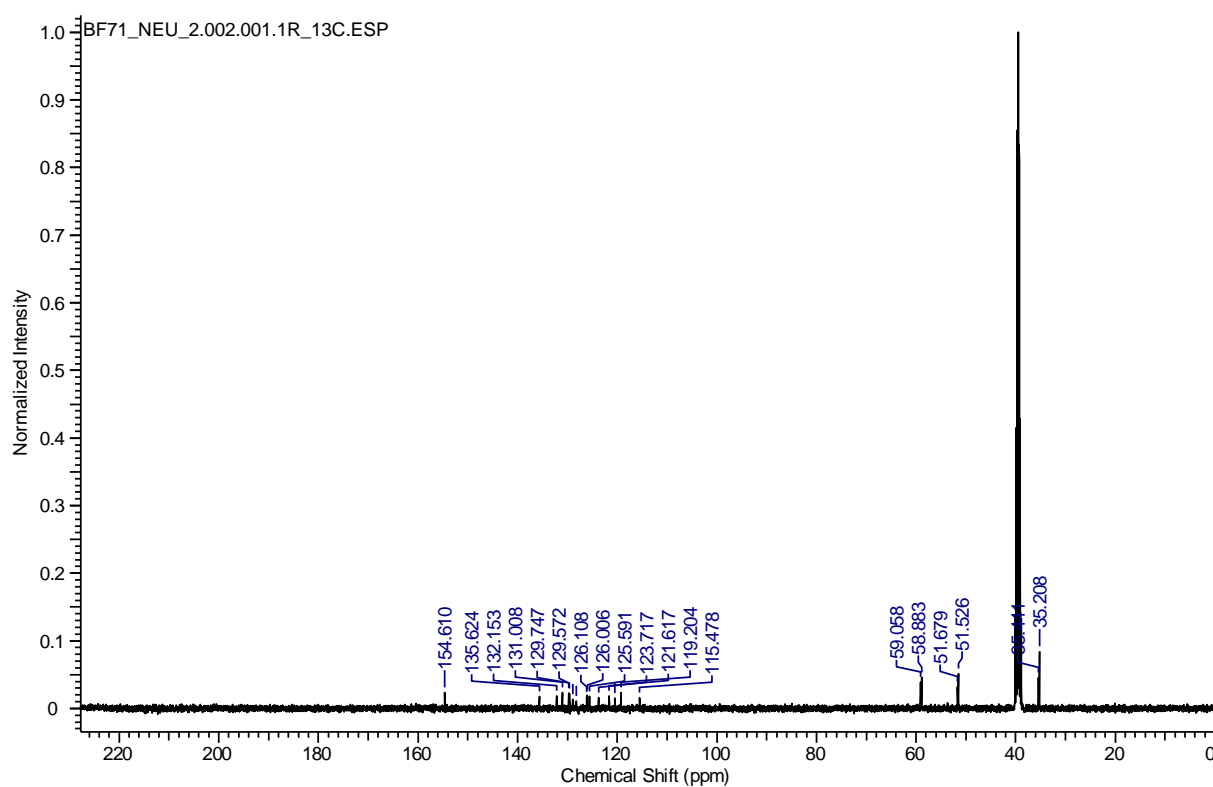
Figure S32: ^{13}C-NMR spectrum of **3e**.
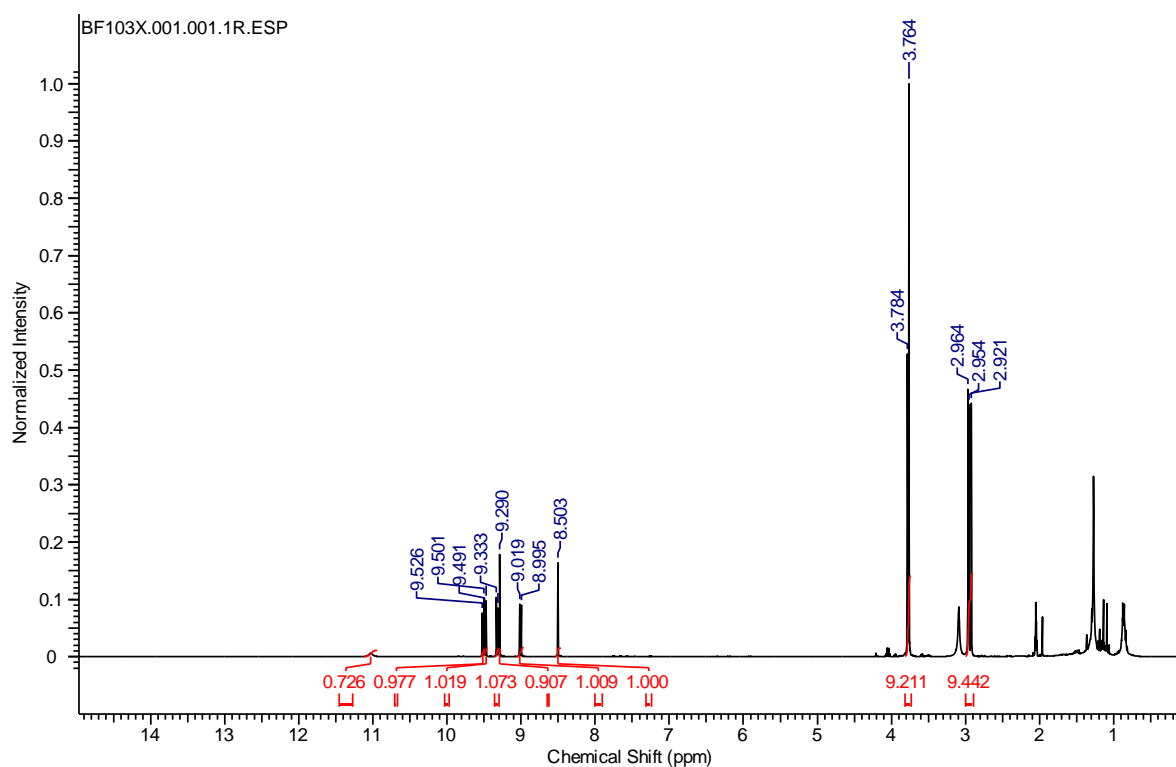
Figure S33: ^{13}C-NMR spectrum of **3e** (zoomed).

Figure S34: mass spectrum of **3e**.

Compound **3f**:

Figure S35: ^{1}H-NMR spectrum of **3f**.

Figure S36: ^{1}H-NMR spectrum of **3f** (zoomed).

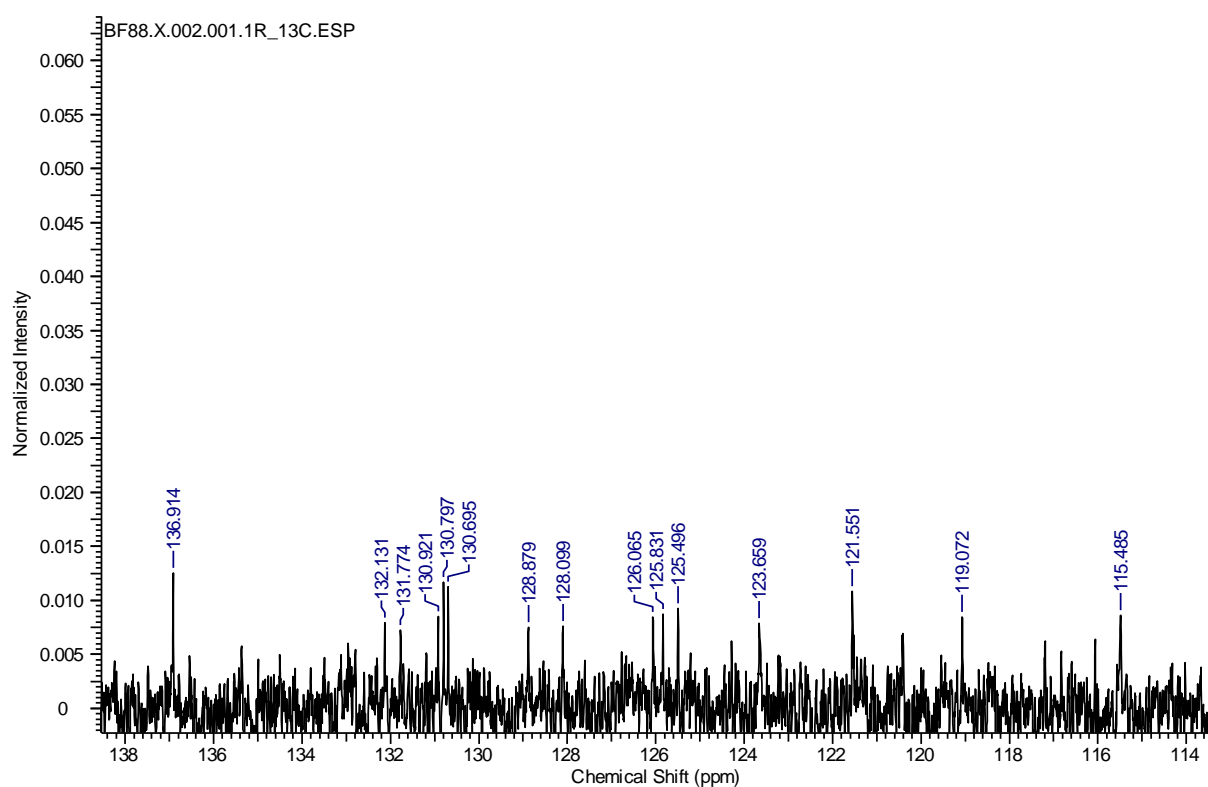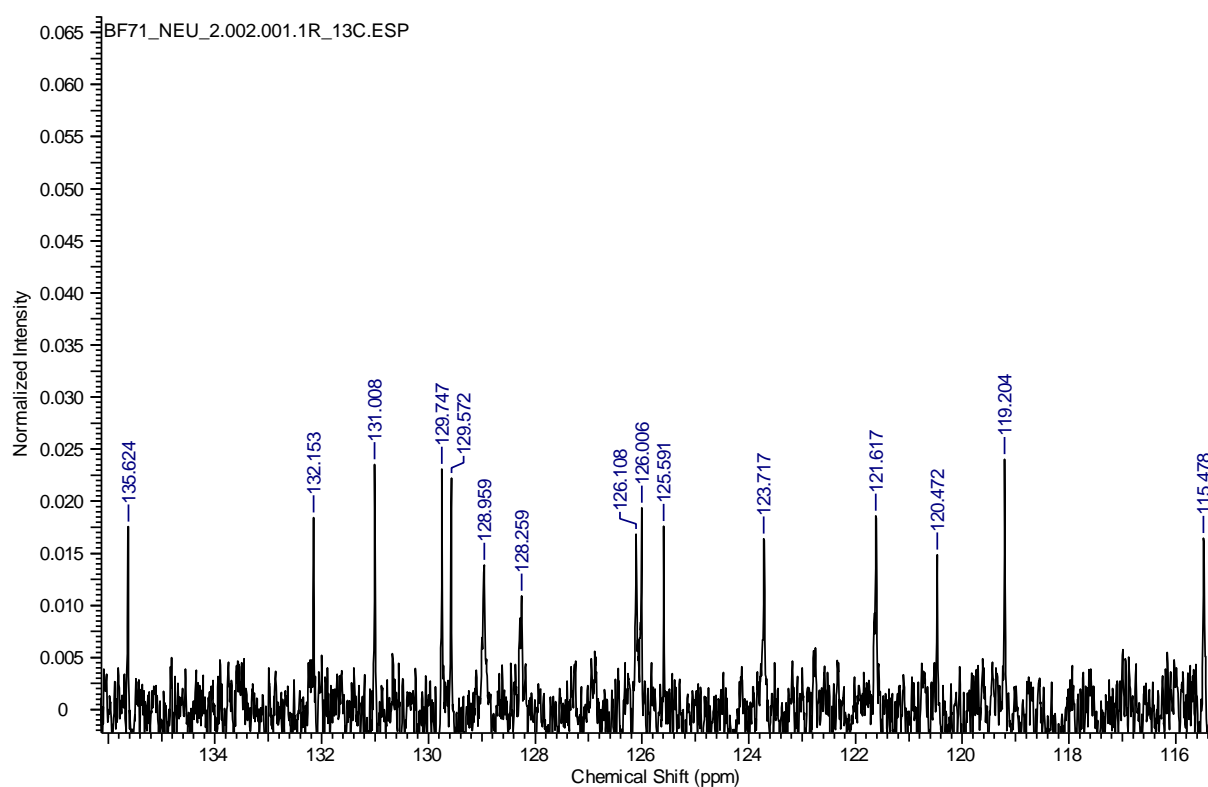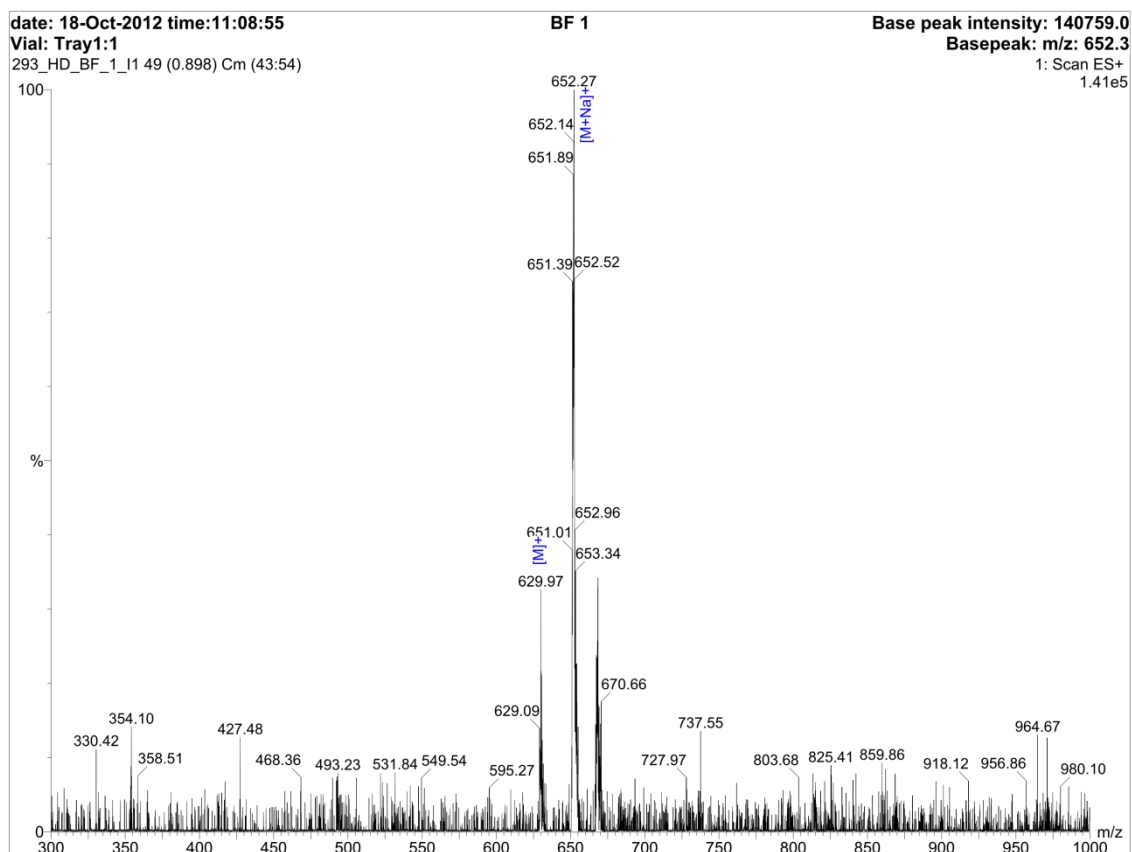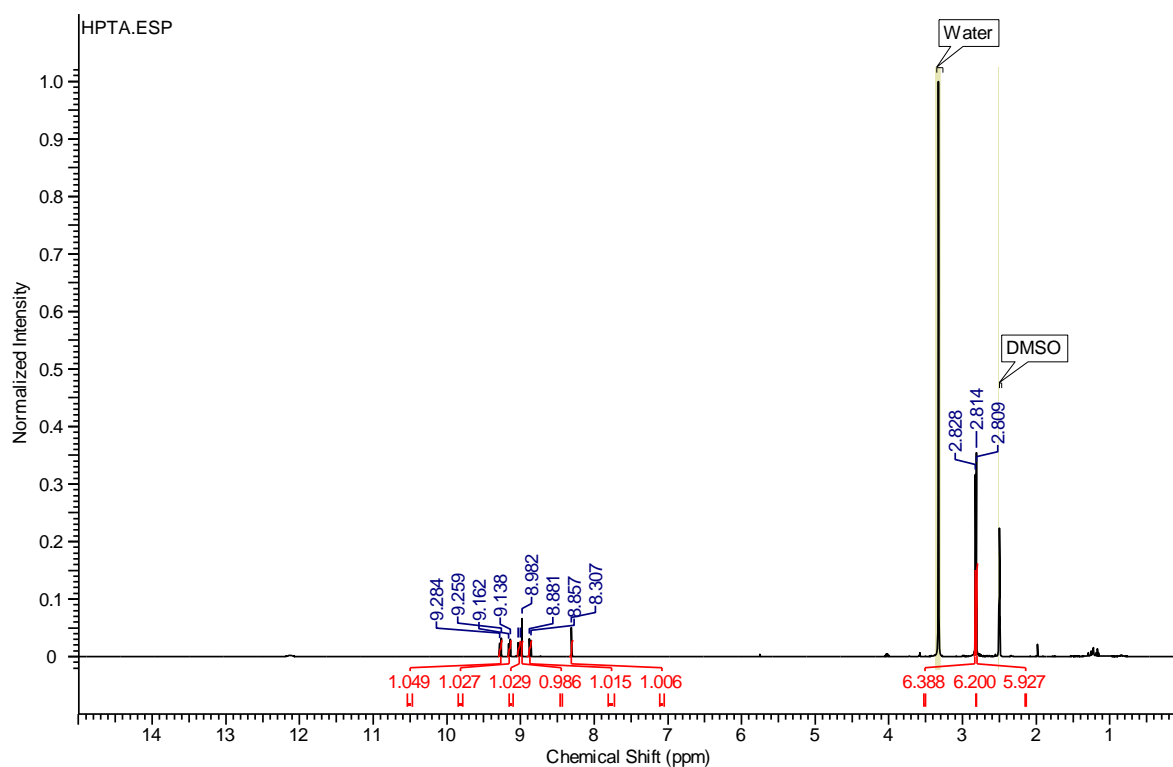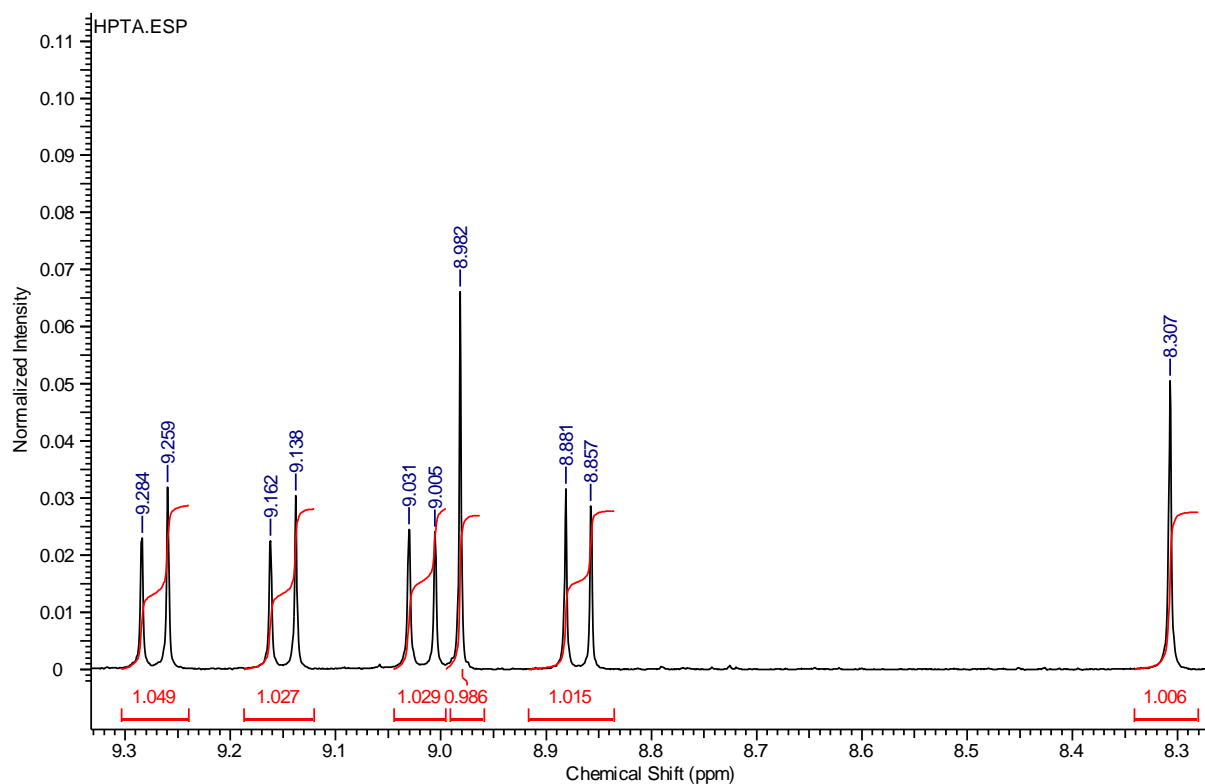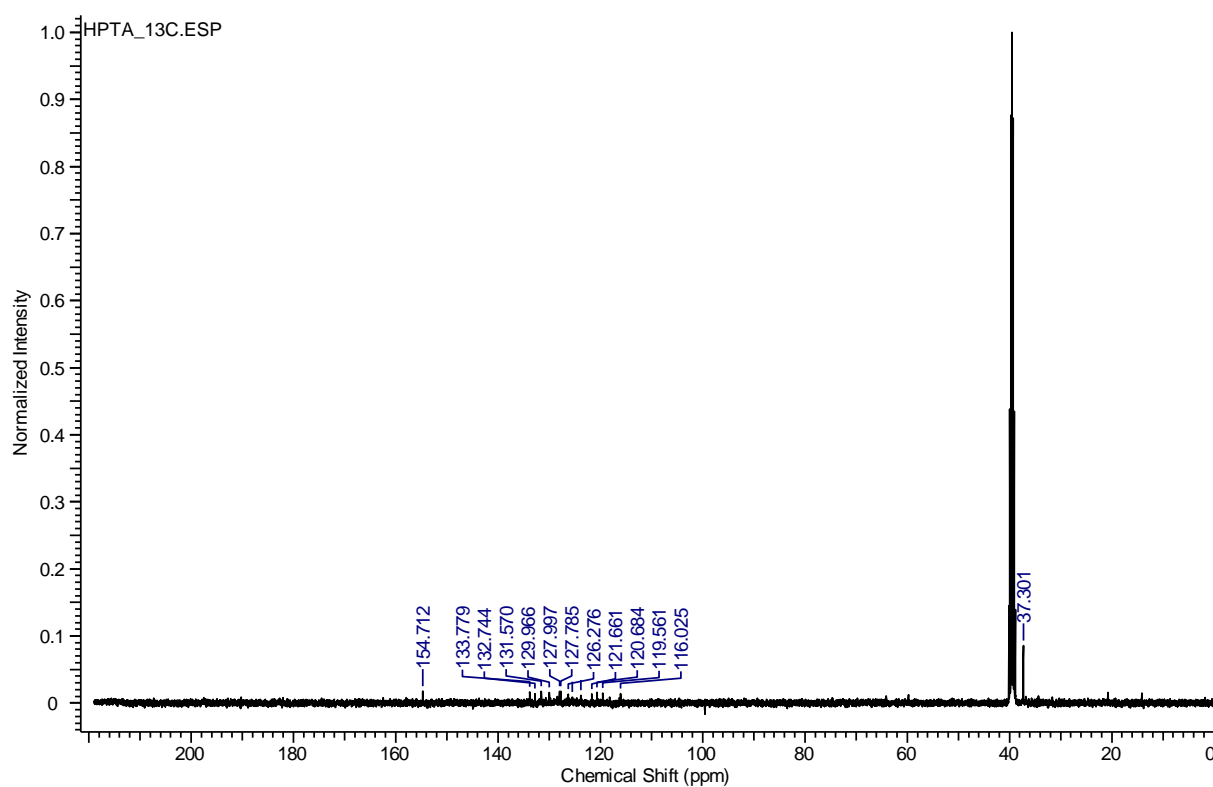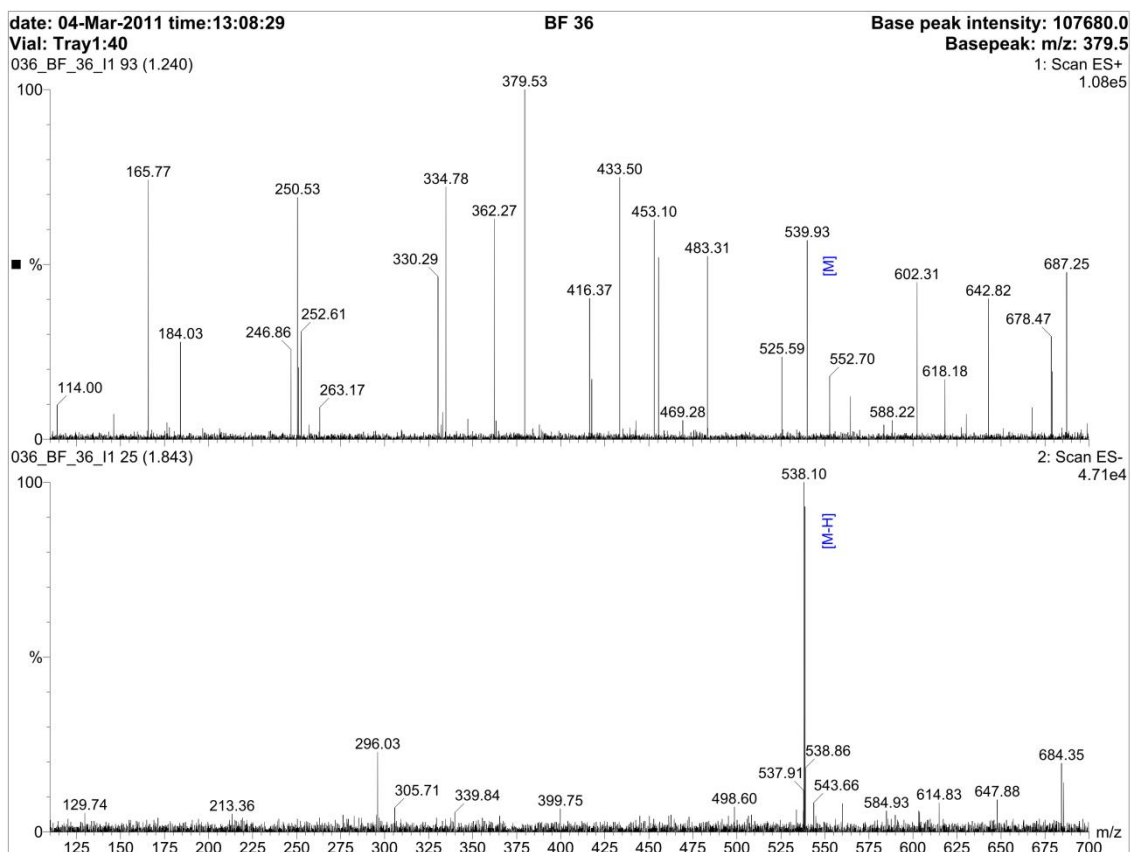Figure S37: ^{13}C-NMR spectrum of **3f**.

Figure S38: mass spectrum of **3f.**

References:

[S1] J. Widengren, B. Terry, R. Rigler, *Chem. Phys.* **1999**, *249*, 259–271.

5

Solvatochromism of pyranine-derived photoacids

Christian Spies,[a] **Björn Finkler,**[a] **Nursel Acar**[b] **and Gregor Jung** [*,a]

₅ **ABSTRACT**

Photoacidity is frequently met in aromatic alcohols where the equilibrium dissociation constant increases by some order of magnitudes upon electronic excitation. In this study we investigated the solvatochromism of a family of recently synthesized super-photoacids and their methylated counterparts based on pyrene. The chemical similarity of these molecules on ₁₀ the one hand and their differing photoacidity with pK_a* values between -0.8 and -3.9 on the other allows for gaining insights into the mechanisms contributing to excited-state proton transfer. Three different solvent scales, namely Lippert-Mataga, Kamlet-Taft and Catalán were independently employed in this study and gave consistent results. We found the strongest correlation of the excited-state acidity with the dipolarity of the excited state, p_{em} ₁₅ ranging from -1775 cm^{-1} to -2500 cm^{-1}, and a concomitant change of the permanent dipole moment of roughly 14 Debye. Spectral changes due to varying basicity of the solvent, which probes the conjugated property of the solute, are found to be less indicative for the graduation of excited-state acidity, i.e. b_{em} values between -700 and -1200 cm^{-1}. The solvent acidity is the only parameter with distinct influence on the electronic spectra of the deprotonated species. ₂₀ The low values of a_{em} ~ 400 cm^{-1} which are 3-4x smaller than a_{abs} and a_{exc}, are monitoring the low basicity of these species in the excited state. Triggered by semiempirical theoretical calculations, the energetic splitting between the two lowest excited states could be related to the excited-state acidity and points to alterations in the electronic mixing of locally excited and charge-transfer states, raised by the substituents. Differences between the threefold ₂₅ negatively charged pyranine and the new neutral photoacids are also discussed.

Introduction

Since its first description by Förster in 1949[1], excited-state proton transfer (ESPT) has gained widespread attention.[2-5] ₃₀ Especially aromatic alcohols have proven to be a valuable tool to investigate the mechanism of proton transfer as they can easily be observed by absorption and fluorescence spectroscopy. Upon electronic excitation the usually weak acids undergo an increase in acidity by some order of ₃₅ magnitudes and are capable of transferring a proton to a suitable acceptor. The underlying reasons for the enhanced excited-state acidity have been subject of research for more than two decades and have been reviewed many times.[2-4, 6, 7] Beside intramolecular charge redistribution[8-11], the ₄₀ influence of the solvent on the excited-state acidity has been intensively studied.[12-15]

Photoacidity is a frequent phenomenon, and many dye molecules[16-20] and proteins[21, 22] are known for releasing a proton in the excited state. The most intensively studied ₄₅ photoacids are those based on naphthol. The good UV-absorption along with their well-known electronic properties makes them well suited to investigate the important ESPT parameters, such as the nature of substituents and their position.[8, 23-29] Another paradigmatic ₅₀ photoacid is 8-hydroxypyrene-1,3,6-trisulfonate (HPTS, pyranine) which exhibits absorption and emission in the

visible part of the electromagnetic spectrum and a high water solubility.[13, 30-36]

ESPT of these photoacids to bases[32, 37] or the solvent[38-40] ₅₅ has been reported. In most examples, the proton-accepting solvent is water because of its high polarity and unique tendency to accept and stabilize protons in a hydrogen-bonding network. Only few molecules with an excited-state acidity constant pK_a* below zero are described, which can ₆₀ transfer the proton to polar, aprotic organic solvents such as dimethyl sulfoxid (DMSO).[41, 42] These so-called "super-photoacids" may offer further insights into a proton transfer mechanism in aprotic environments.[41, 43-46] Further investigations were dedicated to the effects of ₆₅ temperature[18, 36, 47-53], pressure[54], salt concentration[37, 55, 56] or solvent composition[17, 57, 58] on the ESPT process.

The use of time-resolved spectroscopy has given many insights in the mechanism and the dynamics of proton transfer.[16, 34, 59-66] A convenient approach to study the ₇₀ interaction between a probe and the solvent using steady-state spectroscopy is the solvatochromic analysis.[44, 67-72] Absorption and emission wavelengths are collected in different media and correlated to solvent parameters from which solute properties can be deciphered. While ₇₅ absorption spectra are useful for the investigation of ground state properties, emission spectra contain information about the relaxed excited state. Therefore, different solvatochromic shifts of absorption and emission

wavelengths indicate differing interactions in both states.

Many solvatochromic scales have been developed, including empirical scales and those based on physicochemical solvent parameters.[73] An example for the latter is the Lippert-Mataga equation, which correlates the Stokes shift Δv to the solvents relative permittivity ε_r and refractive index n (see experimental section, Equation 1).[74-76] It is used to calculate the change of the static dipole moment of a molecule upon electronic excitation. More detailed information is obtained by empirical multi-parameter approaches that can take account of specific solute-solvent interactions, e.g. hydrogen bonds. Most common are those scales introduced by Kamlet and Taft[77] (Equation 2) and, more recently, by Catalán[78] (Equation 3). Especially the Kamlet-Taft scale has been often used to explore the important parameters for ESPT.[67, 69, 70, 79-81] However, a systematic investigation with a series of similar photoacids that differ in their excited-state acidity is still missing.

In a parallel publication, we report and characterize a new series of highly photostable photoacids with varying photoacidity derived from pyranine.[82] Whereas their ground state pK_a values do not show much alteration, with values between 4.4 and 5.7, their excited state acidity constants pK_a^* vary systematically between -0.8 and -3.9 as computed from spectroscopic data. The present paper provides insight how these photoacids differ in their ESPT ability and describes the important solvent-solute interactions. To accomplish this task we performed a comprehensive solvatochromic analysis of six photoacids and semi-empirical AM1 calculations. To maintain the assignment of hydrogen-bond donation ability to the hydroxylic proton (moiety), a differential solvatochromism method was employed by using the methoxy derivative of the compounds (Scheme 1). By use of HPTA and MPTA, the complexation constant of HPTA in DMSO was determined.[83]

The structure of the paper is as follows: Firstly, we will describe the solvent induced changes in the absorption and emission spectra of the new photoacids. The general solvent effects as well as the photoacid effects will be discussed shortly. We will correlate these changes with various solvent parameters for acidity, basicity and dipolarity. It turns out that the increase of the static dipole moment in the excited state is the most important characteristic for excited-state acidity. Consistent results are obtained from Kamlet-Taft and Catalán analyses. Finally, theoretical calculations give preliminary hints about the molecular energetics.
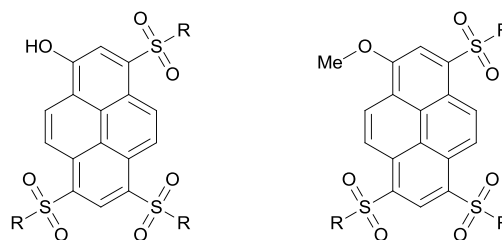
HPTS: R = -O⁻
HPTA: R = -N(CH₃)₂
    1a: R = -OCH₂CF₃
    1b: R = -OCH(CF₃)₂
    1c: R = -N(CH₃)(OCH₃)
    1d: R = -N((CH₂)₂OCH₃)₂
    1e: R = -N(CH₃)((CH₂)₂OH)

MPTS: R = -O⁻
MPTA: R = -N(CH₃)₂
    2a: R = -OCH₂CF₃
    2b: R = -OCH(CF₃)₂
    2c: R = -N(CH₃)(OCH₃)
    2d: R = -N((CH₂)₂OCH₃)₂
    2e: R = -N(CH₃)((CH₂)₂OH)

Scheme 1 Chemical structures of the photoacids and their methoxylated derivatives used in this study. **HPTA** and **HPTS** are known photoacids, **1a – 1e** are the recently synthesized photoacids, **2a – 2e** the methylated forms.

Experimental and Theoretical Methods

Synthesis

Compounds **2a-e** were prepared starting from **HPTS** (98%, Across Organics) as shown in Scheme 2. By deprotonation with sodium hydroxide and reaction with methyl iodide, **HPTS** was converted into **MPTS**. The subsequent route corresponds to a synthetic pathway, which is reported elsewhere.[82] Yields were slightly lower as reported for the photoacids. A detailed description of the procedure is given in the *Supporting Information*. A crystal structure could be obtained for compound **2e**, which is shown in Figure S1 and Table S1.

Spectroscopy

All solvents used for spectroscopic measurements were of spectroscopic quality if available. Moreover, they were checked for fluorescent impurities prior to use. A list of solvents used in this work as well as their solvatochromic and physical parameters are listed in Table 1.

Absorption spectra were taken at micromolar concentration in quartz cuvettes (Hellma) with a Jasco V-650 spectrometer and a bandpass of 1 nm. Fluorescence spectra were measured using the Jasco FP-6500 spectrofluorimeter (wavelength accuracy ± 0.5 nm). All spectra use for the solvatochromic analysis were transformed to the transition dipole moment representation, with the excitation and absorption spectra weighted with v^{-1} and the emission with v^{-3} as suggested by Angulo et al. for solvatochromic analyses.[84] We exclude chloroaliphatics and butyrolactone from any multiparameter regression as they show a deviation of the regression for all compounds.[85]

2a: R³ = –OCH₂CF₃
2b: R³ = –OCH(CF₃)₂
2c: R³ = –N(CH₃)(OCH₃)
2d: R³ = –N((CH₂)₂OCH₃)₂
2e: R³ = –N(CH₃)((CH₂)₂OH)
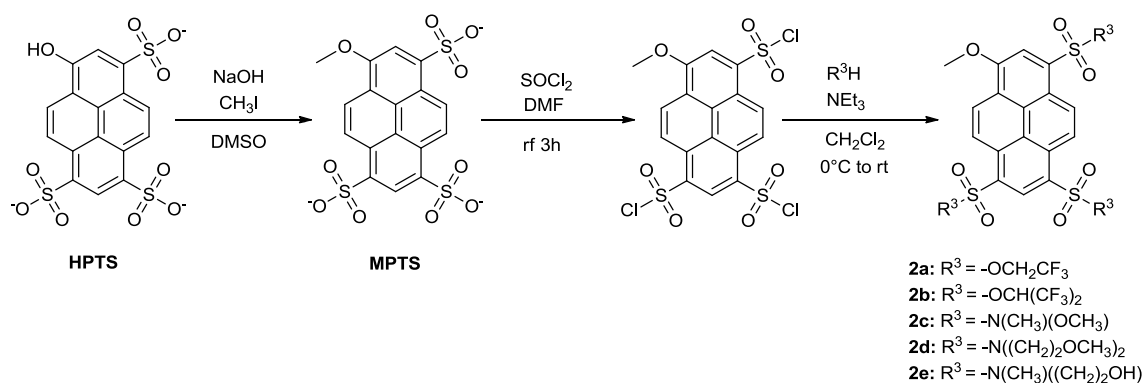
Scheme 2 Reaction Scheme for the synthesis of the methylated compounds.

Table 1 Solvents and their physical (refractive index n and relative permittivity ε_r) and solvatochromic parameters (α, β, π^* and SA, SB, SP, SdP) used in this study.[77, 78, 86]

#	Solvent	ε_r	n	α	β	π^*	SA	SB	SP	SdP
1	Cyclohexane	2.02	1.426	0	0	0	0	0.073	0.683	0
2	Tetrachloromethane	2.30	1.460	0	0	0.28	0	0.044	0.768	0
3	Bromobenzene	5.40	1.557	0	0.07	0.71	0	0.192	0.875	0.497
4	Hexane	1.89	1.375	0	0	-0.11	0	0.056	0.616	0
5	Toluene	2.38	1.497	0	0.11	0.54	0	0.128	0.782	0.284
6	Dioxane	2.21	1.422	0	0.37	0.55	0	0.444	0.737	0.312
7	Sulfolane	42.13	1.484	0	0.39	0.98	0.052	0.365	0.830	0.896
8	Propylene carbonate	64.92	1.422	0	0.4	0.83	0.106	0.341	0.746	0.942
9	Ethyl acetate	6.02	1.372	0	0.45	0.55	0	0.542	0.656	0.603
10	Diethyl ether	4.34	1.353	0	0.47	0.27	0	0.562	0.617	0.385
11	Butyrolactone	40.96	1.437	0	0.49	0.87	0.057	0.399	0.775	0.945
12	Cyclohexanone	18.30	1.451	0	0.53	0.76	0	0.482	0.766	0.745
13	Tetrahydrofuran	7.58	1.407	0	0.55	0.58	0	0.591	0.714	0.634
14	Dimethyl formamide	36.71	1.431	0	0.69	0.88	0.031	0.613	0.759	0.977
15	DMSO	46.45	1.479	0	0.76	1	0.072	0.647	0.83	1.000
16	Tetramethylurea	23.60	1.449	0	0.8	0.83	0	0.624	0.778	0.878
17	HMPT	29.60	1.459	0	1.05	0.87	0	0.813	0.744	1.1
18	Acetone	20.56	1.359	0.08	0.48	0.71	0	0.475	0.651	0.907
19	Acetonitrile	35.94	1.344	0.19	0.31	0.75	0.044	0.286	0.645	0.974
20	Nitromethane	35.87	1.382	0.22	0.06	0.85	0.078	0.236	0.71	0.954
21	Dichloromethane	8.93	1.424	0.3	0	0.82	0.04	0.178	0.761	0.769
22	Chloroform	4.81	1.446	0.44	0	0.58	0.047	0.071	0.783	0.614
23	2-Propanol	19.92	1.377	0.76	0.95	0.48	0.283	0.83	0.633	0.808
24	Ethanol	24.55	1.361	0.83	0.77	0.54	0.4	0.658	0.633	0.783
25	Ethylen glycol	37.70	1.432	0.9	0.52	0.92	0.717	0.534	0.777	0.91
26	Methanol	32.66	1.328	0.93	0.62	0.6	0.605	0.545	0.608	0.904
27	Water	78.30	1.333	1.17	0.47	1.09	1.062	0.025	0.681	0.997
28	2,2,2-Trifluoroethanol	26.53	1.300	1.51	0	0.73	0.893	0.107	0.543	0.922
29	Hexafluoro-2-propanol	16.70	1.275	1.96	0	0.65	-	-	-	-

Theoretical calculations

The Spartan08 software[87] was used to find the starting geometries of MPTA. This program enables us to draw the structure, optimize roughly the geometry using the MM2 force field and to generate the corresponding coordinates by conformational analysis. The ground state geometries of all of the molecules were then optimized by using B3LYP/6-31G* as implemented in Gaussian09[88] (and by AM1 method as implemented in VAMP[89]).

Transition energy $\Delta E_{i \rightarrow j}$ corresponding to the excitation of an electron from the orbital φ_i (occupied in the ground state) to φ_j (unoccupied in the ground state) have been calculated using TD-DFT in Gaussian09 (and using PECI in VAMP).

The excited state geometries were also optimized using AM1 method by taking into account the configuration interaction calculations (CIS = 16).

Solvatochromic scales

To calculate the change of the static dipole moment $\Delta\mu = \left| \mu_e - \mu_g \right|$ of a molecule upon electronic excitation, the Lippert-Mataga equation is used (Equation 1).

$$hc\Delta v = \frac{2|\mu_e - \mu_g|^2}{4\pi\varepsilon_0 a^3}\left[\frac{\varepsilon_r - 1}{2\varepsilon_r + 1} - \frac{n^2 - 1}{2n^2 + 1}\right] = \frac{2|\mu_e - \mu_g|^2}{4\pi\varepsilon_0 a^3}\Delta f \quad (1)$$

In this equation, Δv is the Stokes shift of the molecule in Hz, n the refractive index of the medium, ε_0 and ε_r the vacuum permittivity and the relative permittivity of the medium, respectively. The parameter a is the cavity in the medium, created by the solute, whereas μ_e and μ_g are the static dipole moment of the molecule in the electronic excited and ground state, respectively.

To investigate the hydrogen-bond interactions of the molecules with solvents, the empirical solvent scales of Kamlet-Taft (Equation 2) and Catalán (Equation 3) are used. To further verify the results obtained from the Kamlet-Taft analysis, where we cancel single parameters by appropriate molecule-solvent combinations and straightforward comparisons, we also employ the Catalán solvent scale. In contrast to the former, an unbiased multi-parameter fit is applied here as a separation between the solvent parameters is not convenient. However, both scales express the value of a solvent dependent parameter v_i, i.e. absorption or emission frequency, by its reference value ($v_{0,i}$) and a set of solute and solvent parameters. It should be mentioned, that in the Kamlet-Taft analysis the reference point is cyclohexane, whereas the Catalán scale refers to the gas phase.

$$v_i = v_{0,i} + a_i \cdot \alpha + b_i \cdot \beta + p_i \cdot \pi^* \quad (2)$$

$$v_i = v_{0,i} + A_i \cdot SA + B_i \cdot SB + P_i \cdot SdP + Q_i \cdot SP \quad (3)$$

The solvent parameters for the specific interactions are their acidity (i.e. hydrogen-bond donating ability), expressed by α and SA, respectively, as well as their basicity (or hydrogen-bond accepting ability), expressed by β and SB. The dipolarity and polarizability of the medium, just the single parameter π^* in the Kamlet-Taft relation, is considered in Catalán's equation as the factors SdP and SP, respectively. By doing so, we can also assure that the dipolarity and not a changing polarizability of the molecules is responsible for the observed shifts. Each of these solvent parameters is weighted by a solute-dependent term which, accordingly, correlates the sensitivity of the probe to the respective solvent property. The determination of these prefactors is the key step in every solvatochromic analysis as it provides the corresponding properties of the molecule under investigation, in the ground or excited state. The commonly accepted specific interactions between hydrogen (bond) donors, HB-acceptors and the molecules under investigation are shown in Scheme 3.
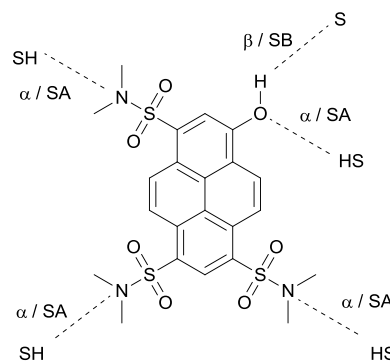
Scheme 3 Possible hydrogen bonds that the molecules can form.

Results and discussion

The fluorescence spectra of the six photoacids in DMSO are shown in Figure 1 (a). All spectra are normalized to the anion emission peak.
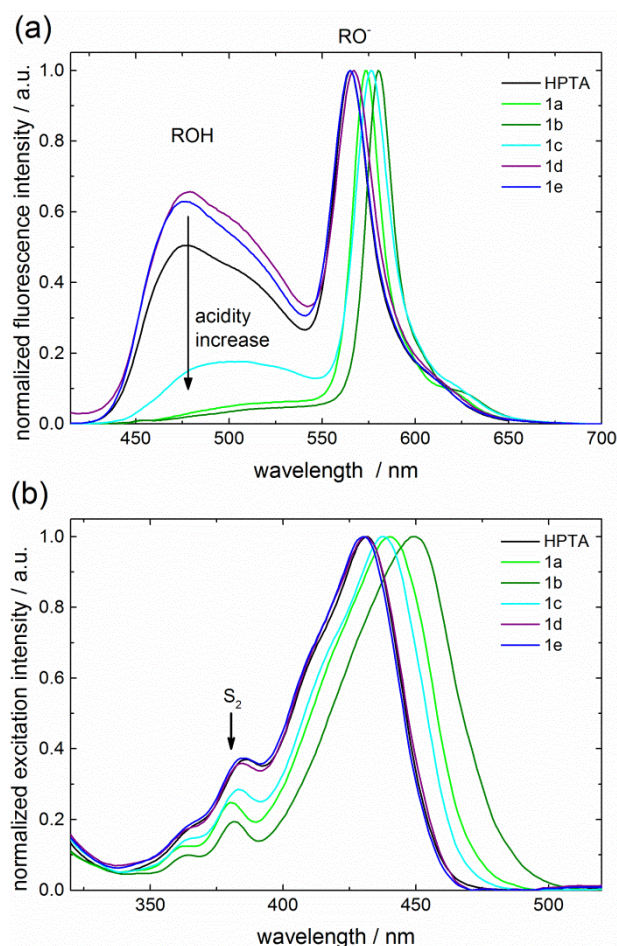
Fig. 1 (a) Normalized fluorescence emission spectra of the investigated photoacids in DMSO (λ_{ex} = 400 nm). The intensity of the acid band decreases with increasing photoacidity. (b) Normalized excitation spectra of the photoacids (λ_{em} = 600 nm). The S_2-state is assigned according to ref. 10.

The solvent DMSO is a vivid choice here because the pK_a^*-values are in a range where all photoacids can undergo ESPT in this medium to a varying extend. The strength of

photoacidity can easily be discussed with respect to this plot (Figure 1a), as with increasing photoacidity the amount of acid fluorescence at λ = 450 - 550 nm decreases (Equation 4).

$$pK_a^* \propto \frac{I_{ROH}}{I_{RO^-}} \qquad (4)$$

It should be mentioned that we rely on the definition of the thermodynamic parameter K_a^* by kinetic parameters, i.e. the rate constant of the process, k_{ESPT} divided by the rate constant for geminate recombination, as observed in the steady state spectra. However, as the fluorescence lifetime and the fluorescence quantum yields of all anionic compounds is very similar and proton diffusion in DMSO was not detected so far [82], our approach to classify the strength of photoacidity on the basis of the emission spectrum (eq. 4) seems valid and more sensitive here.

The strongest photoacid is compound **1b** with hexafluorinated isopropyl substituents as the most electron withdrawing group within this series. A high photoacidity is accompanied by a slight bathochromic shift of the anion emission wavelength, $\lambda_{em,max}(RO^-)$. Concomitantly, the wavelength range of the acid emission also shifts to the red as the extent of ESPT increases. The corresponding excitation spectra are displayed in Figure 1 (b). Also the excitation maxima undergo a bathochromic shift with increasing photoacidity. Most interestingly, the S_2 band[10] at $\lambda_{ex} \approx 380$ nm is hardly affected, only the S_2 state of the strongest photoacids **1a** and **1b** displays a slight hypsochromic shift.

Besides these general effects, some phenomenological solvent effects are exemplified in Figure 2, where the excitation and emission spectra of **1a** and its methylated counterpart **2a** in diffe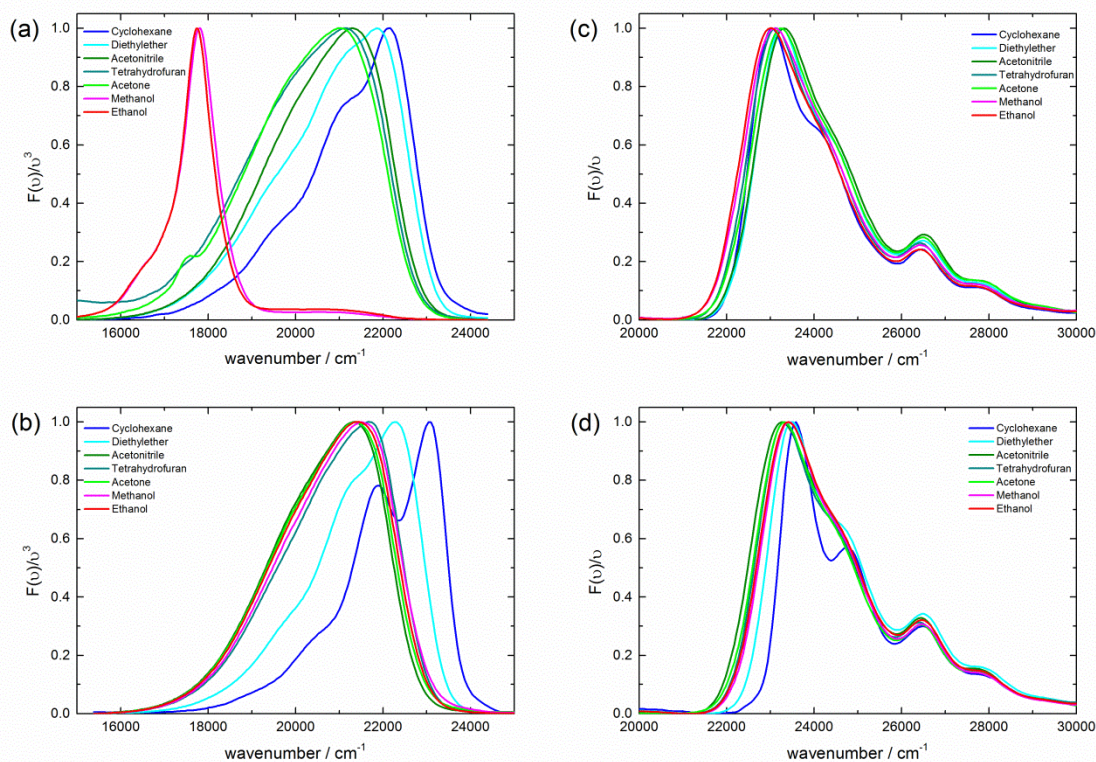rent solvents are shown. Similar results are obtained for the other photoacids emphasizing the generality of these experimental findings.

Fig. 2 Normalized fluorescence emission spectra of (a) **1a** and (b) **2a** in several solvents of differing polarity. The corresponding excitation spectra of **1a** and **2a** in the same solvents are shown in (c) and (d), respectively.

Both emission and excitation spectra exhibit a bathochromic shift in solvents with higher polarity. This shift is more pronounced in emission than in excitation, which gives a first hint that the molecule has a higher polarity in the excited state than in its ground state. The photoacid and its methylated derivtive behave similar. This is to be expected as the electronic effect of a proton and a methyl group is not very different, which is the basis for a differential solvatochromism approach (see next section).[70,]

Another effect observed in Figure 2 is the clear vibronic structure seen in nonpolar cyclohexane with a Franck-Condon progression of $\bar{v} \approx 1160$ cm[-1] for emission of **1a** and **2a**. This value is observed both in emission and excitation, although the latter is less obvious due to the overlap with the second electronic excited state at $\bar{v}_{exc} = 26525$ cm[-1]. A similar progression is found for all other investigated compounds as well. We conclude, therefore, from these coincidences and the wavenumber range that

this progression reflects a bond-length alteration in the O-Pyrene distance but not in the sulfon-substituents. In solvents with a higher polarity, the vibronic structure is blurred out. The effect of hydrogen bonding ability and polarity of the solvent on the vibronic structure of **HPTS** has already been discussed.[12, 13, 33]

From Figure 1 it is already clear that all photoacids studied in this contribution (except the previously investigated[80] **HPTS**) undergo ESPT in DMSO. Further solvents in which ESPT could be observed are the aprotic butyrolactone, dimethyl formamide, tetramethylurea and, to a minor extent, acetone. Furthermore, protic solvents such as methanol, ethanol and 2-propanol are also suitable media to observe ESPT of these photoacids. From these general considerations we can summarize that the photoacids and their corresponding methoxylated counterparts show in principle a similar solvatochromic behavior towards solvent polarity. The main difference is the occurrence of ESPT in protic and very basic, aprotic solvents.

Based on the different solvent dependence of excitation and emission spectra we analyzed the Stokes shift of the photoacids in terms of the Lippert-Mataga equation. To avoid any influence of hydrogen bonding from the hydroxyl group we used the methylated counterparts of the photoacids. As we have shown above, their electronic properties are very similar to those of the acids. In contrast to our findings for **MPTS**[80], a clear dependence according to Equation (1) is found for **MPTA** in non-protic solvents (Figure 3).

As for **MPTA**, a similar strong dependence is seen with the compounds **2a** – **2e**, where the slope correlates with the photoacidity (Figure S2, supporting information). Using a solvent excluded volume a^3 of 414 Å³ determined with Chem3D Pro (CambridgeSoft) for the molecule, a change of the permanent dipole moment $\Delta\mu \approx 14$ D is calculated for **MPTA**. The value of the molecular volume given here is comparable to those listed for molecules of similar size.[90] Despite the rough estimate of the molecular volume, a huge change of the dipole moment is evident for all newly synthesized compounds. Our findings are in agreement with the models of a significant charge transfer (CT) occurring before the proton transfer step, resulting in the high photoacidity of aromatic alcohols. Although it is still unclear whether a larger CT is happening on the acid or the base side[2, 5], these results support a CT before any proton transfer.
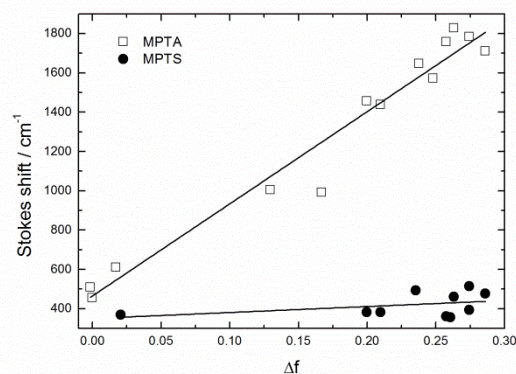
Fig. 3 Lippert-Mataga plot of **MPTA** and **MPTS** for non-acidic solvents. Correlation coefficients are $R^2 = 0.96$ and $R^2 = 0.05$, respectively. The slope of the **MPTA** regression curve is 4690 ($\pm$ 285) cm⁻¹. The values and plots of the other compounds as well as a correlation of the slope with the photoacidity are given in Figure S2 and Table S2.

It has been discussed that a slow charge transfer might occur in all neutral photoacids, in contrast to cationic photoacids.[11] The lack of a Lippert-Mataga correlation seen with **HPTS** may be attributed to the three full negative charges on the sulfonate-substituents, which are supposed to obscure the transfer of partial charges.[61] The stabilizing effect of the solvent continuum is assumed to be the main contribution of the relative acidity increase $\Delta pK_a = pK_a - pK_a^*$ when going from **HPTS** to the here presented photoacids. Whereas the latter compounds undergo changes by up to 8 pK_a-units upon excitation, pyranine shows only an increase by 6 orders of magnitude, i.e. pKa = 7.4 is shifted to pKa* = 1.4.[61]

However, a large CT in the excited state should also be indicated in a Kamlet-Taft analysis (Equation 2) in form of a larger value of p_{em} compared to p_{abs}. A plot of the respective spectroscopic maxima of **MPTA** and compounds **2a** - **2e** is shown in Figure 4. Only non-acidic solvents ($\alpha = 0$) were used for this plot and, as there are no acidic protons identified in those molecules, also $b_i = 0$. Therefore, a linear dependence on solely π^* is expected, which is also observed. The results of this analysis are listed in Table 2.

Table 2 Kamlet-Taft parameter p_{abs} and p_{em} of the methylated compounds. Standard errors are in parenthesis, R^2 is the correlation coefficient. All values are given in cm^{-1}.

Compound	$\nu_{0, abs}$	p_{abs}	R^2	$\nu_{0, em}$	p_{em}	R^2
MPTA	24040 (30)	-445 (50)	0.84	23500 (60)	-1870 (100)	0.96
2a	23550 (55)	-475 (65)	0.69	23045 (130)	-2375 (215)	0.92
2b	23300 (70)	-670 (55)	0.70	22700 (160)	-2500 (260)	0.89
2c	23750 (45)	-455 (75)	0.80	23325 (120)	-2110 (200)	0.92
2d	24045 (40)	-435 (65)	0.85	23300 (95)	-1855 (155)	0.93
2e	23960 (60)	-310 (95)	0.55	23340 (90)	-1775 (130)	0.94

5
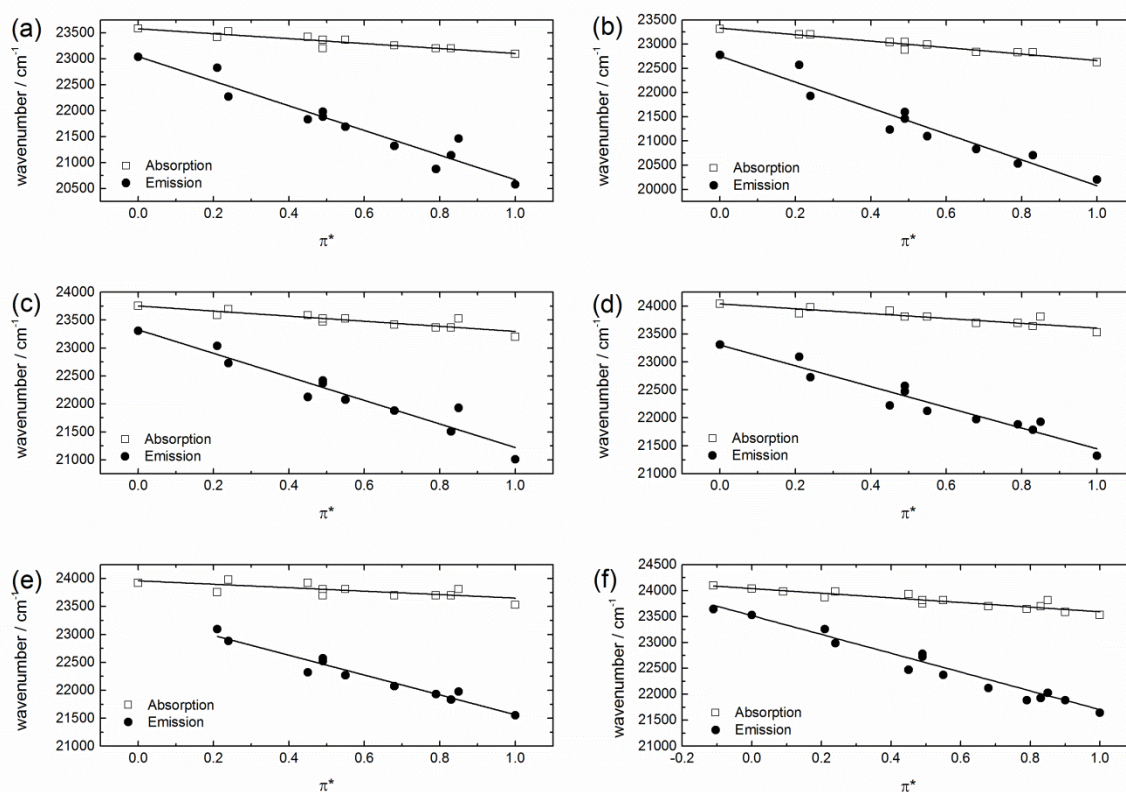
Fig. 4 Absorption (squares) and emission (circles) frequencies of the methylated photoacids in solvents of increasing polarity. (a) **2a**, (b) **2b**, (c) **2c**, (d) **2d**, (e) **2e**, (f) **MPTA**

If protic solvents ($\alpha \neq 0$) are also taken into account, the quality of the regression was improved upon considering an almost negligible dependence on a_{em} in emission ($a_{em} \approx -200 \, cm^{-1}$) for all compounds (Table S3). We attribute this finding to a small interaction of proton donors with the substituents on the pyrene core or, less likely, to an interaction with the methoxy-moiety. For **MPTA**, our values are close to those given by Pines for the emission frequencies although these authors did not exclude a β-dependence a priori.[5]

All methoxy derivatives exhibit an approximately fourfold increase of p thus fulfilling the expectation $p_{em} > p_{abs}$. Furthermore, we found that both the values for p_{abs} and, especially, p_{em} increase with a higher photoacidity of the corresponding free acid as defined in Figure 1. A plot of the acidity according to eq. (4) vs. the p_{em} values obtained from
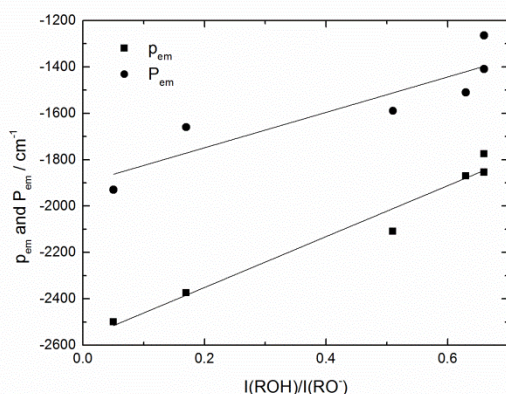
the above analysis is shown in Figure 5.

Fig. 5 Correlation of the photoacidity according to equation (4) with p_{em} ($R^2 = 0.96$) and P_{em} ($R^2 = 0.77$) as obtained from fitting of
5 methylated compounds. Thus, the spectroscopic properties of the methylated derivatives can be connected to the reactivity of the parent molecules.

Comparison was done with the unbiased and independent analysis according to the Catalán-solvent scale. Thus, the
10 methylated compounds could all be fitted by a three-parameter fit, including solvent polarizability SP, solvent acidity SA and solvent dipolarity SdP. Those parameters which were found to be significant ($p < 0.02$) are listed in Table S4. However, any dependence on SB was excluded
15 as no acidic protons are present in these molecules.

All molecules show only a minor dependency on solvent polarity (SdP) in the ground state which strongly increases in emission. As found in the Kamlet-Taft analysis above
20 (Table 2), a systematic increase of the molecules' dipolarity in the excited-state (parameter P_{em}) with higher photoacidity of the corresponding photoacid is noticed (Figure 5). Also the hydrogen-bond donated by a solvent molecule becomes more important in the excited state,
25 parameter A_{em}. However, the molecules **2a** and **2b** with the fluorinated substituents completely lack sensitivity towards SA in the ground state as seen from $A_{abs} = 0$, which may be due to a repulsive effect of the fluorine atoms which hinder the formation of a hydrogen bond with the oxygen atom on
30 the substituents or which might reflect hydrogen-bonds to the electron lone pair of the nitrogen of the sulfonamide bearing photoacids (Scheme 3). Furthermore, solvent polarizability is of importance for the solvatochromism of these dyes. In the ground state this is the most distinct
35 solvatochromic factor which is understandable as neither a distinct dipole moment nor basic sites exist. In the excited state, polarizability and dipolarity are of about equal influence. The slightly higher stabilization due to the solvent polarizability in the excited state can be related to
40 the experimental observation that the optical spectra of neutral compounds are blue-shifted when transferred from solution to the gas phase.[91] Besides this additional information, the overall agreement between the Kamlet-Taft and Catalán analyses of the methylated compounds is
45 large. As can be seen by comparison of Tables S3 and S4 correlation coefficients R^2 are better for the Catalán

analysis which is due to the importance of solvent polarizability.

In the next step we transfer these findings to the analysis of the free photoacids. We start again with the Kamlet-Taft scale and use a differential solvatochromism approach[70, 80] here as the electronic properties between methylated compounds and photoacids are very similar. Furthermore, it facilitates the assignment of the β-dependence to the hydroxyl proton. As in this formalism the p_i values of photoacid and methylated compound are the same, i.e. $p_i(MPTA) = p_i(HPTA)$, equation (5) is used to determine the b_i values.

$$v_i(HPTA) - (v_{i,0}(MPTA) + p_i(MPTA) \cdot \pi^*) = \Delta v_{0,i} + b_i(HPTA) \cdot \beta \qquad (5)$$

The corresponding values for absorption and emission are depicted in Table 3. The corresponding correlation curves are shown in Figure S3 in the supporting information. For
65 most of the molecules beside **HPTA**, only modest R^2 values are obtained for these correlations. One reason for this lies in the broadening of the peaks with increasing solvent polarity (Figure 2) and, in the case of emission, increasing proton transfer efficiency. Another reason could be some
70 residual, yet overlooked CH-acidity of the methyl group which serves as reference in eq. (5). Moreover, good solubility of the various compounds in common solvents minimizes the number of employable solvents.

Table 3 Kamlet-Taft parameters b_{abs} and b_{em} of the photoacids.
75 Standard errors are in parenthesis, R^2 is the correlation coefficient for the plots in Figure S3. All values are given in cm^{-1}.

Compound	b_{abs}	R^2	b_{em}	R^2
HPTA	-560 (90)	0.95	-980 (190)	0.89
1a	-450 (150)	0.76	-935 (330)	0.62
1b	-645 (150)	0.83	-1200 (420)	0.66
1c	-520 (105)	0.79	-700 (210)	0.72
1d	-400 (100)	0.66	-825 (125)	0.84
1e	-330 (120)	0.58	-820 (155)	0.80

As observed before for the solutes dipole moment ($p_{em} > p_{abs}$), also the strength of the hydrogen bond from the
80 hydroxyl group to a solvent molecule increases upon excitation and hence, $|b_{em}| > |b_{abs}|$. This is a general observation within all the photoacids investigated in the literature and a hint that the reason for photoacidity partially is on the acid side.[5, 70, 79] A slight dependence of
85 b_{em} on the photoacidity of the molecules can be deciphered, but not as distinct as expected from the mentioned studies. Whereas the parameter p increased 4-5 times upon electronic excitation, b is just increasing by a factor of about two. Moreover, the variation of b_{em} with the acidity is

less pronounced than that of p_{em}, as shown in Figure S4, supporting information. Concerning the high photoacidity of the investigated photoacids, the parameters b_{em} are also surprisingly small compared to those given in the literature for similar compounds, **HPTS**[3, 81] and (cyano-)naphthols[70, 79]. On the other hand, the values given here are in agreement with our previous findings for pyranine with $b_{em}(\textbf{HPTS}) = 560$ cm^{-1}, concerning its much lower photoacidity.[80]

We also compare the results of the free photoacids with the Catalán solvent scale. Again, multi-parameter fits were performed and compared to the results of the methylated compounds. By doing so we get an unbiased picture of their solvatochromism as the analysis with the Kamlet-Taft scale was somehow driven by chemical intuition (eq. 5). The parameters obtained from the Catalán analysis of the free photoacids are shown in Table S5 and the corresponding correlation curves are displayed in Figure S5. Here, higher correlation coefficients are found than for the Kamlet-Taft analysis as the solvent polarizability is considered.

For the ground state, a rough agreement between the parameters Q_{abs} and P_{abs} of methylated and free photoacids is found, indicating the validity of the multi-parameter approach. The multi-parameter fits of the emission frequencies of the photoacids show a lesser influence of the solvent's dipolarity compared to their methylated counterparts. However, fixing P_{em} to those values of their methylated analogs does not change the values for the basicity significantly (data not shown). Protic solvents become slightly more important for the hydroxylic compounds which may be due to an additional larger interaction of the hydroxyl group than the methoxy group.

This larger interaction amounts to less than 200 cm^{-1} but is observed for all compounds. The main stabilization of the free acids in the electronic ground state according to the Catalán analysis, beyond the solvent's polarizability comes from its basicity. This is in rough agreement with the Kamlet-Taft analysis which shows an equal importance of π^* and β for spectral changes in the electronic ground state. Upon excitation of the molecules, basicity of the solvent becomes more important by a factor of up to two. As in the Kamlet-Taft analysis (parameter b_{em}), no distinct correlation of B_{em} with the photoacidity of the compounds is observed. Furthermore, also the parameter for solvent acidity increases by a factor of about two, $A_{em} \approx 2\ A_{abs}$, as seen for the methylated compounds (Table S3).

From the above considerations we find a significant dependence of a solvatochromic parameter with the photoacidity of the photoacids only for the dipolarity of the solvent. Solvent basicity as well as polarizability also plays a role in the solvatochromic behavior but, from our data, no distinct correlation with the photoacidity could be extracted.

As not only the photoacid is of importance in ESPT reactions but also the product of the proton transfer, we investigated the solvatochromism of the corresponding anion, as well. It can be fully described by an α-dependence (Figure 6 and Table 4) in a Kamlet-Taft analysis. Neither the polarity nor the basicity of the solvent has an obvious influence on absorption or emission wavelengths. It is also worth noting that the Franck-Condon progression, clearly visible for the acids and their methylated counterparts, is almost completely lacking.
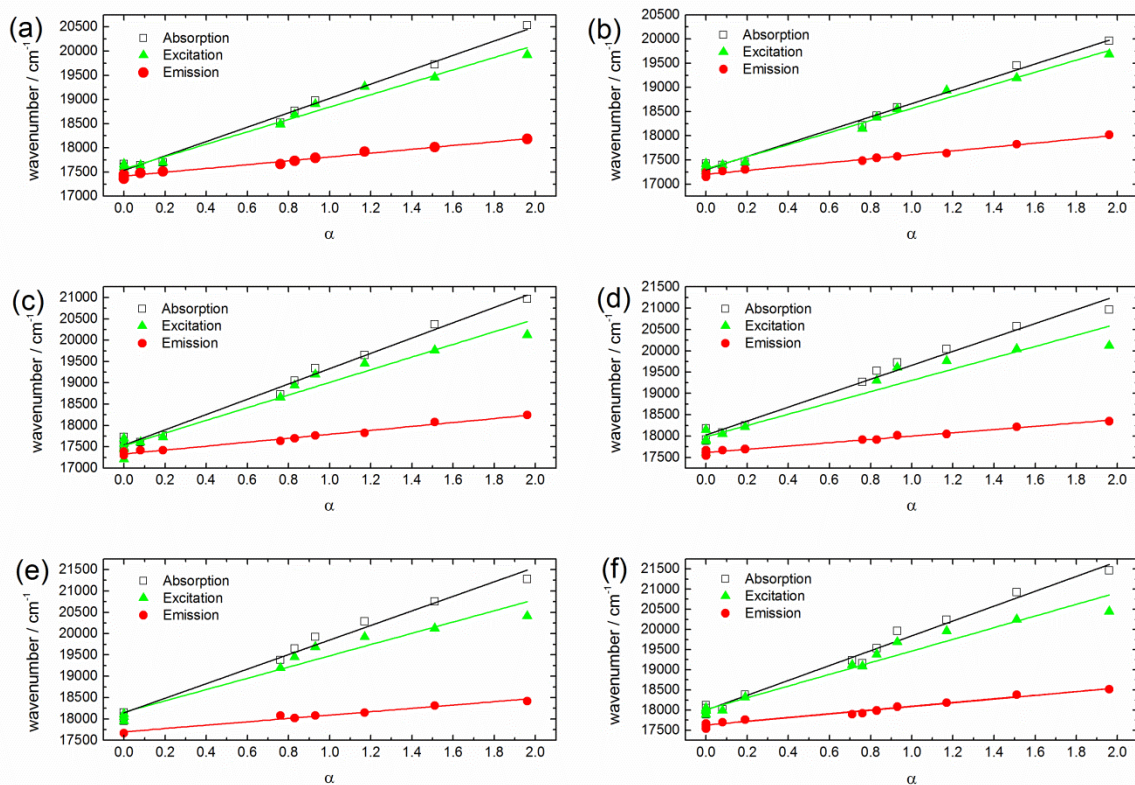
Fig. 6 Absorption (open squares), excitation (triangles) and emission (circles) frequencies of deprotonated photoacids in solvents of increasing acidity. (a) **1a**, (b) **1b**, (c) **1c**, (d) **1d**, (e) **1e**, (f) **HPTA**. The reproducible difference in the slope of excitation and absorption might point to the coexistence of a non-fluorescent complex[92] and will not be discussed further in the present manuscript. Absorption and excitation spectra of two compounds are shown in Figure S6.

Table 4 Kamlet-Taft parameters of the deprotonated photoacids. Standard errors are in parenthesis, R^2 is the correlation coefficient. All values are given in cm^{-1}.

Compound	$\nu_{0,abs}$	a_{abs}	R^2	$\nu_{0,exc}$	a_{exc}	R^2	$\nu_{0,em}$	a_{em}	R^2
HPTA	18000 (45)	1845 (55)	0.97	18015 (60)	1450 (75)	0.96	17630 (20)	460 (20)	0.98
1a	17535 (30)	1485 (35)	0.99	17565 (35)	1280 (45)	0.98	17415 (10)	395 (15)	0.98
1b	17300 (30)	1365 (35)	0.99	17315 (30)	1250 (35)	0.99	17205 (10)	405 (10)	0.99
1c	17540 (45)	1790 (50)	0.99	17530 (70)	1485 (80)	0.96	17335 (15)	460 (20)	0.98
1d	18025 (65)	1630 (75)	0.98	17985 (110)	1320 (120)	0.93	17615 (15)	385 (15)	0.98
1e	18145 (65)	1705 (70)	0.99	18160 (115)	1320 (110)	0.95	17700 (30)	395 (25)	0.97

These findings are in agreement with those results obtained for other photoacids based on naphthol[44, 70] and **HPTS**[80]. Both absorption and emission frequencies are blue-shifted with increasing hydrogen-bond donating strength. The effect is much more pronounced in the ground state, in agreement with a more negatively charged oxygen atom in the ground state. In the excited state, charge density is presumably transferred from the oxygen towards the ring system and hence, the blue-shift is significantly smaller for emission frequencies, i.e. α_{abs} is about 3-4 times larger than α_{em}.

Nevertheless, no stringent correlation of the a_{exc}-values with the acidity of the corresponding photoacid is obtained, just slightly smaller values are determined for **1a** and **1b**. The values for the excited state a_{em} do not change at all for all photoacids investigated within the error margins and might also reflect interactions with the sulfonamide-residues, similar to those observed for the methylated compounds (Table 2). The decrease of a_{em} compared to a_{exc} because of the lower basicity in the excited state has also been noticed in a study of β-naphthol by Solntsev, Huppert and Agmon.[70] They found $a_{exc} = 3100$ cm^{-1} and $a_{em} = 1770$ cm^{-1}, which is two to three times larger than the values given here. However, the photoacidity of β-naphthol is much weaker ($pK_a^* = 2.8$) and those findings support our observation that a_{exc} is lowered with higher photoacidity. Furthermore, in the same paper they predicted this trend by comparison with the 5-cyano derivate of β-naphthol, which is supported by our results. The photoacidity of this molecule is very similar to **HPTA** in terms of pK_a^* but they give $a_{em} = 1100$ cm^{-1} for its anion emission frequency, which is roughly twice as much as the value for **HPTA** (Table 4). We attribute this finding to the much better resonance stabilization of the anion in pyrene based systems compared to naphtholates.

The values found for **HPTS** in our previous study[80] are in disagreement with the above considerations. Although it is a weaker photoacid than the molecules studied here, both a_{exc} and a_{em} of **HPTS** ($a_{exc} = 780$ cm^{-1}, $a_{em} = 240$ cm^{-1}) are smaller than those for the stronger acids. We interpret this finding with the following: **HPTS** has three negatively charged substituents which can act as strong hydrogen-bond acceptors, which may lower the energy of the electronic states as do hydrogen-bond donors for the neutral acids (see Table 2). The interaction of these additional charges is supposed to interfere with any effect of the deprotonated hydroxyl group and, thus, may lower the a_i-values. This explanation is corroborated by the low correlation coefficients obtained for **HPTS** compared to the neutral photoacids.

The results of the multiparameter fitting to Catalán parameters of the photoreaction's products are shown in Table S6. Beside the influence of the solvent's acidity already noticed in the Kamlet-Taft analysis, which is similarly reduced by a factor of ~ 4 in the excited state, the solvent polarizability also contributes to the solvatochromism of the anion, whereas dipolarity and basicity of the solvent do not influence the transition wavelengths for all compounds. The A_{abs} values are not found to change much concerning the large error margins. For all compounds we find $Q_{abs} > Q_{em}$ indicating a higher polarizability in the ground state. We interpret this finding by a partial transfer of electronic charge from the oxygen atom to the pyrene core upon excitation. The shift of the outer, non-bonding electrons to the inner part of the molecule presumably leads to a reduced polarizability. A similar explanation has been made earlier for fluorescent proteins using two-photon absorption[93] and is also exemplified by the red-shifted electronic spectra of other anionic compounds when transferred to the gas phase[94].

In summary, our results from the solvatochromic analysis suggest that the stronger photoacidity change in our pyrene photoacids when compared to **HPTS** is based on the dipolarity of the excited state. Neither a dramatic increase of the hydrogen-bond strength from the hydroxyl group to a solvent molecule, nor that from the solvent to the photoproduct state, nor any evidence for an energy transfer from electronic energy to the OH-stretch, as raised by others,[95] can explain the high photoacidity of the pyranine derivatives.

According to our solvatochromic studies, the clue to photoacidity lies in the charge-transfer but it is unclear at this stage of the study whether CT is mandatory for ESPT as **HPTS** can also undergo ESPT.

To learn more about the electron distribution and a charge transfer state after excitation we investigated prototypical **MPTA** and **MPTS** using semiempirical CIS calculations. Although these calculations basically serve as a first hint, they are nevertheless useful to get insights into the nature of excited states. The properties of the calculated states for **MPTA** in the solvent acetonitrile are shown in Table S7 and the corresponding molecular orbitals are displayed in Figure S7. From these data, states containing different amounts of localized excitation (LE) and charge transfer (CT) character can be identified. The HOMO-LUMO transition shows no strong CT but basically locally excited states on the pyrene core, although a decrease of electron density on the methoxy oxygen can be detected. We find a substantial amount of CT in the states S_3, S_4 and S_5 coming mainly from charge migration from the sulfonamide substituents to the pyrene core ($\Delta\mu \approx 6 - 8$ D). This is an unexpected result when one keeps in mind that the stronger photoacids were produced by introducing stronger electron-withdrawing groups to the pyrene core compared to **HPTA**. Furthermore, the empirical data from the present solvatochromism study hint to a CT from the ring to the substituents as the reason for the increased photoacidity. It is interesting to note that the calculations carried out for **MPTS** showed no significant CT in the first seven excited states (Figure S8 and Table S8). This result can point to differences in the origin of photoacidity of the known pyrene-derived photoacids, as was already pointed out before.[9]

The polar states of **MPTA**, which were also found in gas phase calculations, have a much lower energy in acetonitrile compared to the energy values in vacuo (Figure 7). Concerning the low accuracy of the method in absolute energy values, it might be that those states are closer in energy than the calculations imply, leading to a major role of the charge transfer states for the photophysics of pyrene derivatives. Even a state reversal, as deciphered for **HPTS** by experiments[10, 13, 33], could be imagined and would fit to absorption data (see below). As no CT is evident from our calculations for **MPTS**, no inversion of states is found for this compound.
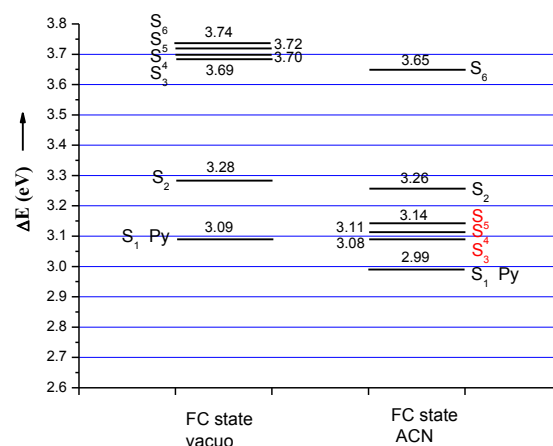
Fig. 7 Comparison of excitation energies in Franck-Condon state in vacuo and acetonitrile (ACN) for **MPTA**, respectively.

Furthermore, a transition involving a CT from the methoxy group to the ring system (H-6 to L+5) is found to contribute around 10 % to the excited-state configuration in the S_1 state. This shows a smaller charge density on the oxygen atom in the excited state, an argument often used to account for the high photoacidity of these systems. More extensive and accurate calculations as well as the use of explicit solvent models are necessary to completely understand the charge redistribution processes in this system.

From these preliminary computations, it seems that the spectroscopically observable second excited state, i.e. the state triple S_3-S_5 from the semiempirical calculations, could be significant for the photoacidity. We therefore investigated the energetics of the S_2–state as well (Figure 2c, d).

It turns out that the energy difference between the first and second excited electronic state increases with higher photoacidity, whereas the absolute position of the second excited state is almost unaffected by the substituents. This is shown in Table 5 and Figure 8a for the values obtained in DMSO. However, the same trend is displayed in other solvents, e.g. diethyl ether, ethanol and cyclohexane (data not shown). Furthermore, the weaker π^* dependence of the S_0-S_2 transition compared to the lowest energetic transition (Figure 8b) contradicts a dominant CT-character of the spectroscopic S_2-state.

Table 5 Energy difference between first and second excited state as observed in DMSO. All values are given in cm^{-1}.

Compound	$\Delta E(S2-S1)$
HPTS	2236
HPTA	2786
1a	3520
1b	3857
1c	3277
1d	2772
1e	2718
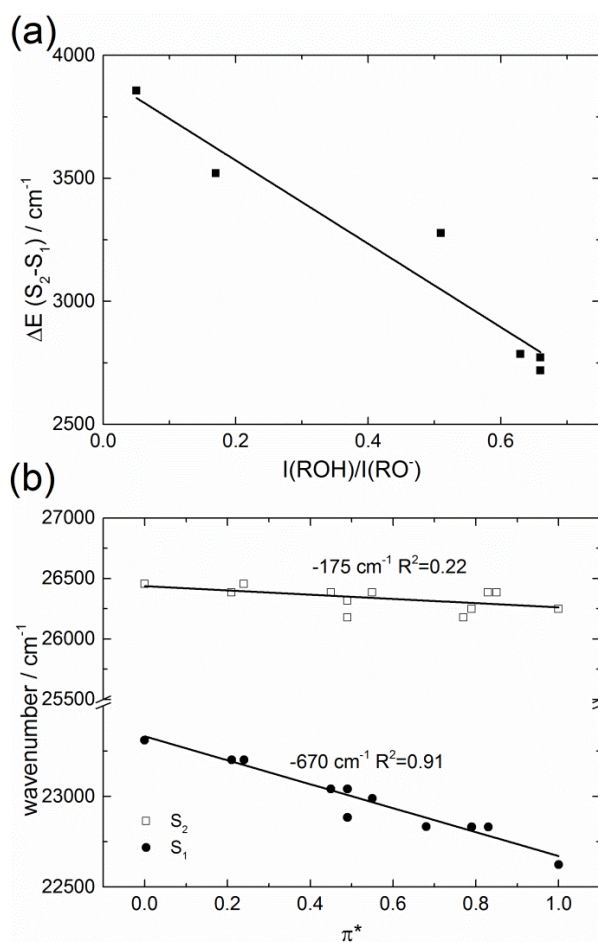
Fig. 8 (a) Correlation of the energy difference between S_1 and S_2 with the photoacidity definition according to eq. 4 (R^2=0.91). (b) Correlation of S_1 and S_2 absorption maxima with solvent polarity parameter π^*.

There are, at least, two possible interpretations how the S_2-state triple found in QC-calculations can influence the photoacidity:

1. These states move below the S_1 state during solvation due to solvent relaxation, i.e. level crossing, and behave as a dark state with relatively low oscillator strength. Consequently, ESPT then only occurs by thermal depopulation of these polar states during the fluorescence lifetime of the molecule. This model could explain why **HPTS** undergoes ESPT without a change of the dipole moment as such stabilization by the solvent is not mandatory for exhibiting ESPT. Photoacidity and intramolecular charge-transfer would be competitive processes in the excited state. However, this explanation is against the accepted model of CT preceding the ESPT step. Secondly, a better stabilization of the dark CT states by polar solvents is in contrast to the experimental findings as ESPT is faster in polar solvents.

2. A real mixing with the S_1 state partially transfers CT-character to the first excited state and this mixing is reduced with increasing $\Delta E(S_2$-$S_1)$. As the calculated CT in these states is a transfer of electron density from the side-groups to the ring,

they are probably counteracting the ESPT process. Suchlike heavy mixing of the lowest energy levels was also pointed out before for **HPTS**[12] and in a recent time-resolved study of 1-naphthol and 2-naphthol.[96] This model can explain why **HPTS**, having the lowest energy gap $\Delta E(S_2$-$S_1)$, is a weaker photoacid and shows that side-chain modifications are a convenient way to manipulate the mixing of states.

A definite answer to the different possibilities can be hardly made on the basis of our experiments, but the solvatochromic analysis indicates that the S_1 state reached in absorption is more polar than the S_2 (see Figures 2 and 8b), whereas the emissive state is of even more CT character. Further research should focus on both time-resolved experiments and theoretical calculations to elaborate the nature and dynamics of the first few excited-states of the here presented photoacids.

Conclusions

We investigated the solvatochromic behavior of several photoacids based on pyrene as well as their methylated derivatives. Different models were exploited to find a correlation between photoacidity and molecular properties. Lippert-Mataga plots reveal a distinct change of the static dipole moment upon excitation. The analyses according to Kamlet-Taft and Catalán, which also take into account specific hydrogen bonding interactions, verify that a high dipole is predominantly formed in the excited state. Moreover, both solvent scales provide a strong correlation of the photoacidity with the amount of intramolecular charge transfer in the excited state. This charge redistribution is not observed for HPTS which presumably results from the shielding by the three permanent negative charges on the substituents. Interestingly, the basicity of the solvent is less important for the ESPT reaction. In contrast, all conjugated bases as the reaction product of ESPT are extremely weak bases in the excited state. A systematic relation to the chemical structure could not be unraveled for the latter.

Inspired by quantum-chemical computations, we could show that the energetic distance between the two lowest excited states is modulated by the substituents in the same direction as the photoacidity. Although being far away from a thorough understanding, the experimental findings including the vibronic progression will guide further elaborated calculations. Future research should also focus on higher electronic states in dependence of the substituents.

Acknowledgement

Notes and references

a Biophysical Chemistry, Saarland University, Campus, Building B2 2, D-66123 Saarbrücken, Germany. Fax: 49-681- 302 64648; Tel: 49-681- 302 64848; E-mail: g.jung@mx.uni-saarland.de

5 *b Ege University, Faculty of Science, Department of Chemistry, 35100 Bornova, Izmir, Turkey*

15 ‡ Footnotes should appear here. These might include comments relevant to but not central to the matter under discussion, limited experimental and spectral data, and crystallographic data.

1 T. Förster, *Naturwissenschaften,* 1949, **36**, 186.

20 2 N. Agmon, *J. Phys. Chem. A,* 2005, **109**, 13.

3 J. T. Hynes, T. Tran-Thi and G. Granucci, *J. Photochem. Photobiol. A,* 2002, **154**, 3.

4 L. G. Arnaut and S. J. Formosinho, *J. Photochem. Photobiol. A,* 1993, **75**, 1.

25 5 E. Pines, *in The Chemistry of Phenols,* ed. Z. Rappoport, John Wiley & Sons, Ltd, 2003, pp.491-527.

6 D. Pines and E. Pines, *in Hydrogen-Transfer Reactions,* ed. J. T. Hynes, J. P. Klinman, H. -H. Limbach and R. L. Schowen, Wiley-VCH Verlag GmbH & Co. KGaA, Weinheim, 2007,

30 pp.377-415.

7 P. M. Kiefer and J. T. Hynes, *in Hydrogen-Transfer Reactions,* ed. J. T. Hynes, J. P. Klinman, H. -H. Limbach and R. L. Schowen, Wiley-VCH Verlag GmbH & Co. KGaA, Weinheim, 2006, pp.303-348.

35 8 N. Agmon, W. Rettig and C. Groth, *J. Am. Chem. Soc.,* 2002, **124**, 1089.

9 L. N. Silverman, D. B. Spry, S. G. Boxer and M. D. Fayer, *J. Phys. Chem. A,* 2008, **112**, 10244.

10 D. B. Spry and M. D. Fayer, *J. Chem. Phys.,* 2007, **127**,

40 204501.

11 D. B. Spry and M. D. Fayer, *J. Chem. Phys.,* 2008, **128**, 084508.

12 O. F. Mohammed, J. Dreyer, B. -Z. Magnes, E. Pines and E. T. J. Nibbering, *ChemPhysChem,* 2005, **6**, 625.

45 13 T. -H. Tran-Thi, C. Prayer, P. Millié, P. Uznanski and J. T. Hynes, *J. Phys. Chem. A,* 2002, **106**, 2244.

14 A. Szemik-Hojniak, L. Wisniewski, I. Deperasinska, A. Makarewicz, L. Jerzykiewicz, A. Puszko, Y. Erez and D. Huppert, *Phys. Chem. Chem. Phys.,* 2012, **14**, 8147.

50 15 J. M. Paredes, L. Crovetto, A. Orte, J. Alvarez-Pez and E. M. Talavera, *Phys. Chem. Chem. Phys.,* 2011, **13**, 1685.

16 F. D. Lewis, L. E. Sinks, W. Weigel, M. C. Sajimon and E. M. Crompton, *J. Phys. Chem. A,* 2005, **109**, 2443.

17 A. A. Freitas, F. H. Quina and A. A. L. Maçanita,

55 *J. Phys. Chem. A,* 2011, **115**, 10988.

18 E. Gould, A. V. Popov, L. M. Tolbert, I. Presiado, Y. Erez, D. Huppert and K. M. Solntsev, *Phys. Chem. Chem. Phys.,* 2012, **14**, 8964.

19 M. Mosquera, J. C. Penedo, M. C. Ríos Rodríguez and F.

60 Rodríguez-Prieto, *J. Phys. Chem.,* 1996, **100**, 5398.

20 A. J. G. Strandjord, D. E. Smith and P. F. Barbara, *J. Phys. Chem.,* 1985, **89**, 2362.

21 B. Cohen, C. M. Álvarez, N. A. Carmona, J. A. Organero and A. Douhal, *J. Phys. Chem. B,* 2011, **115**, 7637.

65 22 Y. Erez, R. Gepshtein, I. Presiado, K. Trujillo, K. Kallio, S. J. Remington and D. Huppert, *J. Phys. Chem. B,* 2011, **115**, 11776.

23 K. M. Solntsev and N. Agmon, *Chem. Phys. Lett.,* 2000, **320**, 262.

70 24 L. M. Tolbert and J. E. Haubrich, *J. Am. Chem. Soc.,* 1990, **112**, 8163.

25 S. G. Schulman, W. R. Vincent and W. J. M. Underberg, *J. Phys. Chem.,* 1981, **85**, 4068.

26 C. M. Harris and B. K. Selinger, *J. Phys. Chem.,* 1980, **84**,

75 891.

27 A. Weller, *Z. Elektrochem.,* 1952, **56**, 662.

28 D. Huppert, L. M. Tolbert and S. Linares-Samaniego, *J. Phys. Chem. A,* 1997, **101**, 4602.

29 S. Mahanta, B. K. Paul, R. Balia Singh and N. Guchhait,

80 *J. Comput. Chem.,* 2011, **32**, 1.

30 S. G. Schulman, S. X. Chen, F. L. Bai, M. J. P. Leiner, L. Weis and O. S. Wolfbeis, *Anal. Chim. Acta,* 1995, **304**, 165.

31 D. B. Spry, A. Goun and M. D. Fayer, *J. Phys. Chem. A,* 2007, **111**, 230.

85 32 S. K. Mondal, S. Ghosh, K. Sahu, P. Sen and K. Bhattacharyya, *J. Chem. Sci.,* 2007, **119**, 71.

33 D. B. Spry, A. Goun, C. B. Bell III and M. D. Fayer, *J. Chem. Phys.,* 2006, **125**, 144514.

34 T. -H. Tran-Thi, T. Gustavsson, C. Prayer, S. Pommeret and J.

90 T. Hynes, *Chem. Phys. Lett.,* 2000, **329**, 421.

35 D. B. Spry and M. D. Fayer, *J. Phys. Chem. B,* 2009, **113**, 10210.

36 P. Leiderman, R. Gepshtein, A. Uritski, L. Genosar and D. Huppert, *J. Phys. Chem. A,* 2006, **110**, 9039.

95 37 L. Genosar, B. Cohen and D. Huppert, *J. Phys. Chem. A,* 2000, **104**, 6689.

38 B. Cohen, J. Segal and D. Huppert, *J. Phys. Chem. A,* 2002, **106**, 7462.

39 T. Htun, *J. Fluoresc.,* 2003, **13**, 323.

100 40 S. Kaneko, S. Yotoriyama, H. Koda and S. Tobita, *J. Phys. Chem. A,* 2009, **113**, 3021.

41 L. M. Tolbert and K. M. Solntsev, *Acc. Chem. Res.,* 2002, **35**, 19.

42 R. Simkovitch, E. Kisin-Finfer, S. Shomer, R. Gepshtein, D.

105 Shabat and D. Huppert, *J. Photochem. Photobiol. A,* 2013, **254**, 45.

43 L. M. Tolbert and J. E. Haubrich, *J. Am. Chem. Soc.,* 1994, **116**, 10593.

44 K. M. Solntsev, D. Huppert and N. Agmon, *J. Phys. Chem. A,*

110 1999, **103**, 6984.

45 K. M. Solntsev, D. Huppert, N. Agmon and L. M. Tolbert, *J. Phys. Chem. A,* 2000, **104**, 4658.

46 C. Clower, K. M. Solntsev, J. Kowalik, L. M. Tolbert and D. Huppert, *J. Phys. Chem. A,* 2002, **106**, 3114.

115 47 T. B. McAnaney, X. Shi, P. Abbyad, H. Jung, S. J. Remington and S. G. Boxer, *Biochemistry,* 2005, **44**, 8701.

48 F. Wong and C. Fradin, *J. Fluoresc.,* 2011, **21**, 299.

49 P. Leiderman, A. Uritski and D. Huppert, *J. Phys. Chem. A,* 2007, **111**, 4998.

120 50 K. Das, K. D. Ashby, J. Wen and J. W. Petrich, *J. Phys. Chem. B,* 1999, **103**, 1581.

51 B. Cohen and D. Huppert, *J. Phys. Chem. A,* 2000, **104**, 2663.

52 B. Cohen, P. Leiderman and D. Huppert, *J. Phys. Chem. A,* 2002, **106**, 11115.

125 53 A. Uritski, I. Presiado, Y. Erez, R. Gepshtein and D. Huppert, *J. Phys. Chem. C,* 2009, **113**, 17915.

54 L. Genosar, P. Leiderman, N. Koifman and D. Huppert, *J. Phys. Chem. A,* 2004, **108**, 1779.

55 R. Barnadas-Rodríguez and J. Estelrich,

130 *J. Photochem. Photobiol. A,* 2008, **198**, 262.

56 P. Leiderman, R. Gepshtein, A. Uritski, L. Genosar and D. Huppert, *J. Phys. Chem. A,* 2006, **110**, 5573.

57 I. Presiado, Y. Erez, R. Gepshtein and D. Huppert, *J. Phys. Chem. C,* 2009, **113**, 20066.

135 58 A. Mirończyk and A. Jankowski, *J. Photochem. Photobiol. A,* 2002, **153**, 89.

59 J. Alvarez-Pez, L. Ballesteros, E. Talavera and J. Yguerabide, *J. Phys. Chem. A,* 2001, **105**, 6320.

60 K. M. Solntsev, D. Huppert and N. Agmon, *Phys. Rev. Lett.,*

140 2001, **86**, 3427.

61 E. Pines, D. Huppert and N. Agmon, *J. Chem. Phys.,* 1988, **88**, 5620.

62 N. Agmon, E. Pines and D. Huppert, *J. Chem. Phys.,* 1988, **88**, 5631.

63 N. Agmon, *J. Chem. Phys.,* 1988, **88**, 5639.

64 N. Agmon and I. V. Gopich, *Chem. Phys. Lett.,* 1999, **302**, 399.

65 P. Leiderman, L. Genosar and D. Huppert, *J. Phys. Chem. A,* 2005, **109**, 5965.

66 S. Park, Y. Lee and D. Jang, *Phys. Chem. Chem. Phys.,* 2008, **10**, 6703.

67 A. Melnichuk, *J. Chem. Phys.,* 2011, **134**, 244303.

68 W. Zhao, L. Pan, W. Bian and J. Wang, *ChemPhysChem,* 2008, **9**, 1593.

69 K. M. Solntsev, D. Huppert, L. M. Tolbert and N. Agmon, *J. Am. Chem. Soc.,* 1998, **120**, 7981.

70 K. M. Solntsev, D. Huppert and N. Agmon, *J. Phys. Chem. A,* 1998, **102**, 9599.

71 A. Bani-Yaseen, *J. Fluoresc.,* 2011, **21**, 1061.

72 R. S. Moog, D. D. Kim, J. J. Oberle and S. G. Ostrowski, *J. Phys. Chem. A,* 2004, **108**, 9294.

73 C. Reichardt, *Solvents and solvent effects in organic chemistry*, VCH, Weinheim, 1988.

74 E. Lippert, *Z. Elektrochem.,* 1957, **61**, 962.

75 N. Mataga, Y. Kaifu and M. Koizumi, *Bull. Chem. Soc. Jpn.,* 1956, **29**, 465.

76 W. Liptay, *Angew. Chem. Int. Ed.,* 1969, **8**, 177.

77 M. J. Kamlet, J. L. M. Abboud, M. H. Abraham and R. W. Taft, *J. Org. Chem.,* 1983, **48**, 2877.

78 J. Catalán, *J. Phys. Chem. B,* 2009, **113**, 5951.

79 B. -Z. Magnes, D. Pines, N. Strashnikova and E. Pines, *Solid State Ionics,* 2004, **168**, 225.

80 G. Jung, S. Gerharz and A. Schmitt, *Phys. Chem. Chem. Phys.,* 2009, **11**, 1416.

81 N. Barrash-Shiftan, B. Brauer and E. Pines, *J. Phys. Org. Chem.,* 1998, **11**, 743.

82 B. Finkler, C. Spies, M. Vester, F. Walte, K. Omlor, I. Riemann, M. Zimmer, F. Stracke, M. Gerhards and G. Jung, *submitted,* 2013.

83 E. Pines, D. Pines, Y. Z. Ma and G. R. Fleming, *ChemPhysChem,* 2004, **5**, 1315.

84 G. Angulo, G. Grampp and A. Rosspeintner, *Spectrochim. Acta A,* 2006, **65**, 727.

85 S. A. Hennessy, S. D. McDermott and S. M. Moane, *J. Forensic Sci.,* 2004, **49**, 1.

86 C. Laurence, P. Nicolet, M. T. Dalati, J. M. Abboud and R. Notario, *J. Phys. Chem.,* 1994, **98**, 5807.

87 I. Wavefunction, *Phys. Chem. Chem. Phys.,* 2006, 3172.

88 M. J. Frisch, G. W. Trucks, H. B. Schlegel, G. E. Scuseria, M. A. Robb, J. R. Cheeseman, G. Scalmani, V. Barone, B. Mennucci, G. A. Petersson, H. Nakatsuji, M. Caricato, X. Li, H. P. Hratchian, A. F. Izmaylov, J. Bloino, G. Zheng, J. L. Sonnenberg, M. Hada, M. Ehara, K. Toyota, R. Fukuda, J. Hasegawa, M. Ishida, T. Nakajima, Y. Honda, O. Kitao, H. Nakai, T. Vreven, J. A. Montgomery, J. E. Peralta, F. Ogliaro, M. Bearpark, J. J. Heyd, E. Brothers, K. N. Kudin, V. N. Staroverov, R. Kobayashi, J. Normand, K. Raghavachari, A. Rendell, J. C. Burant, S. S. Iyengar, J. Tomasi, M. Cossi, N. Rega, J. M. Millam, M. Klene, J. E. Knox, J. B. Cross, V. Bakken, C. Adamo, J. Jaramillo, R. Gomperts, R. E. Stratmann, O. Yazyev, A. J. Austin, R. Cammi, C. Pomelli, J. W. Ochterski, R. L. Martin, K. Morokuma, V. G. Zakrzewski, G. A. Voth, P. Salvador, J. J. Dannenberg, S. Dapprich, A. D. Daniels, Farkas, J. B. Foresman, J. V. Ortiz, J. Cioslowski and D. J. Fox, *Gaussian 09, Revision B.01, Gaussian, Inc., Wallingford CT,* 2009, .

89 T. Clark, A. Alex, B. Beck, F. Burkhardt, J. Chandrasekhar, P. Gedeck, A. Horn, M. Hutter, B. Martin, G. Rauhut, W. Sauer, T. Schindler and T. Steinke, *VAMP 10. 0, CCC, Erlangen,* 2009.

90 A. M. Williams, Y. Jiang and D. Ben-Amotz, *Chem. Phys.,* 1994, **180**, 119.

91 R. Pappalardo and S. Ahmed, *J. Chem. Phys.,* 1972, **56**, 5135.

92 M. Lukeman, M. Burns and P. Wan, *Can. J. Chem.,* 2011, **89**, 433.

93 M. Drobizhev, S. Tillo, N. S. Makarov, T. E. Hughes and A. Rebane, *J. Phys. Chem. B,* 2009, **113**, 12860.

94 D. A. Horke, A. S. Chatterley and J. R. R. Verlet, *Phys. Rev. Lett.,* 2012, **108**, 083003.

95 A. Hakonen and S. Hulth, *Anal. Chim. Acta,* 2008, **606**, 63.

96 F. Messina, M. Prémont-Schwarz, O. Braem, D. Xiao, V. S. Batista, E. T. J. Nibbering and M. Chergui, *Angew. Chem. Int. Ed.,* 2013, **52**, 6871.

Supporting information for:

Solvatochromism of pyranine-derived photoacids

Christian Spies[#], Björn Finkler[#], Nursel Acar[§], Gregor Jung[#]*

[#]Biophysical Chemistry, Saarland University, Campus, Building B2 2, D-66123 Saarbrücken,

Germany

[§]Ege University, Faculty of Science, Department of Chemistry, 35100 Bornova, Izmir, Turkey

Synthesis of Trisodium-8-methoxypyrene-1,3,6-trisulfonate (MPTS)

Trisodium-8-hydroxypyrene-1,3,6-trisulfonate (2.09 g, 4.0 mmol) was dissolved in 80 mL anhydrous DMSO. After addition of sodium hydroxide (0.160 g, 4.1 mmol), the mixture was stirred for 30 minutes at room temperature. Methyl iodide (0.710 g, 5.0 mmol) was added and the resulting solution was stirred for 48 hours at room temperature. Solvent and excess methyl iodide were removed in vacuo. The yellow residue was suspended in 50 ml ethylacetate and filtered. After the filter cake was washed with ethylacetate (2 × 50 mL) and acetone (3 × 50 mL) and dried under vacuum, the crude product was recrystallized from methanol/water. The sodium-salt of **MPTS** was isolated as yellow powder (1.90 g, 88%).

^{1}H-NMR (400MHz, DMSO-d6): δ = 9.12 (1H, d, ^3J (H,H) = 10Hz), 9.04 (1H, d, ^3J (H,H) = 10Hz), 9.02 (1H, s), 8.95 (1H, d, ^3J (H,H) = 10Hz), 8.37 (1H, d, ^3J (H,H) = 10Hz), 8.21 (1H, s), 4.17 (3H, s).

The following steps are based on a synthetic route reported elsewhere.[1]

Compound **2a**:

Yield: 53%

^{1}H-NMR (400MHz, acetone-d6): δ = 9.39 (1H, s), 9.29 (1H, d, ^3J (H,H) = 10Hz), 9.13 (1H, d, ^3J (H,H) = 10Hz), 9.06 (1H, d, ^3J (H,H) = 10Hz), 9.02 (1H, d, ^3J (H,H) = 10Hz), 8.61 (1H, s), 4.90 (6H, m), 4.50 (3H, s). MS (ES-): *m/z* calc. for $C_{23}H_{15}F_9O_{10}S_3$: 717.97; found: 635.20 $[M-CH_2CF_3]^+$.

Compound **2b**:

Yield: 22%

^{1}H-NMR (400MHz, acetone-d6): δ = 9.44 (1H, s), 9.42 (1H, d, ^3J (H,H) = 10Hz), 9.13 (1H, d, ^3J (H,H) = 10Hz), 9.13 (1H, d, ^3J (H,H) = 7Hz), 9.11 (1H, d, ^3J (H,H) = 7Hz), 8.70 (1H, s), 6.39 (3H, m), 4.51 (3H, s). MS (ES+): *m/z* calc. for $C_{26}H_{12}F_{18}O_{10}S_3$: 921.93; found: 921.84 $[M]^+$.

Compound **2c**:

Yield: 34%

^{1}H-NMR (400MHz, acetone-d6): δ = 9.53 (1H, d, ^3J (H,H) = 10Hz), 9.50 (1H, d, ^3J (H,H) = 10Hz), 9.34 (1H, d, ^3J (H,H) = 10Hz), 9.30 (1H,s), 8.98 (1H, d, ^3J (H,H) = 10Hz), 8.43 (1H, s), 4.41 (3H, s), 3.81 (3H, s), 3.78 (3H, s), 3.77 (3H, s), 2.97 (3H, s) 2.94 (3H, s), 2.93 (3H, s). MS (ES+): *m/z* calc. for $C_{23}H_{27}N_3O_{10}S_3$: 601.09; found: 602.32 $[M+H]^+$.

Compound **2d**:

Yield: could not be determined

^{1}H-NMR (400MHz, acetone-d6): δ = 9.27 (1H, d, ^3J (H,H) = 10Hz), 9.24 (1H, s), 9.12 (1H, d, ^3J (H,H) = 10Hz), 9.03 (1H, d, ^3J (H,H) = 10Hz), 8.88 (1H, d, ^3J (H,H) = 10Hz), 8.42 (1H, s), 4.37 (3H, s), 3.67 (12H, m), 3.48 (12H, m), 3.14 (6H, s) 3.06 (6H, s), 3.05 (6H, s). MS (ES+): *m/z* calc. for $C_{35}H_{51}N_3O_{13}S_3$: 817.26; found: 840.27 $[M+Na]^+$.

Compound **2e**:

Yield: 95%

^{1}H-NMR (400MHz, acetone-d6): δ = 9.34 (1H, d, ^3J (H,H) = 10Hz), 9.22 (1H, d, ^3J (H,H) = 10Hz), 9.19 (1H, s), 9.12 (1H, d, ^3J (H,H) = 10Hz), 9.85 (1H, d, ^3J (H,H) = 10Hz), 8.39 (1H, s), 4.37 (3H, s), 3.75 (6H, m), 3.47 (6H, m), 3.08 (3H, s), 3.07 (3H, s), 3.06 (3H, s). MS (ES+): *m/z* calc. for $C_{26}H_{33}N_3O_{10}S_3$: 643.13; found: 666.38 $[M+Na]^+$.

MPTA:

^{1}H-NMR (400MHz, acetone-d6): δ = 9.44 (1H, d, ^3J (H,H) = 10Hz), 9.35 (1H, d, ^3J (H,H) = 10Hz), 9.21 (1H, d, ^3J (H,H) = 10Hz), 9.19 (1H,s), 8.94 (1H, d, ^3J (H,H) = 10Hz), 8.40 (1H, s), 4.41 (3H, s), 2.94 (3H, s), 2.92 (3H, s), 2.91 (3H, s).
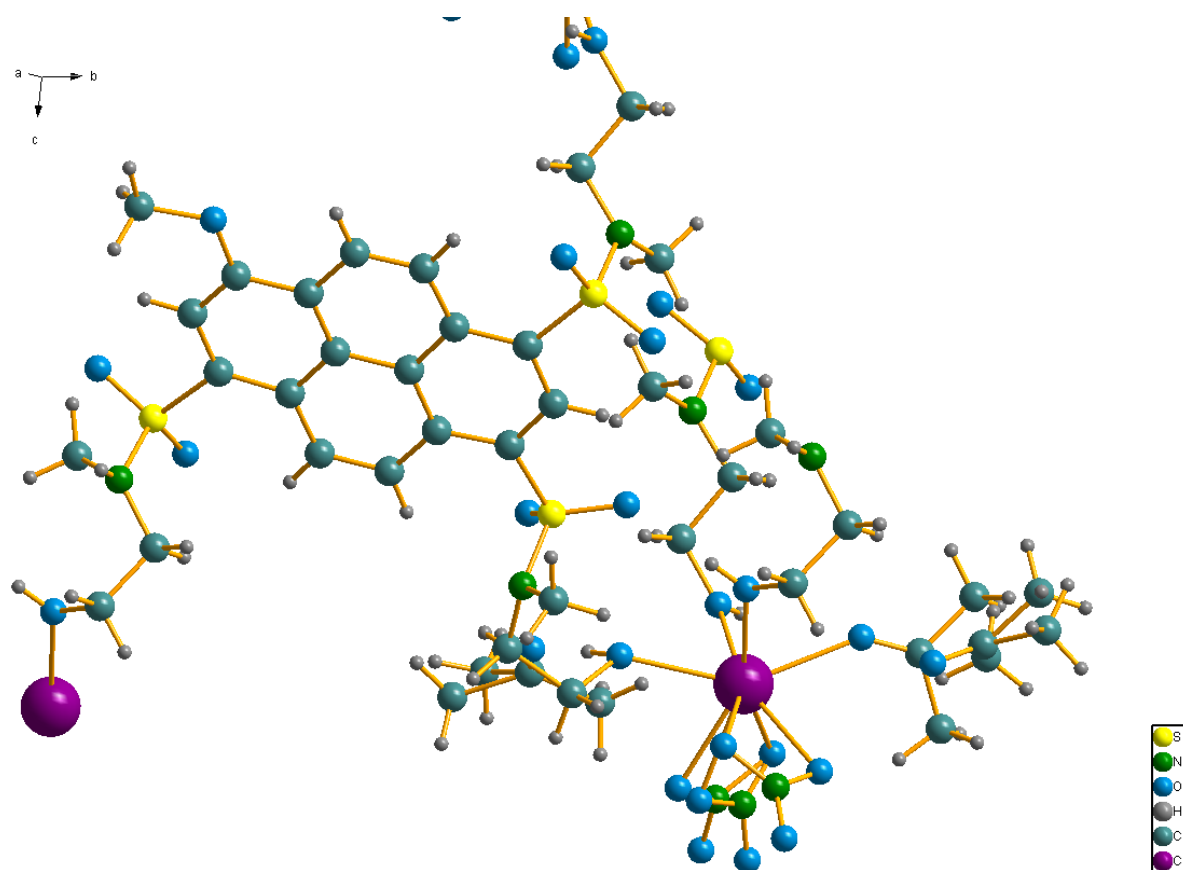
Figure S1. Crystal structure of compound **2e**.

Table 1. Crystal data and structure refinement for **2e**.

Empirical formula	C26 H33 N3 O10 S3 x Ca N2 O6 x 3 C3 H6 O
Formula weight	982.07
Temperature	123(2) K
Wavelength	0.71073 Å
Crystal system	Triclinic
Space group	P-1
Unit cell dimensions	a = 9.9974(6) Å
	b = 13.0768(9) Å
	c = 18.1443(12) Å
Volume	2159.6(2) $Å^3$
Z	2
Density (calculated)	1.510 Mg/m^3
Absorption coefficient	0.374 mm^{-1}
F(000)	1032
Crystal size	0.87 x 0.25 x 0.13 mm^3
Theta range for data collection	1.15 to 26.50°.
Index ranges	-12<=h<=11, -16<=k<=16, -22<=l<=22
Reflections collected	26081
Independent reflections	8729 [R(int) = 0.0381]
Completeness to theta = 26.50°	97.5 %
Absorption correction	None
Max. and min. transmission	0.9530 and 0.7376
Refinement method	Full-matrix least-squares on F^2
Data / restraints / parameters	8729 / 426 / 631
Goodness-of-fit on F^2	1.088
Final R indices [I>2sigma(I)]	R1 = 0.0582, wR2 = 0.1437
R indices (all data)	R1 = 0.0896, wR2 = 0.1609
Largest diff. peak and hole	0.784 and -0.476 $e.Å^{-3}$
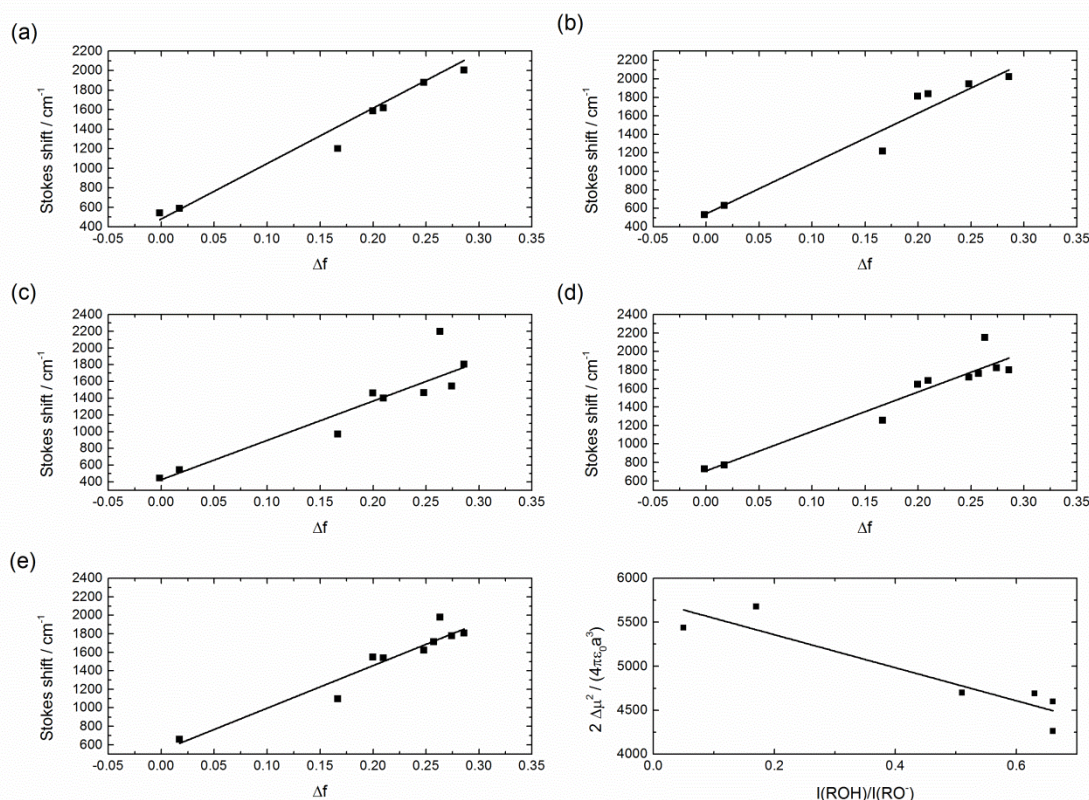
Figure S2. Lippert-Mataga plot of the methylated photoacids in non-acidic solvents. (a) **2a**, (b) **2b**, (c) **2c**, (d) **2d**, ((f)) **2e**, (f) The slope of all Lippert-Mataga plots decreases with decreasing photoacidity (R^2=0.83).

Table S2. The slopes of all Lippert Mataga plots for the methylated compounds. The molecular volume and the calculated change of the dipole moment are also given.

Compound	Slope $(2*(\Delta\mu)^2/(4\pi\varepsilon_0 a^3)$	a^3 [Å³]	$\Delta\mu$ [D]
MPTA	4600 (285)	400	13,6
2a	5680 (710)	410	14,5
2b	5440 (490)	511	15,7
2c	4700 (725)	424	13,6
2d	4260 (425)	686	16,4
2e	4600 (490)	480	14,4

Table S3. Kamlet-Taft parameters of the methylated compounds. Standard errors are in parenthesis, R^2 is the correlation coefficient. All values are given in cm^{-1}.

Compound	$\nu_{0,\,abs}$	p_{abs}	a_{abs}	b_{abs}	R^2	$\nu_{0,\,em}$	p_{em}	a_{em}	b_{em}	R^2
MPTA	24040 (30)	-445 (50)	0	0	0.84	23500 (60)	-1870 (100)	-200 (80)	0	0.83
2a	23550 (55)	-475 (65)	0	0	0.64	23045 (130)	-2375 (215)	-200 (80)	0	0.70
2b	23300 (70)	-670 (55)	0	0	0.63	22700 (160)	-2500 (260)	-200 (80)	0	0.61
2c	23750 (45)	-455 (75)	0	0	0.76	23325 (120)	-2110 (200)	-200 (80)	0	0.77
2d	24045 (40)	-435 (65)	0	0	0.81	23300 (95)	-1855 (155)	-200 (80)	0	0.80
2e	23960 (60)	-310 (95)	0	0	0.58	23340 (90)	-1775 (130)	-200 (80)	0	0.78

Table S4. Catalán parameters of the methylated compounds. Standard errors are in parenthesis, R^2 is the correlation coefficient. All values are given in cm^{-1}.

Compound	$\nu_{0,abs}$	Q_{abs}	P_{abs}	A_{abs}	B_{abs}	R^2
MPTA	25075 (60)	-1585 (85)	-210 (20)	-145 (25)	0	0.97
2a	24475 (250)	-1385 (345)	-230 (65)	0	0	0.86
2b	24240 (205)	-1430 (280)	-360 (70)	0	0	0.77
2c	24880 (105)	-1695 (145)	-235 (35)	-240 (45)	0	0.94
2d	25085 (115)	-1565 (155)	-255 (40)	-305 (50)	0	0.93
2e	25070 (75)	-1675 (105)	-145 (25)	-155 (35)	0	0.96

Compound	$\nu_{0,\,em}$	Q_{em}	P_{em}	A_{em}	B_{em}	R^2
MPTA	24315 (250)	-1305 (355)	-1510 (80)	-350 (95)	0	0.97
2a	25000 (580)	-3130 (800)	-1660 (160)	-505 (205)	0	0.95
2b	24590 (475)	-2975 (655)	-1930 (130)	0	0	0.94
2c	25455 (365)	-3300 (500)	-1590 (100)	-405 (120)	0	0.98
2d	24545 (335)	-2000 (460)	-1410 (90)	-490 (115)	0	0.96
2e	24475 (240)	-1935 (325)	-1265 (75)	-530 (80)	0	0.97
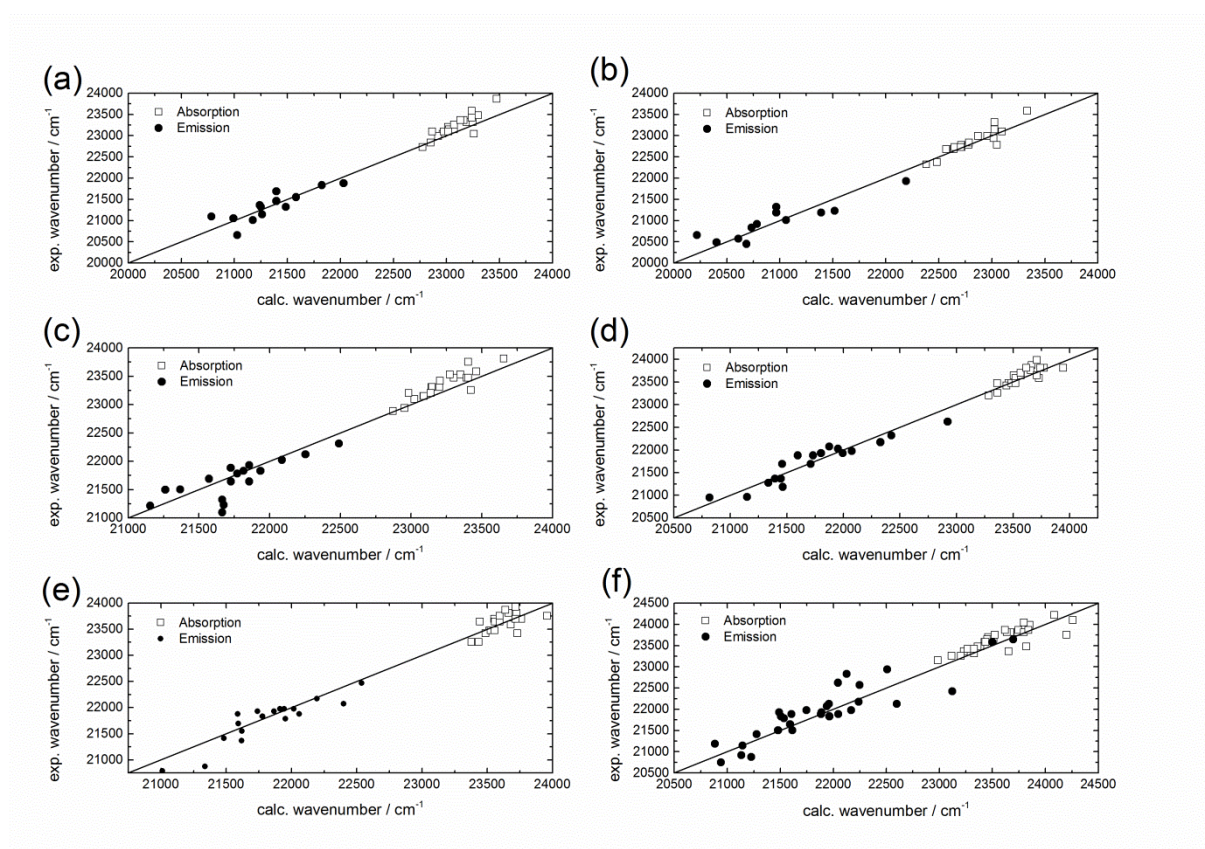
Figure S3. Correlation plots obtained with the Kamlet-Taft analysis of the photoacids. (a) **1a**, (b) **1b**, (c) **1c**, (d) **1d**, (e) **1e**, (f) **HPTA**

Figure S4. Plot of p_{em} (open squares), p_{abs} (full circles), b_{em} (full squares) and b_{abs} (open triangles) of the photoacids vs. the amount acid fluorescence intensity. The strongest dependence and correlation is observed on p_{em}.

Table S5. Catalán parameters of the photoacids. Standard errors are in parenthesis, R^2 is the correlation coefficient. All values are given in cm^{-1}.

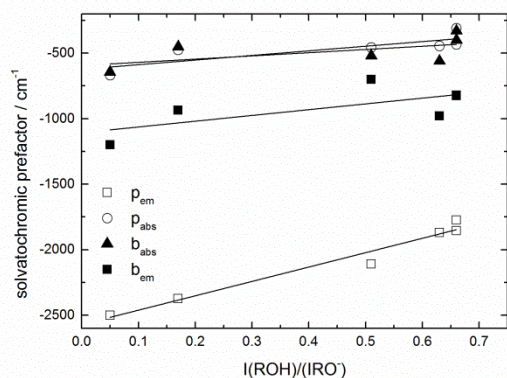| Compound	$v_{0,\,abs}$	Q_{abs}	P_{abs}	A_{abs}	B_{abs}	R^2
HPTA	24945 (290)	-1190 (395)	-130 (105)	-240 (140)	-770 (130)	0.67
1a	24725 (340)	-1200 (440)	-585 (110)	0	-585 (140)	0.84
1b	24480 (370)	-1300 (450)	-505 (155)	0	-820 (180)	0.78
1c	25130 (370)	-1695 (465)	-285 (135)	-430 (145)	-780 (155)	0.78
1d	24885 (360)	-1330 (455)	0	-470 (120)	-625 (135)	0.61
1e	25135 (355)	-1755 (450)	0	-385 (120)	-550 (140)	0.57
Compound	$v_{0,\,em}$	Q_{em}	P_{em}	A_{em}	B_{em}	R^2
HPTA	24900 (620)	-2150 (850)	-1140 (260)	-690 (305)	-1185 (335)	0.82
1a	24765 (1135)	-3255 (1450)	-1040 (205)	0	-1160 (295)	0.87
1b	23290 (700)	-1860 (830)	-930 (240)	0	-1255 (365)	0.87
1c	24660 (475)	-2780 (620)	-705 (145)	-1010 (210)	-890 (185)	0.90
1d	24990 (470)	-3000 (622)	-770 (160)	-995 (235)	-1080 (200)	0.89
1e	26070 (600)	-4400 (760)	-860 (255)	-1040 (280)	-960 (240)	0.80
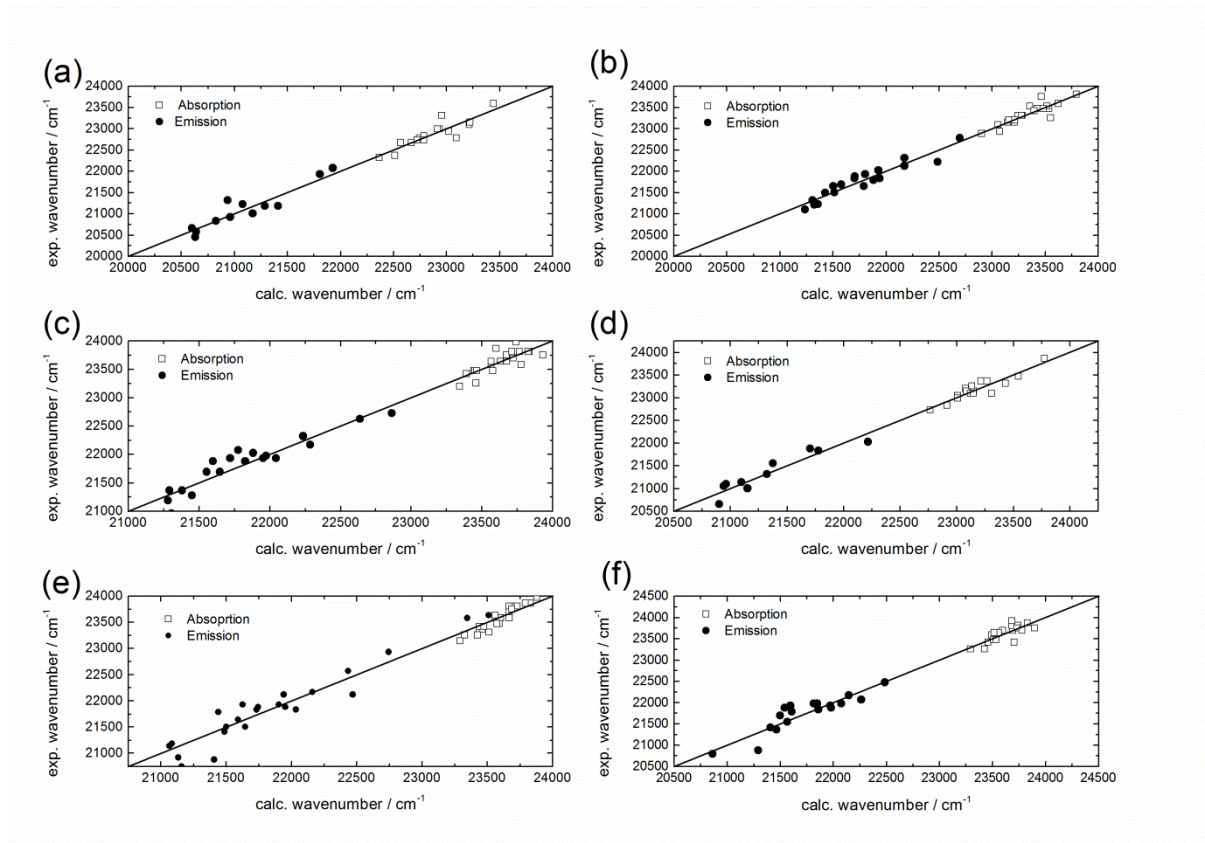
Figure S5. Correlation plots obtained with the Catalán analysis of the photoacids. (a) **1a**, (b) **1b**, (c) **1c**, (d) **1d**, (e) **1e**, (f) **HPTA**
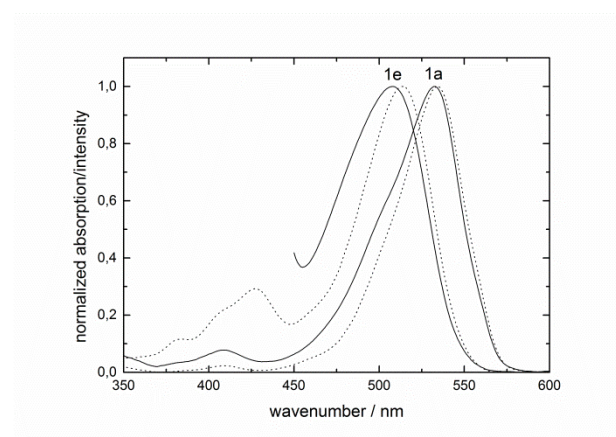

Figure S6. Absorption (full lines) and excitation spectra (dotted lines) of the deprotonated photoacids **1a** and **1e** in ethanol.
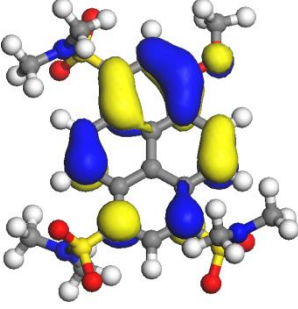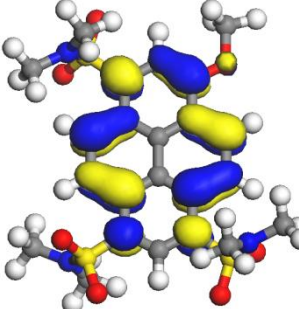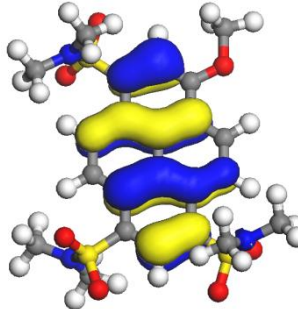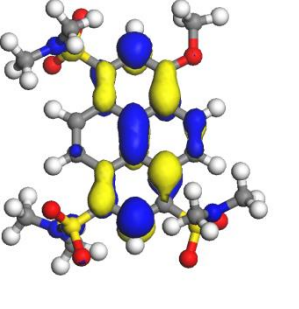
Table S6. Catalán parameters of the deprotonated photoacids. Standard errors are in parenthesis, R^2 is the correlation coefficient. All values are given in cm^{-1}.
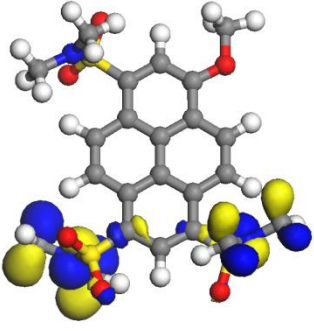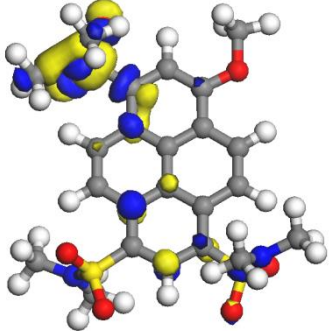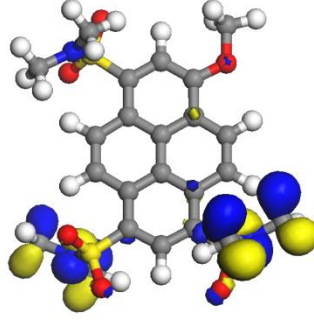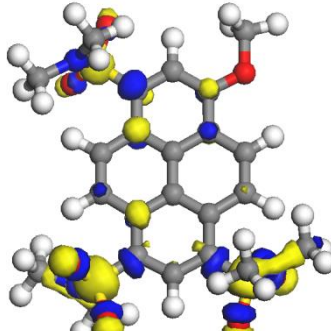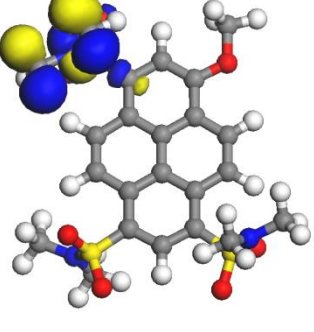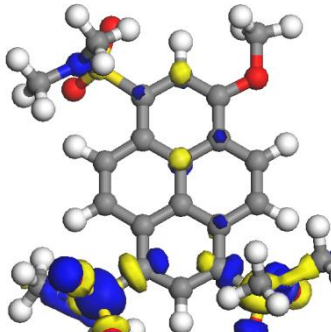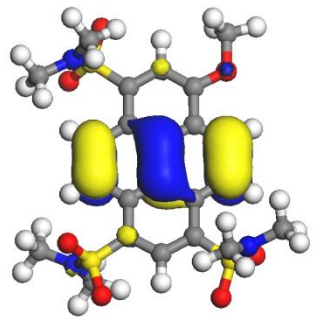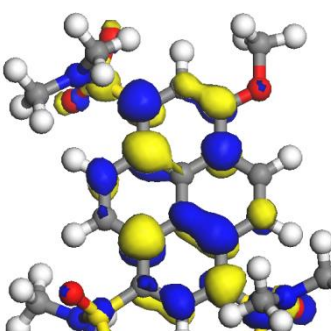
Compound	$\nu_{0, abs}$	A_{abs}	Q_{abs}	R^2	$\nu_{0, em}$	A_{em}	Q_{em}	R^2
HPTA	19800 (530)	1955 (190)	-2365 (700)	0.94	18410 (110)	510 (40)	-1025 (150)	0.97
1a	18435 (430)	2260 (170)	-1210 (590)	0.98	18035 (105)	470 (30)	-840 (145)	0.98
1b	18220 (460)	2125 (180)	-1240 (625)	0.98	17990 (170)	400 (50)	-1045 (235)	0.94
1c	20295 (795)	2060 (245)	-3670 (1090)	0.94	18280 (185)	455 (60)	-1260 (255)	0.95
1d	21325 (900)	1875 (240)	-4515 (1265)	0.95	18420 (165)	395 (50)	-1075 (225)	0.95
1e	21295 (1020)	1715 (365)	-3975 (1300)	0.93	18930 (215)	260 (70)	-1570 (280)	0.96

Table S7. . Excited State Properties Predicted by Quantum Chemical Model Calculations for **MPTA** in Acetonitrile (CIS = 16, LE: locally excited, CT: charge transfer)

state	ΔE, eV	λ_{ex}, nm	$\Delta\mu$, D	f	character	Predominant transitions	% contributions
S1	2.99	414	1.52	0.501	LE(Py)	H→L H-1→L+1 H-6→L+5	62 22 10
S2	3.26	381	0.72	0.034	LE(Py)	H-1→L H→L+1	43 50
S3	3.08	402	7.78	0.025	LE CT CT CT	H-4→L+2 H-4→L+3 H-4→L+1 H-4→L+5	62 17 14 10

S4	3.12	398	5.90	0.032	LE+CT	H-2→L+4	44
					LE+ CT	H-2→L+3	36
					CT (Py)	H-2→L+5	10
S5	3.14	395	6.14	0.013	CT(Py)+LE	H-3→L+3	48
					CT (Py)	H-3→L+5	21
					LE	H-2→L+4	29
S6	3.65	340	0.70	0.003	LE (Py)	H-5→L	61
					LE (Py)	H→L+6	21

	HOMO -9.15 eV		LUMO -2.43 eV
	H-1 -10.06 eV		L+1 -1.25 eV

	H-2 -10.54 eV		L+2 -1.02 eV
	H-3 -10.57 eV		L+3 -0.84 eV
	H-4 -10.70 eV		L+4 -0.79 eV
	H-5 -10.75 eV		L+5 -0.58 eV

	H-6 -11.09 eV		L+6 -0.41 eV
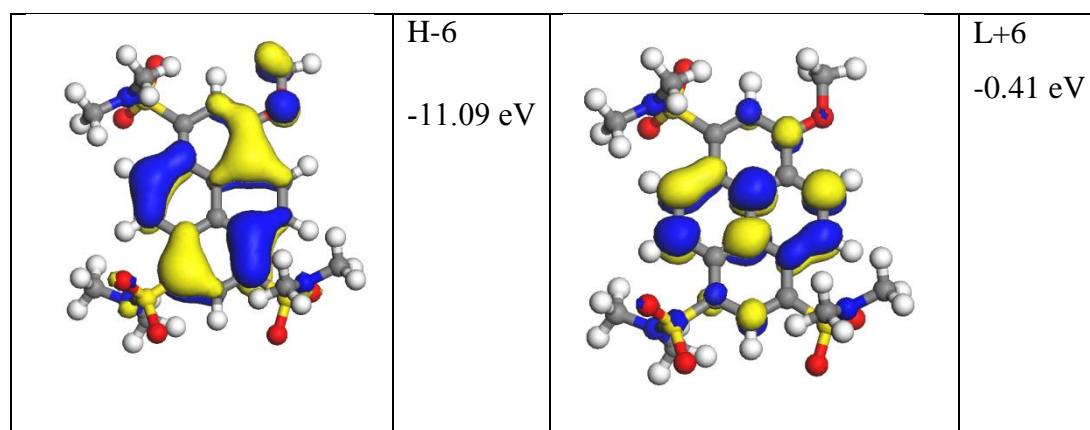
Figure S7. Schematic presentation of the molecular orbitals involved in the CI-description of the excited states of **MPTA** (in acetonitrile).

Table S8. . Excited State Properties Predicted by Quantum Chemical Model Calculations for **MPTS** in Acetonitrile (CIS = 16, LE: locally excited, CT: charge transfer)

state	ΔE, eV	λ_{ex}, nm	$\Delta\mu$, D	f	character	Predominant transitions	%
S1	2.97	416	0.56	0.310	LE (Py)	H→L	55
						H-3→L+2	13
S2	3.18	389	0.19	0.080	LE (Py)	H-1→L	45
						H-3→L+4	12
S3	3.86	321	0.31	0.001	LE (Py)	H-2→L	58
						H-3→L	10
S4	3.91	316	1.11	0.050	LE (Py)	H→L+3	42
						H-3→L+1	23
						H-6→L	16
S5	4.32	286	0.66	0.009	LE (Py)	H→L+2	43
						H-6→L+1	11
S6	4.48	276	3.99	0.565	LE (Py)	H-1→L+1	34
						H-3→L	25

| S7 | 4.66 | 264 | 3.82 | 0.755 | LE (Py) | H→L+1 | 43 |
| | | | | | | H-1→L | 42 |
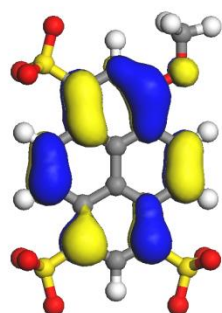
HOMO
-8.40 eV
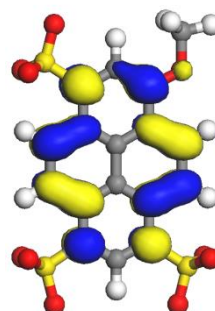
LUMO
-1.50 eV
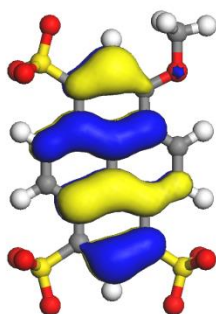
H - 1
-9.25 eV
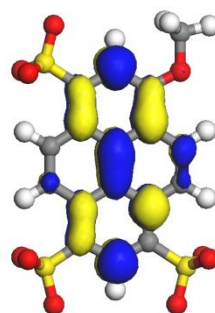
L + 1
-0.50 eV
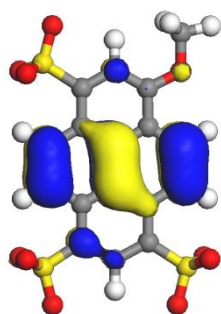
H - 2
-10.11 eV
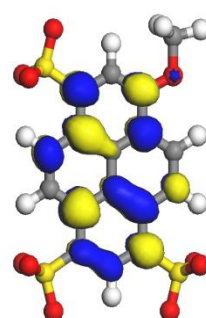
L + 2
0.20 eV
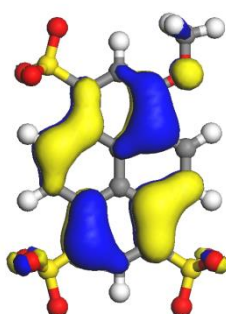
H - 3
-10.28 eV
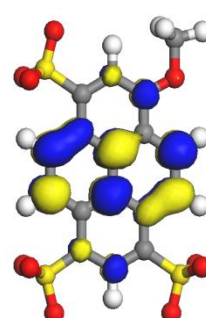
L + 3
0.29 eV
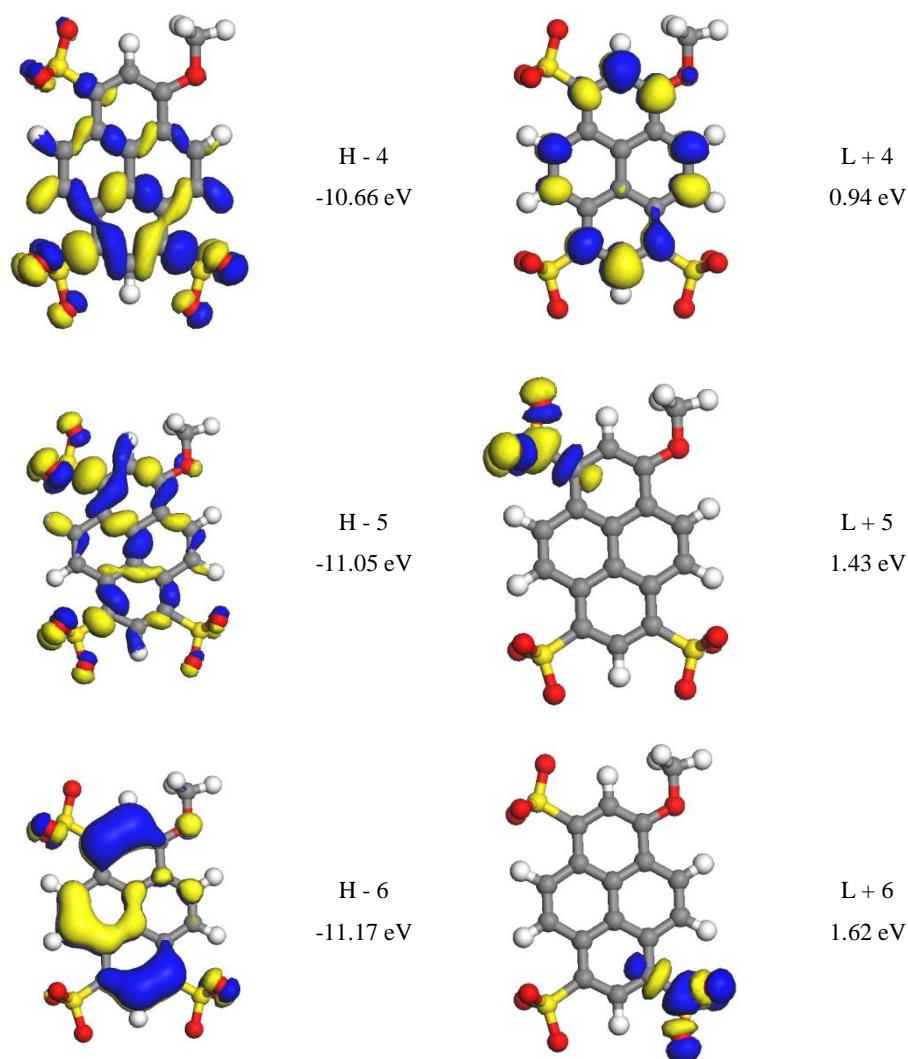
Figure S8. Schematic presentation of the molecular orbitals involved in the CI-description of the excited states of **MPTS** (in acetonitrile).
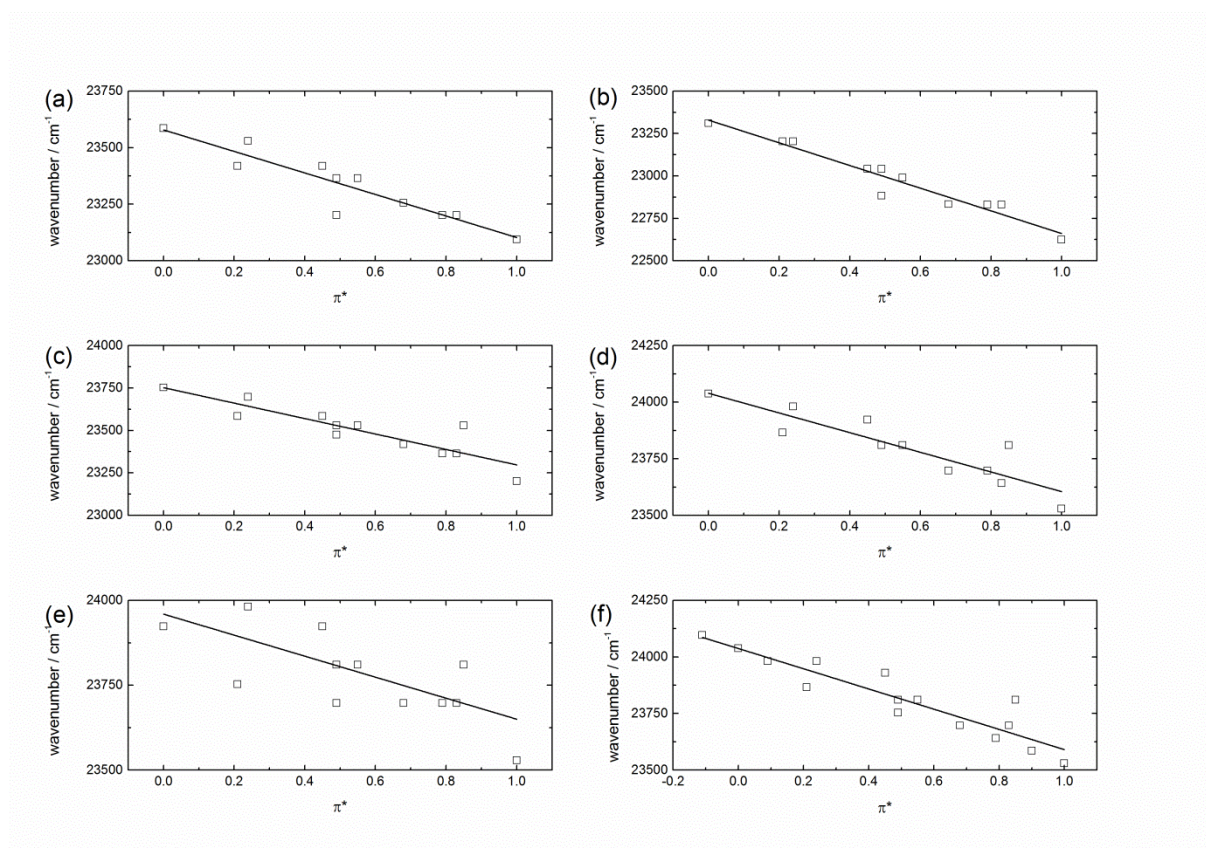
Figure S9. Absorption (squares) frequencies of the methylated photoacids in solvents of increasing polarity. (a) **2a**, (b) **2b**, (c) **2c**, (d) **2d**, (e) **2e**, (f) **MPTA**
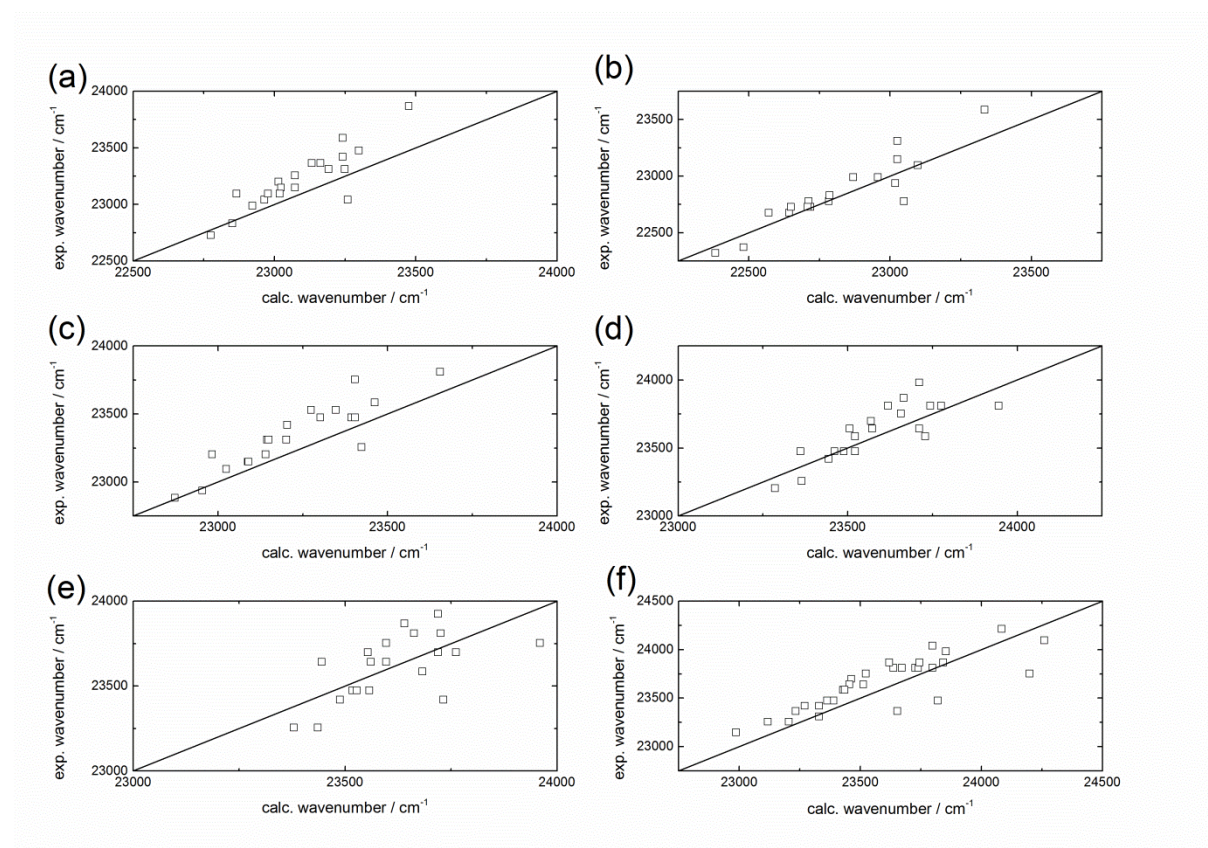
Figure S10. Correlation plots for absorption maxima obtained with the Kamlet-Taft analysis of the photoacids. (a) **1a**, (b) **1b**, (c) **1c**, (d) **1d**, (e) **1e**, (f) **HPTA**
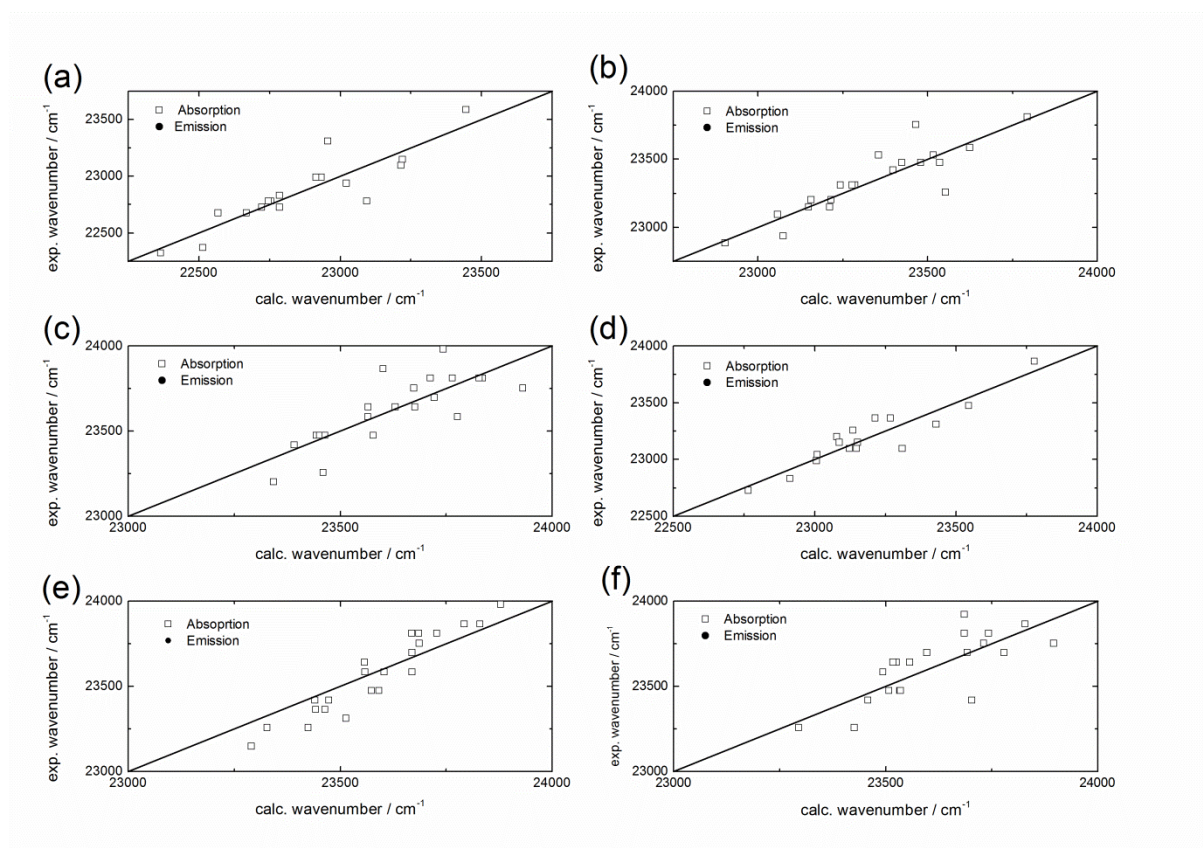
Figure S11. Correlation plots for absorption maxima obtained with the Catalán analysis of the photoacids. (a) **1a**, (b) **1b**, (c) **1c**, (d) **1d**, (e) **1e**, (f) **HPTA**

References

(1) Finkler, B.; Spies, C.; Vester, M.; Jung, G. Versatile Series of Highly Photostable "Super"-Photoacids with High Quantum Yield for Biological and Single-Molecule Investigations. *submitted* **2013** .

Solvent Dependence of Excited-State Proton Transfer from Pyranine-derived Photoacids

Christian Spies,[a] Shay Shomer,[b] Björn Finkler,[a] Dina Pines,[c] Ehud Pines,*[c] Gregor Jung*[a] and Dan Huppert*[b]

Steady-state and time-resolved techniques were employed to study the excited-state proton-transfer (ESPT) rate of two newly synthesized 8-hydroxy-1,3,6-pyrenetrisulfonate (pyranine, HPTS) derived photoacids in three protic solvents, water, methanol and ethanol. The ESPT rate constant k_{PT} of tris(1,1,1,3,3,3-hexafluoropropan-2-yl)-8-hydroxypyrene-1,3,6-trisulfonate, **1a**, whose $pK_a^* \sim -4$, in water, methanol and ethanol is $3 \times 10^{11} s^{-1}$, $8 \times 10^9 s^{-1}$ and $5 \times 10^9 s^{-1}$ respectively. (8-hydroxy-N1,N3,N6-tris(2-hydroxyethyl)-N1,N3,N6-trimethylpyrene-1,3,6 trisulfonamide, **1b**) is a weaker acid than **1a** but still a strong photoacid with $pK_a^* \sim -1$ and the ESPT rate in water, methanol and ethanol is $7 \times 10^{10} s^{-1}$, $4 \times 10^8 s^{-1}$ and $2 \times 10^8 s^{-1}$. We qualitatively explain our kinetic results by a Marcus-like free-energy correlation which was found to have a general form suitable for describing proton transfer reactions in both the proton-adiabatic and the proton-non-adiabatic limits.

Introduction

Photoacids are aromatic organic molecules that are weak acids in their ground electronic state, but of acidity greater by many orders of magnitude in their first excited electronic state. Thus, photo-excitation to the excited state, by short UV-Vis laser pulses, enables one to follow the photoprotolytic processes. Intermolecular excited-state proton transfer (ESPT) from the acidic group of the excited photoacid to a nearby solvent molecule[1-15] is widely researched.

Optically excited hydroxypyrene (HP) is a very weak photoacid with ESPT to water rate that is much smaller than its radiative decay rate of $\sim 10^8$ s^{-1}, so ESPT from HP is barely detectable.[16] The ESPT rate constant of relatively weak photoacids whose $pK_a^* > 0$ in water is considerable, but still relatively small compared to the characteristic solvation times in water which fall in the ps to sub-ps time scale. The observed ESPT rates for this common class of photoacids, $k_{PT} < 5 \times 10^{10} s^{-1}$, diminishes by 3-5 orders of magnitude even in polar, protic solvents like methanol or ethanol. As a result, most commonly used photoacids are incapable of proton dissociating in non-aqueous solvents and so, traditionally, photoacidity has become associated with water as a special solvent for the proton.[17] However, it has become apparent that stronger photoacids ($pK_a^* < 0$) are capable of transferring a proton to polar solvents like alcohols and dimethylsulfoxide (DMSO) within the excited-state lifetime. For pyranine, 8-hydroxy-1,3,6-pyrenetrisulfonate (HPTS), a commonly used photoacid with $pK_a^* = 1.3$, we found[18] that the ESPT rate in water/methanol mixtures decreases as the methanol content in the mixture increases. By extrapolation, we estimate that the ESPT rate constant, k_{PT}, in neat methanol is $\sim 5 \times 10^8 s^{-1}$, whereas in water it is 10^{10} s^{-1}, i.e., three-and-a-half orders of magnitude larger than in methanol. Since the

excited-state decay rate of HPTS is $2 \times 10^8 s^{-1}$, the ESPT efficiency in methanol is only of the order of 1% or less. Another HP derivative, 8-hydroxypyrene-hexamethyl-1,3,6-trisulfonamide (HPTA), with $pK_a^* = -1.5$[19] was found to transfer the proton in 20 ps to water as well 5-cyano-1-naphthol with $pK_a^* = -2.8$[20] was found to transfer proton to water with rate of 1.2×10^{11} s^{-1} and to methanol in 2×10^9 s^{-1}. We found that 5,8-dicyano-2-naphthol (DCN2)[21-23], whose $pK_a^* \sim -4$ efficiently transfers a proton to methanol and ethanol with proton-transfer rates of 1.6×10^{10} s^{-1} and 8.3×10^9 s^{-1}, respectively. N-methyl-6-hydroxy quinolinium, NM6HQ$^+$, is an even stronger photoacid with $pK_a^* \sim -6$.[14, 24, 25] The ESPT rate constant of this photoacid in water, methanol and ethanol is 5×10^{11} s^{-1}, 1.25×10^{11} s^{-1} and 0.5×10^{11} s^{-1}, respectively.[24, 25] In a recent study, slightly smaller values were obtained for alcoholic solutions.[26] In the described cases the difference in the values of k_{PT} in water and in alcohols decreases as the strength of the photoacid increases.

In the current study we report on the photoprotolytic properties of two newly synthesized pyranine derived photoacids shown in scheme 1. The synthesis and basic photophysical parameters of the photoacids have been described elsewhere.[27] Generally, introducing strong electron-withdrawing substituents on the aromatic ring system of a weak photoacid increases the photoacidity considerably.[7, 27] **1a** is a strong photoacid with $pK_a^* \sim -4$ determined by the Förster cycle. Both the ROH and RO$^-$ emission bands of this compound are red shifted with respect to HPTS. The second photoacid is an intermediate strong photoacid with $pK_a^* \sim -1$. We found that both photoacids are capable of transferring a proton not only to water but transfer a proton also to methanol and ethanol. Both photoacids are categorized as super-photoacids according to their rate constants for ESPT. The strongest photoacid **1a** exhibits ESPT rate constants in water, methanol, ethanol of $3 \times 10^{11} s^{-1}$, $8 \times 10^9 s^{-1}$ and $5 \times$

$10^9 s^{-1}$, respectively. The rate constants of both photoacids in all three solvents can be correlated with similar photoacids by the empirical Marcus correlation.
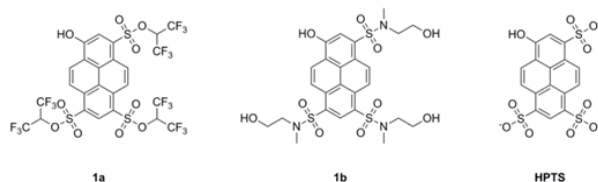
Scheme 1. Structure of the photoacids under investigation in this study.

Table 1. pK_a and pK_a^* values of the photoacids **1a** and **1b**.[27]

	1a	**1b**
pK_a	4.4	5.7
pK_a^*	-3.9	-0.9

Experimental Section

Spectroscopy

For all spectroscopic measurements solvents were of spectroscopic quality and used without further purification. Solvents were always checked for background fluorescence prior to use. Acidification of the samples was achieved by adding 0.1 M hydrochloric acid.

Fluorescence spectra were measured using the Jasco FP-6500 spectrofluorometer (wavelength accuracy ± 0.5 nm). Measurements of time-correlated single-photon counting (TCSPC) were performed with the use of excitation from a cavity-dumped Ti:sapphire femtosecond laser (Mira, Coherent), which provides 150 fs pulses at approximately 800 nm. The second harmonic of the laser, operating over the spectral range of 380-420 nm, was used to excite the samples. The cavity dumper operated with a relatively low repetition rate of 800 kHz. The TCSPC detection system was based on a Hamamatsu 3809U photomultiplier and an Edinburgh Instruments TCC 900 computer module for TCSPC. The overall instrument response was approximately 40 ps (full-width at half-maximum, FWHM) where the excitation pulse energy was reduced to about 10 pJ by neutral-density filters. The fitting of the TCSPC data was carried out by exponential fits and further by solving the Debye-Smoluchowski equation (DSE), using the Spherical Symmetric Diffusion Problem (SSDP) program, developed by Krissinel and Agmon.[28]

The fluorescence up-conversion technique was employed in this study to measure the time-resolved emission of **1a** and **1b** (Scheme 1) compounds in several solvents at room temperature. The laser used for the fluorescence up-conversion was also a cavity-dumped Ti:sapphire femtosecond laser (Mira, Coherent), which provides 150 fs pulses at about 800 nm. The cavity dumper operated with a relatively low repetition rate of 800 kHz. The up-conversion system (FOG-100, CDP, Russia) operated at 800 kHz. The samples were excited by pulses of ≈ 8 mW on average at the SHG frequency. The time response of the up-conversion system is evaluated by measuring the

relatively strong Raman Stokes line of water shifted by 3600 cm^{-1}. It was found that the full width at half-maximum (FWHM) of the signal is 340 fs. Samples were placed in a rotating optical cell to avoid degradation. We found that, during our five-minute time-resolved measurements in a cell rotating at a frequency of 10 Hz, the degradation of the sample was marginal and had no effect on the signal's decay profile

Reversible and irreversible photo-protolytic cycles of the photoacid

Excitation of a photoacid solution of pH lower than its ground-state pK_a, generates a vibrationally relaxed, electronically excited ROH molecule (denoted by ROH*) that initiates a photoprotolytic cycle (Scheme 2).[20, 29-34]
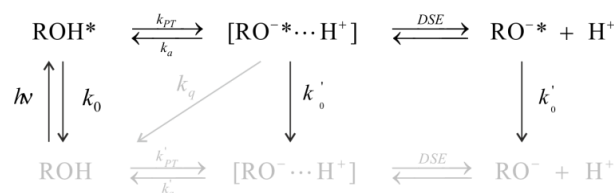
Scheme 2. The photoprotolytic cycle. Steps that are not important for this study are shown in grey.

Proton dissociation, with an intrinsic rate constant k_{PT}, leads to the formation of an ion-pair $RO^-*\cdots H_3O^+$ that subsequently forms an unpaired RO^-* and a solvated proton by diffusion as modeled by the Debye-Smoluchowski Equation (DSE). The proton and the RO^-* may recombine via reversible (adiabatic) geminate recombination with a rate constant k_a and reform the excited acid, ROH*.[29-32] In general, back-protonation may also proceed by an irreversible (non-adiabatic) pathway, involving fluorescence quenching of the RO^-* by a proton with a rate constant k_q, forming the ground-state ROH. 1-naphthol and its derivatives are known to exhibit considerable fluorescence quenching of the deprotonated form, RO^-*, in acidic aqueous solutions.[20, 33, 34]

Removal of an ion-pair from the contact radius a to infinity is described by the transient numerical solution of the DSE.[35, 36] The motion of the transferred proton in water near the photoacid depends strongly on the electrical potential existing between it and RO^-*. The diffusion-assisted geminate recombination (GR) of the RO^-* with the proton could be quantitatively described with the use of the numerical solution of the DSE under the initial and boundary conditions of the photoprotolytic process. In addition, the finite fluorescence lifetimes of all excited species should be taken into account, with $1/k_0 = \tau_{ROH}$ for the acid, and $1/k_0' = \tau_{RO^-}$ for the conjugate base. Generally, k_0' and k_0 are much smaller than both the proton-transfer and the diffusion-controlled rate constants. The decaying amplitude of the long-time delayed fluorescence (long-time 'fluorescence tail') of ROH* depends, beside on k_0, on the intrinsic protonation and deprotonation rate constants, k_a and k_{PT}, on the proton-diffusion constant, D_{H^+}, and on the columbic interaction between RO^-* and the proton.

Results

Figure 1 shows the excitation and emission spectra of the compounds **1a** and **1b** in the three solvents used in this study. All photoacids exhibit excited-state proton transfer in each solvent to a varying extent. While **1a** has only minor differences in ESPT capability in these solvents and transfers the proton very efficiently, the weaker photoacid **1b** shows a more varying amount of ESPT.
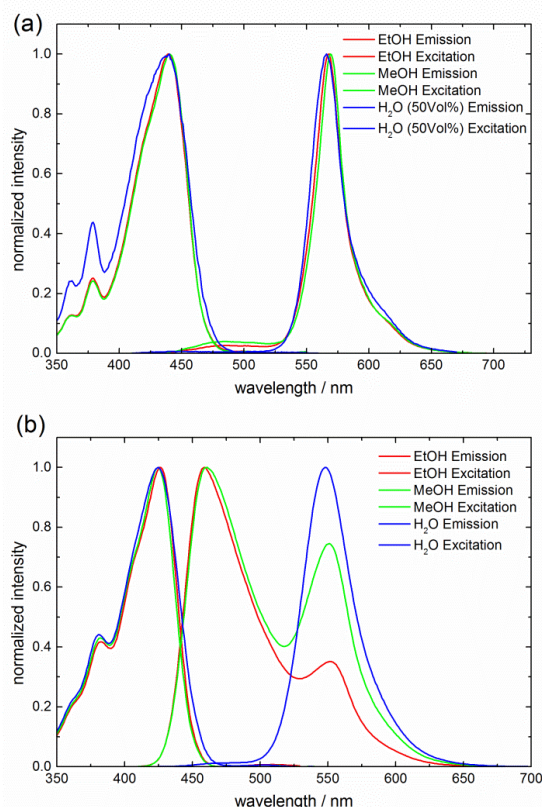
Figure 1. Steady state excitation and emission spectra of compound **1a** (a) and **1b** (b) in the solvents methanol, ethanol and water.

While for the latter, proton transfer in water is also very efficient, the amount of anion emission diminishes with a decrease of solvent polarity in the order methanol to ethanol. The effect of solvent properties on the ESPT in these molecules has been described in detail elsewhere.[35] It should be mentioned here that the emission of both R*OH and R*O⁻ of **1a** is slightly red shifted compared to **1b**. Due to the low solubility of **1a** in water, mixtures of water with methanol were used in this study to measure the properties of the compound in a water-rich environment. The sharp emission band of R*O⁻ and its small solvatochromism in the investigated solvents as well as the very high quantum yield of R*O⁻ is ideal for separating its fluorescence from the broad emission band of the R*OH form in time-dependent experiments.

Proton transfer in methanol

Figure 2 shows the TCSPC emission signals of **1a** in methanol measured at 10 nm intervals in the spectral range 460-600 nm. The R*OH signals plot on a semi-logarithmic scale show that the signals consist of two main

contributions. At short times the proton transfer process takes place with a time constant of about $\tau_{PT} = 120$ ps (Table S1). The non-exponential long-time fluorescence tail shown in figure 2(c) is the "finger print" of the diffusion assisted reversible GR process, which reforms the R*OH form without quenching it back to the ground state. The signal at long wavelength marks the appearance of the deprotonated (anion) form of the photoacid and displays a rise time of about 120 ps, which matches the proton transfer rate as judged by the R*OH decay. The fluorescence decay of R*O⁻ is found as $1/k_0' \approx 6$ ns.
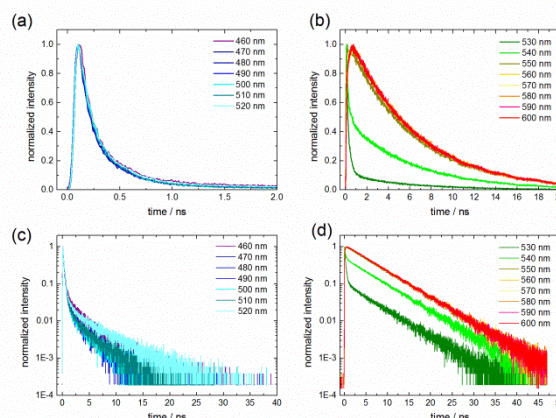
Figure 2. TCSPC curves of **1a** in methanol between 460 nm and 600 nm, on a linear (a), (b) and semi-logarithmic scale (c), (d).

Figure 3 shows the fitting of the TCSPC experimental results measured at 480 nm and 590 nm by the SSDP program described in the experimental section.[28] The adjustable parameters are the radiative lifetimes of both the R*OH and R*O⁻ form of the photoacid as well as k_{PT} and k_a. The Coulomb potential and the reaction sphere radius are important parameters that strongly influence the recombination probability. The reaction sphere radius in our fitting is 6.5 Å. This radius is approximately the molecular size plus one solvent layer.[36] The mutual diffusion constant is $\sim 4.4 \times 10^{-5} \ cm^2 s^{-1}$ and the fitting parameters are the ESPT rate constant k_{PT} and the intrinsic recombination constant k_a. We found $k_{PT} = 8.8 \times 10^9$ s⁻¹ and $k_a = 12.4 \times 10^9$ Ås⁻¹. The latter value can be converted into more convenient units,[33] resulting in $k_a = 5.7 \times 10^9$ s⁻¹.
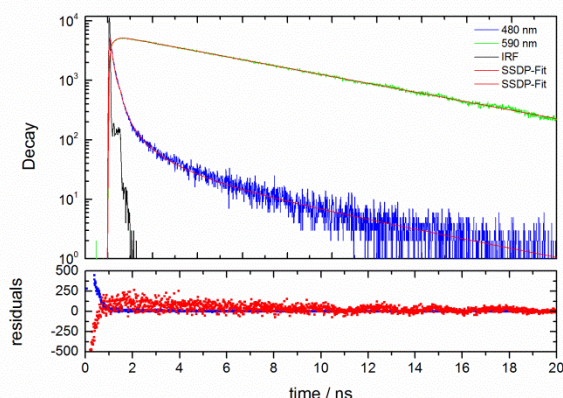
Figure 3. TCSPC data of **1a** in methanol measured at 480 nm and 590 nm and the fit using the SSDP program[28].

As seen in Figure 3, the fit is rather good at both short and long times. The value of k_{PT} is in good agreement with the value estimated from the multi exponential fitting. As we are especially interested in k_{PT}, we consequently omitted extensive consideration of GR. It should be noted at this point that putative proton-hopping along hydrogen bonding chains does not bias the evaluation of k_{PT}, especially as following proton diffusion is much faster than this primary process.

Figure 4 shows the time-resolved emission of **1b** in methanol measured at several wavelengths in 10 nm intervals in the spectral region of 440-570 nm. The R*OH band intensity is larger than the R*O⁻ band as seen in steady-state emission in Figure 1. This fact indicates that the proton transfer rate from **1b** to methanol is comparable to the radiative decay rate of the excited photoacid. Table S2 provides the fitting parameters of the time-resolved emission signals shown in Figure 4. We used a three exponential fit function to fit the data.
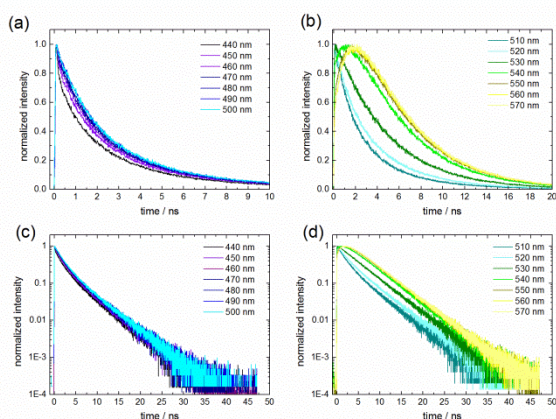
Figure 4. TCSPC curves of **1b** in methanol between 440 nm and 570 nm, on a linear (a), (b) and semi-logarithmic scale (c), (d).

The R*OH signals at short wavelength $\lambda \leq 500$ nm show a short time component of about 0.14 ns with decreasing amplitude when the wavelength is increased. The major decay component has an amplitude of ~0.5 and a lifetime of ~1.6 ns. The third time component of amplitude ~0.3 has a lifetime of ~4.7 ns which is close to the radiative lifetime of

the R*OH form of **1b**. The major component is attributed to the proton transfer process from **1b**, as its rising counterpart is found at $\lambda > 540$ nm. This time constant is strongly influenced by the radiative rate and - to a lesser extent - by the proton geminate recombination process, see Scheme 2. The proton transfer rate constant could be evaluated by equation (1) where $1/k$ is the fitting intermediate time component of 1.6 ns ($k = 6.2 \times 10^8 s^{-1}$).

$$k = k_0 + k_{PT} \qquad (1)$$

We estimate k_0 from the third fitting term, $\tau = 4.7\ ns$, which leads to $k_0 \sim 2.1 \times 10^8 s^{-1}$ and $k_{PT} \sim 4 \times 10^8 s^{-1}$. At longer wavelengths, $\lambda > 540$, nm the signal consists of a rise time that matches the proton transfer rate constant as evaluated from the decay of the ROH form. The fluorescence lifetime of the anionic form of **1b** in methanol is also about 4.7 ns.

Figure S1 shows the time-resolved fluorescence of both the **1a** and the **1b** photoacids in methanol measured by the fluorescence up-conversion technique. The time window of these experiments is rather small, ~ 150 ps and the R*OH and R*O⁻ signals are measured at a large range of wavelength (Tables S3 and S4). As with the TCSPC data, which was taken with much inferior time-resolution, both **1a** and **1b** emission signals show short-time decay components whose amplitude and time-constants depend strongly on the wavelength.[37] With the much better time-resolution at hand, the short-time decay components with $\tau < 10$ ps are attributed to solvation dynamics and possibly to some slow charge rearrangement, that occur prior to the ESPT process.[8, 35] The **1a** compound is a much stronger photoacid and the TCSPC results shown in Figure 3 indicate that the ESPT time constant in methanol is about 120 ps. This result is indeed confirmed in Figure S1. The fluorescence up-conversion signals average decay time at the wavelength range 490-520 nm is about 130 ps. The TCSPC time resolved emission results of **1b** in methanol indicate that the ESPT rate to methanol is rather small and of the order of the radiative rate with $k_{PT} \sim 4 \times 10^8\ s^{-1}$. This slow decay rate is almost not affecting the fluorescence up-conversion signals in the narrow time window of 150 ps. The wavelength-dependent 140 ps component found in the TCSPC measurements of the blue edge emission spectrum of **1b** can neither be attributed to solvation dynamics nor to the ESPT reaction. A possible explanation hints to a σ-complex of a protic solvent molecule and the π-ring system of pyrene as proposed by Wan et al. for hydroxypyrene.[38] This complex may offer a pathway for a fluorescence quenching. However, a detailed analysis of this decay component is out of the scope of the present manuscript and will be addressed in the near future in more detail (see also the SI for a short discussion of the wavelength dependence).

Proton transfer in ethanol

Figure S2 (a) and (b) show the time-resolved emission of compounds **1a** and **1b** in ethanol solution measured by the TCSPC technique at several wavelengths in the spectral

region of 450-600 nm. The ESPT rate of **1a** is about 200 ps as estimated from the average decay time of R*OH and the matching rise time of the R*O⁻ signal. The signals of the R*OH forms measured at 460-500 nm exhibit also the GR non-exponential fluorescence tail. The R*O⁻ signal measured at 560-600 nm displays a distinctive rise time followed by an exponential long time decay attributed to the radiative lifetime of the R*O⁻ form, $1/k_0' = 6$ ns. The weak photoacid **1b** R*OH signals measured at short wavelengths 420-500 nm show a rather slow decay. From the multiexponential fit we deduce that the ESPT rate is slow, about 2.2 ns. The R*O⁻ signals measured at long wavelengths region 540-570 nm exhibit a distinctive long rise time component that matches the decay, followed by an exponential decay. Reconvolution fittings of TCSPC data of **1a** in ethanol using exponential functions are summarized in Tables S5 and S6. Again, a fast decaying signal at the blue edge was found ($\tau \approx 280$ ps) which could neither be attributed to solvation dynamics nor to ESPT.

The fluorescence up-conversion signals measured at several wavelengths of both **1a** and **1b** compounds in ethanol solutions are shown in Figure S3. Reconvolution fittings using exponential functions are summarized in Tables S7 and S8. These measurements confirm that the ESPT rate in ethanol solution is somewhat slower than in methanol solution. The solvation dynamics are also slower than in methanol. The ESPT rate of **1a** in ethanol is about $k_{PT} \sim 5 \times 10^9 \ s^{-1} (\tau_{PT} \sim 200 \ ps)$ in accordance with the results obtained by the TCSPC measurements.

Water methanol mixtures

The compound **1a** is almost insoluble in neat water but could be dissolved in considerable amount in methanol rich water-methanol mixtures. On the other hand, compound **1b** is readily soluble in neat water. Figure S4 shows the TCSPC curves of **1b** and **1a** in water and a water-methanol mixture, respectively. Most of the decay of **1b** in neat water is as fast as the instrument response function (IRF) and occurs on a timescale of about 50 ps. The non-exponential tail at longer times resulting from the GR is also seen in the semi-logarithmic plot. The RO⁻ signal at wavelengths λ > 550 nm consists of a fast rise time, that is hardly discernible in the TCSPC signal and an exponential decay with $\tau_0' = 5.9$ ns. Therefore, it is better to measure the proton transfer rate constant using the up-conversion data, which is shown in Figure 5.
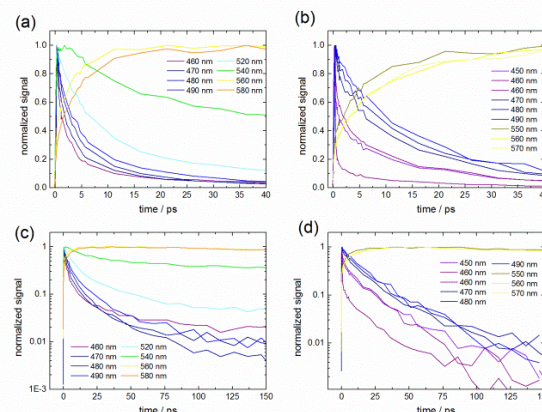
Figure 5. Up-conversion curves of **1a** in 30 vol% water in methanol (a) and **1b** in water (b) between 440 nm and 600 nm, on a linear and semi-logarithmic scale (c), (d).

In this Figure are shown the fluorescence up-conversion signals of the compound **1b** in neat water and of **1a** in water-methanol solution of 30% by volume of water. This mixture composition contains 0.47 mole ratio of water. Water solvation dynamics is ultrafast.[39] It consists of several time components; the short one is of about 50 fs whereas its long-time component is of about 0.8 ps (see Table S9). The solvation dynamics is clearly seen in the **1b** signals since the ESPT rate in this photoacid is rather slow, about $k_{PT} = 15$ ps. In the **1a** fluorescence signals at the ROH emission spectral region the solvation dynamics is faster than the ESPT rate but the two time-components decay times do not differ by much and the overall signal average decay time is about $k_{PT} \approx 4$ ps (see Table S10). The rate constants of both acids in all three solvents studied are summarized in Table 2.

Table 2. The rate constants of proton transfer k_{PT} [s⁻¹] as obtained in this study.

Solvent	1a	1b
Methanol	8×10^9	4×10^8
Ethanol	5×10^9	2×10^8
Water	3×10^{11}	7×10^{10}

Discussion

Alternative models

Modern views of proton transfer along a hydrogen bond in polar solutions invoke two limiting mechanisms, which are termed the quantum adiabatic and the quantum non-adiabatic (tunneling) proton transfer regions.[40-43]

Adiabatic proton transfer reactions occur when the coupling between the reactant and product potential wells is strong. The interaction lowers the activation energy for the proton transfer and the adiabatic reaction limit is achieved when the ground-state proton vibration in the H-bonded complex are above the reaction barrier, a situation which is likely to describe proton transfer reactions along strong H-bonds when the distance between the two heavy atoms is short. In the non-adiabatic (tunneling) limit the interaction is relatively weak and the heavy-atom distance in the H-bonded complex is likely to be large. In this model the two lowest vibrations of the proton are below the reaction

barrier and the proton tunnels in order to transfer to the product well. Below we mainly follow the discussion of the two reaction regions as given by Kiefer and Hynes[44-47]. In the proton adiabatic non-tunneling model the reaction barrier is formed by the solvent. In this view, the ultrafast quantum proton is able to follow adiabatically the continuous change in the solvent structure around the H-bonding complex. The proton transfer event occurs when the solvent reaches a configuration where there is no barrier for the proton transfer. Under such conditions the effective reaction coordinate and the effective activation energy for the proton transfer are that of the solvent. More precisely, the solvent rearranges continuously and the activation energy for the adiabatic proton transfer is that required of the solvent to rearrange so to (temporarily) create solvation conditions suitable for adiabatic proton transfer. The proton transfer rate, k_{PT}, in the proton adiabatic limit is given by a transition-state-like reaction rate eq. 2.

$$k_{PT} = \frac{\omega_s}{2\pi} exp(-\frac{\Delta G^{\#}}{RT}) \qquad (2)$$

R is the gas constant, T the absolute temperature, w_s and $\Delta G^{\#}$ are the frequency factor and the effective activation energy for the proton transfer reaction. The frequency factor ω_s is a property of the solvent and is related to the time needed for the solvent to adopt the configuration which stabilizes the proton transition state in the appropriate adiabatic conditions. It follows, that in such a case ω_s must be associated with some characteristic relaxation time scale of the solvent structure.

Using fundamentally based arguments, Hynes et al [44-47] have shown that the general quadratic form of the Marcus' equation[48-51] relating between the activation free-energy $\Delta G^{\#}$ and the thermodynamic free energy change (ΔG_0) for non-adiabatic electron transfer reactions (NA-ET, eq. 3) is also suitable for describing proton transfer in the adiabatic proton limit. In this reaction model the electronic interaction is strong and hence always adiabatic. However, the proton transfer reaction follows solvent rearrangements in much the same way as in non-adiabatic ET.

$$\Delta G^{\#} = (1 + \frac{\Delta G_0}{4\Delta G_0^{\#}})^2 \Delta G_0^{\#} \qquad (3)$$

Here, $\Delta G_0^{\#}$ is the intrinsic activation energy of a symmetric transfer where the total free energy change ΔG_0 following the charge-transfer is equal to zero.

A very important aspect of Marcus relation when widely employed, semi-empirically, in proton transfer reaction, is the direct correspondence between the acidity constant of the acid, pK_a, and the correlating free-energy change in the reaction ΔG_0 (eq. 4).

$$\Delta G_0 = RTln(10) \cdot pK_a \qquad (4)$$

Marcus' semi-empiric BEBO expression for proton transfer[52] (eq. 5) is an alternative, semi-empiric functional form for the dependence of the proton transfer rate on the free energy of the reaction:

$$\Delta G^{\#} =$$
$$\frac{\Delta G_0}{2} + \Delta G_0^{\#} + \frac{\Delta G_0^{\#}}{ln(2)} ln(cosh(\frac{\Delta G_0 ln(2)}{2\Delta G_0^{\#}})) \qquad (5)$$

The two equations (eqs. 3 and 5) are different in form but almost identical numerically in the normal reaction region, i.e. the non-inverted region, where the reaction barrier becomes progressively smaller with an increase in the reaction exothermicity till the reaction reaches its barrierless rate limit. After reaching the limit, this trend is reversed according to eq. 3, but not according to eq. 5.

In the other widely used model, the non-adiabatic (NA) limit, the ground-state vibration level of the proton lies below the reaction barrier and the proton tunnels through the barrier. In the proton NA model at low temperatures and in the strong solvation limit, the reaction activation energy still depends on the reaction free-energy change by a Marcus' - like quadratic relation. In this model the activation energy for NA proton transfer is that required by the solvent to rearrange so to equally stabilize the reactant and product potential wells. The transition-state for the proton transfer in the solvent reaction coordinate is the symmetric double-well potential (pre-proton transfer and post-proton transfer potential wells) of the proton. However, unlike in the adiabatic model, the reaction frequency factor in the NA description depends on the electronic coupling between the reactant and product states and on the reorganization energy of the solvent. The NA proton transfer rate in the low temperature limit - assuming proton transfer only between the reactant ground vibrational level and the product ground vibrational level of the proton - is given by equation 6.[42, 46, 47]

$$k_{PT} = \frac{2\pi}{\hbar} |C_{AB}|^2 \frac{1}{\sqrt{4\pi\lambda RT}} exp(-\frac{\Delta G^{\#}}{RT})(6)$$

In equation 6, $|C_{AB}|$ is the coupling matrix element and λ the reorganization energy of the solvent ($\lambda = 4G_0^{\#}$). The activation energy of a reaction in the NA model is also given by a Marcus-like free-energy relation, which may be written in a general form resembling eq. 3. As already mentioned, eq. 3 implies the existence of an inverted region at large reaction exothermicities. However, it was shown that inclusion of proton transfer between excited vibration states of the proton tends to delay the appearance of the inverted region to physically unattainable reaction driving forces.[53]

We have been using the Kiefer-Hynes (K-H) theory[44-47] as a justification for utilizing Marcus' quadratic expressions for proton transfer in the normal reaction region in conditions preceding the activationless reaction limit of eq. 3. The K-H theory was developed for ground-state acids, while our experiments involve the electronic excited state of the studied photoacids. This complicates the ground-state picture, where the solvent needs only to equilibrate along the proton transfer reaction coordinate. Adding large electronic rearrangements in the reactant and product sides of the proton transfer reaction must also affect the solvent as well as modify the interaction along the H-bond on a time scale which may be similar to the proton transfer time.

However, no analytic theory to date accounts for all aspects of excited state proton transfer (ESPT). Therefore, we assume that the reaction methodology that was developed for ground state acids is also suitable for ESPT as long as the proton transfer rates (and hence also electronic rearrangements preceding or following the proton transfer) are slower than the characteristic solvent relaxation time scale. We thus use the Marcus relation as a general semi-empiric method for establishing the free-energy relation in families of closely related excited-state proton transfer reactions.[54-61] It follows by the previous discussion that proton transfer reactions in both adiabatic and NA regions may be correlated semi-empirically by the Marcus relation. The results in the previous investigations as well as the new results shown in Figures 6 and 7 show that indeed this assumption is valid.

Our current study involves a family of closely structured hydroxypyrene derivatives where a change in the photoacidity (and ground state acidity) of the acids was achieved by very subtle structural changes in the three polar substituents of the photoacids.[27] As such, this newly synthesized family of photoacids is arguably the best group of photoacids studied to date for the purpose of correlating their respective proton transfer reaction rates using the Marcus' equation as we demonstrate in Fig 6. Similar treatments have been done for correlating the PT rates of acids in the ground state with their respective pK_a's.[62] In these correlations it was found that weak acids of similar structure fit nicely to the Brønsted free-energy correlation[63,64] whereas a large change in the molecular structure of two acids having similar pK_a's can cause large deviations in their proton transfer reaction rate. Figure 9 also includes a few strong photoacids which we have previously studied.[18,19, 21, 24, 56]
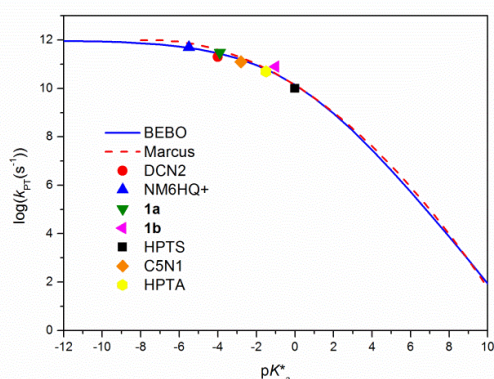
Figure 6. The free-energy correlation found in the proton dissociation reaction of **1a**, **1b**, DCN2, NM6HQ$^+$, HPTS, HPTA and 5C1N in water. The dashed line is for the Marcus equation, eq. (3) and the solid line is for the Marcus BEBO equation, eq. (5). The parameters of the fits are log ($k_{PT}(sec^{-1})$) = 12 for the activationless proton transfer rate and, $\Delta G_0^{\#}$ = 10.5 kJ/mol for the intrinsic barrier common for proton transfer reactions.

The plot of the logarithm of the ESPT rate constant as a function of pK_a (Fig. 6) shows that the slope of the free-energy correlation variably depends on the pK_a values. The rate of the proton transfer from strong photoacids only weakly depends on the pK_a^*, approaching a constant maximum value for the very strong ones with no indication of an inverted region. It is evident from Fig. 9 that the Marcus quadratic and BEBO relations result in practically identical correlations up to about pK_a^* = - 10. At this value, the correlation is already in the inverted region predicted by the quadratic free-energy relation to begin at about pK_a^* = - 7.5 (Figure 6). It is, thus, fortuitous to try to determine which of the two free-energy relations is better for correlating the excited-state proton dissociation reaction of the current pyranol family set of photoacids.

The goodness of the free-energy correlation displayed in Figure 6 shows that, as anticipated, the investigated set of strong photoacids made of pyranol derivatives belong to one family of closely-structured acids. The numerical values of the parameters of the fit are similar to those found in previous correlations which imply that the new pyranol family of photoacids may be correlated with other families of similarly structured photoacids such as the naphthol-based ones. This is not unexpected since HPTS and hydroxypyrene, the parent molecules of the new pyranol family of photoacids, were successfully correlated before with various families of naphthol and a quinoline based photoacid.[54-61]

Below we summarize our general observations based on the kinetic data and its analysis as shown in Fig 6.

1. Intrinsic proton transfer rates to water are ultrafast but do not exhibit an apparent inverted region.

2. The proton transfer rates from different photoacids are well correlated using eqs. 2-5 which are formally adequate for semi-empirically describing proton transfer reactions in the adiabatic and the low temperature NA model.

3. Similarly to what was found in naphthol based families of photoacids, the reaction pre-factor (10^{12} s^{-1}) is relatively slow compared with the inertial and libration time scales of the solvent rearrangements which are both about an order of magnitude faster in water.[65, 66] This finding makes reliable the assumption of a relatively slow change within the solvent, perhaps also involving some translational movements of the solvent, which are controlling the proton dissociation reaction to form the Marcus' product state. According to the Marcus' reaction model the reaction pre-factor is the activation-less rate constant for the formation of the thermodynamic product-state which in our case is the fully solvated solvent-separated ion-pair.

4. The activation energy for the symmetric proton transfer ($\Delta pK_a^* = 0$) is small, about 10.5 kJ/mol. The activation energy becomes progressively smaller for exothermic transfer. This prediction by the correlation is corroborated by direct measurements of the temperature dependence of the proton dissociation reaction of strong photoacids which is typically 4-12 kJ/mol and decreasing with the reaction exothermicity: While it is about 18 kJ/mol for hydroxypyrene (pK_a^* = 4)[19] it decreases to about 10 kJ/mol for HPTS ($pK_a^* \approx 0$)[30, 67] and further decreases to only 6 kJ/mol for HPTA (pK_a^* = -1.5)[19]. In comparison, it is about 10 kJ/mol for the differently structured quinine cyanine 7 (QCy7)

photoacid in ice (pK_a^* ≈ -6).[68]
All of the above suggest, but do not prove, that at room temperature the family set of proton transfer reactions under our considerations likely belongs to the proton adiabatic limit. However, one may also use the general form of eq. 6 which describes the proton transfer rate in the proton NA tunneling limit for the free-energy correlation of the kinetic data as well. Accordingly, one may not completely rule out tunneling as long as there is a barrier for the reaction and the zero point energy (ZPE) of the quantum proton is smaller than the barrier. The main difference between the proton transfer models is the different interpretation of the frequency factor.[40] While in the NA model the frequency factor depends on the electronic coupling between the neutral and proton transfer states when the ground-energy energy levels of the proton in the two states are degenerate (eq. (6),[42, 46, 47] the frequency factor ω_s is assumed to only depend on the solvent in the adiabatic model (eq. (2)). We also note that when approaching in the adiabatic model the barrierless reaction limit, the frequency factor of the reaction as defined by the TS theory becomes increasingly inadequate for the description of the reaction rate. Assuming no inverted region in photoacid proton dissociation reactions such as discussed here, the barrier for the proton transfer is expected to just decrease further with additional increase in the reaction exothermicity until reaching the region where the free-energy correlation shown in Fig. 6 would not hold anymore. In the activationless limit we expect that the rate of the bimolecular proton transfer would approach that observed for ultrafast intramolecular proton transfer reactions which is sub-100 fs.[69-71] The activationless limit might be reached at pK_a ≈ -7.[72] In such cases the rate determining step for the proton transfer would be some vibrational mode of the H-bonded complex which defines the reaction complex. For linear H-bonded complexes this mode is likely to be the H-bond stretch vibration typically about 200 cm^{-1} for photoacid-water H-bond complexes which translates into proton transfer time scale of 100 fs.

Modeling the solvent dependence of photoacid ESPT reaction rate, k_{PT}

Predicting the solvent dependence of outer sphere ET reactions has been considered one of the major triumphs of Marcus Theory[48-51]. Formally speaking, eqs 2 and 6 predict the form of the solvent dependence expected in each of the two limiting cases of proton transfer. However, unlike ET reactions, proton transfer reactions also involve breaking and making of chemical bonds. In addition, protic solvents take part in the reaction complex of acid-base reactions.[4, 5] As a result, in proton transfer reactions, polar solvents act not just as a dielectric medium having some characteristic relaxation times but potentially also as one of the reactants in the reaction. To make things even more complex, it is usually unclear what solvent stoichiometry is involved in proton transfer to associated protic solvents such as water and methanol. Nevertheless, one may use the general form of the Marcus' free-energy dependence of the reaction rate and apply it semi-empirically to various solvent media where the proton transfer reaction takes place. In this case,

the main solvent-dependent parameters of the proton dissociation reaction are the reaction pre-factor and the solvent rearrangement energy. Figure 7(a) summarizes the available solvent effect on the proton transfer reactions of 6 out of the 7 photoacids shown in Fig 6. The kinetic data was taken in water, methanol and ethanol solvents.
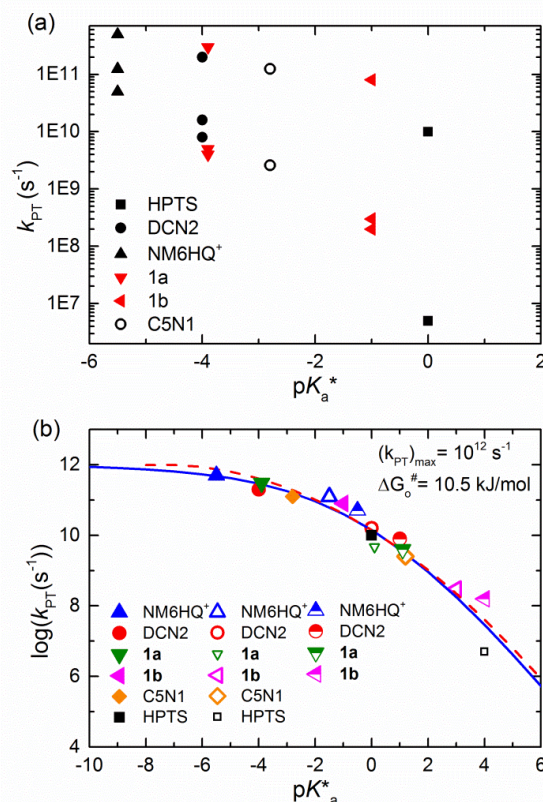
Figure 7. (a) Proton-transfer rate of **1a**, **1b**, DCN2 and NM6HQ$^+$ in three solvents: from top to bottom, water, methanol and ethanol; HPTS and C5N1only have data for water and methanol. Note that the solvent dependence of k_{PT} decreases the smaller pK_a^*. The results from this study are shown in red. (b) The free-energy correlation found in the proton dissociation reaction of **1a**, **1b**, DCN2, NM6HQ$^+$, HPTS and 5C1N in water (solid symbols), in methanol (open symbols) and ethanol (half open symbols). See Figure 6 and discussion for details of the fits.

Comparison of the ESPT rate constants of pyranine derived photoacids and other strong photoacids in water and alcohols

The rate of excited–state proton transfer to the solvent depends on the solvent composition in binary water/alcohols solutions.[21, 24, 56] In contrast to less strong photoacids, it was found that strong photoacids transfer a proton to methanol, ethanol and propanol within the excited state lifetime. The proton dissociation rate for the newly synthesized pyranol derivatives in water, methanol and ethanol was found it to be $3×10^{11}$s^{-1}, $8×10^9$s^{-1} and $5×10^9$s^{-1}, respectively for **1a** and ~$7×10^{10}$ s^{-1}, $4×10^8$ s^{-1}, and $2×10^8$ s^{-1}, respectively, for **1b**. For the comparison of the stronger photoacids with the parent weaker photoacid, HPTS, we could have only used an estimated value of the proton transfer rate of HPTS in methanol by extrapolating the

proton transfer rate measured of HPTS in methanol/water mixtures to pure methanol solutions.

It is clearly seen in Fig 7(a) that the solvent dependence of the proton dissociation rate defined as k_{PT}(water)/k_{PT}(solvent) decreases as the acidity of the photoacid increases. For HPTS there is a difference of more than three orders of magnitude between the values of k_{PT} for water and methanol, whereas for the much stronger photoacid NM6HQ$^+$ it is only about one order of magnitude. It follows that the difference between the ESPT rates of strong photoacids in water and in alcohols such as methanol decreases the stronger the photoacid is.

Below we address the solvent effect as a general consequence of the Marcus- like quadratic dependence between the proton transfer rate and the pK_a* of the photoacids. As benchmark acids, we take ground-state phenols in water, of which the pK^*_a values in methanol are well established.[73] Since the protolytic reaction involves ionic species, a part of this difference in the pK_a^* depends on the dielectric constants that dramatically differ when water (ε=78) is replaced by methanol (ε = 32) or ethanol (ε = 24).

In Fig. 7(b) we plot on one correlation plot the proton transfer rates we have found in water, methanol and ethanol assuming the pK_a*(H_2O) values of the photoacids to be shifted by 4 pK_a units in methanol and by 5 pK_a units in ethanol. The solvent affected pK_a^* values reflect a constant decrease in the acidity of the photoacids in methanol and ethanol. Actually, similar values were found experimentally for many ground state phenols.[73, 74]

Clearly evident in Fig. 7(b) is that a constant shift in the equilibrium acidity of the photoacids when transferred from water to methanol and ethanol is able to account for most of the observed solvent effect on the proton transfer rate. The general form of the Marcus-type free-energy correlation that we have observed in water is nicely maintained in methanol and ethanol. Furthermore, the observed shape of the correlation is similar in all 3 solvents. We are, thus, in a position to conclude that at least on qualitative grounds the general form of the Marcus free-energy correlation is able to account for the observed solvent effect on the proton dissociation rate by using only one solvent-dependent reaction parameter namely, the acidity constant of the photoacid. Other reaction parameters, especially the reaction frequency factor and the solvent rearrangement free-energy around the reaction transition state, are not as sensitive to replacing water by methanol or ethanol for here studied photoacids.

The observed solvent dependence is not immediately understood in either the terms of the rate equation describing the proton adiabatic limit or the rate equation describing the proton NA limit. Possible explanation is additional complexities in the mechanism not taken into account in the current treatments of the two reaction limits. This may cause the reaction to be an intermediate case between the pure tunneling case and the pure over-the-barrier (adiabatic) case. Another possibility is that the solvation dynamics of the studied hydroxylic solvents are intimately convoluted with the proton transfer reaction and much more so than what was generally considered for the treatment of fluorescent probes.[37] Intramolecular charge transfer processes typical of photoacids[6, 35] in the reactant and product sides may also affect the observed proton transfer kinetics. In addition, the reaction complex which undergoes proton transfer may involve more than one solvent molecule. Such reactions are still poorly understood in aqueous solutions and in alcohols.

However, arguing for an invariable reaction frequency factor according to eq. (1) when moving from water to methanol or ethanol cannot be considered trivial and in fact very difficult to account for, assuming that the reaction belongs in all solvents to the proton adiabatic limit. Methanol and especially ethanol are generally much slower solvents than water when considering translational modes of the solvents. It may be that the characteristic solvent frequency ω_s is associated in this case with a hydrogen-bonded complex of the photoacid with several solvent molecules having some cooperative modes which determine the proton transfer rate along the proton transfer coordinate. In fact, proton transfer in protic solvents is expected to be controlled by rearrangements of solvent molecules not belonging to the core solvation of the proton. A well-known example is proton diffusion in water where second solvation shell rearrangements in the extended H-bonded complex of the hydrated proton determine the proton diffusion rate.[75] We also note that in all solvents the inner H-bond between the photoacid and the solvent is of the same form, O-H---O. Intermolecular vibration modulates both the height and width of the reaction barrier. These two parameters determine the probability of proton tunneling in the proton NA limit. But these parameters potentially also determine the configuration of the extended hydrogen-bonding complex at which solvent rearrangements are able to bring the reaction into the proton adiabatic limit. One may envision how relatively slow solvent fluctuations can transiently modulate the reaction rate to fluctuate between the two reaction regions. Alternatively, the O-O distance and the O-H$^{...}$O angle may fluctuate because of solvent rearrangements to a point where the reaction becomes almost adiabatic but not completely getting to be there. This is the limit when the proton tunnels near the top of the reaction barrier from the ground state vibration of the hydrogen bond and transfer adiabatically from the first excited vibration which is already above the barrier. The characteristic time scale for the O-O distance to follow the electronic excitation of the photoacid is sub-100 fs.[76] Once the hydrogen-bonding complex equilibrates with the excited photoacids the typical stretch frequencies are expected to be 200 cm^{-1} at equilibrium O-O separations and about twice faster around the transition state.[43] The H-bond stretching frequencies should be similar for water and for alcohols H-bonded complexes. Thus, following the photoacid excitation, both intramolecular and intermolecular charge and structure relaxations as well as the core H-bond of the photoacid with the solvent (O-H$^{...}$S) are all expected to be much faster than the experimentally found reaction pre-factor. This again implies but does not prove that solvent rearrangements not immediately associated with the intrinsic proton coordinate determine the reaction rate.

The finding that ω_s is insensitive to the solvent is a major outcome of this study and leads to the conclusion that the solvent effect of simple O-H solvents on the k_{PT} mainly arises from equilibrium solvation energies, ΔG_0 (equation 3). These observations should be further verified by temperature-dependent studies while studies exploiting isotope effects should help in elucidating the mechanism of the proton transfer reaction from the OH photoacids in hydroxylic solvents. These experiments will be done in the near future. Furthermore, time-resolved vibrational spectroscopy may give important insights into the initial reaction stage and help understanding the ESPT mechanism.[4, 58, 77-79]

Conclusions

Steady-state and time-resolved emission technique were used to study the excited-state proton transfer (ESPT) rate of two new HPTS (pyranine) derived photoacids. In the new two photoacids the sulfonate groups of the pyranine are modified to stronger electron withdrawing groups which further increase the acidity of the OH group. Unlike the weaker photoacid, HPTS, which only dissociates in water, both **1a** and **1b** are also capable of transferring a proton to alcohols. The pK_a*(water) of **1a** and **1b** is about -4 and -1 respectively. The ESPT rate constants of **1a** in water, methanol and ethanol are $3 \times 10^{11} s^{-1}$, $5 \times 10^9 s^{-1}$ and $4 \times 10^9 s^{-1}$, respectively. The ESPT rate constants of **1b** in these solvents are smaller. The ESPT rate of **1a** in water is comparable to that of N-methyl 6-hydroxy quinolinium (NM6HQ$^+$) pK_a^* ~ -6 which is $5 \times 10^{11} s^{-1}$. We account for the observed solvent effect by using Marcus'-like free-energy correlation between the proton transfer rate and the pK_a^* of the photoacid. Within the context of our analysis, the observed inhibition of k_{PT} in alcohols as compared to water mainly originates from the solvent effect on the equilibrium constant of the photoacids, making them much weaker acids than in water. A major outcome of this study is the finding that the reaction pre-factor is largely independent of the hydroxylic solvent and its magnitude typical of relatively slow solvent rearrangements which enable the proton to transfer. As for the mechanism of the proton transfer, we conclude that additional experimental evidence is needed in order to determine the detailed mechanism of the proton transfer reaction and for elucidating to what reaction limit, adiabatic, NA or mixed adiabatic-NA, proton transfer from strong photoacids belong to. Such additional experimental evidence may be provided in the future by studying the temperature and isotope effects of these reactions, as well as by fs-vibrational spectroscopy.

Acknowledgements

Notes and references

[a] Biophysical Chemistry, Saarland University, Campus, Building B2 2, D-66123 Saarbrücken, Germany, Fax: (+)49 681 302 64648, Tel:
+49-681-302-64848, E-mail: g.jung@mx.uni-saarland.de
[b] Raymond and Beverly Sackler Faculty of Exact Sciences, School of Chemistry, Tel Aviv University, Tel Aviv 69978, Israel. phone: +972-3-6407012, fax: 972-3-6407491, E*mail:* huppert@tulip.tau.ac.il
[c] Department of Chemistry, Ben-Gurion University of the Negev, P.O.B. 653, Beer-Sheva 84105, Israel. phone: +972-8-6461552, Fax: 972-8-6472943, Email: epines@bgu.ac.il.

Electronic Supplementary Information (ESI) available: Tables with the results of fitting procedures. Up-conversion data for the photoacids in ethanol. See DOI: 10.1039/b000000x/

1 J. F. Ireland and P. A. H. Wyatt, in *Advances in Physical Organic Chemistry,* ed. V. Gold, Academic Press, 1976, pp.131-221.
2 M. Gutman and E. Nachliel, *Biochem. Biophys. Acta,* 1990, **1015**, 391.
3 L. M. Tolbert and K. M. Solntsev, *Acc. Chem. Res.,* 2002, **35**, 19.
4 M. Rini, B.-Z. Magnes, E. Pines and E. T. J. Nibbering, *Science,* 2003, **301**, 349.
5 O. F. Mohammed, D. Pines, J. Dreyer, E. Pines and E. T. J. Nibbering, *Science,* 2005, **310**, 83.
6 T.-H. Tran-Thi, T. Gustavsson, C. Prayer, S. Pommeret and J. T. Hynes, *Chem. Phys. Lett.,* 2000, **329**, 421.
7 N. Agmon, *J. Phys. Chem. A,* 2005, **109**, 13.
8 D. B. Spry and M. D. Fayer, *J. Chem. Phys.,* 2008, **128**, 084508.
9 B. J. Siwick, M. J. Cox and H. J. Bakker, *J. Phys. Chem. B,* 2008, **112**, 378.
10 O. F. Mohammed, D. Pines, E. T. J. Nibbering and E. Pines, *Angew. Chem. Int. Ed.,* 2007, **46**, 1458.
11 S. K. Mondal, K. Sahu, P. Sen, D. Roy, S. Ghosh and K. Bhattacharyya, *Chem. Phys. Lett.,* 2005, **412**, 228.
12 P. K. Mandal and A. Samanta, *J. Phys. Chem. A,* 2003, **107**, 6334.
13 B. Bhattacharya and A. Samanta, *J. Phys. Chem. B,* 2008, **112**, 10101.
14 J. L. Pérez Lustres, S. A. Kovalenko, M. Mosquera, T. Senyushkina, W. Flasche and N. P. Ernsting, *Angew. Chem. Int. Ed.,* 2005, **44**, 5635.
15 J. L. Pérez-Lustres, F. Rodriguez-Prieto, M. Mosquera, T. A. Senyushkina, N. P. Ernsting and S. A. Kovalenko, *J. Am. Chem. Soc.,* 2007, **129**, 5408.
16 E. Pines, in *Isotope Effects In Chemistry and Biology,* ed. A. Kohen and H. Limbach, CRC Press, 2005, pp.451-464.
17 G. W. Robinson, *J. Phys. Chem.,* 1991, **95**, 10386.
18 N. Agmon, D. Huppert, A. Masad and E. Pines, *J. Phys. Chem.,* 1991, **95**, 10407.
19 T. Barak, Ph.D. Thesis, Ben-Gurion University of the Negev, 2005.
20 E. Pines, D. Tepper, B.-Z. Magnes, D. Pines and T. Barak, *Ber. Buns. Phys. Chem.,* 1998, **102**, 504.
21 I. Carmeli, D. Huppert, L. M. Tolbert and J. E. Haubrich, *Chem. Phys. Lett.,* 1996, **260**, 109.
22 L. M. Tolbert and J. E. Haubrich, *J. Am. Chem. Soc.,* 1990, **112**, 8163.
23 L. M. Tolbert and J. E. Haubrich, *J. Am. Chem. Soc.,* 1994, **116**, 10593.
24 E. Gould, A. V. Popov, L. M. Tolbert, I. Presiado, Y. Erez, D. Huppert and K. M. Solntsev, *Phys. Chem. Chem. Phys.,* 2012, **14**, 8964.
25 T. G. Kim and M. R. Topp, *J. Phys. Chem. A,* 2004, **108**, 10060.
26 M. Veiga-Gutiérrez, A. Brenlla, C. Carreira Blanco, B. Fernández, S. A. Kovalenko, F. Rodríguez-Prieto, M.

Mosquera and J. L. Lustres, *J. Phys. Chem. B,* 2013, **117**, 14065.

27 B. Finkler, C. Spies, M. Vester, F. Walte, K. Omlor, I. Riemann, M. Zimmer, F. Stracke, M. Gerhards and G. Jung, *Photochem. Photobiol. Sci.,* 2014, **13**, 548.

28 E. B. Krissinel' and N. Agmon, *J. Comput. Chem.,* 1996, **17**, 1085.

29 E. Pines and D. Huppert, *J. Chem. Phys.,* 1986, **84**, 3576.

30 E. Pines, D. Huppert and N. Agmon, *J. Chem. Phys.,* 1988, **88**, 5620.

31 E. Pines and D. Huppert, *Chem. Phys. Lett.,* 1986, **126**, 88.

32 N. Agmon, E. Pines and D. Huppert, *J. Chem. Phys.,* 1988, **88**, 5631.

33 E. Pines and G. R. Fleming, *Chem. Phys.,* 1994, **183**, 393.

34 E. Pines, B.-Z- Magnes and T. Barak, *J. Phys. Chem. A,* 2001, **105**, 9674.

35 C. Spies, B. Finkler, N. Acar and G. Jung, *Phys. Chem. Chem. Phys.,* 2013, **15**, 19893.

36 E. Pines, D. Huppert and N. Agmon, *J. Chem. Phys.,* 1988, **88**, 5620.

37 M. L. Horng, J. A. Gardecki, A. Papazyan and M. Maroncelli, *J. Phys. Chem.,* 1995, **99**, 17311.

38 M. Lukeman, M. Burns and P. Wan, *Can. J. Chem.,* 2011, **89**, 433.

39 R. Jimenez, G. R. Fleming, P. V. Kumar and M. Maroncelli, *Nature,* 1994, **369**, 471.

40 D. C. Borgis, S. Lee and J. T. Hynes, *Chem. Phys. Lett.,* 1989, **162**, 19.

41 D. Borgis and J. T. Hynes, *Chem. Phys.,* 1993, **170**, 315.

42 D. Borgis and J. T. Hynes, *J. Phys. Chem.,* 1996, **100**, 1118.

43 A. Staib, D. Borgis and J. T. Hynes, *J. Chem. Phys.,* 1995, **102**, 2487.

44 P. M. Kiefer and J. T. Hynes, *J. Phys. Chem. A,* 2002, **106**, 1834.

45 P. M. Kiefer and J. T. Hynes, *J. Phys. Chem. A,* 2002, **106**, 1850.

46 P. M. Kiefer and J. T. Hynes, *Solid State Ionics,* 2004, **168**, 219.

47 P. M. Kiefer and J. T. Hynes, in *Hydrogen-Transfer Reactions,* ed. J. T. Hynes, J. P. Klinman, H.-H. Limbach and R. L. Schowen, Wiley-VCH Verlag GmbH & Co. KGaA, Weinheim, 2006, pp.303-348.

48 R. A. Marcus, *J. Phys. Chem.,* 1968, **72**, 891.

49 R. A. Marcus, *J. Am. Chem. Soc.,* 1969, **91**, 7224.

50 R. A. Marcus, *Faraday Discuss. Chem. Soc.,* 1982, **74**, 7.

51 R. A. Marcus and N. Sutin, *Biochim. Biophys. Acta,* 1985, **811**, 265.

52 A. O. Cohen and R. A. Marcus, *J. Phys. Chem.,* 1968, **72**, 4249.

53 S. J. Edwards, A. V. Soudackov and S. Hammes-Schiffer, *J. Phys. Chem. B,* 2009, **113**, 14545.

54 E. Pines and D. Pines, in *Ultrafast Hydrogen Bonding Dynamics and Proton Transfer Prosesses in the Condensed Phase,* ed. T. Elsaesser and H. Bakker, Springer Netherlands, 2002, pp.155-184.

55 E. Pines, B. Magnes, M. J. Lang and G. R. Fleming, *Chem. Phys. Lett.,* 1997, **281**, 413.

56 E. Pines, D. Pines, T. Barak, B. Magnes, L. M. Tolbert and J. E. Haubrich, *Ber. Buns. Phys. Chem.,* 1998, **102**, 511.

57 D. Pines and E. Pines, in *Hydrogen-Transfer Reactions,* ed. J. T. Hynes, J. P. Klinman, H.-H. Limbach and R. L. Schowen, Wiley-VCH Verlag GmbH & Co. KGaA, Weinheim, 2007, pp.377-415.

58 O. F. Mohammed, D. Pines, E. Pines and E. T. J. Nibbering, *Chem. Phys.,* 2007, **341**, 240.

59 N. Munitz, Y. Avital, D. Pines, E. T. J. Nibbering and E. Pines, *Isr. J. Chem.,* 2009, **49**, 261.

60 M. Prémont-Schwarz, T. Barak, D. Pines, E. T. J. Nibbering and E. Pines, *J. Phys. Chem. B,* 2013, **117**, 4594.

61 K. Adamczyk, M. Prémont-Schwarz, D. Pines, E. Pines and E. T. J. Nibbering, *Science,* 2009, **326**, 1690.

62 R. P. Bell, *The proton in chemistry*, Chapman and Hall, London, 1973.

63 J. N. Brönsted, *Chem. Rev.,* 1928, **5**, 231.

64 J. N. Brönsted, *Recl. Trav. Chim. Pay-B,* 1923, **42**, 718.

65 N. Huse, S. Ashihara, E. T. J. Nibbering and T. Elsaesser, *Chem. Phys. Lett.,* 2005, **404**, 389.

66 S. Ashihara, N. Huse, A. Espagne, E. T. J. Nibbering and T. Elsaesser, *Chem. Phys. Lett.,* 2006, **424**, 66.

67 P. Leiderman, R. Gepshtein, A. Uritski, L. Genosar and D. Huppert, *J. Phys. Chem. A,* 2006, **110**, 9039.

68 R. Simkovitch, S. Shomer, R. Gepshtein, D. Shabat and D. Huppert, *J. Phys. Chem. A,* 2013, **117**, 3925.

69 T. Elsaesser, in *Ultrafast Hydrogen Bonding Dynamics and Proton Transfer Prosesses in the Condensed Phase,* ed. T. Elsaesser and H. Bakker, Springer Netherlands, 2002, pp.119-153.

70 S. Lochbrunner, A. J. Wurzer and E. Riedle, *J. Chem. Phys.,* 2000, **112**, 10699.

71 S. Lochbrunner, A. J. Wurzer and E. Riedle, *J. Phys. Chem. A,* 2003, **107**, 10580.

72 R. Simkovitch, N. Karton-Lifshin, S. Shomer, D. Shabat and D. Huppert, *J. Phys. Chem. A,* 2013, **117**, 3405.

73 G. H. Parsons and C. H. Rochester, *J. Chem. Soc. , Faraday Trans. 1,* 1975, **71**, 1058.

74 I. Um, Y. Hong and D. Kwon, *Tetrahedron,* 1997, **53**, 5073.

75 P. Kiefer and J. Hynes, in *Ultrafast Hydrogen Bonding Dynamics and Proton Transfer Prosesses in the Condensed Phase,* ed. T. Elsaesser and H. Bakker, Springer Netherlands, 2002, pp.73-92.

76 E. Pines, D. Pines, Y. Z. Ma and G. R. Fleming, *ChemPhysChem,* 2004, **5**, 1315.

77 Y. Wang, W. Liu, L. Tang, B. Oscar, F. Han and C. Fang, *J. Phys. Chem. A,* 2013, **117**, 6024.

78 W. Liu, F. Han, C. Smith and C. Fang, *J. Phys. Chem. B,* 2012, **116**, 10535.

79 D. E. Moilanen, D. B. Spry and M. D. Fayer, *Langmuir,* 2008, **24**, 3690.

Supporting information for

Solvent Dependence of Excited-State Proton Transfer from Pyranine-derived Photoacids

Christian Spies[†], Shay Shomer[‡], Björn Finkler[†], Dina Pines[α], Ehud Pines[α*], Gregor Jung[†*] and Dan Huppert[‡*]

[‡]Raymond and Beverly Sackler Faculty of Exact Sciences, School of Chemistry,

Tel Aviv University, Tel Aviv 69978, Israel

[α]Department of Chemistry, Ben-Gurion University of the Negev, P.O.B. 653, Beer-Sheva 84105, Israel

[†]Biophysical Chemistry, Saarland University, Campus, Building B2 2, D-66123 Saarbruecken, Germany

Table S1. Reconvolution fitting of TCSPC data of **1a** in methanol using exponential functions.

λ [nm]	τ_1 [ns]	A_1	τ_2 [ns]	A_2	τ_3 [ns]	A_3	χ^2
460	0.14	0.88	0.48	0.10	3.21	0.02	1.66
470	0.10	0.78	0.32	0.20	2.58	0.02	1.17
480	0.13	0.88	0.45	0.10	2.70	0.02	1.61
490	0.13	0.89	0.45	0.10	2.55	0.01	1.27
500	0.12	0.85	0.39	0.14	2.41	0.01	1.36
510	0.13	0.85	0.40	0.14	3.25	0.01	1.23
520	0.13	0.86	0.47	0.12	4.76	0.02	1.15
530	0.09	0.62	0.29	0.31	5.85	0.07	1.20
540	0.14	0.50	0.31	0.14	6.12	0.36	1.12
550	0.72	0.45	0.92	-0.39	6.02	0.94	1.65
560	0.15	-0.34	6.12	0.95			1.34
570	0.13	-0.36	6.11	0.54			1.31
580	0.12	-0.47	6.09	0.73			1.35
590	0.13	-0.36	6.12	0.63			1.19
600	0.12	-0.40	6.11	0.75			1.38

Table S2. Reconvolution fitting of TCSPC date of **1b** in methanol using exponential functions.

λ [nm]	τ_1 [ns]	A_1	τ_2 [ns]	A_2	τ_3 [ns]	A_3	χ^2
440	0.14	0.42	1.54	0.36	4.51	0.22	1.05
450	0.17	0.31	1.59	0.43	4.55	0.26	1.06
460	0.18	0.26	1.62	0.46	4.59	0.28	1.23
470	0.14	0.23	1.60	0.49	4.59	0.28	1.50
480	0.11	0.21	1.64	0.51	4.72	0.28	1.43
490	0.14	0.13	1.53	0.52	4.44	0.35	1.26
500	0.09	0.16	1.52	0.50	4.48	0.34	1.92
510	0.18	0.16	1.66	0.49	4.65	0.35	1.05
520	0.19	0.14	1.58	0.32	4.57	0.54	1.19

530	0.31	0.13	0.82	-0.06	4.73	0.93	1.34
540	0.32	0.13	0.83	-0.07	4.73	0.94	1.34
550	1.62	-0.60	4.72	0.91			1.11
560	1.59	-0.53	4.75	0.73			1.12
570	1.57	-0.53	4.77	0.73			1.09
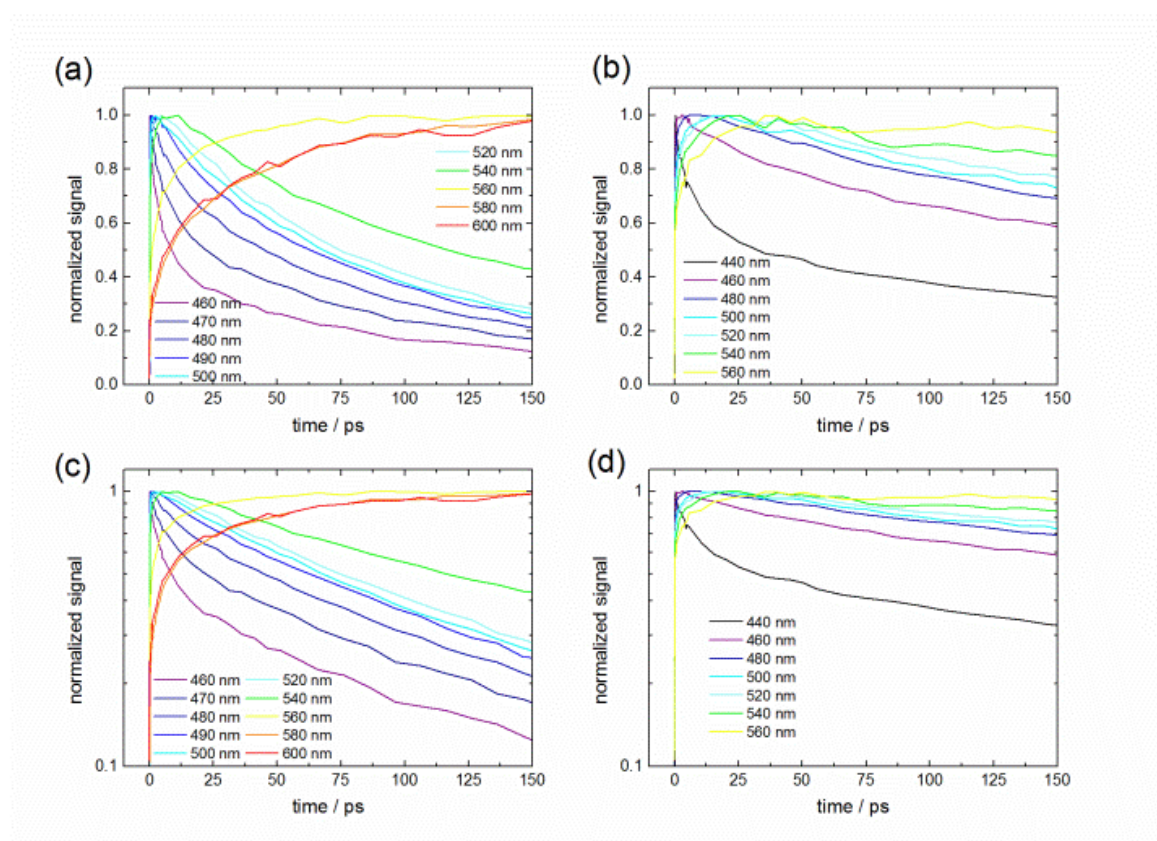
Figure S1. Up-conversion curves of **1a** (a) and **1b** (b) in methanol between 440 nm and 600 nm, on a linear and semi-logarithmic scale (c), (d).

Table S3. Reconvolution fitting of upconversion data of **1b** in methanol using exponential functions.

λ [nm]	τ_1 [ps]	A_1	τ_2 [ps]	A_2	τ_3 [ps]	A_3	χ^2
440	0.22	0.23	8.99	0.30	279	0.47	1.48
460	2.01	-0.03	31.9	0.19	440	0.84	4.69
480	2.79	-0.18	140	0.55	1500[a]	0.75	2.57
500	4.00	-0.25	150	0.37	1500[a]	0.58	2.84
520	4.21	-0.18	367	0.42	1500[a]	0.16	2.17
540	4.71	-0.19	183	0.09	1500[a]	0.46	1.62
560	1.00	-0.27	12.7	-0.64	1500[a]	1.98	1.38

[a] Variable fixed at this value.

Table S4. Reconvolution fitting of upconversion data of **1a** in methanol using exponential functions.

λ [nm]	τ_1 [ps]	A_1	τ_2 [ps]	A_2	τ_3 [ps]	A_3	χ^2
460	0.17	0.35	5.36	0.34	125	0.31	3.93
470	0.04	0.46	6.71	0.22	123	0.32	3.27
480	0.003	0.40	12.2	0.17	126	0.43	2.48
490	0.001	0.32	35.5	0.23	155	0.45	4.68
500	1.72	-0.07	62.2	0.72	319	0.35	3.48
520	2.17	-0.23	49.0	0.50	174	0.73	3.34
540	2.26	-0.20	101	0.54	6100[a]	0.17	2.59
560	2.28	-0.12	23.6	-0.15	6100[a]	0.44	2.23
580	3.32	-0.06	42.4	-0.16	6100[a]	0.27	3.99
600	0.99	-0.14	31.5	-0.33	6100[a]	0.57	3.15

[a] Variable fixed at this value.

Figure S2. TCSPC curves of **1a** (a) and **1b** (b) in ethanol between 420 nm and 600 nm, on a linear and semi-logarithmic scale (c), (d).

Table S5. Reconvolution fitting of TCSPC data of **1b** in ethanol using exponential functions.

λ [nm]	τ_1 [ns]	A_1	τ_2 [ns]	A_2	τ_3 [ns]	A_3	χ^2
420	0.28	0.28	2.18	0.39	3.71	0.33	1.14
440	0.28	0.23	2.17	0.42	3.75	0.35	1.04
450	0.26	0.35	2.48	0.50	4.51	0.15	1.09
460	0.35	0.16	1.80	0.29	3.54	0.55	1.11
480	0.41	0.14	2.83	0.29	5.05	0.57	1.42
500	2.32	-0.31	5.24	0.55			1.32
520	2.28	-0.35	5.27	0.54			1.21
540	2.23	-0.36	5.28	0.54			1.16
560	2.16	-0.35	5.35	0.51			1.27
570	2.11	-0.35	5.37	0.50			1.26

Table S6. Reconvolution fitting of TCSPC date of **1a** in ethanol using exponential functions.

| λ [nm]	τ_1 [ns]	A_1	τ_2 [ns]	A_2	τ_3 [ns]	A_3	χ^2
460	0.08	0.69	0.34	0.27	2.54	0.04	1.41
480	0.09	0.57	0.33	0.39	2.55	0.04	1.18
500	0.12	0.65	0.39	0.32	2.57	0.03	1.06
560	0.22	-0.19	5.98	1.01			1.10
580	0.20	-0.42	5.98	0.91			1.65
600	0.18	-0.27	6.01	0.62			1.14

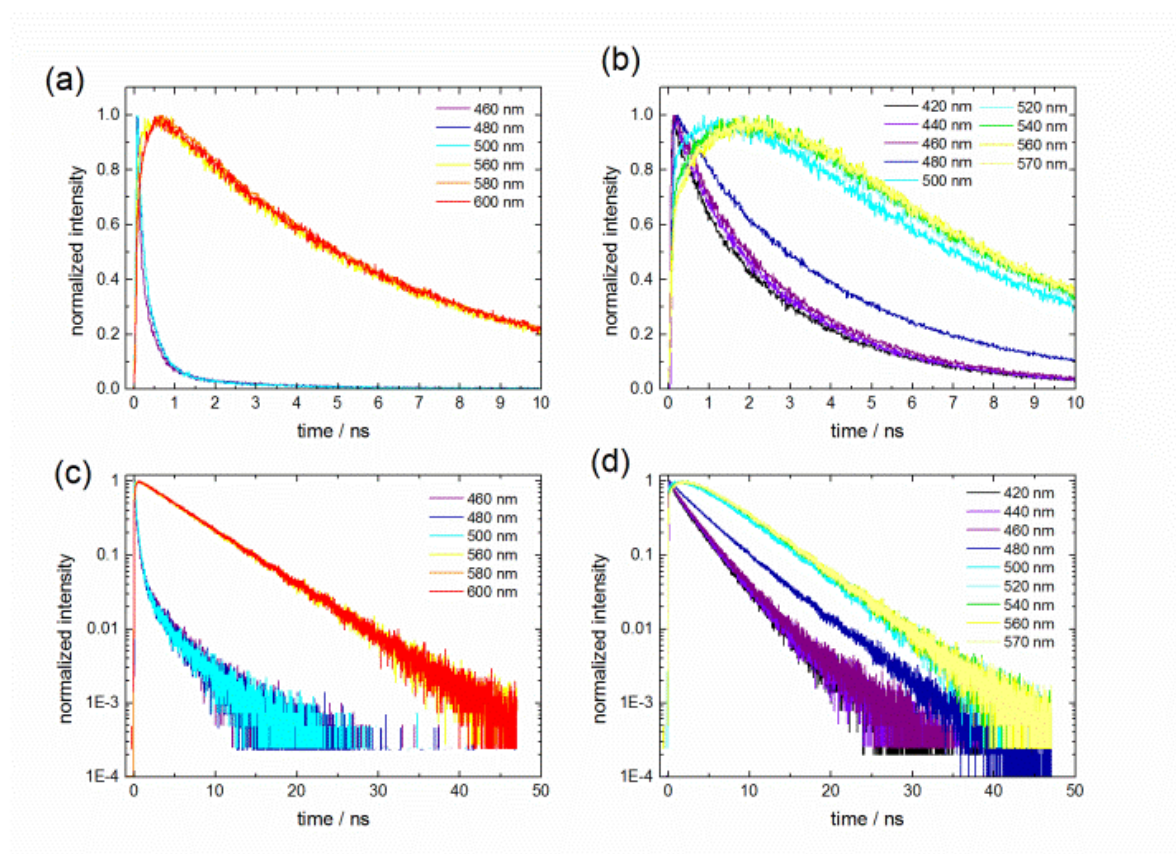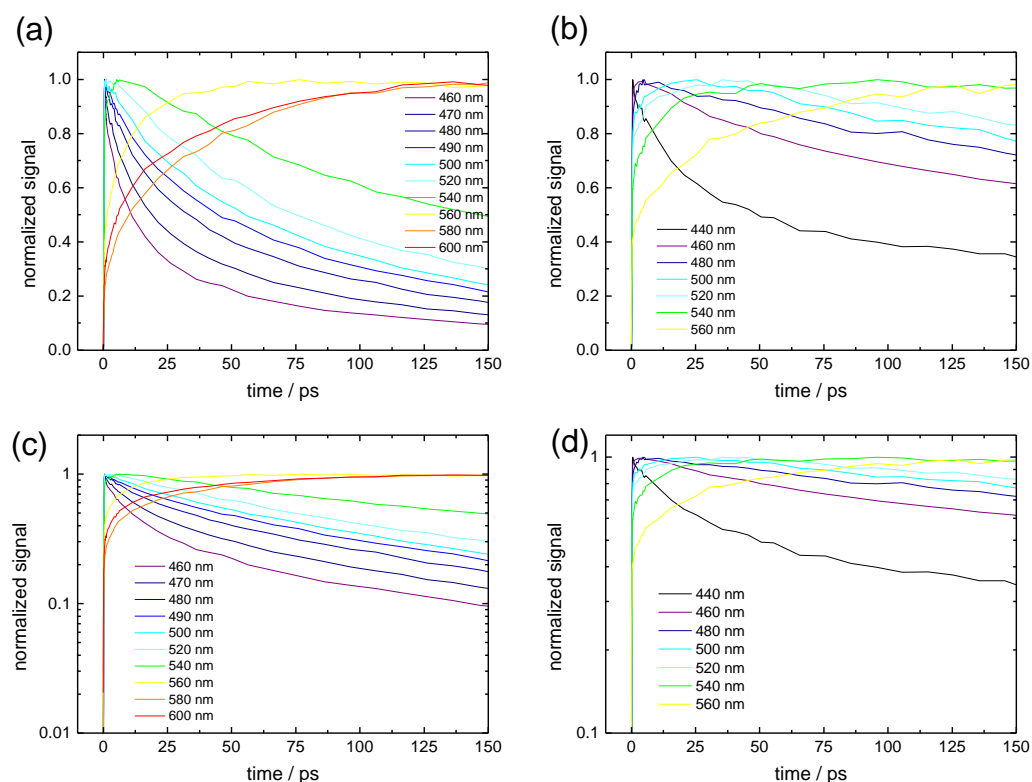**Figure S3**. Up-conversion curves of **1a** (a) and **1b** (b) in ethanol between 440 nm and 600 nm, on a linear and semi logarithmic scale (c), (d).

Table S7. Reconvolution fitting of upconversion data of **1b** in ethanol using exponential functions.

λ [nm]	τ_1 [ps]	A_1	τ_2 [ps]	A_2	τ_3 [ps]	A_3	χ^2
440	0.05	0.40	20.6	0.27	369	0.33	1.25
460	2.35	-0.09	39	0.23	524	0.86	0.55
480	2.12	-0.12	175	0.42	5500[a]	0.49	2.93
500	7.63	-0.10	197	0.22	5500[a]	0.25	
520					5500[a]		
540	0.81	-0.02	13.4	-0.07	5500[a]	0.20	1.51
560	2.86	-0.12	44.5	-0.55	5500[a]	1.12	0.87

[a] Variable fixed at this value.

Table S8. Results of reconvolution fitting of upconversion data of **1a** in ethanol.

Wavelength	τ_1 [ps]	A_1	τ_2 [ps]	A_2	τ_3 [ps]	A_3	χ^2
460	0.06	0.52	9.3	0.29	114	0.19	4.65
470	0.07	0.38	12	0.32	121	0.3	2.87
480	0.003	0.5	16	0.21	131	0.29	3.08
490	0.003	0.46	20	0.19	143	0.35	1.65
500	0.003	0.4	29	0.21	158	0.39	2.98
520	3.4	-0.08	49	0.52	235	0.56	2.64
540	2.8	-0.02	1003		115	0.07	
560	1.1	-0.12	13	-0.38	6000[a]	0.78	2.86
580	2.5	-0.01	41	-0.04	6000[a]	0.07	4.11
600	0.18	-0.2434	5.46	-0.2653	6000[a]	0.07	2.28

[a] Variable fixed at this value.
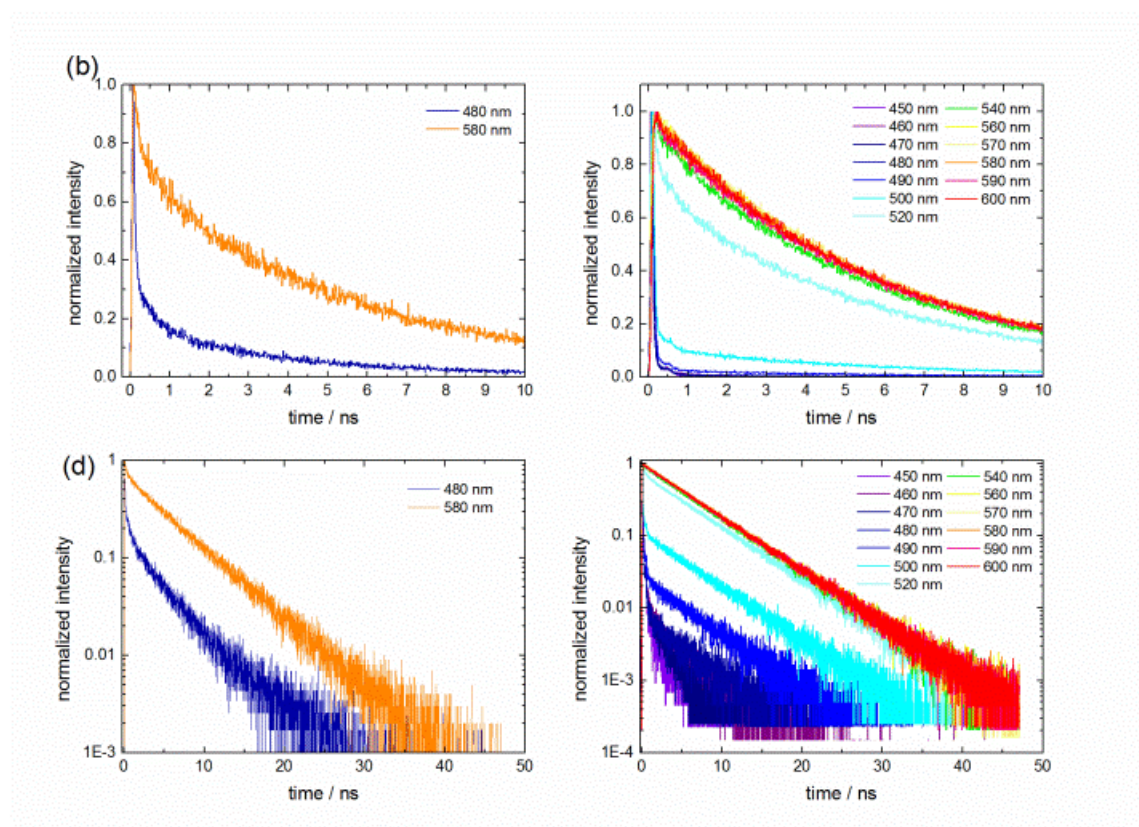
Figure S4. TCSPC curves of **1a** in 30 vol% water in methanol (a) and **1b** in water (b) between 450 nm and 600 nm, on a linear and semi-logarithmic scale (c), (d).

Table S9. Results of reconvolution fitting of upconversion data of **1b** in water.

Wavelength	τ_1 [ps]	A_1	τ_2 [ps]	A_2	τ_3 [ps]	A_3	χ^2
450	0.038	0.82	2.61	0.085	23.48	0.09	1.63
460	0.0032	0.79	4.46	0.143	34.09	0.06	5.17
470	0.349	0.37	12.68	0.54	70.3	0.09	1.53
480	0.274	0.267	13.11	0.623	71.28	0.11	1.4
490	0.43	0.162	15.4	0.743	100.76	0.095	1.56
550	4.15	-0.36	23.67	-0.31	594	1	1.18
560	0.982	-0.149	13.54	-0.627	616	1	1.18
570	4.37	-0.326	19.5	-0.411	673	1	0.83

Table S10. Results of reconvolution fitting of upconversion data of **1a** in water.

Wavelength	τ_1 [ps]	A_1	τ_2 [ps]	A_2	τ_3 [ps]	A_3	χ^2
460	0.30	0.54	3.58	0.40	152	0.06	2.52
470	0.49	0.47	4.90	0.47	113	0.07	5.29
480	0.73	0.43	6.78	0.52	105	0.05	7.37
490	1.30	0.40	9.09	0.52	143	0.08	4.42
520	0.77	0.15	9.06	0.68	142	0.17	2.11
540	1.10	-0.16	14.0	0.58	398	0.58	0.96
560	0.39	-0.41	4.67	-1.69	842		1.34
580	0.49	-0.58	5.70	-2.83	1005		1.23

Correction of pK$_a$ values by electrostatic work term

The two new strong pyranine-derived photoacids shown in scheme 1 were found to have pK_a^* of ~ -4 (**1a**) and ~ -1 (**1b**) determined by the Förster cycle.[227] The ESPT rate of **1a** in water was measured to be 3×10^{11} s^{-1} (Table 2). The weaker photoacid, **1b,** exhibits a smaller ESPT rate as expected from the higher pK_a^* value. The ESPT rate constant of **1b** in water was found to be ~8×10^{10} s^{-1}. In comparison, the much studied parent (and also weaker) photoacid, the triply negatively charged HPTS molecule transfers a proton only in water with k$_{PT}$ ≈ 10^{10} s^{-1}. We have correlated the HPTS photoacid together with the neutral photoacids after adjusting its pK_a^* value (1.4) to contact ion-pair formation rather than using the conventional value which include the electrostatic work needed to separate the ion pair to infinite separation distance, using eq. 7:

$$pK_a^* = pK^*(contact) + \frac{R_D}{2.3a} \tag{1}$$

where the Debye Radius R_D is given by eq. 8:

$$R_D = \frac{|z_1 z_2|e^2}{\varepsilon k_B T} \tag{8}$$

k_B is the Boltzmann constant, a = 6.5 Å is the reaction contact radius, ε is the permittivity of the solution, e is the elementary charge, and z_1 = 1, z_2 = -3 are the

charge numbers of the proton and HPTS respectively. We find $pK^*(contact) = 0$ for HPTS and use this value for the free-energy correlation.

Sensitivity of change in proton transfer rate with pK_a^*
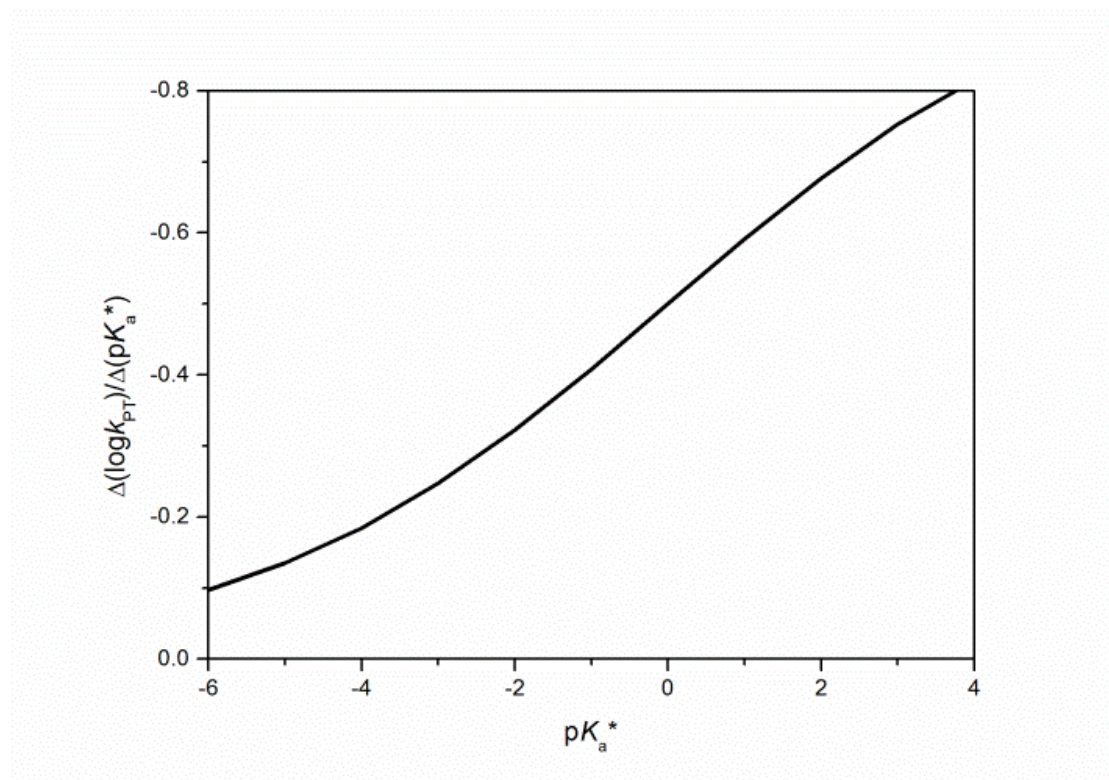
Figure S4. $\Delta(\log k_{PT})/\Delta(pK_a^*)$ of free-energy correlation found in the proton dissociation reaction (solid line in Fig. 11) vs pK_a^*.

In Fig. S4 we have plotted the derivative of the logarithm of the proton transfer rate k_{PT}, given by eqs. 2-5, as a function of the pK_a^*. This derivative of the Marcus free-energy function scales the sensitivity of the proton transfer rate to a pK_a^* change as a function of the absolute pK_a^* of the photoacid. The stronger the photoacid the less sensitive is the proton transfer rate to a pK_a^* change due to a solvent or a substituent change which do not alter the general mechanism of the proton transfer reaction in water. The derivative distinctly increases in the range of the acidities that were considered in this study (pK_a^* from -6 to 4) when moving from the stronger photoacids to the weaker ones and unambiguously reproduces the observed trend in the solvent effect on the dissociation rate of the photoacids.

Discussion of the wavelength dependence

As indicated in the manuscript, the strong wavelength dependence observed especially for compound **1b**, can have several reasons. In the manuscript we mention a quenching reaction competing with the ESPT reaction as a possible explanation for this finding. However, this may not be the solely answer to it. In fact, the values for the time constants in tables S9 and S10 are also varying with the wavelength. This could be due to the reconvolution fitting procedure and the non-exponential nature of solvation dynamics. In this case, the numbers in these tables may not be strictly correct, although the extraction of the ESPT rate should not be affected. Another possible explanation may be the vibrational structure of the bands. Due to the excitation at about 400 nm, higher vibrational levels are populated by the laser puls. Vibrational cooling may occur, although it usually should be completed within 10 ps, and hence have an impact in wavelength-resolved emission decays.

4 Bibliography

[1] H. Lischka, V. Dyczmons, *Chemical Physics Letters* **1973**, *23*, 167-172.

[2] P. A. Kollman, C. F. Bender, *Chem. Phys. Lett.* **1973**, *21*, 271-274.

[3] M. C. R. Symons, *J. Am. Chem. Soc.* **1980**, *102*, 3982-3982.

[4] M. D. Newton, S. Ehrenson, *J. Am. Chem. Soc.* **1971**, *93*, 4971-4990.

[5] R. Vuilleumier, D. Borgis, *J. Chem. Phys.* **1999**, *111*, 4251-4266.

[6] M. H. Begemann, R. J. Saykally, *J. Chem. Phys.* **1985**, *82*, 3570-3579.

[7] F. H. Stillinger, C. W. David, *J. Chem. Phys.* **1978**, *69*, 1473-1484.

[8] B. Kirchner, *ChemPhysChem* **2007**, *8*, 41-43.

[9] C. A. Reed, *Acc. Chem. Res.* **2013**, *46*, 2567-2575.

[10] M. Eigen, *Angew. Chem. Int. Ed.* **1964**, *3*, 1-19.

[11] G. Zundel, *The Hydrogen Bond: Recent Developments in Theory and Experiments*, North-Holland, Amsterdam, **1976**.

[12] Zundel G., Metzger H., *Z. Phys. Chem. N. F.* **1968**, *59*, 225-241.

[13] E. S. Stoyanov, I. V. Stoyanova, C. A. Reed, *J. Am. Chem. Soc.* **2010**, *132*, 1484-1485.

[14] E. S. Stoyanov, I. V. Stoyanova, F. S. Tham, C. A. Reed, *J. Am. Chem. Soc.* **2008**, *130*, 12128-12138.

[15] J. A. Morrone, M. E. Tuckerman, *J. Chem. Phys.* **2002**, *117*, 4403.

[16] J. R. Roscioli, L. R. McCunn, M. A. Johnson, *Science* **2007**, *316*, 249-254.

[17] T. Förster, *Naturwissenschaften* **1949**, *36*, 186-187.

[18] T. Förster, *Z. Elektrochem.* **1950**, *54*, 42-46.

[19] K. Weber, *Z. Phys. Chem.* **1931**, *B15*, 18-44.

[20] T. Förster, *Pure Appl. Chem.* **1970**, *24*, 443-450.

[21] L. M. Tolbert, K. M. Solntsev, *Acc. Chem. Res.* **2002**, *35*, 19-27.

[22] A. Weller, *Z. Elektrochem.* **1952**, *56*, 662-668.

[23] A. Weller, *Z. Elektrochem.* **1954**, *58*, 849-853.

[24] A. Weller, *Z. Phys. Chem. N. F.* **1958**, *17*, 224-245.

[25] A. Weller *, in Progr. in Reaction Kinetics* (Ed:. G. Porter), Pergamon Press **1961**, pp. 187-214.

[26] A. Weller, *Naturwiss.* **1955**, *42*, 175-176.

[27] N. M. Trieff, B. R. Sundheim, *J. Phys. Chem.* **1965**, *69*, 2044-2059.

[28] R. Simkovitch, N. Karton-Lifshin, S. Shomer, D. Shabat, D. Huppert, *J. Phys. Chem. A* **2013**, *117*, 3405-3413.

[29] G. Granucci, J. T. Hynes, P. Millié, T.-H. Tran-Thi, *J. Am. Chem. Soc.* **2000**, *122*, 12243-12253.

[30] E. Pines, *in The Chemistry of Phenols* (Ed:. Z. Rappoport), John Wiley & Sons, Ltd **2003**, pp. 491-527.

[31] M. T. Nguyen, E. S. Kryachko, L. G. Vanquickenborne, *in The Chemistry of Phenols* (Ed:. Z. Rappoport), John Wiley & Sons, Ltd, Chichester, UK, **2003**, pp. 1-198.

[32] J. F. Ireland, P. A. H. Wyatt, *in Advances in Physical Organic Chemistry* (Ed:. V. Gold), Academic Press **1976**, pp. 131-221.

[33] M. Gutman, E. Nachliel, *Biochem. Biophys. Acta* **1990**, *1015*, 391-414.

[34] L. G. Arnaut, S. J. Formosinho, *J. Photochem. Photobiol. A* **1993**, *75*, 1-20.

[35] N. Agmon, *J. Phys. Chem. A* **2005**, *109*, 13-35.

[36] M. Kasha, *Discuss. Faraday Soc.* **1950**, *9*, 14-19.

[37] J. R. Platt, *J. Chem. Phys.* **1949**, *17*, 484-495.

[38] T. -H. Tran-Thi, C. Prayer, P. Millié, P. Uznanski, J. T. Hynes, *J. Phys. Chem. A* **2002**, *106*, 2244-2255.

[39] D. B. Spry, A. Goun, C. B. Bell III, M. D. Fayer, *J. Chem. Phys.* **2006**, *125*, 144514.

[40] D. Pines, E. Pines, *in Hydrogen-Transfer Reactions* (Eds.: J. T. Hynes, J. P. Klinman, H. -H. Limbach, R. L. Schowen), Wiley-VCH Verlag GmbH & Co. KGaA, Weinheim, **2007**, pp. 377-415.

[41] G. Jung, S. Gerharz, A. Schmitt, *Phys. Chem. Chem. Phys.* **2009**, *11*, 1416-1426.

[42] D. B. Spry, A. Goun, M. D. Fayer, *J. Phys. Chem. A* **2007**, *111*, 230-237.

[43] P. W. Atkins, *Physikalische Chemie*, VCH, Weinheim, **1990**.

[44] T. Engel, P. J. Reid, *Physikalische Chemie*, Pearson-Studium, München u.a., **2006**.

[45] S. Kaneko, S. Yotoriyama, H. Koda, S. Tobita, *J. Phys. Chem. A* **2009**, *113*, 3021-3028.

[46] L. Stryer, *J. Am. Chem. Soc.* **1966**, *88*, 5708-5712.

[47] J. Sühnel, *J. Phys. Org. Chem.* **1990**, *3*, 62-68.

[48] E. Pines*, in Isotope Effects In Chemistry and Biology* (Eds.: A. Kohen, H. Limbach), CRC Press **2005**, pp. 451-464.

[49] P. M. Kiefer, J. T. Hynes, *J. Phys. Chem. A* **2003**, *107*, 9022-9039.

[50] E. Pines, D. Pines, T. Barak, B. Magnes, L. M. Tolbert, J. E. Haubrich, *Ber. Buns. Phys. Chem.* **1998**, *102*, 511-517.

[51] M. Prémont-Schwarz, T. Barak, D. Pines, E. T. J. Nibbering, E. Pines, *J. Phys. Chem. B* **2013**, *117*, 4594-4603.

[52] A. Uritski, I. Presiado, D. Huppert, *Isr. J. Chem.* **2009**, *49*, 235-249.

[53] A. Uritski, I. Presiado, Y. Erez, R. Gepshtein, D. Huppert, *J. Phys. Chem. C* **2009**, *113*, 17915-17926.

[54] N. Karton-Lifshin, I. Presiado, Y. Erez, R. Gepshtein, D. Shabat, D. Huppert, *J. Phys. Chem. A* **2012**, *116*, 85-92.

[55] B. Cohen, J. Segal, D. Huppert, *J. Phys. Chem. A* **2002**, *106*, 7462-7467.

[56] A. Uritski, D. Huppert, *J. Phys. Chem. A* **2008**, *112*, 4415-4425.

[57] C. Clower, K. M. Solntsev, J. Kowalik, L. M. Tolbert, D. Huppert, *J. Phys. Chem. A* **2002**, *106*, 3114-3122.

[58] K. M. Solntsev, D. Huppert, N. Agmon, *J. Phys. Chem. A* **1999**, *103*, 6984-6997.

[59] G. W. Robinson, *J. Phys. Chem.* **1991**, *95*, 10386-10391.

[60] R. Simkovitch, S. Shomer, R. Gepshtein, D. Shabat, D. Huppert, *J. Phys. Chem. A* **2013**, *117*, 3925-3934.

[61] R. Simkovitch, E. Kisin-Finfer, S. Shomer, R. Gepshtein, D. Shabat, D. Huppert, *J. Photochem. Photobiol. A* **2013**, *254*, 45-53.

[62] A. Mirończyk, A. Jankowski, *J. Photochem. Photobiol. A* **2002**, *153*, 89-100.

[63] T. Htun, *J. Fluoresc.* **2003**, *13*, 323-329.

[64] M. Veiga-Gutiérrez, A. Brenlla, C. Carreira Blanco, B. Fernández, S. A. Kovalenko, F. Rodríguez-Prieto, M. Mosquera, J. L. Lustres, *J. Phys. Chem. B* **2013**, *117*, 14065-14078.

[65] J. L. Pérez-Lustres, F. Rodriguez-Prieto, M. Mosquera, T. A. Senyushkina, N. P. Ernsting, S. A. Kovalenko, *J. Am. Chem. Soc.* **2007**, *129*, 5408-5418.

[66] A. A. Freitas, F. H. Quina, A. A. L. Maçanita, *J. Phys. Chem. A* **2011**, *115*, 10988-10995.

[67] J. N. Brönsted, *Recl. Trav. Chim. Pay-B* **1923**, *42*, 718-728.

[68] O. F. Mohammed, D. Pines, E. Pines, E. T. J. Nibbering, *Chem. Phys.* **2007**, *341*, 240-257.

[69] O. F. Mohammed, D. Pines, E. T. J. Nibbering, E. Pines, *Angew. Chem. Int. Ed.* **2007**, *46*, 1458-1461.

[70] M. Rini, B.-Z. Magnes, E. Pines, E. T. J. Nibbering, *Science* **2003**, *301*, 349-352.

[71] A. Staib, D. Borgis, J. T. Hynes, *J. Chem. Phys.* **1995**, *102*, 2487-2505.

[72] E. Pines, B. Magnes, M. J. Lang, G. R. Fleming, *Chem. Phys. Lett.* **1997**, *281*, 413-420.

[73] S. K. Mondal, S. Ghosh, K. Sahu, P. Sen, K. Bhattacharyya, *J. Chem. Sci.* **2007**, *119*, 71-76.

[74] W. Liu, F. Han, C. Smith, C. Fang, *J. Phys. Chem. B* **2012**, *116*, 10535-10550.

[75] B. J. Siwick, M. J. Cox, H. J. Bakker, *J. Phys. Chem. B* **2008**, *112*, 378-389.

[76] L. Genosar, B. Cohen, D. Huppert, *J. Phys. Chem. A* **2000**, *104*, 6689-6698.

[77] F. Han, W. Liu, C. Fang, *Chem. Phys.* **2013**, *422*, 204-219.

[78] P. Maurer, V. Thomas, U. Rivard, R. Iftimie, *J. Chem. Phys.* **2010**, *133*, 044108.

[79] G. H. Parsons, C. H. Rochester, *J. Chem. Soc. , Faraday Trans. 1* **1975**, *71*, 1058-1068.

[80] K. M. Solntsev, D. Huppert, N. Agmon, L. M. Tolbert, *J. Phys. Chem. A* **2000**, *104*, 4658-4669.

[81] N. Agmon, D. Huppert, A. Masad, E. Pines, *J. Phys. Chem.* **1991**, *95*, 10407-10413.

[82] P. Leiderman, R. Gepshtein, A. Uritski, L. Genosar, D. Huppert, *J. Phys. Chem. A* **2006**, *110*, 9039-9050.

[83] J. S. Seixas de Melo, C. Cabral, J. C. Lima, A. L. Maçanita, *J. Phys. Chem. A* **2011**, *115*, 8392-8398.

[84] S. Das, M. Ali, S. Saha, *J. Solution Chem.* **2011**, *40*, 299-306.

[85] A. A. Freitas, A. A. L. Macanita, F. H. Quina, *Photochem. Photobiol. Sci.* **2013**, *12*, 902-910.

[86] S. J. Formosinho, L. G. Arnaut, *J. Photochem. Photobiol. A* **1993**, *75*, 21-48.

[87] A. Szemik-Hojniak, L. Wisniewski, I. Deperasinska, A. Makarewicz, L. Jerzykiewicz, A. Puszko, Y. Erez, D. Huppert, *Phys. Chem. Chem. Phys.* **2012**, *14*, 8147-8159.

[88] T. Lin, K. Tang, S. Yang, J. Shen, Y. Cheng, H. Pan, Y. Chi, P. Chou, *J. Phys. Chem. A* **2012**, *116*, 4438-4444.

[89] S. Lochbrunner, A. J. Wurzer, E. Riedle, *J. Phys. Chem. A* **2003**, *107*, 10580-10590.

[90] J. M. Paredes, L. Crovetto, A. Orte, J. Alvarez-Pez, E. M. Talavera, *Phys. Chem. Chem. Phys.* **2011**, *13*, 1685-1694.

[91] A. J. G. Strandjord, D. E. Smith, P. F. Barbara, *J. Phys. Chem.* **1985**, *89*, 2362-2366.

[92] M. Mosquera, J. C. Penedo, M. C. Ríos Rodríguez, F. Rodríguez-Prieto, *J. Phys. Chem.* **1996**, *100*, 5398-5407.

[93] K. Das, K. D. Ashby, J. Wen, J. W. Petrich, *J. Phys. Chem. B* **1999**, *103*, 1581-1585.

[94] H. H. Richtol, Fitch. B. R., *Anal. Chem.* **1974**, *46*, 1749-1754.

[95] L. M. Tolbert, J. E. Haubrich, *J. Am. Chem. Soc.* **1994**, *116*, 10593-10600.

[96] S. G. Tajc, B. S. Tolbert, R. Basavappa, B. L. Miller, *J. Am. Chem. Soc.* **2004**, *126*, 10508-10509.

[97] J. Alvarez-Pez, L. Ballesteros, E. Talavera, J. Yguerabide, *J. Phys. Chem. A* **2001**, *105*, 6320-6332.

[98] Y. Avnir, Y. Barenholz, *Anal. Biochem.* **2005**, *347*, 34-41.

[99] R. Barnadas-Rodríguez, J. Estelrich, *J. Photochem. Photobiol. A* **2008**, *198*, 262-267.

[100] T. G. Kim, M. R. Topp, *J. Phys. Chem. A* **2004**, *108*, 10060-10065.

[101] L. P. Hammett, A. J. Deyrup, *J. Am. Chem. Soc.* **1932**, *54*, 2721-2739.

[102] C. Hansch, A. Leo, R. W. Taft, *Chem. Rev.* **1991**, *91*, 165-195.

[103] E. Pines, G. R. Fleming, *Chem. Phys.* **1994**, *183*, 393-402.

[104] E. Pines, D. Tepper, B. Magnes, D. Pines, T. Barak, *Ber. Buns. Phys. Chem.* **1998**, *102*, 504-510.

[105] E. Pines, B. Magnes, T. Barak, *J. Phys. Chem. A* **2001**, *105*, 9674-9680.

[106] N. Agmon, *J. Chem. Phys.* **1999**, *110*, 2175-2180.

[107] D. Huppert, L. M. Tolbert, S. Linares-Samaniego, *J. Phys. Chem. A* **1997**, *101*, 4602-4605.

[108] D. Jacquemin, E. A. Perpete, I. Ciofini, C. Adamo, *J. Phys. Chem. A* **2008**, *112*, 794-796.

[109] V. Thomas, P. Maurer, R. Iftimie, *J. Phys. Chem. B* **2010**, *114*, 8147-8155.

[110] W. Gu, T. Frigato, T. Straatsma, V. Helms, *Angew. Chem.* **2007**, *119*, 2997-3001.

[111] E. L. Wehry, L. B. Rogers, *J. Am. Chem. Soc.* **1965**, *87*, 4234-4238.

[112] N. Mikami, *Bull. Chem. Soc. Jpn.* **1995**, *68*, 683-695.

[113] S. G. Schulman, W. R. Vincent, W. J. M. Underberg, *J. Phys. Chem.* **1981**, *85*, 4068-4071.

[114] A. Bryson, R. W. Matthews, *Aust. J. Chem.* **1963**, *16*, 401-410.

[115] A. V. Popov, E. Gould, M. A. Salvitti, R. Hernandez, K. M. Solntsev, *Phys. Chem. Chem. Phys.* **2011**, *13*, 14914-14927.

[116] O. S. Wolfbeis, M. Leiner, P. Hochmuth, H. Geiger, *Ber. Buns. Phys. Chem.* **1984**, *88*, 759-767.

[117] Y. A. Dávila, M. I. Sancho, M. C. Almandoz, S. E. Blanco, *J. Chem. Eng. Data* **2013**, *58*, 1706-1716.

[118] B. H. Milosavljevic, J. K. Thomas, *Photochem. Photobiol. Sci.* **2002**, *1*, 100-104.

[119] E. Pines, D. Huppert, N. Agmon, *J. Chem. Phys.* **1988**, *88*, 5620-5630.

[120] I. Presiado, N. Karton-Lifshin, Y. Erez, R. Gepshtein, D. Shabat, D. Huppert, *J. Phys. Chem. A* **2012**, *116*, 7353-7363.

[121] M. S. Baranov, K. A. Lukyanov, A. O. Borissova, J. Shamir, D. Kosenkov, L. V. Slipchenko, L. M. Tolbert, I. V. Yampolsky, K. M. Solntsev, *J. Am. Chem. Soc.* **2012**, *134*, 6025-6032.

[122] K. Winkler, J. Lindner, V. Subramaniam, T. M. Jovin, P. Vohringer, *Phys. Chem. Chem. Phys.* **2002**, *4*, 1072.

[123] S. S. Stavrov, K. M. Solntsev, L. M. Tolbert, D. Huppert, *J. Am. Chem. Soc.* **2006**, *128*, 1540-1546.

[124] S. R. Meech, *Chem. Soc. Rev.* **2009**, *38*, 2922-2934.

[125] Y. Erez, R. Gepshtein, I. Presiado, K. Trujillo, K. Kallio, S. J. Remington, D. Huppert, *J. Phys. Chem. B* **2011**, *115*, 11776-11785.

[126] I. Presiado, Y. Erez, R. Simkovitch, S. Shomer, R. Gepshtein, d. S. Pinto, d. S. Esteves, D. Huppert, *J. Phys. Chem. A* **2012**, *116*, 10770-10779.

[127] Y. Erez, I. Presiado, R. Gepshtein, d. S. Pinto, d. S. Esteves, D. Huppert, *J. Phys. Chem. A* **2012**, *116*, 7452-7461.

[128] B. Cohen, C. M. Álvarez, N. A. Carmona, J. A. Organero, A. Douhal, *J. Phys. Chem. B* **2011**, *115*, 7637-7647.

[129] S. K. Mondal, K. Sahu, P. Sen, D. Roy, S. Ghosh, K. Bhattacharyya, *Chem. Phys. Lett.* **2005**, *412*, 228-234.

[130] D. B. Spry, A. Goun, K. Glusac, D. E. Moilanen, M. D. Fayer, *J. Am. Chem. Soc.* **2007**, *129*, 8122-8130.

[131] D. E. Moilanen, D. B. Spry, M. D. Fayer, *Langmuir* **2008**, *24*, 3690-3698.

[132] T. Mondal, A. K. Das, D. K. Sasmal, K. Bhattacharyya, *J. Phys. Chem. B* **2010**, *114*, 13136-13142.

[133] E. Gould, A. V. Popov, L. M. Tolbert, I. Presiado, Y. Erez, D. Huppert, K. M. Solntsev, *Phys. Chem. Chem. Phys.* **2012**, *14*, 8964-8973.

[134] D. B. Spry, M. D. Fayer, *J. Chem. Phys.* **2008**, *128*, 084508.

[135] N. Agmon, W. Rettig, C. Groth, *J. Am. Chem. Soc.* **2002**, *124*, 1089-1096.

[136] J. T. Hynes, T.-H. Tran-Thi, G. Granucci, *J. Photochem. Photobiol. A* **2002**, *154*, 3-11.

[137] L. M. Tolbert, J. E. Haubrich, *J. Am. Chem. Soc.* **1990**, *112*, 8163-8165.

[138] A. G. Crawford, A. D. Dwyer, Z. Liu, A. Steffen, A. Beeby, L. Pålsson, D. J. Tozer, T. B. Marder, *J. Am. Chem. Soc.* **2011**, *133*, 13349-13362.

[139] I. Carmeli, D. Huppert, L. M. Tolbert, J. E. Haubrich, *Chem. Phys. Lett.* **1996**, *260*, 109-114.

[140] B. Hinkeldey, A. Schmitt, G. Jung, *ChemPhysChem* **2008**, *9*, 2019-2027.

[141] J. N. Brönsted, *Chem. Rev.* **1928**, *5*, 231-338.

[142] O. F. Mohammed, D. Pines, J. Dreyer, E. Pines, E. T. J. Nibbering, *Science* **2005**, *310*, 83-86.

[143] E. Pines, D. Huppert, *Chem. Phys. Lett.* **1986**, *126*, 88-91.

[144] E. Pines, D. Huppert, *J. Chem. Phys.* **1986**, *84*, 3576-3577.

[145] F. C. Goodrich, *J. Chem. Phys.* **1954**, *22*, 588-594.

[146] N. Agmon, *J. Chem. Phys.* **1984**, *81*, 2811-2817.

[147] N. Agmon, E. Pines, D. Huppert, *J. Chem. Phys.* **1988**, *88*, 5631-5638.

[148] N. Agmon, *J. Chem. Phys.* **1988**, *88*, 5639-5642.

[149] D. Pines, E. Pines, *J. Chem. Phys.* **2001**, *115*, 951-953.

[150] K. M. Solntsev, N. Agmon, *Chem. Phys. Lett.* **2000**, *320*, 262-268.

[151] K. M. Solntsev, D. Huppert, N. Agmon, *Phys. Rev. Lett.* **2001**, *86*, 3427-3430.

[152] N. Agmon, I. V. Gopich, *Chem. Phys. Lett.* **1999**, *302*, 399-404.

[153] I. V. Gopich, K. M. Solntsev, N. Agmon, *J. Chem. Phys.* **1999**, *110*, 2164-2174.

[154] B. Cohen, D. Huppert, N. Agmon, *J. Am. Chem. Soc.* **2000**, *122*, 9838-9839.

[155] E. B. Krissinel', N. Agmon, *J. Comput. Chem.* **1996**, *17*, 1085-1098.

[156] K. Ando, J. T. Hynes, *J. Phys. Chem. B* **1997**, *101*, 10464-10478.

[157] K. Ando, J. T. Hynes, *J. Phys. Chem. A* **1999**, *103*, 10398-10408.

[158] P. Leiderman, L. Genosar, D. Huppert, *J. Phys. Chem. A* **2005**, *109*, 5965-5977.

[159] R. Gepshtein, P. Leiderman, L. Genosar, D. Huppert, *J. Phys. Chem. A* **2005**, *109*, 9674-9684.

[160] T. -H. Tran-Thi, T. Gustavsson, C. Prayer, S. Pommeret, J. T. Hynes, *Chem. Phys. Lett.* **2000**, *329*, 421-430.

[161] B.-Z. Magnes, N. V. Strashnikova, E. Pines, *Isr. J. Chem.* **1999**, *39*, 361-373.

[162] F. Messina, M. Prémont-Schwarz, O. Braem, D. Xiao, V. S. Batista, E. T. J. Nibbering, M. Chergui, *Angew. Chem. Int. Ed.* **2013**, *52*, 6871-6875.

[163] D. B. Spry, M. D. Fayer, *J. Chem. Phys.* **2007**, *127*, 204501.

[164] O. F. Mohammed, J. Dreyer, B. -. Magnes, E. Pines, E. T. J. Nibbering, *ChemPhysChem* **2005**, *6*, 625-636.

[165] L. N. Silverman, D. B. Spry, S. G. Boxer, M. D. Fayer, *J. Phys. Chem. A* **2008**, *112*, 10244-10249.

[166] R. Knochenmuss, P. L. Muiño, C. Wickleder, *J. Phys. Chem.* **1996**, *100*, 11218-11227.

[167] R. A. Marcus, *J. Phys. Chem.* **1968**, *72*, 891-899.

[168] R. A. Marcus, *J. Am. Chem. Soc.* **1969**, *91*, 7224-7225.

[169] R. A. Marcus, *Angew. Chem. Int. Ed.* **1993**, *32*, 1111-1121.

[170] A. O. Cohen, R. A. Marcus, *J. Phys. Chem.* **1968**, *72*, 4249-4256.

[171] N. Munitz, Y. Avital, D. Pines, E. T. J. Nibbering, E. Pines, *Isr. J. Chem.* **2009**, *49*, 261-272.

[172] K. Adamczyk, M. Prémont-Schwarz, D. Pines, E. Pines, E. T. J. Nibbering, *Science* **2009**, *326*, 1690-1694.

[173] H. S. Johnston, C. Parr, *J. Am. Chem. Soc.* **1963**, *85*, 2544-2551.

[174] K. S. Peters, A. Cashin, P. Timbers, *J. Am. Chem. Soc.* **2000**, *122*, 107-113.

[175] K. S. Peters, G. Kim, *J. Phys. Chem. A* **2004**, *108*, 2598-2606.

[176] N. Agmon, R. D. Levine, *Chem. Phys. Lett.* **1977**, *52*, 197-201.

[177] N. Agmon, R. D. Levine, *J. Chem. Phys.* **1979**, *71*, 3034-3041.

[178] E. Pines, G. R. Fleming, *J. Phys. Chem.* **1991**, *95*, 10448-10457.

[179] A. J. C. Varandas, S. J. Formosinho, *J. Chem. Soc. , Chem. Commun.* **1986**, 163-165.

[180] A. J. C. Varandas, S. J. Formosinho, *J. Chem. Soc. , Faraday Trans. 2* **1986**, *82*, 953-962.

[181] M. Barroso, L. G. Arnaut, S. J. Formosinho, *J. Photochem. Photobiol. A.* **2002**, *154*, 13-21.

[182] P. M. Kiefer, J. T. Hynes, *J. Phys. Chem. A* **2002**, *106*, 1834-1849.

[183] P. M. Kiefer, J. T. Hynes, *J. Phys. Chem. A* **2002**, *106*, 1850-1861.

[184] K. S. Peters, *Acc. Chem. Res.* **2009**, *42*, 89-96.

[185] D. C. Borgis, S. Lee, J. T. Hynes, *Chem. Phys. Lett.* **1989**, *162*, 19-26.

[186] D. Borgis, J. T. Hynes, *Chem. Phys.* **1993**, *170*, 315-346.

[187] D. Borgis, J. T. Hynes, *J. Phys. Chem.* **1996**, *100*, 1118-1128.

[188] P. M. Kiefer, J. T. Hynes, *Solid State Ionics* **2004**, *168*, 219-224.

[189] B. J. Ka, W. H. Thompson, *J. Phys. Chem. A* **2012**, *116*, 832-838.

[190] B. Cohen, D. Huppert, *J. Phys. Chem. A* **2001**, *105*, 2980-2988.

[191] B. Cohen, P. Leiderman, D. Huppert, *J. Phys. Chem. A* **2002**, *106*, 11115-11122.

[192] C. Reichardt, *Solvents and solvent effects in organic chemistry*, VCH, Weinheim, **1988**.

[193] W. Liptay, G. Walz, *Z. Naturforsch.* **1971**, *26a*, 2007.

[194] W. Liptay, *Angew. Chem. Int. Ed.* **1969**, *8*, 177-188.

[195] E. Lippert, *Z. Elektrochem.* **1957**, *61*, 962-975.

[196] N. Mataga, Y. Kaifu, M. Koizumi, *Bull. Chem. Soc. Jpn.* **1956**, *29*, 465-470.

[197] A. Bani-Yaseen, *J. Fluoresc.* **2011**, *21*, 1061-1067.

[198] V. Gutmann, *Coord. Chem. Rev.* **1967**, *2*, 239-256.

[199] A. Leo, C. Hansch, D. Elkins, *Chem. Rev.* **1971**, *71*, 525-616.

[200] E. Grunwald, S. Winstein, *J. Am. Chem. Soc.* **1948**, *70*, 846-854.

[201] E. M. Kosower, D. Hofmann, K. Wallenfels, *J. Am. Chem. Soc.* **1962**, *84*, 2755-2757.

[202] E. M. Kosower, *J. Am. Chem. Soc.* **1958**, *80*, 3253-3260.

[203] K. Dimroth, C. Reichardt, T. Siepmann, F. Bohlmann, *Justus Liebigs Ann. Chem.* **1963**, *661*, 1-37.

[204] C. Reichardt, *Justus Liebigs Ann. Chem.* **1971**, *752*, 64-67.

[205] C. Reichardt, E. Harbusch-Görnert, *Liebigs Ann. Chem.* **1983**, *1983*, 721-743.

[206] H. Langhals, *Angew. Chem. Int. Ed.* **1982**, *21*, 724-733.

[207] R. W. Taft, M. J. Kamlet, *J. Am. Chem. Soc.* **1976**, *98*, 2886-2894.

[208] M. J. Kamlet, R. W. Taft, *J. Am. Chem. Soc.* **1976**, *98*, 377-383.

[209] M. J. Kamlet, J. L. Abboud, R. W. Taft, *J. Am. Chem. Soc.* **1977**, *99*, 6027-6038.

[210] M. J. Kamlet, J. L. M. Abboud, M. H. Abraham, R. W. Taft, *J. Org. Chem.* **1983**, *48*, 2877-2887.

[211] J. Catalán, C. Díaz, V. López, P. Pérez, J. G. De Paz, J. G. Rodríguez, *Liebig Ann.* **1996**, *1996*, 1785-1794.

[212] J. Catalán, C. Díaz, *Liebigs Ann.* **1997**, *1997*, 1941-1949.

[213] J. Catalán, H. Hopf, *Eur. J. Org. Chem.* **2004**, *2004*, 4694-4702.

[214] J. Catalán, *J. Phys. Chem. B* **2009**, *113*, 5951-5960.

[215] C. Laurence, P. Nicolet, M. T. Dalati, J. M. Abboud, R. Notario, *J. Phys. Chem.* **1994**, *98*, 5807-5816.

[216] J. Jayabharathi, V. Thanikachalam, M. Perumal, K. Jayamoorthy, *J. Fluoresc.* **2012**, *22*, 213-221.

[217] A. Rosspeintner, G. Angulo, M. Weiglhofer, S. Landgraf, G. Grampp, *J. Photochem. Photobiol. A* **2006**, *183*, 225-235.

[218] G. Angulo, G. Grampp, J. Grilj, P. Jacques, S. Landgraf, A. Rosspeintner, *J. Photochem. Photobiol. A* **2008**, *199*, 204-210.

[219] A. Filarowski, M. Kluba, K. Cieslik-Boczula, A. Koll, A. Kochel, L. Pandey, W. M. De Borggraeve, d. A. Van, J. Catalan, N. Boens, *Photochem. Photobiol. Sci.* **2010**, *9*, 996-1008.

[220] W. Zhao, L. Pan, W. Bian, J. Wang, *ChemPhysChem* **2008**, *9*, 1593-1602.

[221] R. S. Moog, D. D. Kim, J. J. Oberle, S. G. Ostrowski, *J. Phys. Chem. A* **2004**, *108*, 9294-9301.

[222] M. Bauer, A. Rollberg, A. Barth, S. Spange, *Eur. J. Org. Chem.* **2008**, *2008*, 4475-4481.

[223] K. M. Solntsev, D. Huppert, L. M. Tolbert, N. Agmon, *J. Am. Chem. Soc.* **1998**, *120*, 7981-7982.

[224] K. M. Solntsev, D. Huppert, N. Agmon, *J. Phys. Chem. A* **1998**, *102*, 9599-9606.

[225] B. -Z. Magnes, D. Pines, N. Strashnikova, E. Pines, *Solid State Ionics* **2004**, *168*, 225-233.

[226] C. Spies, B. Finkler, N. Acar, G. Jung, *Phys. Chem. Chem. Phys.* **2013**, *15*, 19893-19905.

[227] B. Finkler, C. Spies, M. Vester, F. Walte, K. Omlor, I. Riemann, M. Zimmer, F. Stracke, M. Gerhards, G. Jung, *Photochem. Photobiol. Sci.* **2014**, *13*, 548-562.

5   List of abbreviations

DNA	Deoxyribonucleic acid
UV	Ultraviolet
Vis	visible (part of the electromagnetic spectrum)
IR	infra-red
fs	femtosecond
TCSPC	time-correlated single photon counting
ESPT	excited state proton transfet
PT	proton transfer
e.g.	exempli gratia (for the sake of an example)
ES	excited (electronic) state
GS	ground (electronic) state
HPTS	8-hydroxy-1,3,6-pyrenetrisulfonate, pyranine
HPTA	8-hydroxypyren-N,N,N',N',N'',N''-hexamethyl-1,3,6-trisulfonamide
H	hydrogen
D	deuterium
i.e.	id est (lat.); that is to say
KIE	kinetic isotope effect
DMSO	dimethyl sulfoxide
ICT	intramolecular charge transfer
CT	charge transfer
DSE	Debye-Smoluchowski equation
GR	geminante recombination
ESIPT	excited state intramolecular proton transfer

6 List of publications

6.1 Articles that appeared in peer-reviewed scientific journals

Christian Spies, Shay Shomer, Björn Finkler, Dina Pines, Ehud Pines, Dan Huppert and Gregor Jung, *Phys. Chem. Chem. Phys.*, **2014**, DOI: 10.1039/C3CP55292F.

Björn Finkler, Christian Spies, Michael Vester, Frederick Walte, Kathrin Omlor, Iris Riemann, Manuel Zimmer, Frank Stracke, Markus Gerhards and Gregor Jung, *Photochem. Photobiol. Sci.* **2014**, *13 (3)*, 548.

Christian Spies, Björn Finkler, Nursel Acar and Gregor Jung, *Phys. Chem. Chem. Phys.*, **2013**, *15*, 19893-19905.

Christian Spies, Anh-Minh Huynh, Volker Huch and Gregor Jung, *J. Phys. Chem. C*, **2013**, *117*, 18163-18169.

Xavier Le Guével, Vanessa Trouillet, Christian Spies, Gregor Jung and Marc Schneider, *J. Phys. Chem. C*, **2012**, *116*, 6047-6051.

Xavier Le Guével, Christian Spies, Nicole Daum, Gregor Jung and Marc Schneider, *Nano Res.*, **2012**, *5*, 379-387.

Xavier Le Guével, Vanessa Trouillet, Christian Spies, Ke Li, Timo Laaksonen, Dagmar Auerbach, Gregor Jung and Marc Schneider, *Nanoscale*, **2012**, *4*, 7624-7631.

6.2 Contributions to scientific conferences

Christian Spies, Shay Shomer, Björn Finkler, Dina Pines, Ehud Pines, Dan Huppert and Gregor Jung, "Solvent Dependence of Excited-State Proton Transfer from Pyranine-derived Photoacids" Talk at *DPG meeting* **2014**, Berlin.

Christian Spies, Shay Shomer, Björn Finkler, Dina Pines, Ehud Pines, Dan Huppert and Gregor Jung, "Solvent Dependence of Excited-State Proton Transfer from Pyranine-derived Photoacids" Scientific poster at *MAF* **2013**, Genoa.

Christian Spies, Michael Vester and Gregor Jung, "Photophysics of Photoacids based on Pyrene", Talk at *Photochemietagung* **2012**, Potsdam.

Christian Spies, Michael Vester and Gregor Jung, "Photophysics of Photoacids based on Pyrene", Scientific poster at *MAF* **2011**, Strasbourg.

Christian Spies, Michael Vester, Björn Finkler and Gregor Jung, "Excited-state proton transfer – Synthesis and Characterization of Photoacids", Scientific poster at *Bunsentagung* **2011**, Berlin.